A Novel Thermal Energy Storage based Air Conditioning System for Rail Transport

by

Binjian Nie

Submitted in accordance with the requirements for the degree of

Doctor of Philosophy

The University of Birmingham

School of Chemical Engineering

April 2019

The candidate confirms that the work submitted is his own and that appropriate credit has been given where reference has been made to the work of others.

ACKNOWLEDGEMENTS

Time elapses quickly, when submitting this thesis, I would like to express my sincere gratitude to my supervisor Prof. Yulong Ding. With his continuous support and encouragement, combined with great vision and immense knowledge, I was able to enter the energy storage field, learn while performing research. Without his patient supervision and precious experience, I could not have finished the research work reported in this thesis.

I appreciate the suggestions from my co-supervisor, Dr Yongliang Li.

I very much appreciate the advices by academic, technical, administrative staff members, fellow and PhD colleagues of Birmingham Centre for Energy Storage, particulary, A Sciacovelli, H Navarro, Xiaohui She, Ping Ding, D P Smith, Chunping Xie, Xiaodong Peng, Chuan Li.

My deep thanks also go to my family members, particulary, my parents and brothers for their support.

Finally, I wish to express my thanks to my wife Dan Zhang and my little boy Shangchu Nie. My wife's understanding and contributions to the family have always motivated me during difficult life during the research and writing periods.

ABSTRACT

Thermal energy storage system using phase change materials (PCMs) has a potential for a wide range of applications, particulary dealing with the mismatch between energy demand and supply. The work reported in this PhD thesis concerns the use of PCM in temperature regulation in cabins of rail transportation.

The focus of the work is on: (a)enhancing the heat transfer from heat exchanger side by using extended surfaces(fins), and (b)PCM side by using additives. Air was used as heat transfer fluid as such a fluid can be used for air circulation. Both modelling and experimental work was carried out on the PCM based heat exchanger.

The modelling results show that the heat transfer coefficient can be significantly improved by the presence of fins with the charging and discharging durations reduced by ~ 85% and 74% respectively. The modelling results revealed that the use of fins in airside is more efficient than that in PCM side. In the absence of the fins in the PCM side, the same level of enhancement of heat transfer can be achieved by increasing thermal conductivity of the model PCM by 4-5 times. The modelling results were validated by experimental data. Based on the experimentally validated modelling results, an air-conditioning system consisting of a PCM heat exchanger was designed, constructed and tested in the lab. The results show that, for both charging and discharging processes, the heat transfer performance of the system is significantly improved with fins used in both air and PCM sides, leading to the increased thermal comfort, decreased outlet temperature fluctuation, an excellent heat transfer rate, a large energy storage capacity and a long working time.

Based on the above work, a novel compact thermal energy storage (TES) device containing a commercial PCM (RT 18 HC) was designed and experimentally investigated with an aim to improve thermal comfort and smooth cooling load of a rail air conditioning system. Two different types of fins were employed to in the TES device for the thermal performance enhancement, one is with serrated fins used in the air side and other is perforated straight fins employed in the PCM side. The time evolutions of PCM temperature during the discharging process of both in the axial and radial directions were presented. The discharging time, discharging depth, discharging power, thermal efficiency and exergy efficiency were studied as function of inlet air temperature and velocity. The results showed that hot air in the cabin could be cooled down to the desired temperature range of 16-20^{o}C in seconds. Both the energy and exergy analyses revealed that the designed device performed excellent discharging depth, higher than 97%. The results also showed favourable air temperature around 18^{o}C

for extended period of time, a flexibility for cooling load adjustment and had an ability to smooth out the frequent fluctuations of cooling load of transport compartments.

The charging behaviour was then investigated and the effects of charging time, transient charging rate, overall thermal efficiency and exergy efficiency at different inlet air temperatures and velocities were examined. The time evolutions of PCM temperature in both the axial and radial directions were also measured. The dynamic exergy efficiency was studied for the first time to assess the optimal charging depth and charging time. The experimental results showed that the designed storage device had a flexible charging rate with the maximum rate at 1.3 kJ/s, a high thermal efficiency of 87% and an overall exergy efficiency of 70%. Decreasing the inlet air temperature or increasing the air velocity shortened the whole charging time, which varied from 50 to 174.2 mins. The analysis of the dynamic exergy efficiency showed that the maximum exergy efficiency was around 90% with the optimal charging time varying from 10 to 52 mins. The corresponding optimal charging depth increased with increasing inlet air temperature or velocity, ranging from 46% to 58% under the studied conditions.

Further analyses were performed on the heat transfer characteristics of the storage device for transport air conditioning systems. The charging and discharging times, the transient heat flux and the heat transfer coefficient were obtained. Comparison of the overall heat transfer coefficient for the charging and discharging processes was used to explain the difference between the charging and discharging kinetics. The variation in Nusselt number with Reynolds number under different Prandtl number for the discharging and charging processes were established.

Such an empirical relationship was experimentally validated. Validations between the empirical and experimental Nusselt number were carried out. The average error for the charging and discharging processes between the empirical and experimental Nusselt is 2.33% and 1.65% respectively which shows a good reliability. This indicates that the obtained equations can be used for the design of such novel TES device for transport air conditioning application.

Finally, the PCM based storage device integrates with a conventional air conditioner(AC). Comparisons were carried out between the AC and PCM-AC, with respect to the space temperature fluctuation, the coefficient of performance (COP), energy savings, and emergency ventilation/cooling. The experimental results show that, compared with the AC, space temperature fluctuation of the PCM-AC is decreased to 2.56°C; the ON-OFF cycles of the compressor in the PCM-AC are reduced by 27%; the overall COP is increased by 19.05%; the emergency ventilation and cooling time is prolonged by up to 9 times. What's more, the economic evaluation

shows that the electrical cost of the PCM-AC could be saved by up to 17.82%; the payback period is around 3.3 years and can be reduced to 1.83 years when using industrial grade PCM.

List of Figures

List of Tables

NOMENCLATURE

c_p Specific heat of capacity (kJ/(kg·K))

k Thermal conductivity (W/(m·K))

m Mass(kg)

$\dot{m}$ Mass flow rate (kg/s)

T Temperature ($^{\circ}$C or K)

t Time (s)

RH Relative Humidity

H Latent heat (kJ/kg)

V Velocity vector (m^3)

ρ Density(kg/m^3)

h Specific enthalpy (kJ/kg)

γ Liquid fraction

p Pressure(Pa)

μ Liquid viscosity (Pa·s)

δ Error

y_{exp} Experimental value

y_{num} Numerical value

ΔR Total error

δX_n Error factor

T_0 Ambient temperature, °C/K

W Power kJ s^{-1}

Q Energy kJ

η Efficiency

η_{th} Thermal efficiency

η_{ex} Exergy efficiency

e Specific exergy kJ kg^{-1}

E Exergy kJ

a air

pcm phase change material

TES thermal energy storage

i initial

e end

Al Aluminum

v Vapor

LMTD logarithmic mean temperature difference

EV Emergency ventilation and cooling

LHTES Latent heat energy storage

ω Humidity ratio kg kg^{-1}

D Discharging depth kJ kJ^{-1}

D_{ch} charging depth

LHES latent heat energy storage

v velocity, m/s

μ dynamic viscosity, kg/m^2 s

ρ density, kg/m^3

Q heat flux, kJ/s

d hydraulic diameter, m

A area, m^2

K heat transfer coefficient, W $m^{-2}K^{-1}$

Re Reynolds number ($=\rho\, vd/\,\mu$)

Pr Prandtle number ($=\mu\, c_p/\,k$)

Nu Nusselt number ($=Kd/k$)

Subscripts

l Liquid

s Solid

e End

m Melting

i Initial

Al Aluminum

ref Reference

max Maximum

ave Average

exp Experimental

num Numerical

η efficiency

η_{th} thermal efficiency

η_{ex} exergy efficiency

ω humidity ratio, kg kg^{-1}

tr transient

ov overall

AC Air Conditioner

Contents

Chapter 1 Introduction

General description

Rail transport has played a vital and rising role in urban development. Mechanical air-conditioning systems are usually employed to provide thermal comfort for people. However, passenger load is always flexible, and the peak load can surpass 30% of the designed condition[1]. What's more, the fast-changing operating ambient due to the train movement causes frequent fluctuation of the cooling load of the air-conditioning systems. Besides, the unstable cooling load will be brought in by air infiltration during opening and closing of rail transport doors [2]. The traditional air-conditioning systems could not be sufficient to handle such frequent load changes, which causes comfort degradation and even healthy concern. On the other hand, the general air conditioning system is designed to deal with the expected worst weather. However, the average cooling load is much lower than that of the peak period, which means that the air conditioning system is overdesigned in most cases [3]. Hence, the effective method is urgently needed to smooth the cooling load, eliminate the mechanical overdesign and back up the inadequate capacity of the rail transport air-conditioning systems.

PCM based cold energy storage

Latent heat thermal energy storage systems (LHTESS) which benefit from the natural characters of phase change materials (PCMs) have been employed to shift peak and off-peak energy and show great potentials in various fields. The large energy storage capacity to store energy at a relatively constant temperature[4][5][6] is particularly attractive for solving the existing fluctuations and the backup problem of transport air-conditioning systems.

Disadvantages of previous research

Firstly, previous research on PCM based cold energy storage for air conditioning systems is mostly for building applications. There are only a few papers on the utilization of PCM for transport air conditioning system. The past work mainly focuses on the performance in building applications without considering the compactness. For the transport application, it has a strict requirement of the compactness of the system with suitable volume and weight. Hence, it's important to develop the compact TES device for transport application.

Secondly, there is still no work published to reveal the heat transfer coefficient of such a novel TES device for transport air conditioning system. This work endeavours to determine the heat transfer characteristics including the charging and discharging time, heat flux and especially the heat transfer coefficient of the PCM based TES device. The charging and discharging characteristics including time and heat flux under different inlet air temperature and velocity were compared. Besides, the charging and discharging transient heat transfer

coefficients with various inlet air parameters were revealed. The overall heat transfer coefficients for both the charging and discharging process were concluded. The innovative results of this study can be used as the guideline for the future design of the novel PCM based device for transport air conditioning system.

Finally, emergency ventilation and cooling is another problem which the transport air conditioning is facing. Currently, only fresh air from ambient can be blown to the carriage when the sudden accident of the electricity supply occurs. This is due to that the emergency battery can only drive the emergency fan without enough power for the compressor. This leads to a shortage of emergency ventilation and cooling which can cause thermal comfort reduction and even the health concern. When the ambient temperature is high, the fresh air will bring more heat load into the carriage. Hence, it's quite necessary to develop the emergency ventilation and cooling for the rail transport field. There are still no sufficient publications to involve the proposed system.

Feasibility of integration with cold energy storage

In order to introduce cold energy storage to a traditional air conditioning system, a real case was cited to show the feasibility of integration. The mechanical unit is designed with a cooling power of 44Kw. The inlet air flowrate is 5000 m^3/h which consists of two parts. The first part is new air from the ambient with the flowrate at 1600 m^3/h, the other part is recycling air from the carriage. **Table 1.1** gives the operating and mechanical parameters of the traditional air conditioner used in a rail carriage.

Aspen plus was employed to simulate the whole process. With the cooling power of 44kW, when the new air temperature changes between 35 ˚C and 25 ˚C, the outlet air temperature varies from 20 ˚C to 14 ˚C, shown in **Figure 1.1 a-d**. It can be seen that the cooling power is designed according to the highest ambient temperature. Obviously, the ambient temperature is lower which will lead to excess power. This will further lead to the cooler outlet air temperature which can cause thermal comfort reduction and even health concern. Hence, the excess cold energy needs to be absorbed when the outlet temperature is lower than the 18 ˚C.

Table 1.1: Operating and mechanical parameters of the traditional air conditioner in a rail carriage.

Catalogue	Highest	Lowest
New air temperature (˚C)	35	25
New air flowrate (m^3/h)	1600	
Recycle air flowrate(m^3/h)	3400	
Recycle air temperature(˚C)	28	
Cooling power(kW)	44	
Outlet temperature requirement(˚C)	20	18

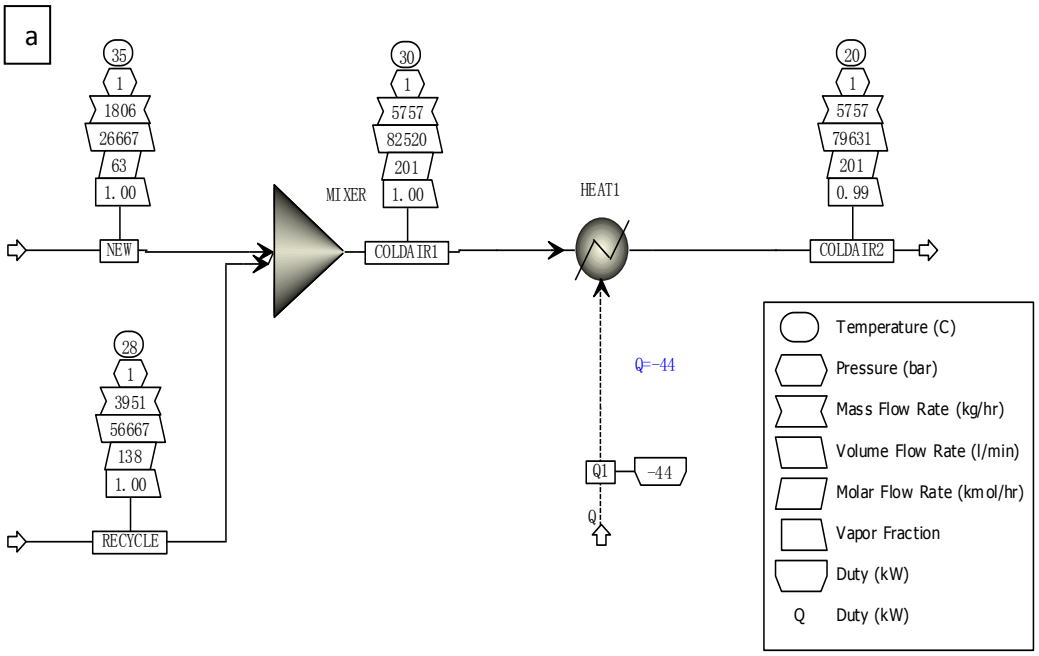

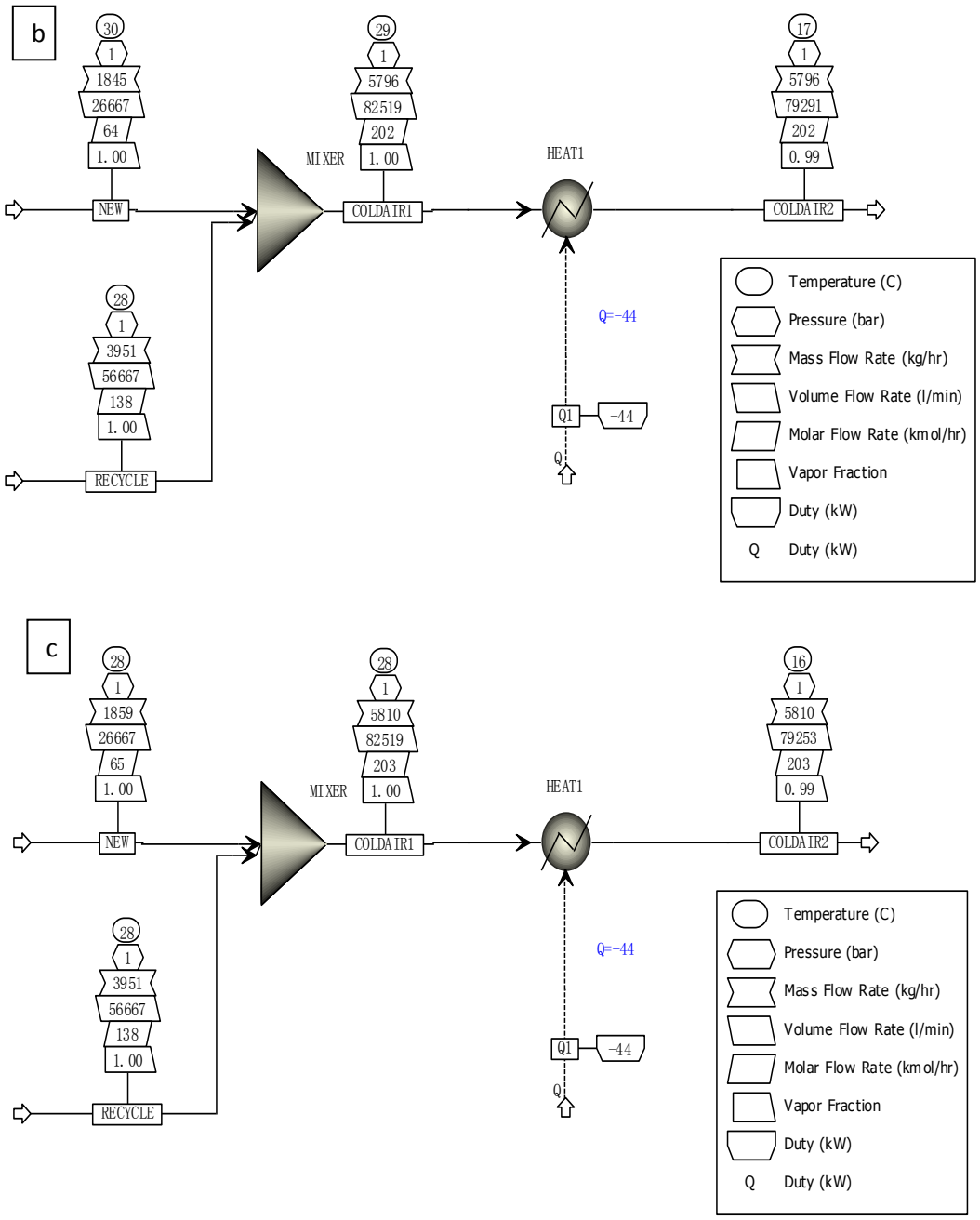
b
30
1
1845
26667
64
1.00
NEW
MIXER
29
1
5796
82519
202
1.00
COLDAIR1
HEAT1
17
1
5796
79291
202
0.99
COLDAIR2
28
1
3951
56667
138
1.00
RECYCLE
Q=-44
Q1
-44
Q
Temperature (C)
Pressure (bar)
Mass Flow Rate (kg/hr)
Volume Flow Rate (l/min)
Molar Flow Rate (kmol/hr)
Vapor Fraction
Duty (kW)
Q Duty (kW)

c
28
1
1859
26667
65
1.00
NEW
MIXER
28
1
5810
82519
203
1.00
COLDAIR1
HEAT1
16
1
5810
79253
203
0.99
COLDAIR2
28
1
3951
56667
138
1.00
RECYCLE
Q=-44
Q1
-44
Q
Temperature (C)
Pressure (bar)
Mass Flow Rate (kg/hr)
Volume Flow Rate (l/min)
Molar Flow Rate (kmol/hr)
Vapor Fraction
Duty (kW)
Q Duty (kW)

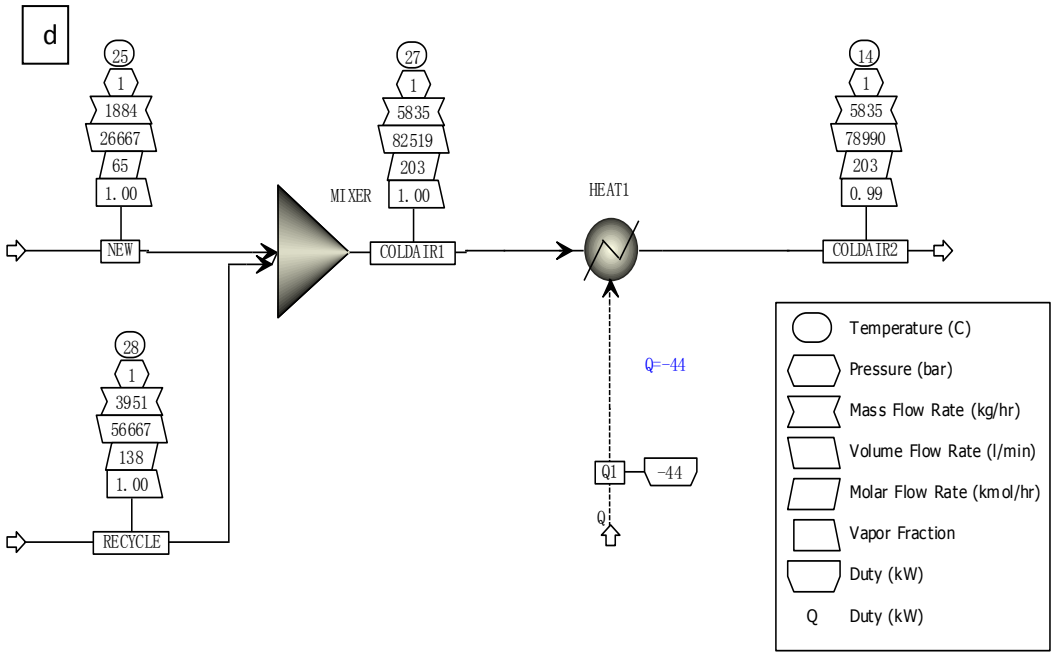

Figure 1.1: The outlet air temperature simulated by Aspen Plus under different inlet new air temperature (a: 35 ˚C, b: 30 ˚C, c: 28 ˚C; d: 25 ˚C).

When setting the outlet temperature between 18 ˚C and 20 ˚C, the actual cooling power needed with the new air temperature of 28 ˚C is 36 kW and 26 kW which is only 82% and 59% of the designed capacity respectively, given in **Figure 1.2 a-b**. With the new air temperature decreases to 25 ˚C, the real power is 61% and 39% of the full capacity, which can be found in **Figure 1.3 a-b**. This furtherly indicates the excess design of cooling power which shows the feasibility of using energy storage which can absorb the excess cold energy to ensure the desired outlet air temperature.

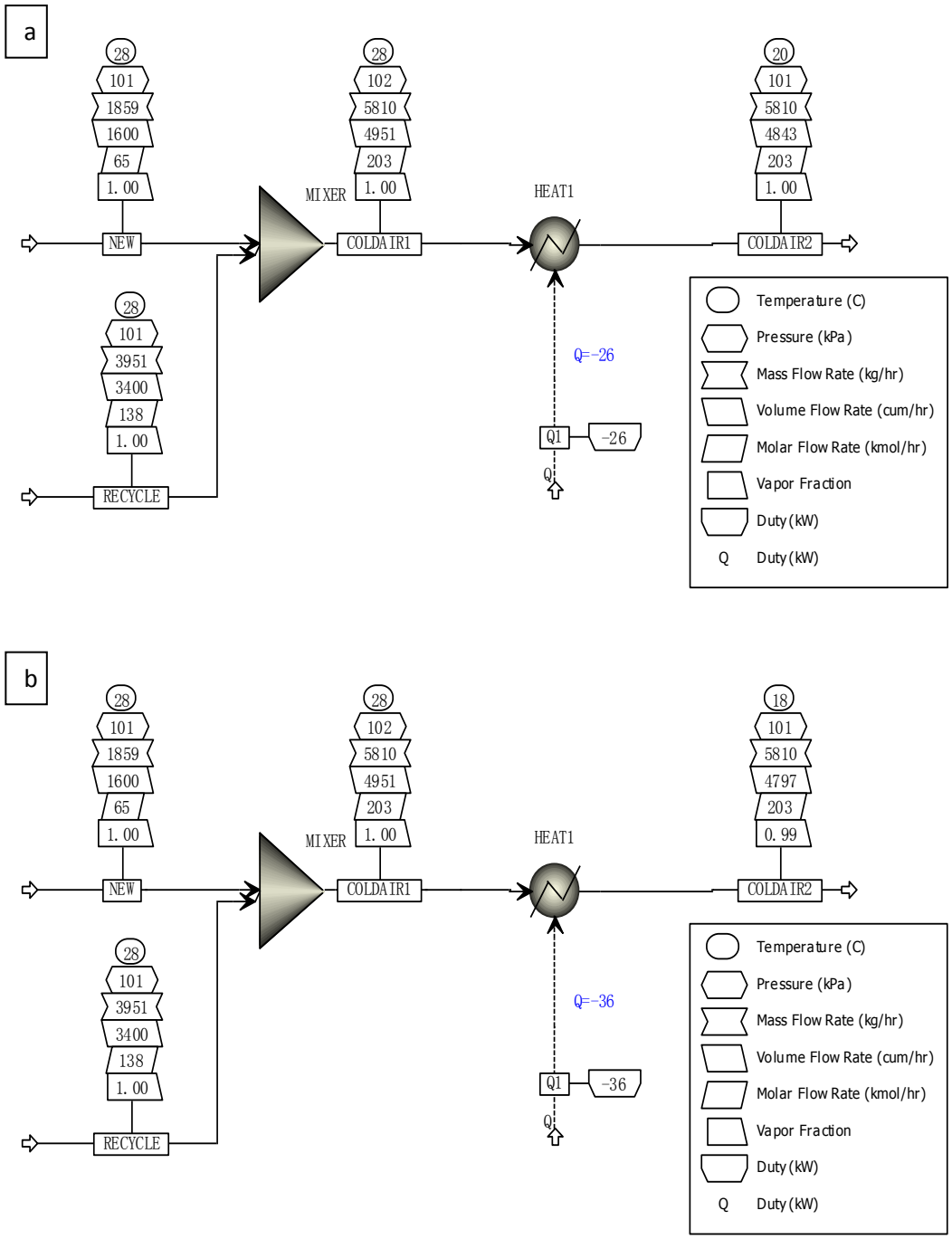

Figure 1.2: The actual cooling power for different outlet air temperature (a: 20 ˚C, b: 18 ˚C) with new air temperature at 28 ˚C.

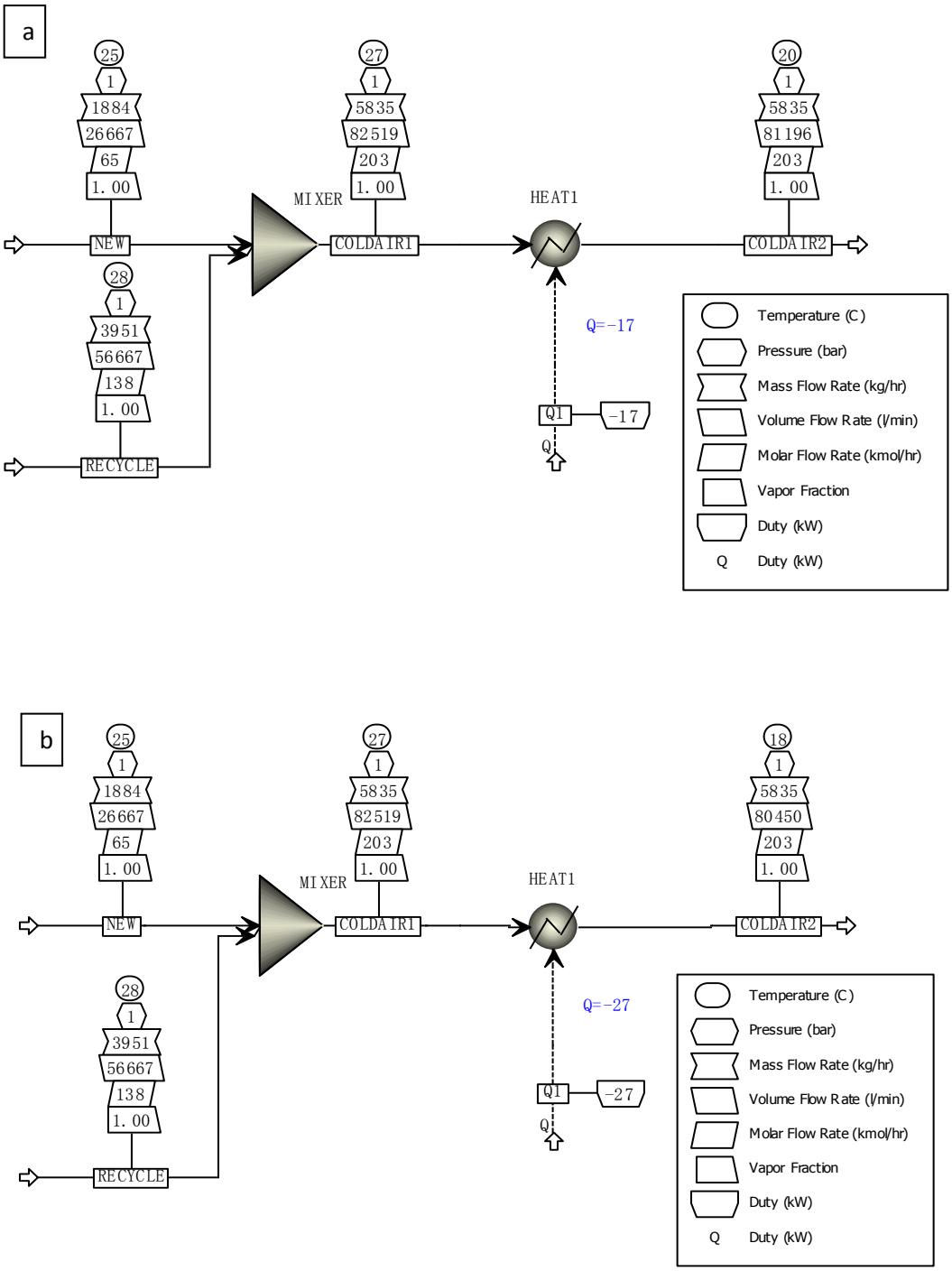

Figure 1.3: The actual cooling power for different outlet air temperature (a: 20 ˚C, b: 18 ˚C) with new air temperature at 25 ˚C.

A Newly Proposed Air conditioning system

In this study, a compact TES device filled with PCM was introduced to the air conditioning system which has a great potential in transport application. The TES device was designed and optimized through modelling and experimental methods.

The experimental rig shown in **Figure 1.4** is set up to test its performance. The whole system is mainly consisted of an air conditioner, a TES device, and an insulated room. The heat load inside the room is generated from an electrical heater. A centrifugal fan with a frequency converter is added to ensure the required air velocity. Cold air provided by the air conditioner flows through the TES device and then enters the room for cooling. The return air from the room enters the air conditioner.

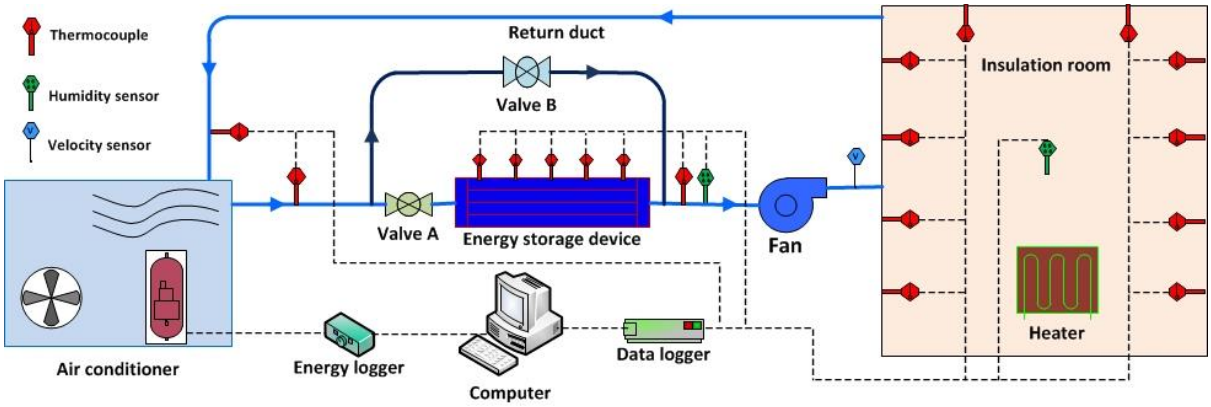

Figure 1.4: Schematics of the experimental rig for the PCM-AC.

Aims and objectives

The primary aim of this study is to apply phase change material based cold energy storage in transport air conditioning system, including the design and performance of the device and system. Both mathematical modelling and experimental are used to achieve the aim.

The specific objectives of this work are to develop the newly proposed technology for transport air conditioning applications. The comparison of the effects of fins on air or PCM sides with the modified PCMs of different conductivities, the charging and discharging performance of the TES device including the discharging and charging time, the transient discharging charging rate, thermal efficiency and exergy efficiency at different inlet air temperatures and velocities combined with the thermo-economic analysis and emergency cooling effect of the PCM added system are expected to achieve. All these results to be obtained can provide guidelines for the design and optimum operating conditions for air conditioning system integrated with the compact TES device in transport applications.

Methodologies

Both experimental work and mathematical modelling are carried out to investigate the discharging and charging performance of the TES device. Numerical modelling combined with experiments has been employed to optimize the configurations of the compact TES device.

Firstly, numerical models were applied to simulate the energy storage system with 4 different configurations: no fins on both sides (no fins), serrated fins on the air side (air fins), straight fins on the PCM side (PCM fins), both serrated fins on air side and straight fins on PCM side (both fins). The results were compared with those when using model PCMs with different thermal conductivities. Secondly, the modelling results were used as guidelines for the design of the phase change TES device and a both fins type was designed and manufactured based on the numerical results. Finally, an experiment rig consisted with the TES device-air conditioner system was built up and its thermos-economic performance was tested.

Organisation of the Thesis

The thesis is organized in the following manner. Chapter Two reviews the literature relevant to this study including applications of energy storage technology, existed problems of the PCM and device, modelling and experimental design of TES device, energy storage for cold applications, cold energy storage for air conditioning systems. Chapter Three explains the theoretical background and details of the mathematical modelling used in the present study. The characterizations and thermos-physical properties of PCM, experimental set-up and procedure are described in this chapter as well. Modelling results and experimental validation are discussed in Chapter Four. Chapter Five presents the experimental results for the charging and discharging of the TES device. The heat transfer characteristics especially the heat transfer coefficient was also discussed in the Chapter Six. Chapter Seven shows the thermos-economic analysis of the PCM air conditioning system. Finally, a summary of the main conclusions is given in Chapter Eight.

Chapter 2 Literature Review

This chapter reviews previous research relevant to the PCM based cold energy storage. Section 2.1 generally reviews the current cold energy storage applications, mainly includes free cooling and refrigeration. Section 2.2 shows the limit applications of cold energy storage due to low heat conductivity, and the two methods including composite PCM and solid mesh to enhance the thermal conductivity. Section 2.3 examines the modelling and experimental research on the cold TES devices. Section 2.4 provides the work of the PCM based air conditioning system in the past. Finally, Section 2.5 summarizes the problems of past work on PCM based air conditioning systems and indicates the importance of the current study revealed by this thesis.

2.1 Energy storage for cold applications

Latent heat energy storage (LHES) techniques based on phase change materials (PCM) present innovative potential for the thermal management. A great amount of past work has revealed the advantages of LHES, which includes high energy storage density and constant temperature during phase change period. PCM integrated applications have been applied in many fields including solar energy systems [7][8], building heating and cooling systems [9][10], and heat recovery systems[11][12] .

2.1.1 Free cooling

Free cooling is referred to the cooling supply during the day by coldness stored during the night. It enables to capture and store the night-time sensible free-cooling which can save the power consumption of conventional air conditioning system. Many approaches have been conducted using PCM to store the night time coolness which is then used for cooling the hot ambient air during daytime.

Chiu et al [13] employed the latent heat thermal energy storage for active free cooling. The cold energy stored during night time was used as a heat sink for cooling when the cooling capacity was not sufficient. Techno-economic feasibility was studied with multi-objective optimization in comparison to a conventional air conditioning system. The results obtained through techno-economic feasibility study show that the proposed system can make the indoor comfort range meet 75% of the cooling requirement under half of the electricity consumption combined with less than half of the conventional air conditioning cost. Barzin et al [14] experimentally used the low-temperature outdoor air to charge the PCM-impregnated gypsum boards which was then used for building free cooling purposes. Two identical fully instrumented test huts with interior dimensions

of 2.4*2.4*2.4 m were designed. PT20 from PureTemp company was used as the PCM. A 20W fan was employed to blow outdoor cold air into the Hut through the entrance door during night period which was between 9 pm until 7 am. It was concluded that impressive electricity saving of 73% over a one-week period was achieved. Medved et al [15] studied the potential of latent heat thermal energy storage in building application. The energy savings and thermal comfort improvement was achieved. The thermal response of the packed-bed PCM unit was numerically modelled using an experimentally verified model. A mechanical ventilation system with an integrated PCM unit and an advanced control unit was set up as **Figure 2.1**. The ventilation system was operated by the control unit according to the air temperature at the PCM unit's inlet (ambient air temperature, T_a) and outlet T_o. When $T_o > T_a$ (mostly during the nights), the PCM unit was ventilated directly using the cold ambient air, the PCM was charged. When $T_a > T_o$ (normally during the daytime) the building was ventilated through the charged PCM unit, then the building was cooled down by releasing the coldness stored inside the PCM. The results showed that the optimal size of the LHTES for the free cooling of buildings was between 1 and 1.5 kg of PCM per m^3/h of fresh ventilation air.

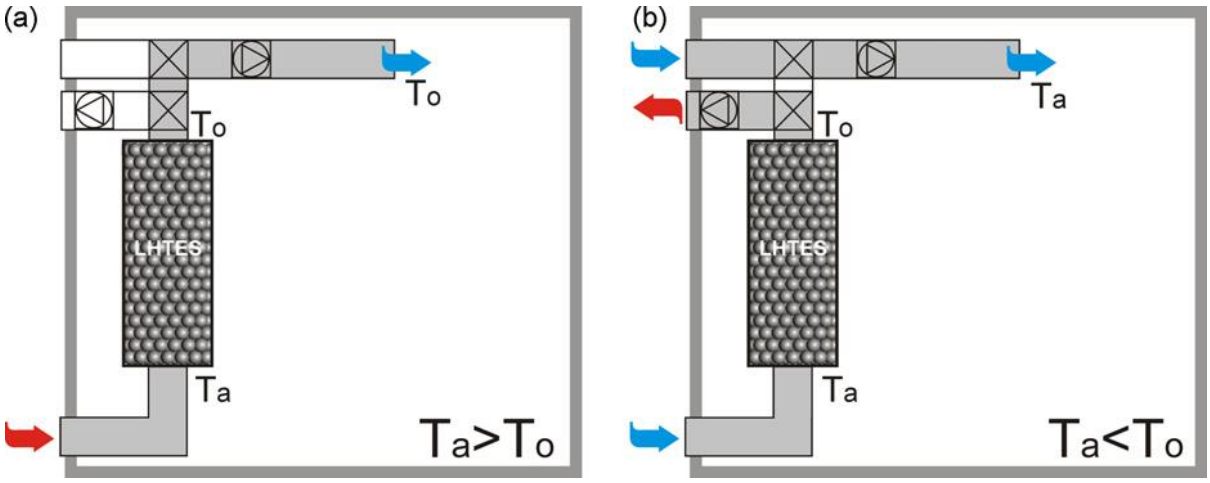

Figure 2.1: Outline of the free-cooling system: (a) air flow when $T_a > T_o$ (daytime); (b) air flows when $T_a < T_o$ (night-time)[15].

Takeda et al[16] developed a ventilation system containing the PCM. A schematic diagram of the experimental apparatus is shown in **Figure 2.2**. The dimensions of the air unit are 140*140*900 mm with a PCM unit packed in the centre at a height of 300 mm. The PCM granules consist of 65% ceramic materials and 35% paraffinic hydrocarbon by weight. When outdoor air temperature T_a is below 26 °C, cold air from ambient was blown through the PCM and cold energy was stored inside the PCM. While when T_a was above 26 °C, the ambient air

was cooled down and then was supplied into the room. By integrating the PCM unit with the air duct, it could be found that a 62.8% reduction of ventilation load was obtained. The cooling load was also decreased by the ventilation system.

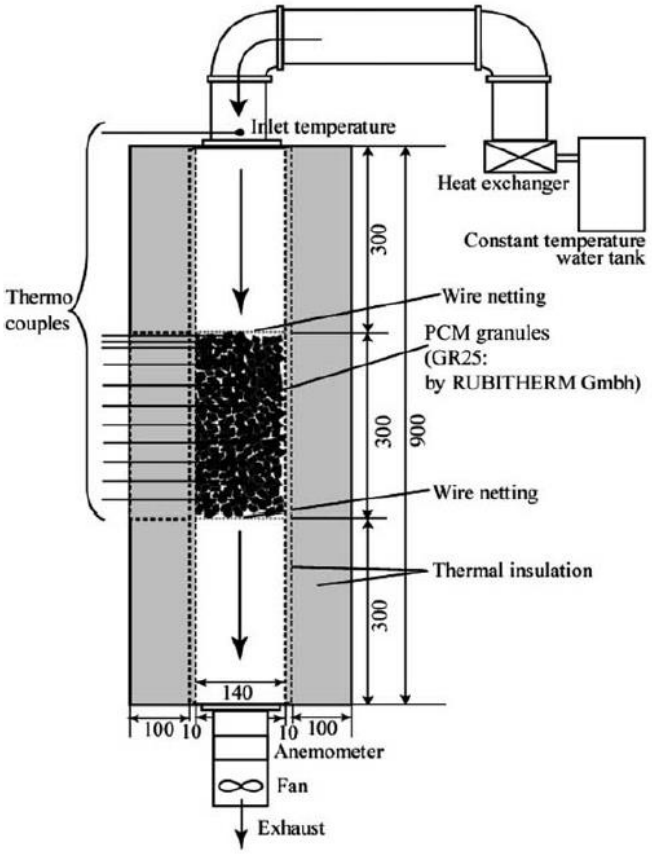

Figure 2.2: Schematics of the experimental apparatus for the ventilation system[16].

Arkar et al[17] presented the free cooling of building using a latent-heat thermal TES device integrated into a mechanical ventilation system. It showed that the free cooling with PCM is an effective cooling technique for suitable thermal comfort. Zalba et al[18] technically and economically evaluated a real free-cooling system using PCM. The system was proven to be not only technically feasible, but also economically advantageous with a pay-off period of 3-4 years. Walsh et al[19] applied PCMs based free cooling to an evaporative cooling system installed in a chemical plant. The obtained results showed that the new system was able to reduce energy costs by improving demand-side management. The salt hydrate with a freezing temperature of 17 °C which was encapsulated in the blow-moulded High-Density Polyethylene containers was used for the PCM unit. Cold water passed through the PCM unit and freezed the PCM inside while the water was cooled down by the coldness stored in the PCM during the following day. Subsequently, the cooled water passed through the absorber where

it dissipated the heat load. The chiller was run as a supply of coldness when the temperature was not low enough to charge (freeze) the PCM. In this way, the reduction of chiller peak-time operation could be achieved by up to 67% combined with a saving of less than 2% in electrical cost.

A PCM free cooling system using cold stored during nights to reduce day cooling load was presented by Osterman et al[20] numerically and experimentally. Plates with outer dimensions at 30 cm × 45 cm × 1.5 cm were vertically installed in the storage tank. The longer side of the plates were parallel to the air flow direction. The average mass of filled plate was 1361 g, with 1003 g of paraffin RT22HC from Rubitherm Company inside. The energy consumption in an office could be annually reduced by approximately 142 kWh. Sun et al[21] developed a free air cooling system using PCM to reduce the cooling energy consumption of the telecommunications base stations. PCMs were used to absorb excess cold energy from the ambient air. The stored coldness would be released when the conventional air conditioners could not meet the cooling requirements of the telecommunications base stations. The cooling capacity of the PCM unit was 3 kW with a dimension of 68 cm × 65 cm × 1.68 m. It was concluded that the energy savings ratio could reach a maximum value of 67% with replacement of the operation of conventional air conditioners from 82.6% to almost 100%. What's more, the authors indicated that the PCM unit could be powered by portable energy suppliers such as the batteries inside the stations. This would increase the feasibility and security of the PCM based system for free cooing of the telecommunications base stations. Gracia et al[22] investigated the potential of night free cooling in reducing the cooling loads of a building. The ventilated facade presented an air channel with a thickness of 15 cm which represented a 0.36 m^2 of channel area. The cold air was pumped by mechanical fans through the channel from the environment to solidify the PCM during the night time. For the cooling process, the hot air from ambient was blown through the fully charged PCM and was then pumped to the inner environment. The macro-encapsulated CSM panels containing salt hydrate SP-22 from Rubitherm company was employed as PCM in this study. This PCM presented a heat storage capacity of 150 kJ/kg in a temperature range from 15 °C to 30 °C with the melting and solidification temperature at 22 °C and 18 °C, respectively. A total number of 112 PCM panels (1.4 kg of SP-22 each) were distributed inside the facade which formed 14 air flow channels. During night time, typically from 2 to 8 a.m., the PCM was solidified. When the demand requires a cooling supply, the coldness inside the PCM was released to the air with mechanical ventilation. The conclusions showed that the free cooling could produce a reduction in the energy consumed by the heat pump of the building. The cooling capacity varied under different conditions with a maximum capacity at 42.8 MJ per day in the study. Mosaffa et al[23] numerically studied the performance enhancement of a free cooling system using a TES unit

with multiple PCMs. It was concluded that the COP (coefficient of performance) of the proposed system could achieve up to 7.0 which is significantly better than that of the traditional air conditioning systems. The conclusions obtained could be used for the guideline of optimum design for PCM free cooling air conditioning.

It can be easily concluded that by introducing the PCM to free cooling applications, a reduction of energy consumption of the mechanical air conditioning system was observed obviously. The potential of thermal comfort improvement and reduction of equipment size was noticed as well.

2.1.2 Refrigeration

Refrigeration is necessary for maintaining the quality and prolonging the shelf-life of fresh, frozen and perishable products. The predominant technology in refrigeration is mechanical vapor compression refrigeration. This method performs low energy efficiency and contributes to global warming. It was analyzed that the greenhouse gas emissions from conventional diesel engine driven vapor compression refrigeration systems used in food transport refrigeration can be as high as 40% of the greenhouse gas emissions from the vehicle's engine. PCM based energy storage systems used for refrigeration applications can offer energy savings and greenhouse gas emissions by replacement of the mechanical refrigeration system combined with a decrease of the frequency of on/off cycling. Several studies[24][25] have been done to compare the performance of PCM based and conventional refrigeration system.

Liu et al.[26] [27] simulated a PCM based refrigeration system using a proposed TRNSYS model for mobile transport application. The refrigerated space was set up with a size of 3 m × 2m × 1.8 m and insulated with 50 mm polyurethane. The PCM used for the refrigeration has a discharging (melting) temperature of -26.7 °C and a latent heat of 154 kJ/kg. The PCM was encapsulated into thin flat containers and parallel stacked. For charging process, the PCM unit was solidified by an off-vehicle refrigeration unit when the vehicle parked. When cooling was needed, the cold energy stored inside the PCM was released to cool down the refrigerated space. The brief configuration of the refrigeration system was shown in **Figure 2.3**. The charging process is expected to be accomplished in 8 h during the off-peak electricity tariff period from 11:00 p.m. to7:00 a.m.. The fully charged PCM unit could discharge the stored cooling capacity when it moved. Results showed that in order to maintain the temperature of the products at -18 °C for 10 h, a total of 250 kg and 390 kg of PCM was needed. When compared with a mechanical system, the proposed system incorporating PCM consumed less energy and produced significantly lower greenhouse gas emissions. Besides, the authors indicated that due to the stationary

operation, the electrically driven refrigeration units are highly efficient, extremely quiet and highly reliable. The energy cost for the refrigeration system was up to 86.4% less than conventional systems.

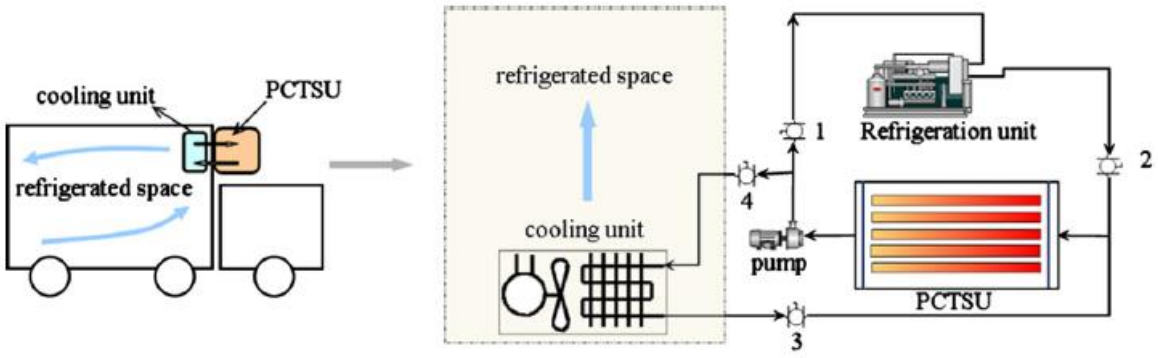

Figure 2.3: Configuration of the refrigeration system[26].

Glouannec et al.[28] developed a design of an insulation wall consisted of reflective multi-foil insulation, aerogel and PCM for refrigerated vans. It was concluded that the peak heat transfer and energy consumption during the daytime period could be reduced. Yusufoglu et al.[29] compared four kinds of PCMs in two different refrigerator models on the household refrigerator. By incorporating PCM on the evaporator tubes, the energy saving can be increased by a maximum of 9.4% when using only 0.95 kg of PCM. It also revealed that using PCMs in household refrigerators was economically beneficial combined with reducing harmful emissions. The performance of a PCM-based cooling system for automotive refrigerated containers under different ambient conditions was carried out by Shukla et al.[30].It was found that the newly developed container containing PCM plates could maintain the required inside temperature between -8 and -5 °C for 40 hours after charging 10 hours. The main advantage of this system was to eliminate fuel consumption for cooling and making a green system with zero pollution. What's more, a saving of 68 % of the cost was observed with the use of this application. Azzouz et al.[31] introduced an experimentally validated model for the dynamic behaviour of a refrigerator using a PCM storage system. A eutectic aqueous solution was used as PCM which was added on the outside face of a refrigerator evaporator. The location of PCM was shown in the **Figure 2.4**. It was found that by adding a phase change material (PCM) slab, a higher evaporating temperature was allowed, which increased the energy efficiency of the system. Besides, the energy stored in the PCM released to the refrigerator cell during the off cycle could provide the duration of several hours of continuous operation without power supply. A 5-15% increase in the coefficient of performance was achieved, a significant decrease in the number of ON/OFF cycles of the compressor and the temperature fluctuations inside the refrigerated cell was noticed as well. For a 5 mm

thick PCM slab, the refrigerator allowed safe food preservation without electrical supply ranges for up to 8 hours.

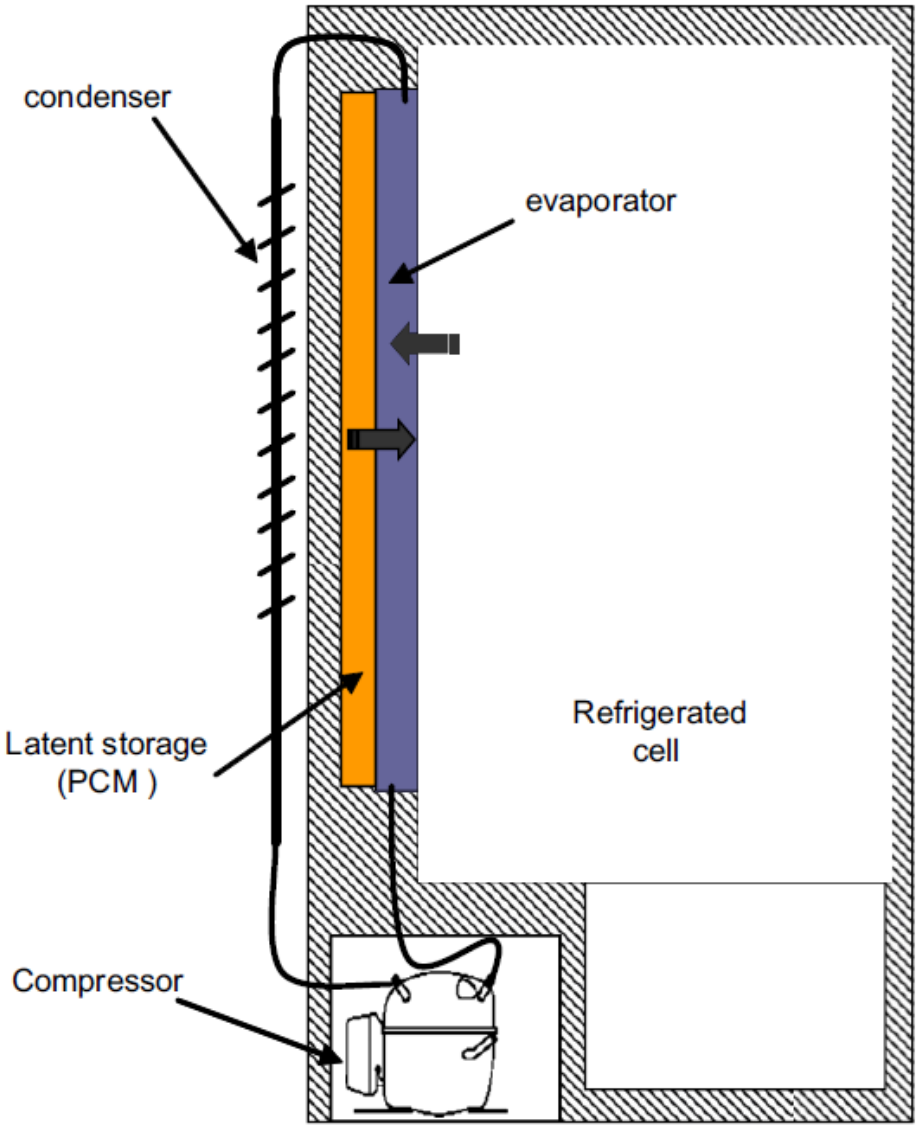

Figure 2.4: The description of PCM location on the evaporator of a household refrigerator[31].

Ahmed et al.[32] constructed a PCM insulation wall to decrease the heat load input to the refrigeration compartment. The paraffin-based PCM with a melting point at 7 °C was selected. Two test truck trailer simulators with a dimension of 1.22 m ×1.22 m × 1.22 m were built, with one was set-up with standard trailer walls, while the other one was outfitted with the PCMs inside the walls. The obtained results revealed that the peak heat transfer rate could be reduced by 29.1%, with overall average daily heat flow reductions into the refrigerated compartment at 16.3%. It would lead to energy savings and pollution abatement from mechanical

refrigeration units. The reduction of the refrigeration equipment size and extension of the equipment operational life was expected to be achieved due to the enhanced stability of operation of the compressor. Zarajabad et al[33].modelled the performance of PCM based household freezer. NaCl-H_2O was selected as PCM. The cold could be released to the freezer's cabin when the compressor was off. The proposed system could keep the freezer's cabin in the standard thermal condition for 4.5 hours, without using a compressor. A considerable reduction in energy consumption (45.7 kWh/year) was obtained. This reduction, not only diminished fossil fuel consumption about 13.7 liters/year, but also decreased CO_2 emission from 165.5 to 135.52 kg/year. Wang et al.[34] investigated the performance of applications of PCMs in refrigeration systems at different positions of the refrigeration cycle circuit with a shell and tube structure. It was observed that the refrigerant temperature entering the compressor was stabilized which caused a reduction on the peak compressor inlet temperature.

Gin et al.[35] installed the PCM panels on the internal walls of a freezer. A eutectic composition of water and ammonium chloride with a melting and freezing point of -15.4 °C was selected. For the conventional freezer, the product temperature rose to -3 °C caused by 3 h power loss, while the peak temperature could reach -11 °C when using the PCM. Meantime, the lower temperature fluctuations could be achieved due to PCM which was able to guarantee better food quality. For two weeks, the drip loss of product was 10%, which was nearly halved than that of the conventional one. Cheng et al.[36] set up a household refrigerator with PCM energy storage condensers. The experimental results show that the energy efficiency could be increased by approximately 12% with smaller starting power and shorter time to obtain the operation stability. Fioretti et al.[37] used PCM in a refrigerated container to improve the thermal performance. The paraffin wax with a melting temperature of 35°C was used as PCM. PCM acted as an energy storage medium which absorbed and displaced the incoming heat flux during its melting phase. Through the insertion of the PCM in a reefer container envelope, the heat transfer rate coming from the outside environment was reduced. It was observed that 1-2 °C reduced internal surface temperature compared with the conventional container. A reduction in peak heat transfer rate of 5.55% and 8.57% was concluded respectively as well. The results obtained from the above research show that when using PCM for the refrigeration system, the peak heat load can be reduced with stabilized temperature, energy saving, system efficiency improvement combined with a prolonged operational life of equipment can be achieved as well. Sepe et al.[38] installed twelve eutectic plates with six was placed on the ceiling and the other six on the right of a 20 feet an International Organization Standardization (ISO) container. The eutectic with a melting temperature at −26°C was selected as the phase change material. The air passing through the plates was cooled and transported cold air through a shaped duct placed in the upper part of the container for both fresh

(+4°C− ±1°C) and frozen (−18°C− −20°C) products. It was found the PCM based refrigeration container could maintain the required temperature values for almost seven days. Khan et al.[39] experimentally studied the effects of PCM on temperature fluctuation inside the cabinet of a household refrigerator during the door opening and power failure. The Polyethylene glycol-400 with a phase change temperature at 5-6°C was packaged inside a stainless steel container which was then placed inside the refrigerator cabinet. It was found that when integrating PCM, a significantly lower temperature fluctuation (about 2°C) was achieved. Under the door opening condition, the rise of air temperature in the cabinet decreased by about 3-5°C with PCM compared with that of the traditional system. During power failure time, PCM could work as a backup for up to 2 hours to maintain the lower temperature inside the chamber. Kilic et al[40]. used PCM for refrigeration room kept at -18°C to deal with the operational failure or electricity shortage problem. The results showed that the PCM load covering 10% of the total heat transfer surface area provided significant temperature maintenance under all ambient conditions. Elarem et al[41]. carried out experiments to improve the energy efficiency of a household refrigerator by integrating a PCM with the phase change temperature at 4 °C. It was shown that when using PCM, the power consumption was reduced by 12% and the COP was increased by 8% compared to the refrigerator without PCM. Raja et al[42]. designed the cold storage plant of the cascade refrigeration system using ethylene glycol as PCM. Compared with the conventional system, the max COP of the refrigeration system using PCM was increased by 16.4%. Bruno et al[43]. designed a PCM thermal storage system incorporated with an ammonia refrigeration system for a farm. The PCM could provide heat transfer fluid temperatures of around -6°C to -8°C which made it possible for food storage which temperature requirement was typically around -1°C to 3°C. It showed that the refrigeration system integrated with the energy storage system achieved a peak demand reduction during the summer period. The system was able to shift the electricity load from the peak to off-peak electricity period using PCM. It demonstrated that a PCM thermal storage system could be used to shift the electricity load for cold storage from peak to off-peak periods.

From the mentioned above, PCMs placed at the evaporator section provided slower fluctuation of compartment temperature and more stable conditions against thermal load variations. A higher COP, lower energy consumption, lower condensation temperature and lower condensation pressure was achieved. When incorporating PCM inside the food storage compartment, a stable temperatures inside the compartment were observed[44].

2.1.3 Other cold applications

Beyond the applications on the free cooling and refrigeration, approaches in cold applications using PCM on other fields were also made in recent years. Krishnan et al.[45] proposed a hybrid heat sink which was consist of a parallel-plate heat sink with a portion of the fin tips immersed in the PCM. When the air cooling was reduced, the heat was absorbed by the PCM. It was observed that the performance of the hybrid heat sink can be improved compared to a finned heat sink without PCM. Hasan et al.[46] used the PCM to improve heat sink performance for cooling electronic packaging. Under natural ventilation for the same heat load up to 6 W, when using PCM, the time for the device to operate under safety temperature (below 60 °C) extended from 5min to 15 min. While under the forced ventilation, the operating time increased from 15 min to 60 min. Behi et al[47]. introduced a new PCM-assisted heat pipe module to improve the cooling process and avoid inside system heat dissipation in electronic devices. It was revealed that the module could contribute 86.7% to the cooling application and 11.7% avoidance of heat dissipation by providing additional heat absorption. In this way, the proposed module could eliminate or at least minimize thermal damage in electronic components. Krishna et al[48]. experimentally tested the cooling performance for electronic cooling using a heat pipe containing nano-enhanced PCM. The PCM was prepared by dispersing Al_2O_3 nanoparticles (50 nm) in Tricosane using ultrasonic methods. The evaporator temperature of the heat pipe with nano-enhanced PCM was reduced by about 25.75%, which was able to save 53% of the fan power compared to a conventional heat pipe. It was also found that the nano enhanced PCM could store almost 30% of the energy supplied at the evaporator which contributed to the reduction in fan power consumption. Yang et al. [49] developed a passive thermal management system using paraffin as PCM for $LiFePO_4$ battery modules. Comparison between the thermal response of battery packs with and without PCM was carried out. **Figure 2.5**. illustrated the heat fluxes in the battery pack with the PCM cooling method.

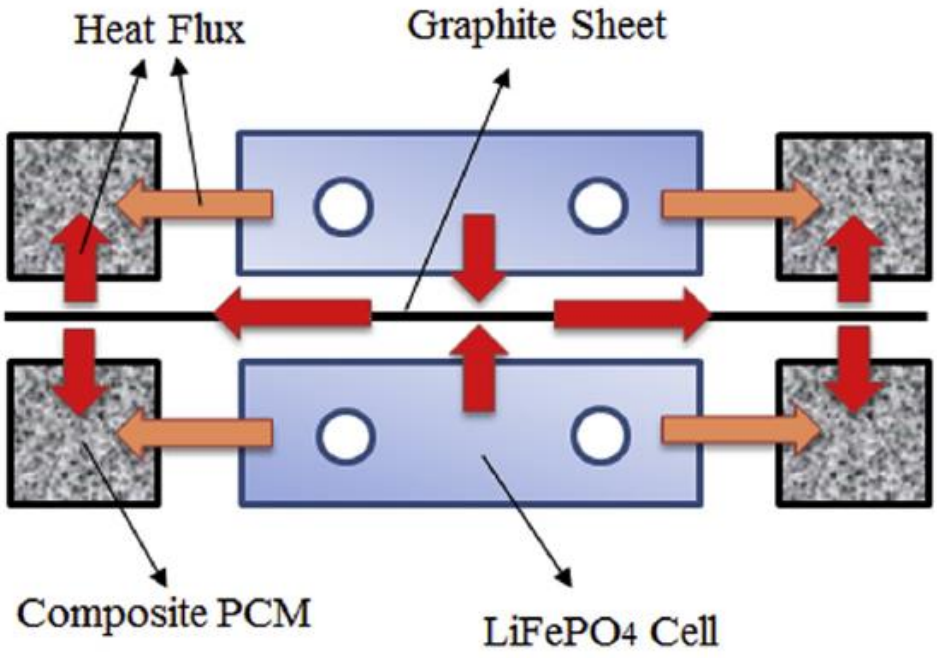

Figure 2.5: Schematic diagram of the heat flux in the battery pack with the composite PCM[49].

The experimental results revealed that under constant current discharges, the presence of PCM was able to reduce the temperature of the battery module by 37%. The thermal uniformity on the battery was far more than 5°C which could meet the real requirement. The proposed cooling system could effectively maintain the battery within its optimum operating temperature for a long period.

Commercial PCM RT42 from Rubitherm was used by Sharma et al[50]. to regulate the thermal performance of Building-Integrated Concentrated Photovoltaic systems. An increase in relative electrical efficiency of 7.7% and an average reduction in module centre temperature by 3.8 °C was observed when incorporating with the PCM.

Karthick et al[51]. used the inorganic glauber salt ($Na_2SO_4 \cdot 10H_2O$) with melting temperature at 32 °C for the thermal regulation of the Building-Integrated Concentrated Photovoltaic systems. The experimental results showed that PCM based system had an electrical efficiency increase by 10% and temperature reduction up to 8°C. Duan et al.[52] experimentally studied thermal management of battery modules using PCM with a phase change temperature at 18 °C. A battery cell was experimentally simulated by an electric heater. It indicated that the PCM system can realize good effectiveness in maintaining the heater within the desired temperature range. The passive cooling component utilizing PCM was added by Fathabadi et al. [53]with the active part of the hybrid thermal management system to optimize the thermal performance of the battery pack. Paraffin wax with melting temperature at 58.9°C was employed as PCM. The simulation results showed that the proposed battery pack could operate below 60°C for ambient temperature until 55°C. Lu et al.[54] studied the performance of a

new hybrid personal cooling system incorporating both ventilation fans and phase change materials. The cooling uniform set consisted of two ventilation units and 24 PCM packs. The main ingredients of PCMs are sodium sulfate and water with a melting temperature at 21°C. The total mass of each PCM pack was 86 g with the total weight of the hybrid unit at 3589g. The hybrid personal cooling system was illustrated in **Figure 2.6**.

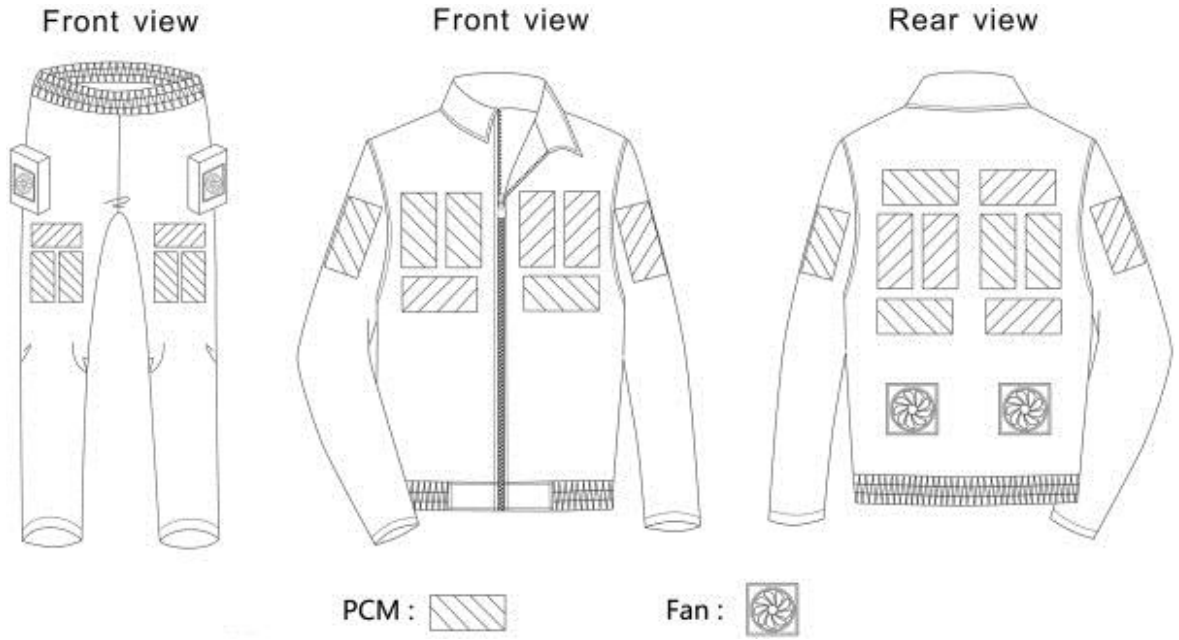

Figure 2.6: The hybrid personal cooling uniform contained PCMs and ventilation fans[54]**.**

Compared with existing portable air ventilation systems, the PCM based system performed better cooling effect at the initial working stages. The newly proposed system could be used for pre-cooling or post-exercise cooling athletes to improve thermal comfort, reduce the recovery time and thereby to improve the exercise performance. Yazdi et al[55][56][57]. employed a cooling garment using PCM with melting temperature at 18-20 oC on the body's thermal situation. The surface covered by PCM packets was 26% of the torso. The simulation results showed that the PCM bags could increase the efficiency of cool-vest up to 20% and 34% in case of using an ordinary insulating layer or a reflective coating, respectively. Itani et al.[58] incorporated phase change material packets into vests to improve the comfort of workers in hot environments. A polyester cooling vest equipped with 20 equally-sized PCM packets was used in the study. The experiments results showed effectively improved thermal comfort. Park et al.[59] experimentally investigated the electrical performance improvement a vertical PV module with the phase change material. With PCM attaching onto the rear side, the overheating of the PV module was prevented because the excess heat was absorbed by the phase change material. The obtained results showed that the PV cell temperature of the PV/PCM module was lower by up to 5 °C compared to the

conventional PV module. What's more, the electric power output of the PV module was increased by 3.1% when using the PCM. Atkin et al[60]. used the paraffin wax PCM with an approximate melting point of 40 °C for the thermal regulation of the PV panel. It was found that the overall efficiency of the PV panel could be increased 12.97%. Luo et al.[61] developed a PV-PCM system to control the temperature of a PV panel by applying paraffin/expanded graphite composite PCM. Compared with the temperature of the conventional PV panel, the temperature of the PV-PCM panel was maintained below 50 °C for 200 min which was extended by 146 min. The output power was averagely increased by 7.28% in heating process. The output voltage of the PV-PCM panel kept above 20.55 V for 128 min with the maximum value of 20.99 V, which was 0.51 V above the maximum output voltage of the conventional PV panel. The output power of the PV-PCM panel kept above that of the conventional PV panel for 230 min with the maximum increment of 11.50% and an average increment of 7.28%. Nada et al[62]. set up an experimental rig using PCM to regulate the thermal performance of the PV. By integrating the PCM to the back side of the building integrated PV module, the improvements of the module power and efficiency was increased. The obtained results showed that when integrating the PV with PCM, the temperature of the modules dropped 10.6 °C with efficiency rising by 13.2%. Hasan et al[63]. compared the temperature drop and power savings of the PV panels using $CaCl_2 \cdot 6H_2O$ and a eutectic mixture of fatty acids, capric acid-palmitic acid. It was found that $CaCl_2 \cdot 6H_2O$ achieved a 3-4 °C higher PV temperature drop and resulted in a 3% more power saving than that of capric–palmitic acid. Stropnik et al[64].using organic paraffin as PCM for the improvement of the electric generation performance of the PV panel. The PV cell temperature of the PV-PCM panel was lower by a maximum of 35.6 °C compared to the conventional PV panel, confirming the effect of a decrease in the temperature by the PCM. The obtained results showed that the generated electrical power output increased by 4.3%-8.7% and energy generation efficiency increased by 0.5%-1%, compared to the conventional PV module. The annual increase for production of electric energy was 7.3% and for energy generation efficiency was 0.8%, compared to the traditional PV panel. Aelenei et al[65]. studied an innovative building integrated system made of photovoltaic panels and PCMs. The thermal and electric efficiencies were calculated to reach about 10% with the overall system efficiency (electrical and thermal) at about 20%. Hasan et al[66].selected five different PCMs to regulate the building integrated photovoltaics. When integrating with PCMs, the temperature of the PV front surface was reduced to a maximum of 18 °C for 30 min. The temperature could keep a 10 °C temperature reduction for the longest duration of 5 h with 1000 W/m^2 insolation. Qiu et al[67]. experimentally investigated into the energy performance of a novel PV/T thermal and power system using the Microencapsulated Phase Change Material (MPCM) slurry. Paraffin

wrapped with the polymer shells was used as the Micro-encapsulated Phase Change Material (MPCM) slurry. The copper serpentine tube attached to the back surface of the PV module which allowed the PCM slurry to flow across. The heat generated within the PV cells was taken away by the MPCM slurry. It was concluded that with solar radiation of 500-700 W/m^2, the PCM based system could obtain the net overall solar efficiencies at 80.8-83.9%. The authors confirmed that the MPCM slurry based PV/T thermal and power system was superior to conventional air-sourced heat pump systems (ASHP) and solar assisted heat pump systems (ISAHP), and could potentially reduce fossil fuel consumption and carbon emission. Gao et al.[68] introduced phase-change chairs (PCC) and phase-change plates (PCPs) to isolated environments for cooling purposes. It was found that the combined system had the possibility to improve indoor thermal comfort and reduce the occupied space. With every 1 °C decrease in the cold storage temperature, the amount of PCPs reduced by 21-44%. Compared to the PCPs alone, the proposed system had a better performance in terms of temperature control and space saving.

2.2 Heat transfer enhancement

Among the previous studies on PCM cold applications, the overall performance of the new system can be improved when integrating with PCM. In the previous applications, both the inorganic and organic PCMs have been used.

2.2.1 Phase change materials

The phase change materials used for cold energy storage are classified into organic, organic materials and Eutectic, shown in **Figure 2.7**. The organic materials are generally classified as paraffin and non-paraffin while inorganic PCMs are generally metallic and hydrated salts. Eutectic PCM is a mixture of two or more PCMs in order to achieve the desired melting point[69]. The inorganic PCMs have limitations for widespread applications, it's mainly due to the corrosion[70][71][72][73][74][75][76], super cooling[77][78][4][79] and phase segregation under thermal cycling problems[80][81][82]. Compared with inorganic PCMs, organic PCMs have been widely used due to their outstanding properties such as non-toxicity, low or no supercooling and good thermal reliability[83][84][85][86][87][88][89].

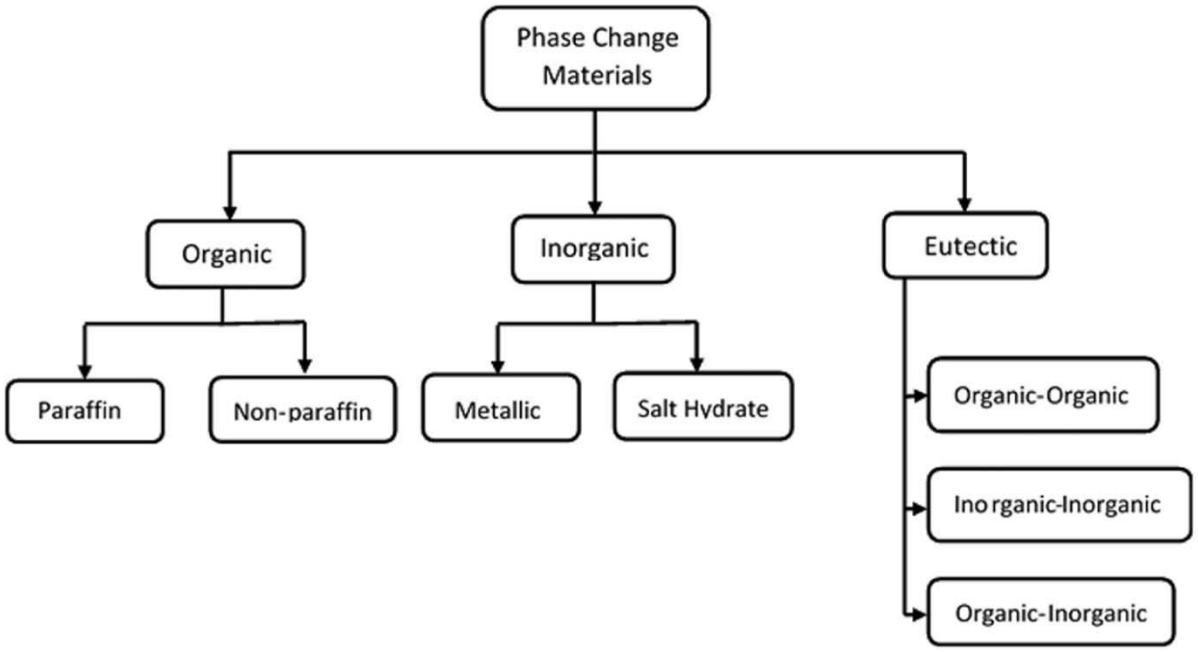

Figure 2.7: Classification of PCM for cold thermal energy storage[90]**.**

Paraffin is widely used not only due to the suitable phase change temperature, but also because paraffin is of chemically inert, stable and recyclable properties and exhibits no supercooling due to the self-nucleating character [83][91][92][93]. Hence, paraffin is normally used as organic PCM and also used in this study. However, the relatively low thermal conductivity of paraffin strongly suppresses the energy transfer rate and limits the widespread utilization of the latent heat energy storage system in transport air conditioning systems. Hence, efficient measures should be employed to promote the thermal conductivity of the latent heat energy storage system [94][95].

Hence, various approaches have been attempted to overcome the poor thermal conductivity drawback. Besides, for the cold applications, the temperature difference between the heat transfer fluid and PCM phase change point is normally small which leads to a poorer heat transfer performance. Among the existed research, it mainly focuses on two aspects. The first is adding high thermal conductivity additives and the other is extending the heat transfer surface area.

2.2.2 Composite PCM

For enhancing the heat transfer performance of energy storage system by modifying PCMs composite phase change materials (CPCMs) are normally used, which usually consist of a PCM, a thermal conductivity enhancement material and a ceramic supporting material for shape stabilization.

Li et al. [96] doubled the thermal conductivity of the PCM by adding 2.7%wt graphite. Karaipekli et al.[97] employed carbon nanotubes to enhance the thermal conductivity of paraffin which used as PCM for thermal energy storage system by 113.3%. Atinafu et al.[98] used porous carbons to increase the thermal conductivity of eutectic PCM up to 117.65%. Zou et al. [99]proposed a composite PCM for battery thermal management system. By adding multi-walled carbon nanotubes and graphene, the thermal conductivity of the PCM can reach 124% higher than that of pure PCM. Ji [100] et al. employed continuous ultrathin-graphite foam additives to increase the thermal conductivity of PCM by up to 18 times. Deng[101] et al. demonstrated that the PCM thermal conductivity was enhanced by up to 11.3 times through physically adding the polyethylene glycol-silver nanowire. Şahan[102] et al. concluded that with the addition of Fe_3O_4 nanoparticles, the thermal conductivity of PCM was improved with a maximum of 60% in their study. Yang [103] et al. revealed that the thermal conductivity of composite PCM presented 12 times enhancement by adding hexagonal boron nitride. The reduction of solidification time of the mixture of 60% n-tetradecane and 40% n-hexadecane by embedding with alumina and aluminum nanoparticles was revealed by Kalaiselvam et al [104]. It was found that the solidification rate was improved by up to 12.97% which indicated the potential for increasing the energy efficiency of the conventional LTES system in building cold applications. Xia et al.[11] added the expanded graphite into carnauba wax to form the composite PCM. It was shown that the thermal conductivity was increased by 16.4 times by adding one-tenth of expanded graphite which leaded to the reduction of the melting and solidification time at 81.7% and 55.3% respectively. The composite PCM exhibited good potential for recovery of condensation heat from cold storage refrigeration systems. Chandrasekaran et al.[105] dispersed 37-59 nm copper oxide nanoparticles into water to generate nanofluid phase change material. A significant reduction in solidification time at about 35% was noticed. It was proposed that the enhanced heat transfer rate of the composite PCM had a potential of energy savings of cool thermal energy storage by operating the evaporator at a higher temperature. Wang et al. [106] put PCM emulsions without and with graphite nanoparticles into two separated tubes which were placed inside a thermo-scientific bath. The transient temperature inside both tubes and the bath were recorded by a data logger with thermocouples. Compared with the pure PCM, the thermal

conductivity of the composite PCM containing 2wt% graphite was increased to 0.578W m^{-1} K^{-1}, with an 88.9% improvement. The enhanced thermal conductivity with excellent thermal reliability of the composite PCM was advised for using as highly efficient cold energy storage. Parameshwaran et al.[107] embedded Ag-TiO_2 hybrid nanocomposite particles into organic ester phase change material to form the composite PCM used for the cool thermal energy storage in buildings. The scheme for the preparation of the composite PCM was shown in **Figure 2.8**. The TiO_2 powder was dispersed in ethanol using ultrasonicator and silver nitrate was dissolved subsequently. It was found the nanocomposite PCM exhibited an improvement in thermal conductivity which was from 0.286 W m^{-1} K^{-1} to 0.538 W m^{-1} K^{-1} without changing the phase change temperature. Besides, compared to the pure PCM, the freezing and the melting times of the composite PCMs were reduced by 23.9% and 8.5% respectively.

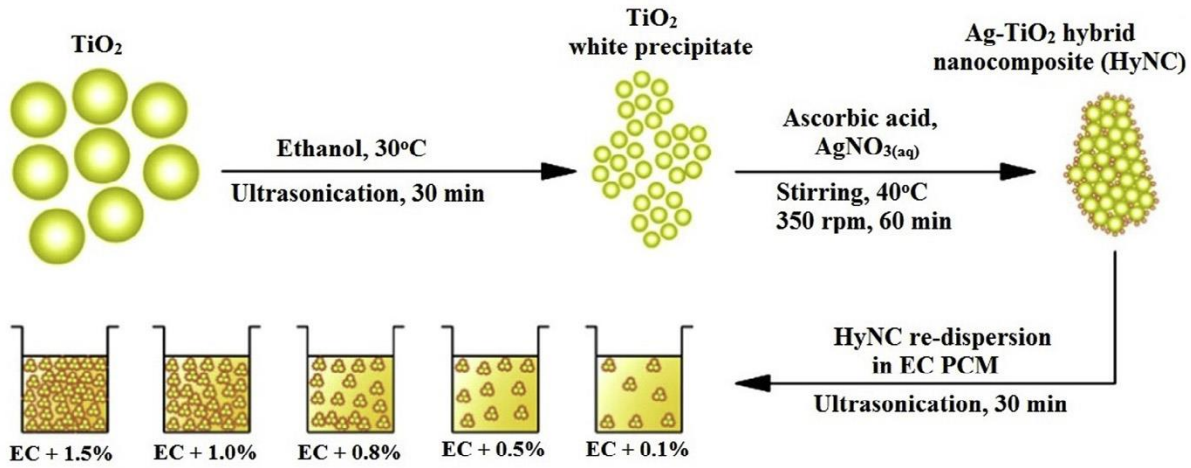

Figure 2.8: Scheme for preparation of the composite PCM[107]**.**

A water-based nanofluid phase change material containing the multi-wall carbon nanotubes which has potential application in cool thermal energy storage was prepared by Kumaresan et al.[108] The solidification time was shortened by 20.1% and 14% with a volume fraction 0.6% of the multi-wall carbon nanotubes at the surrounding temperature of -12 °C and -9 °C respectively which was mainly contributed by the thermal conductivity improvement. An n-tetradecane@polystyrene-silica (Tet@PS-SiO_2) composite nanoencapsulated phase change material for cold energy storage was synthesized by Fu et al.[109]. It was observed that the thermal conductivity of the composite PCM was improved by 8.4% which could reach 0.4035 W m^{-1} K^{-1} through the grafting of SiO_2. The formulation of the composite PCM was illustrated in **Figure 2.9**.

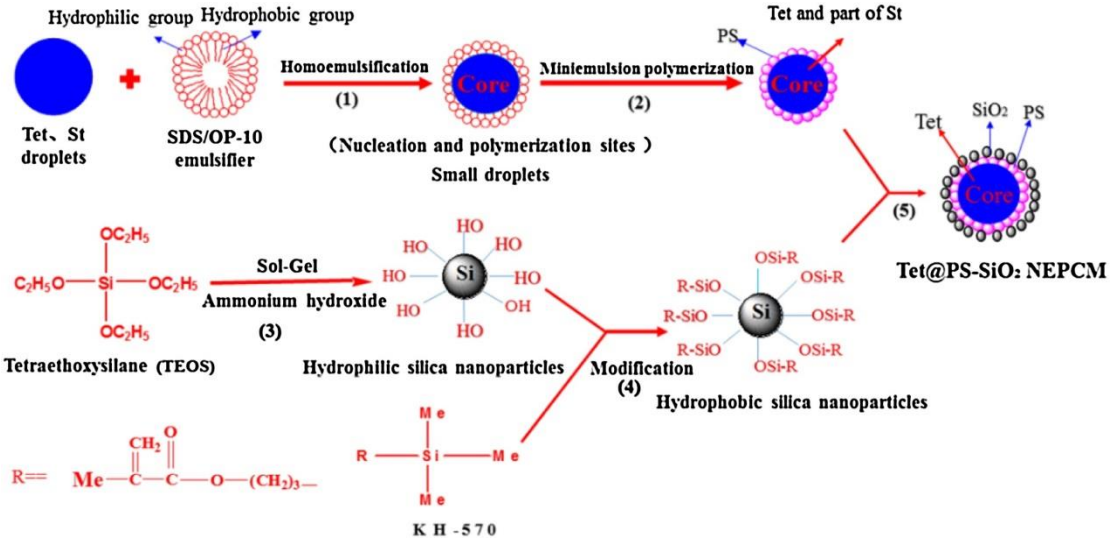

Figure 2.9: Synthesis schematic of the -tetradecane@polystyrene-silica composite PCM [109].

2.2.3 Solid mesh

It can be noticed that by adding heat transfer additives, the thermal conductivity can be improved considerably. However, the formulation processes are most complicated. Hence, some other research focused on employing metal foam for the thermal performance enhancement[110][111].

Tian et al.[112] embedded metal foam into the PCM. By using metal foams, the heat conduction rate was improved significantly which could be about 10 times higher. Besides, the authors indicated that with smaller porosities and bigger pore densities, the better heat transfer performance could be achieved. Yang et al.[113] experimentally investigated the dynamic thermal performance of a shell-and-tube latent heat thermal storage unit. Through the vacuum impregnation, a paraffin-copper foam composite was formed with the impregnation ratio at 96.7%. It was found that the melting time of the paraffin-copper foam composite was shortened over 1/3 compared with that of pure paraffin. **Figure 2.10**. shows the photos of copper foam and the paraffin- copper foam composite.

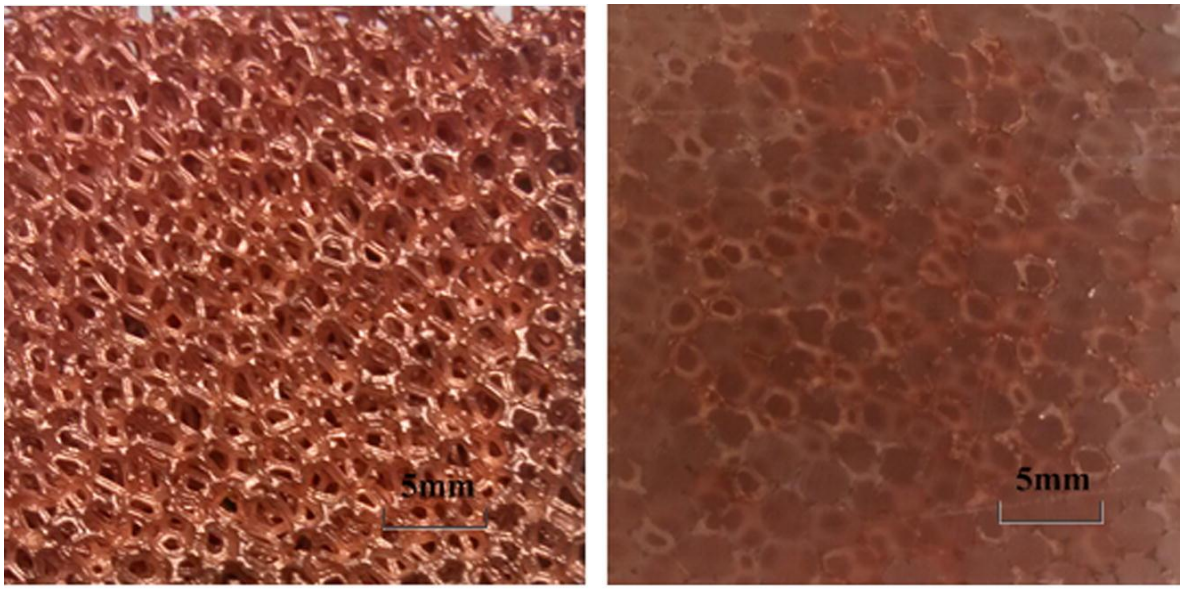

Figure 2.10: Copper foam (a) and paraffin-copper foam composite (b) [113]**.**

The influence of aluminum foam porosity and pore size on melting performance of low-temperature paraffin wax was experimentally studied by Lafdi et al.[114]. It was revealed that both the higher porosity and bigger pore size could contribute to the greater effect of convection which led to faster achievement of the steady-state temperature. Xiao et al.[115] used a vacuum impregnation method to prepare the paraffin/nickel foam and paraffin/copper foam composite phase change materials for solar energy storage applications. The impregnation ratios of the paraffin/nickel foam composite PCMs can reach the range of 96.0-98.6%. Compared with pure paraffin, the thermal conductivities of the composite PCMs were drastically improved. The thermal conductivity of the paraffin/nickel foam composite was enhanced by nearly three times while the thermal conductivity of the paraffin/copper foam composite PCM was improved by 15 times. Wang et al[116]. experimentally studied the performance of the paraffin/aluminum foam composite phase change material (PCM) for the Li-ion battery cooling. It was observed that the addition of aluminum foam could intensively improve the effective thermal conductivity of the PCM which led to a higher melting rate. The temperature uniformity of the PCM was increased as well. When the heat fluxes were 7000 W/m^2 and 12,000 W/m^2, the heat storage time of the composite PCM is 73.6% and 74.4% of that of pure paraffin, respectively. Zhao et al.[117] embedded the copper foam with 95% porosity into the paraffin wax RT58 to enhance the heat transfer performance. It was concluded that the overall heat transfer rate was improved by 3-10 times. The effects of copper foam on the heat transfer on melting performance of paraffin was numerically and experimentally studied by Li et al.[118]. An experimental apparatus, shown in **Figure 2.11**, was set up to investigate the melting performance of the

PCM-copper foam composite. The paraffin-saturated metal foam was put inside a plexiglass cavity to prevent the leakage of the liquid. An electric insulated film heater was glued to the left side of the metal foam to provide constant heat flux. T type thermocouples were employed to obtain the temperature distribution of the composite PCM. It was revealed that the enhancement of heat conduction was more prominent than the suppression of natural convection of molten liquid by the copper matrix in the foam-PCM composite.

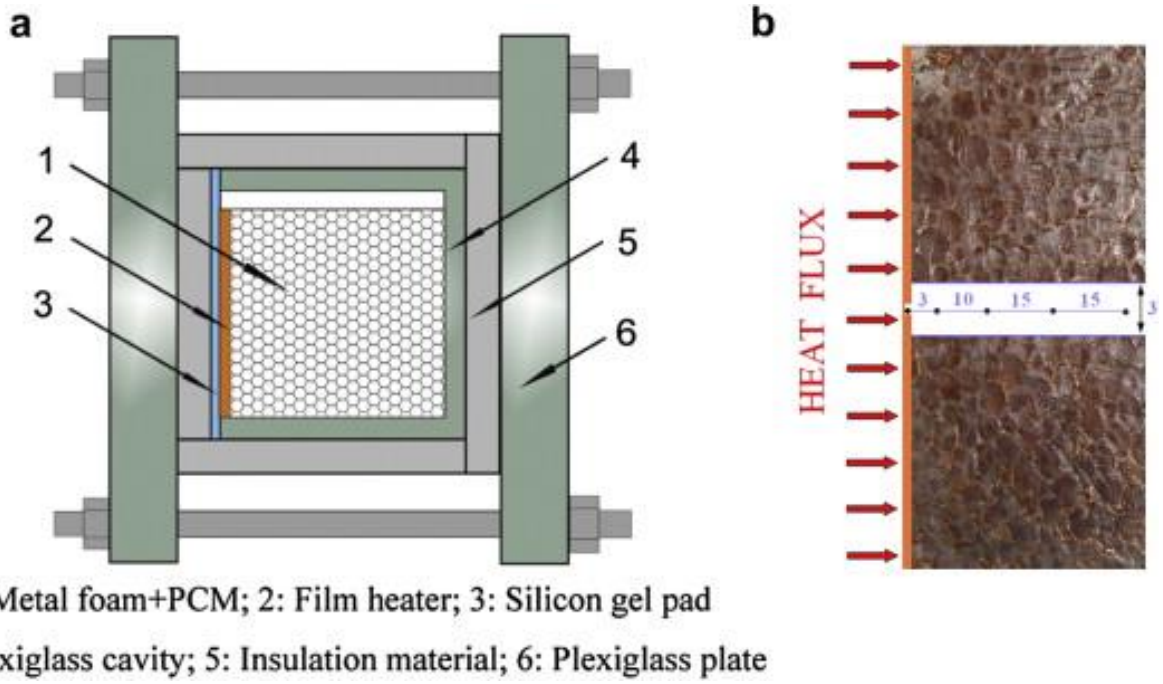

Figure 2.11: Experimental apparatus and test section. (a) Experimental apparatus, (b) Test section[118]**.**

Zhou et al[119]. experimentally studied the heat transfer characteristics of PCMs embedded in open cell metal foams. The paraffin wax RT 27 from Rubitherm Company and calcium chloride hexahydrate were used in the study. The foam was composed of interconnected dodecahedral-like cells, which had 12-14 pentagonal or hexagonal faces. The cells could be considered to be homogeneous in size and shape. The heat transfer rate of the PCMs was enhanced significantly by adding metal foams with the whole melting time was shortened to a quarter of that for paraffin and to a third for calcium chloride hexahydrate respectively under the same heat flux. Li [120]et al. experimentally employed the copper metal foam to the PCM based cooling system for the Li-ion battery package. The obtained results show that when compared with pure PCM system, the foam-PCM composite can furtherly decrease the battery's surface temperature and perform a more uniform temperature distribution due to the thermal conductivity improvement. Hussain [121] et al. employed a PCM based thermal management system for lithium-ion batteries. It was observed that the surface temperature could be reduced by

PCM significantly. The effect was enhanced by inserting the nickel foam which showed a 24% reduction compared to pure PCM. Research by [122] et al. showed that copper foam could decrease the total energy storage time of PCM by 40%.

2.3 TES device for cold applications

As reviewed above, adding thermal enhancement additives and solid mesh can improve the thermal performance of the PCMs. However, it's obvious to notice that the manufacture processes of composite PCM are complicated, and will lead to segregation and cost concern. It's also difficult for realizing widespread applications through inserting solid mesh. This is mainly due to that the shape of mesh can restrict the geometries of the TES devices. Hence, it will be more feasible by designing devices with high heat transfer performance, as the manufacture can be easily achieved without any geometry limit for various applications. The previous research studies on heat transfer enhancement of TES devices both by modelling and experimental methods were reviewed in this section.

2.3.1 Modelling

Numerical simulation is always proven to be an effective method to optimize the design of TES device, especially for investigating the behaviours of different geometries. El Qarnia et al.[123] employed a numerical model to simulate the influence of different key parameters on the thermal performance of the PCM-based heat sink. The conclusion was used for the design of PCM-based cooling systems. Jmal et al.[124] numerically compared four different geometry configurations of coaxial tubes. Yang et al. [49] modelled the energy transfer behaviours of an energy storage unit including time, temperature and liquid fraction using the plate-fin device. Their conclusions revealed that numerical results could give a good estimation of the melting and solidification processes of PCMs which could provide guidelines for thermal performance and design optimization of the latent thermal energy storage unit.

Mat [125] et al. used an experimentally validated model to investigate the heat transfer enhancement of fins on a PCM triplex-tube heat exchanger. It was concluded that the fins could decrease the melting time by up to 56.7%. Ogoh [126] et al. numerically studied the fins effects on the heat transfer characteristics of a cylindrical latent heat energy storage system. The obtained results revealed that fins could enhance the heat transfer rate

significantly by reducing the thermal resistance on the PCM side. Liu [127] et al. experimentally investigated the effects of copper fins on the heat transfer performance of PCM system. The fins can accelerate the PCM charging rate by up to 250% through improving both the conduction and the natural convection of the PCM. Using fins already has lots of approaches in PCM energy storage systems [128][129][130] and performs great potential for extended applications. Bourne et al.[131] numerically studied performance of the TES device which was used to shift peak cooling loads to off-peak hours or to periods when intermittent renewable energy sources were available. The device was a containment tank packed with cylindrical tubes with PCM. It was concluded that the two-dimensional model could predict the performance of this type of energy storage unit with sufficient accuracy. Tay et al.[132] used the effectiveness-NTU model to design and optimise a tube-in-tank phase change thermal energy storage unit for low energy cooling of buildings. Water was used as heat transfer fluid which flew through the copper tube, while PCM was put inside the tank. The three-dimensional PCM energy storage unit was shown in **Figure 2.12**. The optimized parameters obtained by modelling using the effectives-NTU model could provide a realistic size for the commercial building applications.

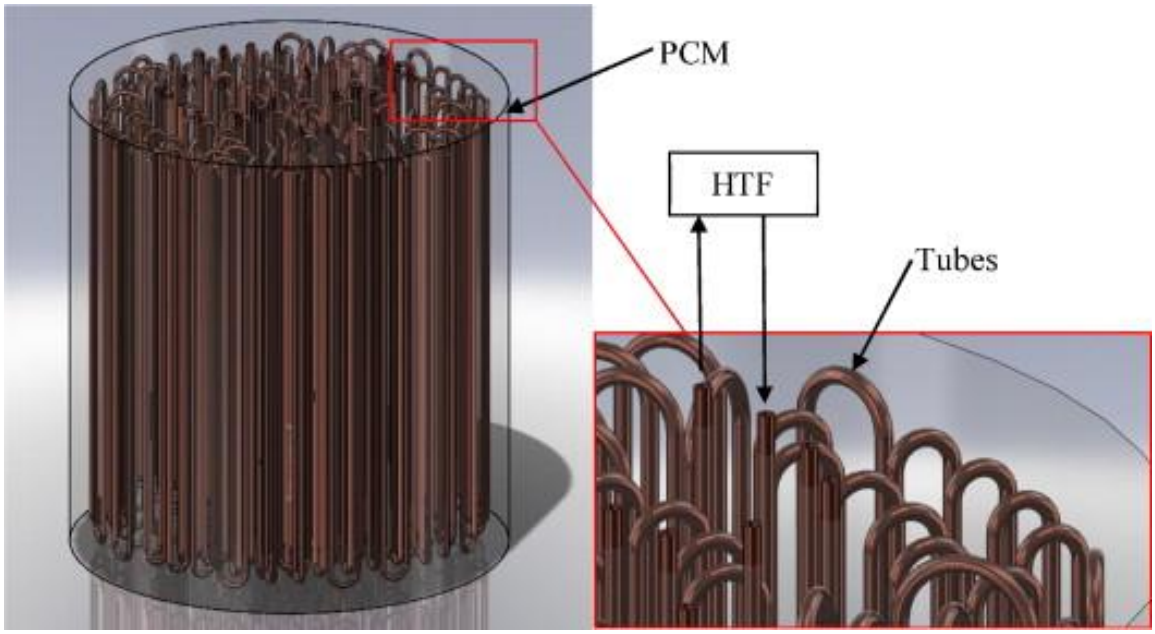

Figure 2.12: Tube-in-tank PCM energy storage unit[132]**.**

Wu et al.[133] dynamically modelled the discharging characteristics of a coil pipe unit for cool thermal energy storage. The rectangular storage tank consisted of horizontal parallel curved pipes which were submerged in n-tetradecane. The effects of operating and geometric parameters including the inlet temperature and the flow rate of the heat transfer fluid, and the diameter of coil pipes was studied through the evaluation of the outlet

temperature of the heat transfer fluid, the melting fraction and cool releasing rate of PCM. It was found that the higher inlet temperature of the heat transfer fluid and the larger diameter of coil pipes led to higher heat transfer rate. It was also shown that the inlet temperature and flow rate of the fluid had more obvious effect on the discharging process than the diameter of coil pipes. Zhai et al.[134] experimentally investigated a fin tube phase change cold storage unit containing C-L acid (capric and lauric acid) PCM with solidification temperature at 14.97◦C which could be used for cooling application. The unit was a 500 mm long cylinder with the diameter of 110 mm. The copper pipe with a diameter of 20 mm was centred which was used for the flow passage of water. Four annular fins were firstly used to divide the inner space into five identical segments with four rectangular fins orthogonally welded along the central tube in each segment. All the fins were made of copper with the thickness of 1 mm. The whole unit was filled with PCM. The schematic diagram of the unit was shown in **Figure 2.13**. The structural parameters including annular fin pitch, number of rectangular fins, the height of rectangular fins and fin thickness were numerically evaluated through the charging performance. Finally, an optimal scheme of the fin tube phase change cold storage unit was proposed based on modelling results.

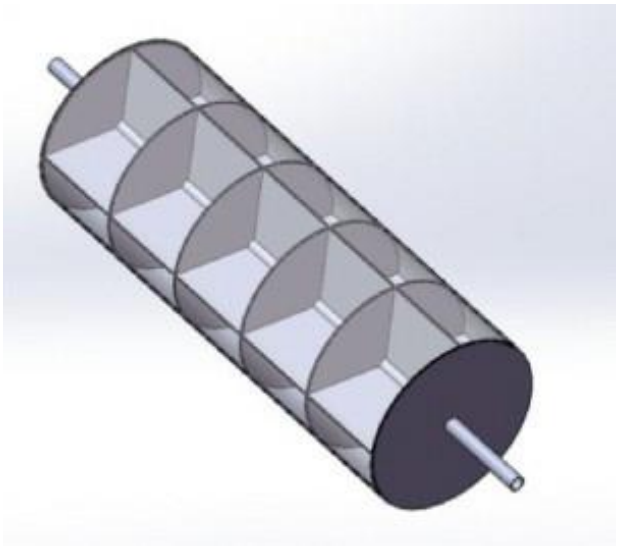

Figure 2.13: Schematic diagram of the fin tube phase change cold storage unit[134]**.**

Raj et al.[135] developed a tube and shell heat exchanger for free cooling application with PCM in the shell and air flowing through the tube channel. Both the transient and steady-state CFD modelling was carried out for a single module and two air spacers. The study indicated that the flow state and temperature variation of air was determined which could be used to select the geometrical and flow parameters for given surface temperature and inlet condition. The transient analysis results which reflected the PCM solidification behaviours could be used to

verify the suitability of the selected geometrical dimensions. A mathematical model of the PCM air heat exchanger for building free cooling was developed by Hed et al.[136]. The PCM with the phase change temperature at 24 ^{o}C was packed in the 8 mm thick aluminum pouches which were stacked in layers. The air flew through the gap between the Al plates with a velocity at 4m/s. The modelling results showed how the specific heat capacity-temperature curve affected on the cooling power of a PCM heat exchanger. Zhao et al.[137] numerically studied TES device consisted of a finned inner tube, an outer tube and an insulated rectangular envelope. The annulus space between inner tube and outer tube was filled with PCM which had a melting temperature between 19-23 ^{o}C. The device was proposed to be used with conventional air-conditioner to increase the overall cooling coefficient of performance. Water was used for charging loop while air was used for discharging loop. Optimum fin height, optimum mass flow rate of charging fluid and discharging fluid was achieved through the modelling. When replacing the conventional cooling tower using the proposed PCM thermal storage device for a water-cooled air-conditioner, the COP value was increased by about 25.6%. Teggar et al.[138] numerically studied the plate type TES device containing phase change material for air conditioning. The device was equipped with a set of parallel plates and had a gap between every two successive plates, shown in **Figure 2.14**. The parallel plates were fulfilled with water as PCM. Cold ethylene glycol as heat transfer fluid was circulated during nights through the parallel plates to charge the PCM. The indoors warm air during days was cooled down when circulating through the charged parallel plates.

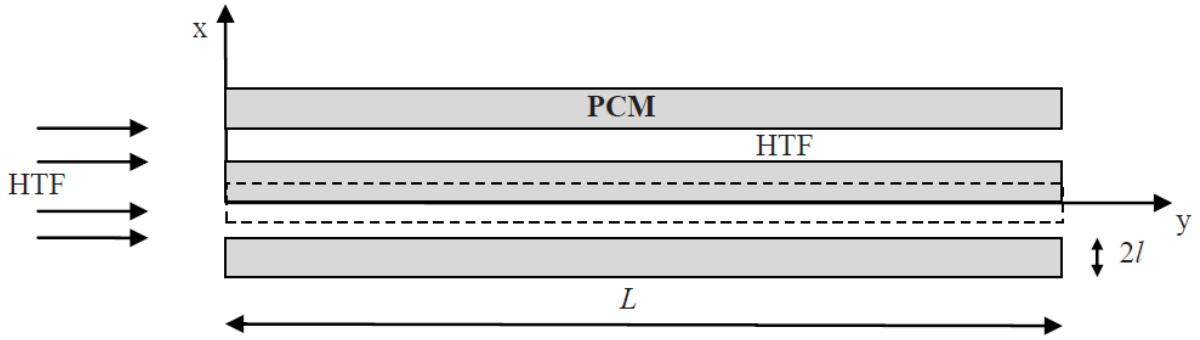

Figure 2.14: Scheme of the plate type latent heat exchanger[138]**.**

It was concluded that the complete charging time of the cool storage device was within 3 h 37 mins. The charging rate decreased over time due to the drop of the temperature gradient between the liquid fluid and the PCM. A proportion of 81% of PCM was charged within 57% of the total charging time.

Mosaffa et al.[139] numerically studied the solidification process of PCM in a shell and tube device with radial fins. The geometry of the device was shown in **Figure 2.15**. The calcium chloride hexahydrate, $CaCl_2 \cdot 6H_2O$, with a melting temperature of 29.7 ◦C was selected as PCM and atmospheric air was chosen as heat transfer fluid which flew through the tube. The outer side was insulated to prevent heat loss. The effects of air velocity and inlet air temperature on the performance of the thermal energy storage were studied. The obtained results were expected to determine optimum designs for air conditioning systems for various climatic conditions.

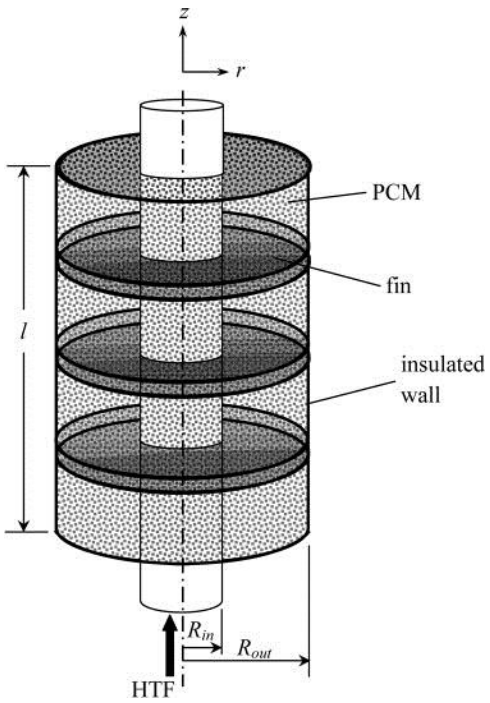

Figure 2.15: Schematic of the thermal TES device for air conditioning[139]**.**

Hu et al.[140] numerically studied a PCM heat exchanger for ventilated window application. The heat exchanger was made of a wooden frame, a glazing cover, and parallel vertical PCM boards which contained paraffin wax with a temperature at 22°C as PCM. The PCM heat exchanger was discharged through cold air during nights and recharged by high-temperature ambient air. The authors recommended the suitable correspondence of plate thickness with discharging time. For a 4-5 h discharging time, 10 mm plate thickness for the heat exchanger was recommended, when the discharging time decreased to 0-3.6 h, 5 mm plate thickness for the heat exchanger was recommended. For a 10 mm plate thickness heat exchanger, the discharging efficiency of the heat exchanger was 89.85%, the efficiency increased to 90.32% when the plate thickness decreased to 5 mm. Dolado et al[141]. simulated the thermal behaviour of a phase change material-air heat exchanger for a solar cooling system which aimed to increase the COP of the absorption chillers. The PCM-air

heat exchanger, shown in **Figure 2.16**. which consisted of a series of microencapsulated PCM plates arranged as parallel plate-walls, separated by air gaps. The air flow was driven between the PCM plate-walls by a centrifugal fan and exchanged heat with PCM. The RT27 from Rubitherm Company with melting temperature at 27 ˚C was selected.

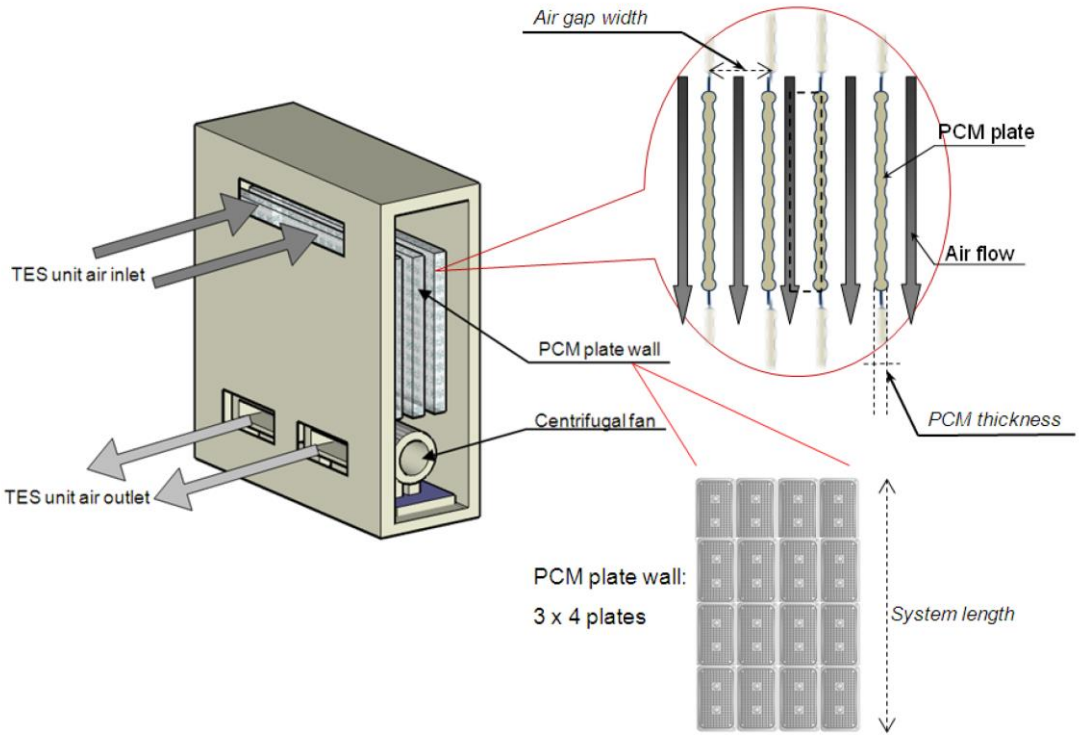

Figure 2.16: Schematic view of the PCM-air heat exchanger[141]**.**

It was found that a COP improvement of 14% was obtained compared to the same system without the air heat exchanger.

2.3.2 Experimental

Allouche et al.[142] experimentally investigated the performance of the low temperature thermal energy storage tank which could be used for air conditioning applications. The tank had a capacity of 100L with bundle tube inside, shown in **Figure 2.17**. Two parallel tube bundle heat exchangers were put in the top of the tank used for the charging process. Meanwhile, another two parallel tube bundle heat exchangers located in the bottom of the tank for the discharging process. Each tube bundle heat exchanger was composed of 7 tubes with a pitch of 22 mm. The comparison of water, PCM tank released cold energy more quickly. It indicated that the tube bundle storage tank showed a better heat transfer performance than a coil-in-tank configuration.

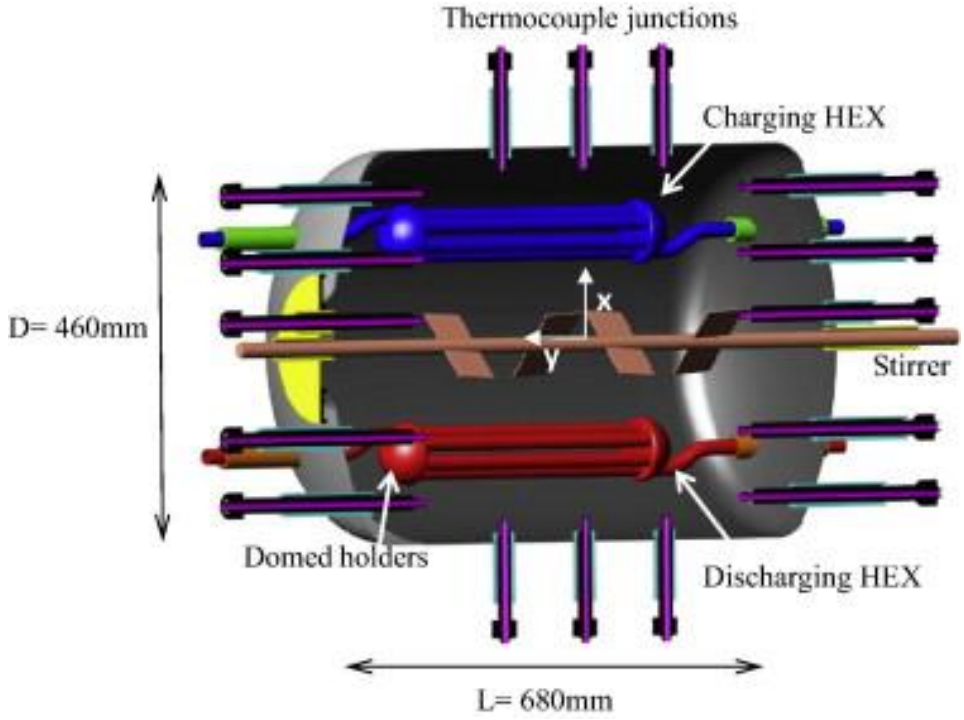

Figure 2.17: Longitudinal cross section view of the storage tank[142]**.**

Marı´n et al.[143] designed a plate type PCM-air heat exchanger mainly for free cooling applications and tested it experimentally. Through embedding the paraffin in the graphite matrix, the flat plate encapsulations were formed. As can be seen in **Figure 2.18**, the external shell was made with plates of polystyrene, with an air chamber in between. When air flew through PCM plates set, heat was transferred between the PCM and air. The power of fan was decreased by up to 50% by adding graphite matrix into the PCM plates.

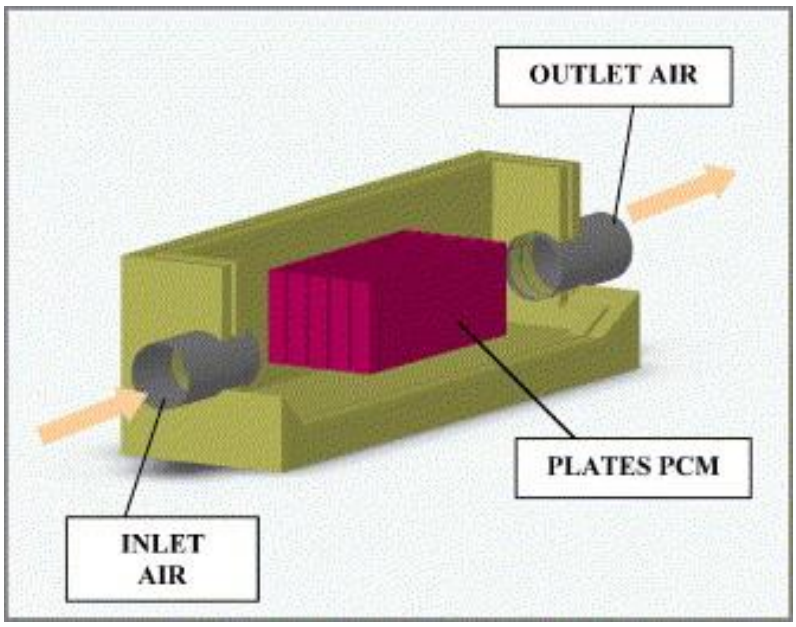

Figure 2.18: Configuration of the thermal TES device.[143]

Castell et al.[144] experimentally studied of a PCM tank for cold storage applications. As shown in **Figure 2.19**, a coil was inserted in the tank and the tank was filled with the low temperature PCM. The coil was looped to be evenly distributed through the PCM. Through the study, a new equation of the effectiveness as a function of the ratio of the mass flow rate over the heat transfer surface was proposed which could be used as the design of the coil in tank type TES device. It was also shown that the effectiveness of the PCM energy storage unit decreased with the increasing flow rate of water flow and increased with increasing heat transfer area. The coil in tank design combined with a low-temperature PCM was advised by the authors as a thermal storage facility for cold storage.

Figure 2.19: Schematic and photo of the experimental PCM device.[144]

The suitability for the integration of a helically coiled tube device into a low-temperature energy storage system for solar air conditioning applications was carried out by Diaconu et al.[145]. A helically coiled copper tube immersed in a tank was built. The helix diameter was 140 mm, consisting of eight turns and a pitch of 37 mm. The helically coiled tube was inserted coaxially in a tank of 240 mm in diameter and 550 mm in height. Distilled water was selected as the heat transfer fluid which circulated through the helically coiled tube. It was found that the values of the heat transfer coefficient for the phase change material slurry were higher than for water. Weng et al.[146] experimentally studied the thermal performances of a heat pipe with phase change material for electronic cooling. The flat heat pipe was made of Cu with a length of 120 mm and a diameter of 6 mm. The photo of the phase change module was shown in **Figure 2.20**. The working fluid inside the copper tube was

water. The heat sink has 29 fins with a fin height, width and thickness at 5 mm, 40 mm and 0.2 mm respectively. The energy storage tank was made of acrylic.

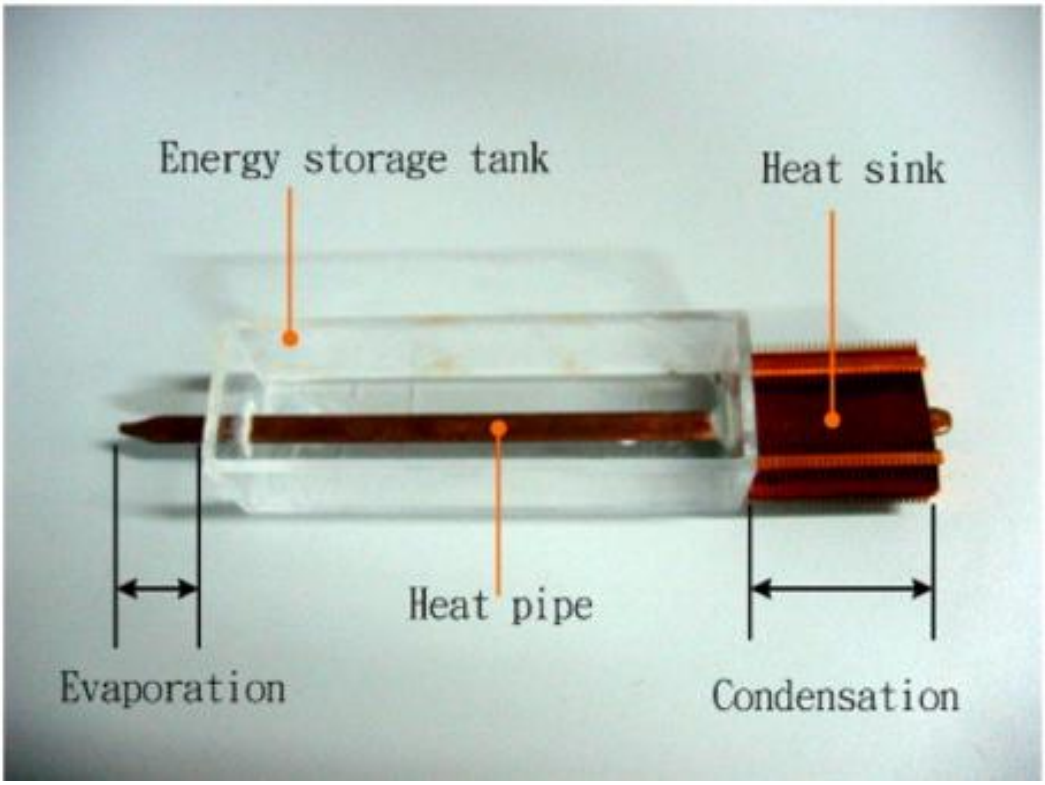

Figure 2.20: The photo of phase change cooling module[146]**.**

It was concluded that the heat pipe module with tricosane as PCM could reduce fan power consumption up to 46%. Usman et al.[147] experimentally compared the thermal performance of unfinned and finned PCM based heat sinks for passive cooling of electronics. Thermal enhancement by pin-fins with inline and staggered pin-fin arrangements was studied. Organic PCM was incorporated inside the heat sink to absorb the heat generated by the electronics. The obtained results showed that triangular inline pin-fin heat sink geometry was most efficient for passive thermal management of electronic devices. Garg et al.[148] presented the thermal performance of encapsulated phase change material based TES device for thermal management of the building. The high-density polyethylene (HDPE) containers with copper tubes circulating inside were used as the TES device. The inorganic chemical compound with a melting range of 23-32 °C was used as PCM and water was used as the heat transfer fluid. PCM was used to absorb heat from air present in the room and water was used to extract heat absorbed by the PCM. The TES device was placed on the top of the test room for cooling. The schematic of the TES device and the placement of the device inside the room were shown in **Figure 2.21**.

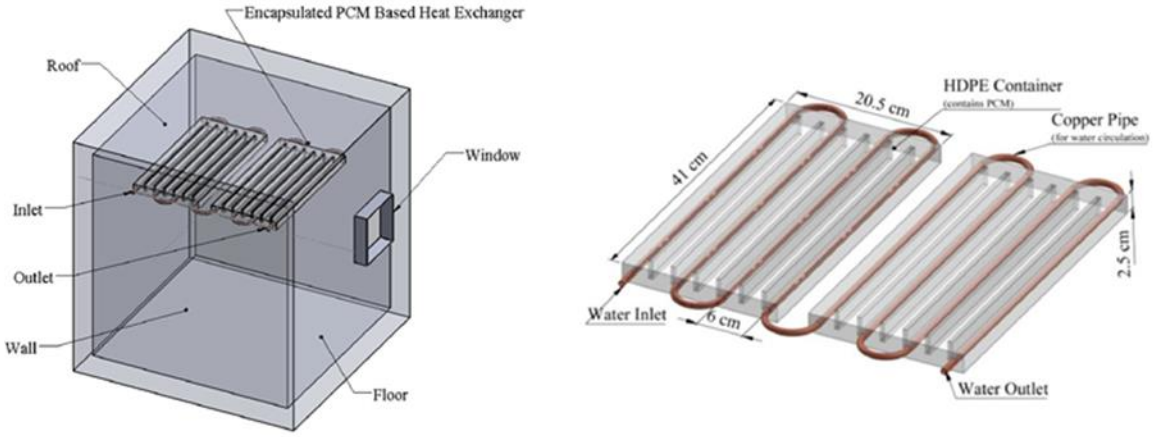

Figure 2.21: Schematic of the encapsulated PCM based TES device cooling system and its placement in the test chamber[148]**.**

It was found that the encapsulated PCM based TES device could reduce the heat gain of the test room by approximately 50% with the mean air temperature decreasing by more than 6 °C. It was proposed that the encapsulated PCM based heat exchanger was beneficial in flattening the peak for longer duration and reducing the fluctuation in mean air temperature of the test room.

2.3.3 Summary

For the optimal design of the TES device, among the published results, adding fins were very attractive and effective. For the existed types of heat exchangers, the plate-fin type heat exchanger has been proven to have a high degree of surface compactness and better thermal performance.

Al-Abidi et al. [149] used fins in a triplex tube heat exchanger for PCM melting and shortened the total melting time by 34.7%. Peng et al.[150][49] reported that the plate-fin type heat exchanger represented compact configuration and a good heat transfer performance compared to the traditional ones. The charging performance of the phase change system with tube and fins was experimentally investigated by Tao et al. [151]. Results showed that by using two types of enhanced fins, the energy adsorbing time decreased by 71.2% compared with the system without fins. Sciacovelli et al. [152] employed fins to increase the energy transfer rate of a shell-and-tube TES device. System efficiency was increased by 24% when using the Y-shaped fins with two bifurcations. Ye et al.[153] numerically modelled energy transfer characteristic using a plate-fin energy device. The obtained conclusion revealed that a remarkable vortex of air was formed during the energy release process.

Stritih[154] experimentally compared the energy transfer behaviours of a TES device with a fin-extended surface. The results showed that by adding fins, total heat transfer release time reduced by 40%. It was concluded that the compact finned heat storage exchanger provided superior performance.

Meanwhile, the simplicity in structure, ease in fabrication and low cost of manufacture can contribute to the widespread and commercial application of fins in latent heat energy storage system. Besides, for transport air conditioning applications, the limited volume and weight requires the compactness of the device due to the mobility. Hence, a novel compact TES device with fins was designed and manufactured in this study.

2.4 Air conditioning system performance

Air conditioner used in vehicles or buildings consumes the significant part of the rolling stock's total auxiliary energy approximately 20%. However, the frequent heat load causes a low energy efficiency and poor economic performance of the traditional air conditioning system. Besides, it leads to a thermal comfort reduction. Hence, effective methods have been employed to solve the current issues.

For the transport applications, the air conditioning system is the essential component which supplies thermal comfort to the occupants. However, it significantly increases the energy consumption which shortens the driving range[155][156]. It was reported that the air conditioner unit in small commercial vehicles could consume 12% to 17% of available engine power, with most of the energy being used by the compressor[157]. Research also shows that the air-conditioning unit is responsible for the largest proportion of energy consumption of the urban rail onboard auxiliary systems[158].

Therefore, the reduction in the energy consumption of the air-conditioning unit has become a major concern in the transport field. Energy storage using phase change materials performs great potential to reduce energy consumption due to its high latent heat storage capacity and nearly isothermal phase change behaviour [159][160][161][162][163][36][164]. Utilizations of PCM have been investigated for a long period to reduce air conditioning system energy usage by maintaining comfortable temperatures[165][166].

Hence, the PCM based energy storage has been performing increasing importance in air conditioning systems. When integrating with energy storage, the new air conditioning systems are able to provide more stable operation and lower energy consumption than conventional systems[167][168][169]. The thermal comfort improvement combined with emission reduction also shows the prospect of PCM based air conditioning systems [170][171][172][26].

Hence, the effective method is needed to smooth the heating and cooling power of air conditioners which can keep the output energy stable. This can increase energy efficiency and reduce the noise, and maintain the output temperature constant. Latent heat energy storage systems which benefit from the natural characters of phase change materials (PCMs) have been used to shift peak and off-peak energy and show great potentials in various applications. It is particularly attractive for solving the existed fluctuations problem of transport air conditioner owning to its large energy storage capacity to store energy at a relatively constant temperature[4] [5][6].

Attempts using LHTESS to settle the mismatch issues of demand and supply have been made in air conditioning systems. The gained experience showed that the peak cooling electric demand could be declined by a maximum of 90% when applying the cold energy storage in a conventional air conditioning system[173]. Research also revealed that the system efficiency could be improved when integrating the LHTESS with the air conditioning system [174][175][176].

Previous work has concluded that the LHTESS is an important apparatus to manage and adjust the cold energy balance and stability. It is feasible for mobile transport leading to the lower temperature fluctuation, large energy savings, more stable operation and control, reduced pollution and noise, decreased mechanical equipment size and extended equipment operating time [177][26].

Obviously, the conventional air conditioning systems are proven to be energy intensive with temperature and power fluctuations. It can even bring a health concern due to gas and noise pollution.

The LHES can store excess energy in off-peak time and release it with a constant temperature in peak time, which is attractive for relieving the cooling load fluctuations and improve thermal comfort. What's more, LHES has a large energy storage density and will not occupy much space in the carriage which has strict spatial constraints. Attempts using LHES in building air-conditioning have been widely reported, which shows significant energy and cost savings, and thermal comfort improvement.

2.4.1 Temperature stabilization

Allouchal et al. [167] dynamically simulated an air conditioning system with PCM cold storage. They indicated that integrating the PCM based latent heat storage with the air conditioning system lead to a more stable system with higher indoor comfort. Fang et al[178]. experimentally studied the performance of a PCM based air-conditioning system with separate helical heat pipes. Two groups of parallel inner whorl copper tubes installed in cool storage tank were used as the evaporation part of a separate heat pipe for cool storage. Water

was used as the PCM which released cold the heat transfer fluid in the form of ice. It was found that the cool discharge rate in the cool storage tank stabilized between 3.5 and 3.0 kW during ice latent heat discharging period with the cooling capacity achieving at 35,000 kJ. The outlet water temperature from the cool storage tank was kept between 4.2 °C and 5.5 °C, and the outlet air temperature inside the room unit maintained quite stably between 8 °C and 9 °C when using the PCM energy storage tank.

2.4.2 Energy savings

Al-Aifan et al[179]. applied dimethyl adipate with phase change temperature at around 9.92 °C to the combined variable refrigerant volume and cool thermal energy storage air conditioning system. It was found that the indoor temperature was maintained at 24 °C for year-round operational conditions. The reduced cooling capacities and reduced combined power consumption contributed to the improved performance of the combined system. The authors concluded that the proposed system would be beneficial to meet indoor comfort cooling without sacrificing energy efficiency. Sun et al [180]introduced a PCM based air conditioning technique for telecommunications base stations. The simulations combined with the experimental evaluations showed that the adjusted energy efficiency ratio of the new system can enhance up to more than 4 times compared with the normal air conditioner with an estimated energy saving potential at 50%.

Jia [181]et al set up a storage-enhanced heat recovery room air-conditioner test rig containing a PCM based heat recovery tank. The obtained results showed that the overall performance could be increased by PCM with the overall coefficient of performance (COP) improving by 6.9%-9.8%. The heat retention time of the tank water was also extended by 21.1%. Zhao et al[137]. numerically proposed a new air conditioning system integrated with a finned shell-and-tube based PCM energy storage unit. The general effectiveness of the PCM energy storage system exceeds 0.5 with the COP of the system increasing by 25.6%. Karaipekli [97]et al. used the PCMs for building ventilating and air conditioning purposes. The results show that the indoor thermal comfort can be improved due to the lasting comfortable period. It is also concluded that the energy consumption can be decreased.

Zhao et al [182] introduced the PCM heat storage unit to the prototype thermoelectric system for space cooling application. The obtained results show that 35.3% of electrical energy can be saved with the maximum system cooling COP up to 1.22. Parameshwaran et al[183]. used silver nano-based PCM to improve the thermal performance and energy efficiency of chilled water-based variable air volume air conditioning system.

Compared with the conventional system, the proposed air conditioning system achieved an on-peak and per day average energy savings up to36-58% and 24-51% respectively. Castell [184] et al. applied alveolar bricks with PCM in building passive cooling field. They revealed that the PCM could reduce the daily temperature fluctuations with energy savings at about 15%. The PCM-impregnated gypsum boards used for building cooling were experimentally studied by Barzin [14] et al. They concluded that the daily cost and energy could be saved up to 93% and 92% respectively with weekly electricity saving of 73%. Zhao et al. [182] proposed a PCM energy storage system for water-cooled air conditioning application. Results showed that the integrated system had a general efficiency higher than 50%. Integration of the latent heat energy storage with the conventional cooling tower can increase the coefficient of performance (COP) value of the conventional water-cooled air-conditioner by about 25.6%. Chaiyat [185]used PCM to improve the cooling efficiency of an air conditioner under Thailand climate. The electrical power of the modified system could be saved by 9%. Allouche et al.[186] presented the simulation of a solar driven ejector cooling system integrating with PCM cold storage for space air conditioning. The system which was mainly consisted of a solar loop, an ejector cycle and a PCM cold storage tank was designed to provide air-conditioning for a 140 m^3 office space during the summer. The obtained maximum COP and solar thermal ratio (STR) were 0.193 and 0.097 respectively. It was also found that using a large cold storage tank capacity resulted in a high cooling cycle COP. Said et al.[187] integrated the phase change material based plates with the condenser of the air conditioning unit. The PCM material with the melting temperature at 24-25^oC was enclosed in a thin aluminum cuboid of 1 mm thickness. By discharging the charged cold storage energy at night at day, the coefficient of performance (COP) of the air conditioning unit with PCM plates increased. Through decreasing the condenser pressure and increasing the evaporator cooling capacity, the PCM based system reduced the consumed power of the air conditioning unit by up to 11.2%. Aljehani et al.[188] proposed a phase change composite material consisting of paraffin wax (n-Tetradecane) and expanded graphite based cold thermal energy storage systems for air conditioning applications. The system consisted of a stack of 28 slabs of composite PCM with the size and weight of each slab at 46×26×2.54 cm and 2.79 kg (22% graphite and 78% graphite) respectively. The copper tubes passed back and forth in between the 28 slabs. A stream of Ethylene Glycol (EG) was circulated through the copper tubes for charging and discharging the PCM. By integrating the PCM with the conventional air conditioning unit, the compressor could be designed by a 50% drop in size, which led to an electricity consumption drop by 30%. This doubled the efficiency during mid and off-peak hours with lowering CO_2 emissions by 30%. Chen et al[189]. tested a PCM based air conditioning system which was proposed to be used for data centre and telecommunication station cooling management. The

whole system consisted an outdoor and an indoor unit which was illustrated in **Figure 2.22**. A commercial PCM with melting temperature at 17-21 ^{o}C was selected. The PCM was filled in aluminum panel containers, and a total number of 30 containers were arranged in 10 layers parallel to each other in a cold storage tank. The total amount of PCM used in the study was about 58.5 kg. The gap between two adjacent PCM containers was used for the water channel which acted as heat transfer fluid.

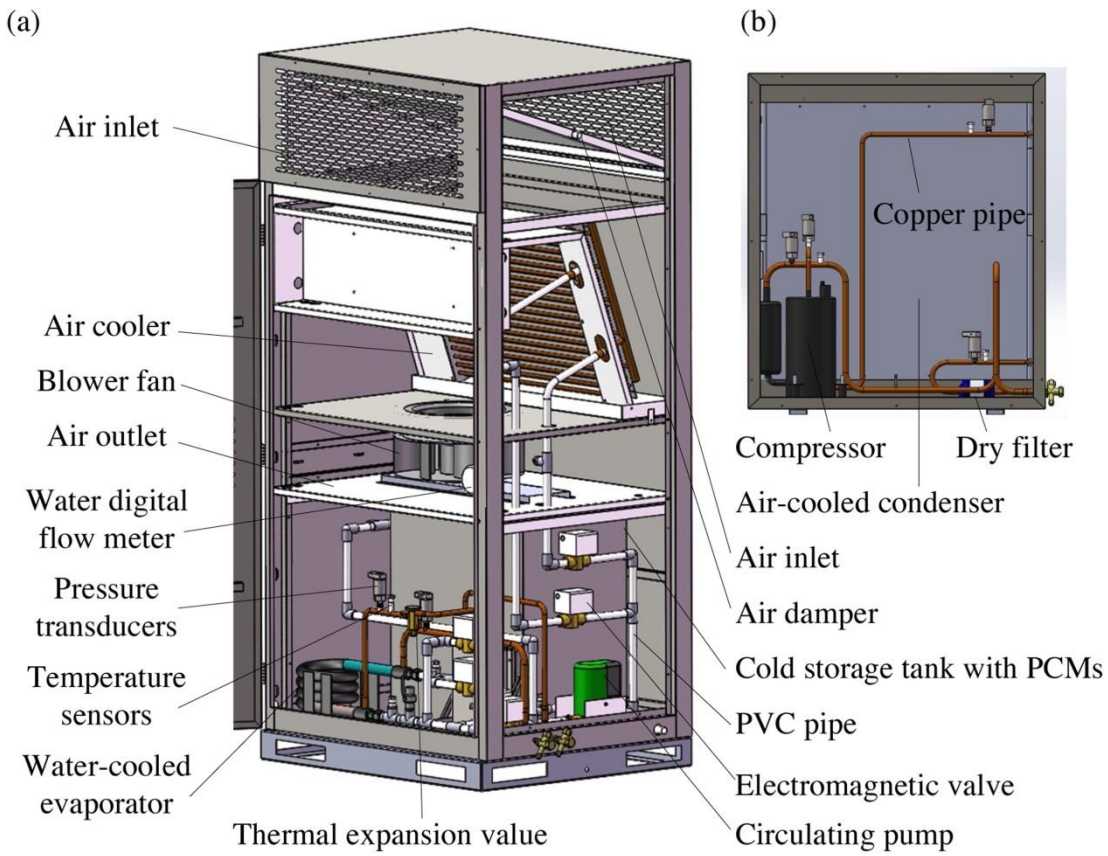

Figure 2.22: Schematic of the experimental system: (a) indoor and (b) outdoor units[189]**.**

It was found when using PCM to release the cold which was extracted from ambient air during nights, the COP of the air conditioning system could be increased by about 14% compared to that of the conventional system. Jarzyna et al[190]. used distilled water to store thermal energy in public transport vehicles. Significant reduction of financial expenses and the total weight of all batteries with the same amount of stored energy were observed. This cold energy stored by the PCM was from electricity which could be drawn from the network at bus stops. It was also concluded that the thermal storage tank could be an alternative to electrochemical cells and might contribute to reducing the cost of transport.

2.4.3 Economic analysis

Chaiyat [185] employed the experimentally verified model to investigate the PCM integrated air conditioning system. It was concluded that the cost of the PCM based air conditioning system could perform a 9.10% drop with the payback period at around 4.15 years. The energy economic performance of PCM integrated air conditioning system was carried out by Chaiyat [185]. It was found that the electrical and cost savings could be achieved up to 9% and 9.10% with the payback period at around 4.15 years. Kabeel et al[191].economically compared a solar energy assisted desiccant air conditioning system with four different kinds of PCMs. The numerical results showed that the life cycle savings could be achieved at 1727.5, 1997.6, 1766.1, and 1534.6$ for using paraffin wax, stearic acid, capric-palmitic and $CaCl_2 \cdot 6H_2O$ as PCM respectively. It was also concluded that when using the above the PCMs, the payback time was 4.93, 3.19, 3.94, and 4.33years respectively. Mosaffa et al[192]. studied the economic performance of a PCM based air conditioning system. By comparing three different kinds of PCMs, the best PCM was selected through the exergoeconomic analysis, with the lowest total cost rate at 4094 $/year. Navidbakhsh et al[193]. modelled the system performance of an ice thermal energy storage system (ITES) incorporating a PCM as the partial cold storage. Calcium chloride hexahydrate was selected as the PCM. When integrating PCM with the system, the annual electricity consumption decreased by 6.7% and 17.1% relative to simple ITES and conventional air conditioning systems respectively. Compared to the conventional system and the ITES system, the payback period could be 3.97 years and 3.39 years respectively.

The thermal performance of cold energy storage integration with solar-assisted air conditioning was carried out by Diaconu et al[194]. The thermal comfort improvement was observed through the numerical study. Akeiber et al[195]. evaluated the thermal performance and economy of a PCM based building air conditioning system. PCM (paraffin) was enclosed inside the aluminum container. It was demonstrated that the room without PCM encapsulation consumed the highest energy at 24 °C than the one with PCM. A reduced internal heat flux (38.45%) and temperature fluctuation was achieved with PCM encapsulation in the room. The authors concluded that the proposed PCM system was advantageous for efficient building construction in hot climate conditions.

2.5 Summary

The above applications show that employing the latent heat energy storage based on PCMs have great advantages and potentials on temperature stabilization, energy savings, cold energy balance and stability, emission and noise pollution abatement, equipment size reduction, extended operational life, and easier operation and control compared to the conventional mobile refrigeration systems.

Among the existed approaches, integrating PCM cold energy storage with air conditioning system has shown great potential for industrial applications due to the advantages of peak energy demand shift and thermal comfort improvement. Implementation of PCM in air conditioning system shows great potential for increasing the COP with a reasonable payback period.

However, there are only few industrial applications of PCM based air conditioning system. This is mainly due to the relative thermal conductivity of PCMs which leads to a poor overall thermal performance of the system. As mentioned above, it's much easier and more effective to increase the overall performance by optimizing the devices instead of increasing the thermal conductivity of PCMs. Besides, the past work in this field mainly focuses on the performance in building applications without considering the compactness. For the transport application, it has a strict requirement of the compactness of the system with suitable volume and weight.

Hence, it's important to develop the compact TES device for transport application. In this study, a compact TES device filled with PCM was introduced to the air conditioning system which has a great potential in transport application.

Emergency ventilation and cooling is another problem which the transport air conditioning is facing. Currently, only fresh air from ambient can be blown to the carriage when the sudden accident of the electricity supply occurs. This leads to a shortage of emergency ventilation and cooling which can cause thermal comfort reduction and even the healthy concern. Hence, it's quite necessary to develop the emergency ventilation and cooling for the transport field.

There is still no sufficient study to involve the proposed system. In this study, a PCM based air conditioning system by adding a compact TES device filled with PCM to normal air conditioning system was experimentally investigated. The device design and performance, system performance combined with economic analysis, and emergency ventilation and cooling have been carried out in this study.

Chapter 3 Methodologies

The effects of utilizing fins in both air and PCM sides were investigated numerically and experimentally validated in this chapter. The effects of air fins, PCM fins and model PCMs with different thermal conductivities on the total heat transfer rate during the melting and solidification processes were compared. The charging and discharging behaviours of air conditioning system with the TES device installed were investigated experimentally.

3.1 Mathematical modelling

In this part, the four configurations of the PCM based TES device are described first, followed by boundary and initial conditions. Mathematical model and numerical method are then briefly discussed.

A three-dimensional view of the TES device is shown in **Figure 3.1**. It consisted of PCM chambers and air channels. The PCM chambers are rectangular-shaped with vertically oriented straight fins; see Figs 3.1 and 3.2. Air channels are horizontally arranged with serrated fins with each 10mm long in the flow direction and orthogonal to the PCM chambers. The air channels and the PCM chambers are periodically arranged and connected with clapboards. The used of serrated fins in the air side was for disturbing air flow to create turbulence for enhancing heat transfer while minimizing pressure drop. Air was used as the heat transfer fluid and flowed through horizontal air channels where serrated fins were installed[196][197].The use of straight fins in the PCM side was to minimise difficulties in PCM filling process which achieve a required level heat transfer enhancement for the purpose of his study. As the TES device is large, only a small section (marked with the red dotted line) was modelling in this study.

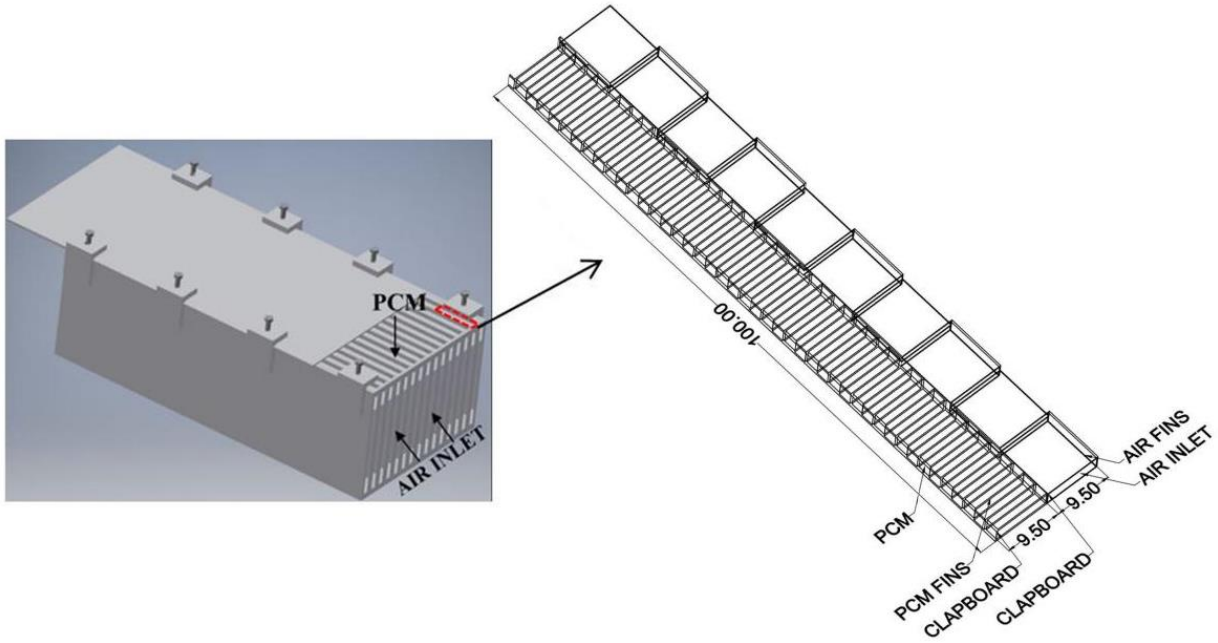

Figure 3.1: TES device for numerical simulation (unit: mm).

3.1.1 Boundary and initial conditions

As mentioned above, only a small section of the TES device was modelled. The main reasons for the only modelling the small portion are: first, modelling the whole TES device is very time consuming; and second, the geometrical structure of air channels and PCM chambers are symmetrical and periodically arranged.

Figure 3.2 shows the detailed geometries of the selected portion for numerical simulation, which has a length of 100mm containing a periodical unit of air channels, PCM chamber and clapboard. The height, width and thickness of fins in both air and PCM sides are respectively 9.5mm, 2.5mm and 0.2mm and the offset length of air fins is 10mm. The width and thickness of the clapboard are 2.5mm and 0.2mm, respectively.

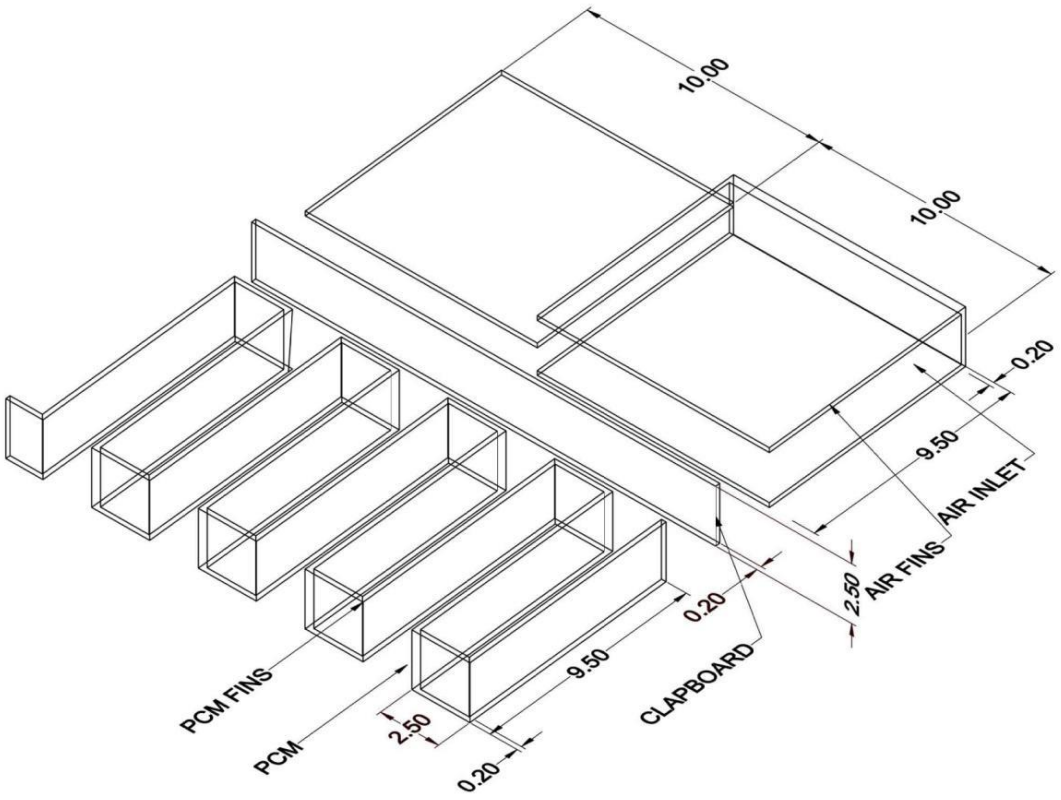

Figure 3.2: Geometrical dimensions of the fins and clapboards.

The boundary conditions were set on the basis of a normal operation of a traditional air conditioning system with air temperature ranging from 284.15K to 312.15K and air velocity 1.20 m/s. During discharging, both the PCM (in solid form) and straight fins were initially set at a temperature of 289.15K. The inlet air velocity and temperature of air were given as 1.20 m/s and 312.15K, respectively. During charging, both the PCM (in liquid form) and straight fins were initially at the temperature of 298.15K. The inlet air velocity and temperature were initially at 1.20 m/s and 284.15K, respectively. The initial conditions for the simulations are summarized in **.**

Table 3.1.

Table 3.1: Initial conditions of the numerical simulation for the charging and discharging process.

Catalogue	Charging	Discharging
Inlet air temperature (K)	284.15	312.15
Inlet air velocity (m/s)	1.20	1.20
Initial PCM phase and temperature (K)	Liquid, 298.15	Solid, 289.15
Initial air fins and clapboard temperature (K)	298.15	289.15
Initial PCM fins temperature (K)	298.15	289.15

3.1.2 Numerical simulation

The numerical simulations were performed in the Ansys Fluent environment. For each of the configurations, the following assumptions were made with rationales also included:

- PCM is uniformed distributed in the PCM chambers and homogeneous in terms of thermophysical properties-this is justified through carefully PCM filling and degassing processes.
- No heat loss from the modelled parts-this could be achieved by carefully insulating the TES device.
- Negligible effect of natural convection-this is due to densely distributed fins within PCM and little space for PCM to flow [198].

Under the above assumptions, the governing equations for the PCM include the flowing mass, momentum and energy balance equations:

$$\frac{\partial \rho}{\partial t} + \nabla \cdot (\rho \mathbf{v}) = 0 \tag{3.1}$$

$$\rho \frac{\partial \mathbf{v}}{\partial t} + \rho(\mathbf{v} \cdot \nabla)\mathbf{v} = -\nabla p + \mu \nabla^2 \mathbf{v} + \rho \vec{g}(T - T_0) + \vec{S} \tag{3.2}$$

$$\frac{\partial}{\partial t}(\rho h) + \nabla \cdot (\rho \mathbf{v} h) = \nabla \cdot (k \nabla T) \tag{3.3}$$

Where v represents the velocity vector, ρ denotes the density, k is the thermal conductivity, h is the specific enthalpy and T is temperature. Phase change process was accounted by using the enthalpy-porosity method which allows tracking the presence of solid/liquid PCM by using the liquid fraction. The specific enthalpy h is written as:

$$h = h_{ref} + \int_{T_{ref}}^{T} c_p dT + \gamma H \tag{3.4}$$

where H is the latent heat of fusion of the PCM and liquid fraction γ is defined as:

$$\gamma = \begin{cases} 0 & T < T_s \\ \dfrac{T - T_s}{T_l - T} & T_s < T < T_l \\ 1 & T > T_l \end{cases} \tag{3.5}$$

Where T_s and T_l are respectively the solidification and melting temperature. The air velocity and temperature were obtained by solving continuity, Navier-Stokes and the energy equations. A tetrahedral mesh was used for the discretisation of the governing equations. The Semi-Implicit Method for pressure –Linked Equations (SIMPLE) algorithm was employed for velocity-pressure coupling. The Second Order scheme was used for pressure spatial discretization and the Second Order Upwind was used for the discretization of the momentum and energy terms. A fine mesh is applied at positions close to walls and the cell size was taken as half of the fin's thickness (0.1mm), which was found to be appropriate through sensitivity analyses. The total number of nodes and corresponding tetrahedral cells of various geometries are list in **liquid fraction** was monitored.

Table 3.2.

A time step of 0.1s was chosen to ensure time-step independent results. The convergence was checked with the scaled residuals less than 10^{-6} for the continuity, momentum, and energy equations. The volume average of PCM liquid fraction was monitored.

Table 3.2: Number of nodes and corresponding cells for different geometries.

Geometries	Number of nodes	Number of cells
No fins	7261302	41915191
PCM fins	7269132	42047419
Air fins	7264475	41999148
Both fins	7283028	42143549

3.1.3 Mesh independent

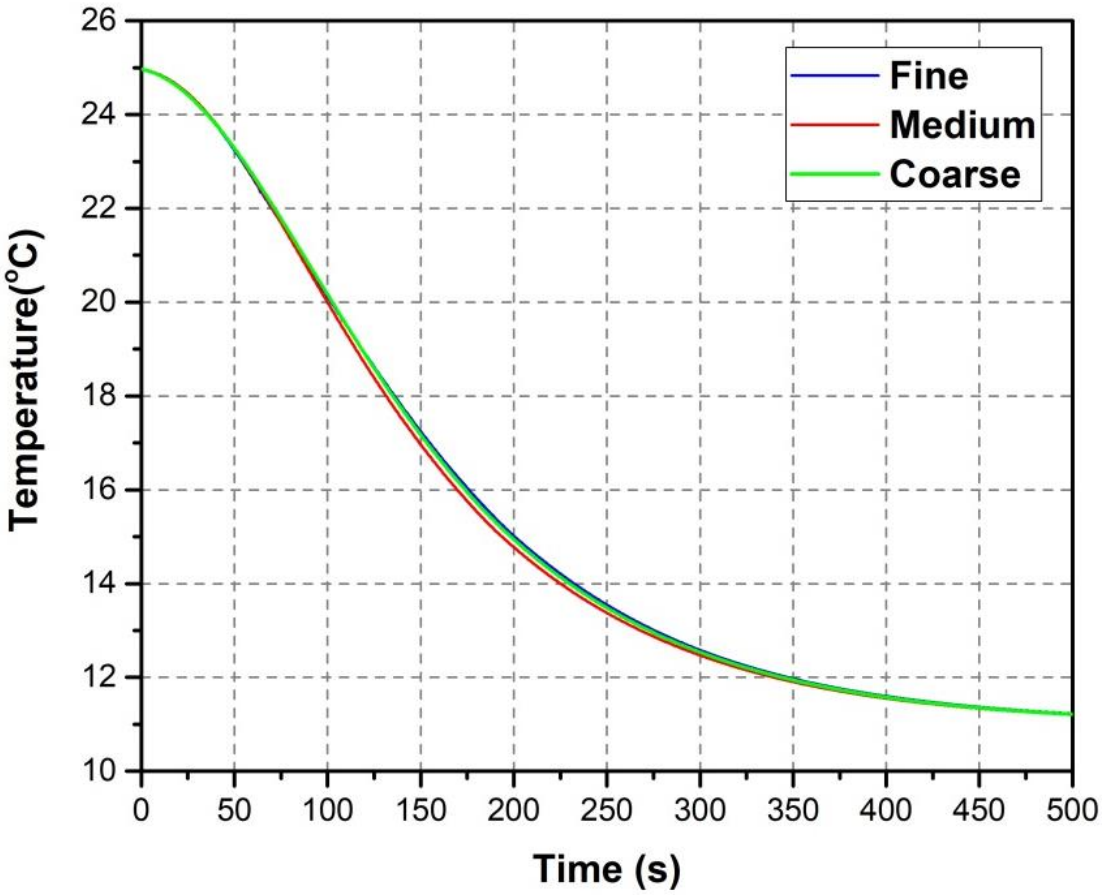

Figure 3.3: Grid independency of the simulation.

The mesh independent test(shown in **Figure 3.3**) for charge process was carried out at first, with 351,059, 2,693.220 and 5,362,100 cells for coarse, medium and fine mesh, respectively. The results are shown in Fig. 1, it could be confirmed that the mesh effect could be neglectable when the mesh is greater than 5M.

3.1.4 Experimental validation

(1) Phase Change Material

A commercial PCM, RT 18 HC, purchased from Rubitherm Technologies GmbH, Germany, was used in the work. A Mettler Toledo Differential Scanning Calorimeter (DSC-2) was used to characterise the thermal properties of the PCM (melting point, latent heat and specific heat capacity). The measurements used aluminum

crucibles containing ~10 mg sample. To obtain reliable and repeatable results, three different samples were measured with each sample measured for three times. A sapphire standard material was used as a reference to obtain the specific heat capacity. The measurements were done between 0°C and 50°C with heating/cooling rate of $1^{o}C\ min^{-1}$ under a nitrogen atmosphere. **Table 3.3** gives a summary of the measurement data. One can see a latent heat of 220kJ/kg and a melting and freezing range between17°C and 19°C. The specific heat capacities at solid (10°C) and liquid (30°C) state were measured to be 1.9 ±0.2 kJ/ (kg·K) and 2.0 ±0.2 kJ/ (kg·K), respectively.

A laser flash analyser (LFA427, Netzsch) was used to measure the thermal diffusivity of the PCM with a platinum crucible. The measurements were carried out in an air atmosphere. A three-layer model was used to determine the thermal diffusivity. One can see that the average thermal conductivity of the PCM for both solid and liquid phases is 0.2 W/(m·K) (

Table 3.3).

Table 3.3: Thermal-physical properties of RT18 HC for the numerical and experimental investigation.

Density (kg/m^3)	Latent heat (kJ/kg)	Melting range (main peak) (°C)	Congealing range (main peak) (°C)	Specific heat capacity (10 °C) (kJ/(kg·K))	Thermal Conductivity (both phases) (W/(m·k))
880	220	17-19 (18)	19 -17 (17)	2	0.2

(2) Experiment rig

Figure 3.4 gives a schematic diagram of the experimental set-up, which mainly consists of the TES device as described in Section 3.1.1, a commercial air conditioner, an air flow and temperature stabilisation chamber and a data acquisition connected to various sensors. A Leister Hot wind system was used to provide hot air and air conditioning unit was from Tripp Lite Company. The exterior size of the TES device including insulation was 600mm (length) ×300mm (width) ×200mm (height). A total of 10 kg PCM was used in the TES unit. The fins, channels, chambers, and clapboards were made of aluminum. To make the PCM filling easier, some holes with 2 mm diameter were made on the PCM fins to facilitate the PCM filling process.

The air chamber has a dimension of 800mm (height) × 800mm (width) ×1000mm (length) to ensure thorough mixing of cold air from air conditioner and the hot air from the heater for a precise air temperature control

before entering the TES device. The outer covering was the insulation layer to prevent the heat loss. The whole device was made of aluminum. Slightly different from the simulated unit (**Figure 3.2**), perforated straight fins were used in PCM side with holes of 2 mm in diameter as these holes could keep the liquidity of PCM being good for natural convection and materials filling.

Ten K- type thermocouples with 0.3% accuracy were installed in the inlet and outlet of the device with five in each of the ends. This allowed an average inlet and outlet air temperatures to be obtained from the measurements of the five thermocouples. Ten extra K-type thermocouples were inserted into the PCM chambers to track the PCM temperature at different positions as a function of time. The locations of the thermocouples inside the PCM are shown in **Figure 3.5**, where the axial distances from the inlet were denoted respectively by T1 and T2 (50mm), T3 and T4 (150mm), T5 and T6 (300mm), T7 and T8 (450mm), and T9 and T10 (550mm).

The thermocouples were interfaced to an Orchestrator data logger with 64 channels, which included a 7320 measurement module and a 7020 Analog I/P module. The data-logging unit was connected to a desktop computer, allowing all the measurement data to be recorded. A thermal anemometer with 1% accuracy (Air flow Instruments) was employed to measure the inlet air velocity. The anemometer measured air velocity at different positions at the inlet plane enabling accurate estimation of the average air velocity. `

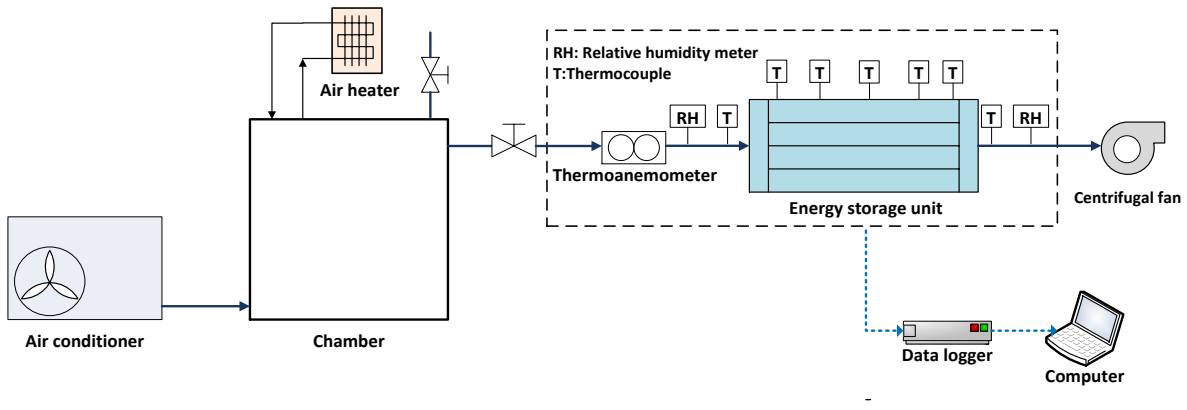

Figure 3.4: Brief schematics of experimental rig for testing the TES device.

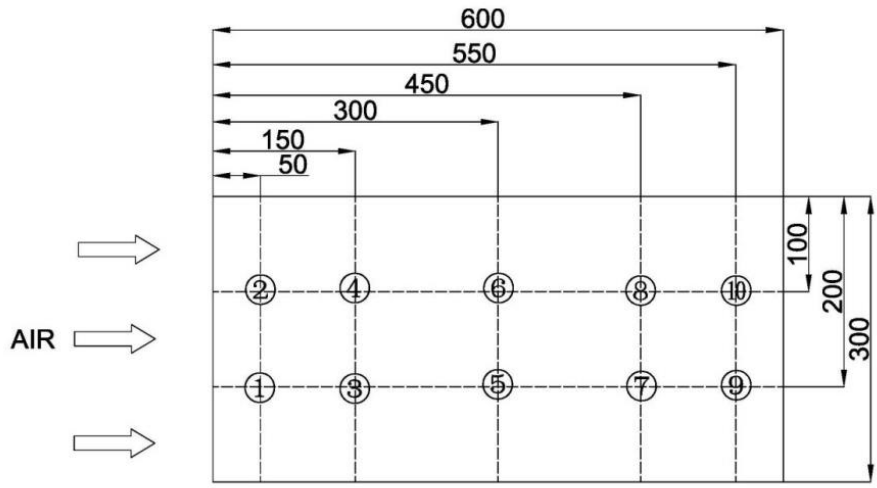

Figure 3.5: Distributions of the thermocouples inside the TES device, the number i in the cycles corresponding to the Ti in the text (i=1-10), (unit: mm).

(3)Validation of the model

Figure 3.6 shows a comparison of modelling and experimental results of the outlet air temperature for the charging and discharging processes under a constant inlet air temperature of 11 °C and 39 °C, respectively. One can see the modelling results capture the main feature of experimental results though the experimental curve is more diffusive, which could be attributed to two reasons with one being that the axial thermal conduction via the aluminum wall of the PCM chambers was not accounted in the modelling, and the other being a wider phase change temperature range of the PCM than the DSC measurements. To quantify the derivation of the modelling results from experimental data, a relative maximum error (δ_{max}) and average error (δ_{ave})[199] are introduced here:

$$\delta_{\max}(100\%) = \max_{1,2,\ldots N}\left\{\left(\left|\frac{y_{\exp} - y_{num}}{y_{\exp}}\right|\right)\times 100\right\} \tag{3.6}$$

$$\delta_{ave}(100\%) = \sum_{1,2,\ldots N}\left\{\left(\left|\frac{y_{\exp} - y_{num}}{y_{\exp}}\right|\right)\times 100\right\} / N \tag{3.7}$$

Where y represents a measurement parameter; the subscripts *exp* and *num* denote respectively the experimental data and modelling results; and N is the number of positions where the parameter is measured or calculated. One

finds that the δ_{max} and δ_{ave} values are less than 9.67 % and 4.24 % respectively for the charging process with an inlet air temperature and 11 °C and an inlet velocity at 1.20m/s , and are lower than 12.37 % and 6.56 % for the discharging process with an inlet air temperature of 39 °C and an inlet velocity of 1.20m/s.

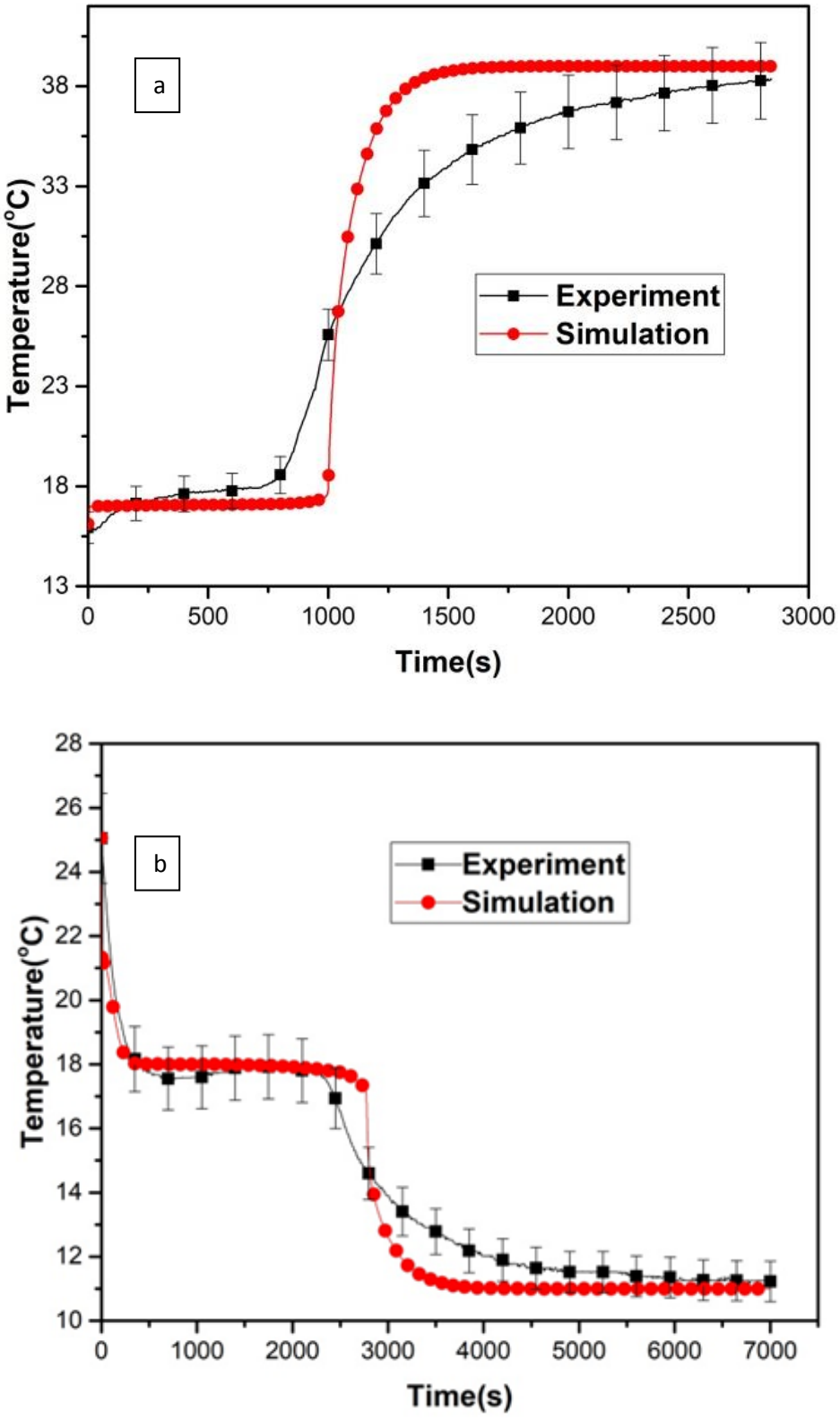

Figure 3.6: Comparison of the results between simulation and experiment for discharging (a) and charging (b) processes.

3.2. Experiments

This part gives details of design and inside structure of the devices. The experimental system design and construction, data-logging, experimental procedure, the materials used in the experiments and their characterisation were also discussed in this part.

3.2.1 Phase Change Material

The commercial PCM (RT 18 HC) was used in the TES device, the characterisations and thermal-physical properties of the PCM were indicated in Section 3.1.3. The outside dimensions of the device were 300 mm (length)×400 mm (width)×300 mm (height), and all parts were made of aluminum. The device was covered by the insulation layer to prevent the heat loss to the environment. The mass of PCM is 10 kg, and the mass of aluminum is 18 kg.

The device consisted of PCM and air channels as shown in **Figure 3.7**. Each PCM channel consisted of rectangular shaped passages formed by straight perforated fins. PCM was filled and stored in these channels. In air channels serrated fins were installed. One air channel was connected to one PCM channel with clapboard as a separation. The unit of one air channel and one PCM channel was repeatedly installed until it was filled the whole chamber of energy stage device. In both channels, the height of fins and the pitch between fins were 12.8 mm and 2.5 mm respectively, with the thickness of 0.2 mm. The offset length of the serrated fins in the air flow direction is 10 mm. Both fins were used to enhance heat transfer. Besides, holes on perforated fins could keep the liquidity of PCM, which would be definitely good for natural convection and materials filling.

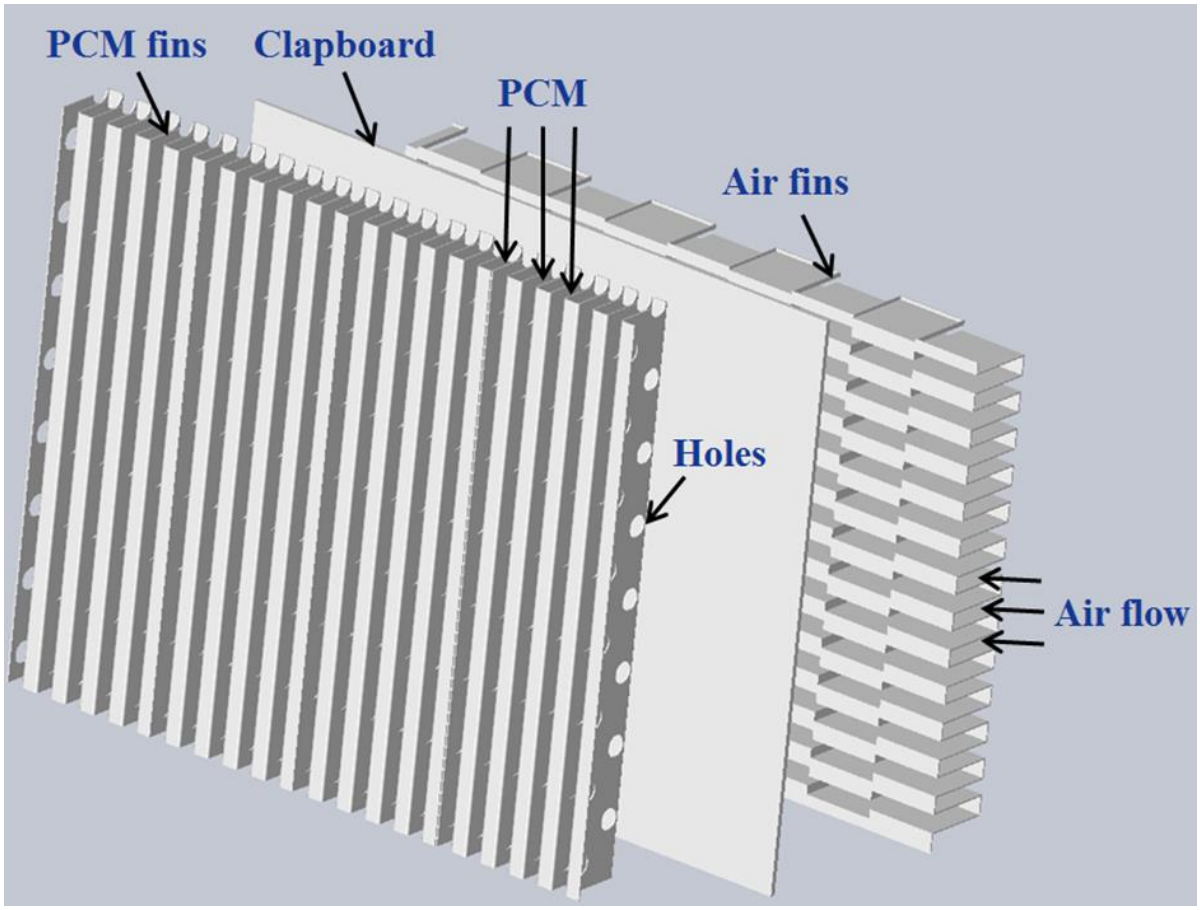

Figure 3.7: Inside structure of the device.

3.2.2 Discharging experiments

For the real operation of the rail carriage, the inlet air temperature for the charging process is selected between 11-15 ^{o}C, as the temperature of the cold air after the evaporator locates in this range. The discharging temperature is chosen based on the real ambient which varies from 25 to 30 ^{o}C. The inlet air velocity is also selected due to the real operating conditions which is between the 0.75 and 1.2 m/s.

(1) Experimental rig

An experimental rig was set up mainly with the TES device, a commercial air conditioner and a data acquisition instrument as shown in **Figure 3.8**. The air heater was used to provide hot air. Cold air was acquired from the commercial air conditioner. In order to acquire the stable properties of the inlet air, a chamber with the size of

800 mm (height) ×800mm (width) ×1000 mm (length) was employed to uniformly mix the air from the air conditioner and air heater. Then, the mixed air with a given temperature was blown through the TES device.

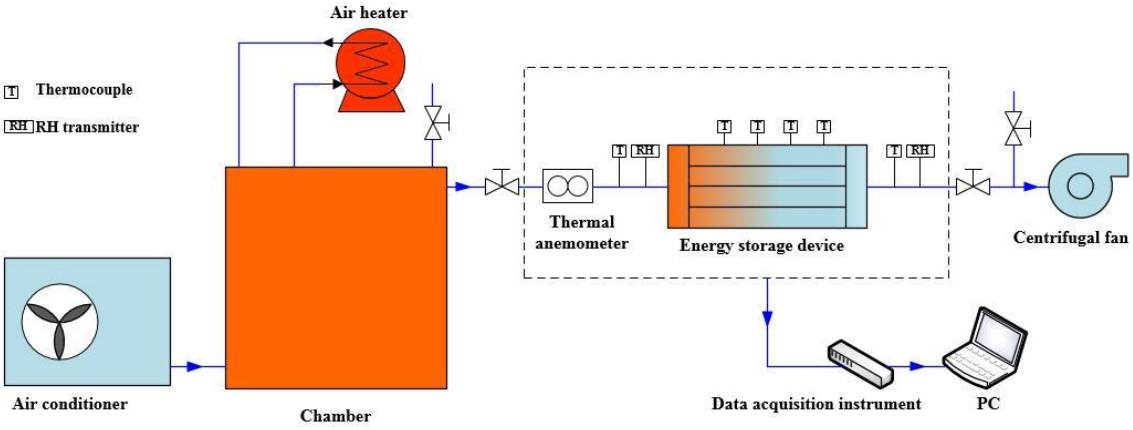

Figure 3.8: Schematics of the experimental rig for testing the TES device.

In order to monitor the air and PCM temperature through the TES device, 8 K-type thermocouples were placed at the inlet and outlet of the device, with 4 at each side, and 20 K-type thermocouples were placed inside the PCM to determine its melting and solidification temperatures. The thermocouples were installed in 4 layers along air flow direction with 5 thermocouples in each layer as shown in **Figure 3.9**(a). The depth of the thermocouples, which was the distance from the top surface of the device to the position of the thermocouples, for T6-9, T10-13, T14-17, T18-21 and T22-25 was 250 mm, 200 mm, 150 mm, 100 mm and 50 mm respectively, as shown in **Figure 3.9**(b).

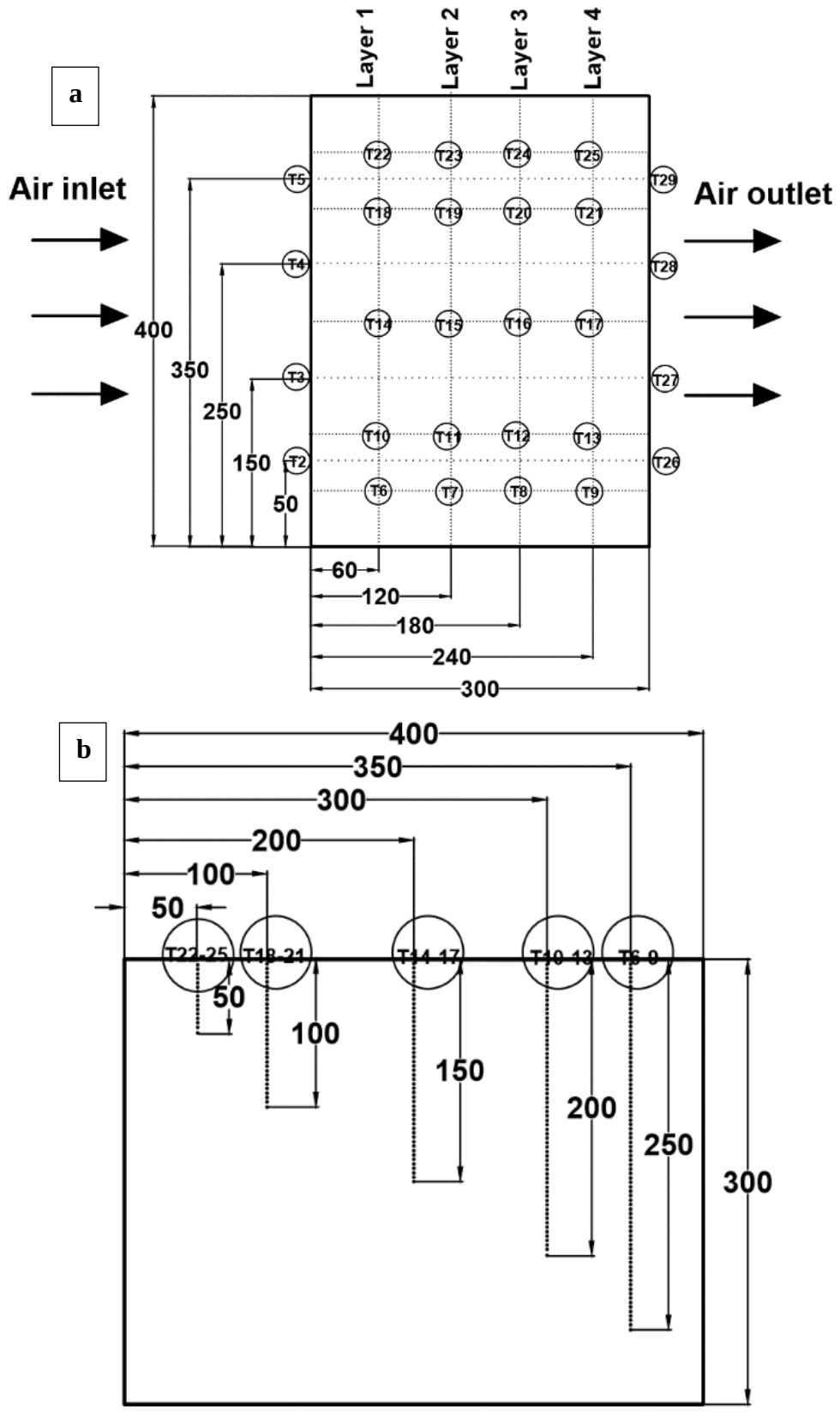

Figure 3.9: The locations of thermocouples in the TES device, (a) Top view and (b) cross section, unit: mm.

An orchestrator data logger system with 64 channels, including a 7320 Measurement module and a 7020 Analog I/p module, was used to collect all the data. Two RH transmitters (of 3.0 % accuracy) were used to measure the inlet and outlet air relative humidity. A thermal anemometer (of 1% accuracy) was employed to measure the inlet air velocity. Air velocities at different positions were measured to acquire the average value.

(2) Performance indexes

(a).The working period

For a rail carriage, the supply air temperature is required to be in the range of 16-20 ^{o}C. Therefore, the working period, *t*, is defined as the period when the air outlet temperature of the TES device is between 16 and 20^{o}C during the discharging process.

(b).The discharging power

The discharging power of the TES device, W_a, is defined as the amount of cold energy absorbed by the air, and can be calculated as follows.

$$W_a = \dot{m}_a \left(\sum_0^t H_{a,in} - \sum_0^t H_{a,out} \right) \tag{3.8}$$

where, $\dot{m}_a$ is the average air mass flow rate; t is the discharging time; $H_{a,in}$ and $H_{a,out}$ are the inlet and outlet air enthalpies, respectively.

(c).The discharging thermal efficiency

The total energy absorbed by the air during discharging, Q_a, is calculated using Eq. (3.9).

$$Q_a = \int_0^t W_a dt \tag{3.9}$$

whereas total energy released by the PCM, Q_{PCM}, is calculated using the Eq. (3.10).

$$Q_{PCM} = m_{PCM} \left[c_{p,s} \left(T_{m,low} - T_i \right) + \Delta H_{PCM} + c_{p,l} \left(T_e - T_{m,high} \right) \right] \tag{3.10}$$

where, the first part is the subcooling capacity; the second part is the latent heat capacity and the third part is the superheating capacity. The m_{PCM} and ΔH_{PCM} are the mass and latent heat capacity of PCM, respectively; $c_{p,l}$ and

$c_{p,s}$ are the liquid and solid specific heat capacities respectively; T_e and T_i are the end temperature and initial temperature of PCM respectively. $T_{m,low}$ and $T_{m,high}$ are the low (17 ^{o}C) and high (19 ^{o}C) melting temperatures.

The total energy released by the aluminum (frame of the TES device), Q_{Al}, can be calculated by Eq. (3.11).

$$Q_{Al} = m_{Al} c_{p,Al} (T_e - T_i) \tag{3.11}$$

where, m_{Al} and $c_{p,Al}$ are the mass and specific heat capacity of aluminum, respectively. The discharging thermal efficiency, η_{th}, is defined by Eq. (3.12).

$$\eta_{th} = \frac{Q_a}{Q_{PCM} + Q_{Al}} \tag{3.12}$$

(d).The discharging exergy efficiency

The specific flow exergy of the moist air, e_a, is given by Eq. (3.13).

$$e_a = (c_{p,a} + \omega c_{p,v}) T_0 \left(\frac{T_{a,out} - T_{a,in}}{T_0} - \ln \frac{T_{a,out}}{T_{a,in}}\right) \tag{3.13}$$

where, $c_{p,a}$ and $c_{p,v}$ are the specific heat capacity of dry air and vapor, respectively. T_0 is the ambient temperature. $T_{a,in}$ and $T_{a,out}$ are resepectively the air temperature at the inlet and outlet of the TES device.

The total flow exergy of moist air, E_a, is given by

$$E_a = \dot{m}_a \int_0^t e_a dt \tag{3.14}$$

The total exergy released by PCM, E_{PCM}, is acquired by Eq. (3.15).

$$E_{PCM} = m_{PCM} c_{p,s} [(T_i - T_{m,low}) - T_0 \ln(\frac{T_i}{T_{m,low}})] + m_{PCM} \Delta H_{PCM} [(\frac{T_0}{T_{m,ave}}) - 1] + m_{PCM} c_{p,l} [(T_{m,high} - T_e) - T_0 \ln(\frac{T_{m,high}}{T_e})] \tag{3.15}$$

where, the first part is the subcooling exergy; the second part is the latent heat exergy, and the last part is the supheating exergy. $T_{m,ave}$ is the average melting temperature, 18 ^{o}C.

The total exergy released by the aluminum (frame of the TES device), E_{Al}, is calculated in the following.

$$E_{Al} = m_{Al} c_{p,Al} T_0 [(\frac{T_i - T_e}{T_0}) - \ln(\frac{T_i}{T_e})] \tag{3.16}$$

The discharging exergy efficiency, η_{ex}, is defined by Eq.(3.17).

$$\eta_{ex} = \frac{E_a}{E_{PCM} + E_{Al}} \tag{3.17}$$

(e). The discharging depth

Given the air temperature requirement of 16-20 ^{o}C for the rail cabins, the discharging process will stop when the air outlet temperature of the TES device is equal or higher than 20 ^{o}C. This can occur due to two cases-either or both of insufficient cold energy in the TES device and the heat transfer process does not allow the exit air to be cooled down the air to below 20 ^{o}C. Considering that there may still be cold energy left, it is therefore of interest to understand the amount of cold energy remaining in the TES device. The discharging depth, *D*, is defined as the ratio of exergy released for cooling the air to the exergy stored in the TES device.

The total exergy stored in the PCM, $E_{PCM,store}$, is determined by,

$$E_{PCM,store} = m_{PCM} c_{p,s} [(T_i - T_0) - T_0 \ln(\frac{T_i}{T_0})] \tag{3.18}$$

The total exergy stored by the aluminum (frame of the TES device), $E_{Al,store}$, is calculated as follows.

$$E_{Al,store} = m_{Al} c_{p,Al} [(T_i - T_0) - T_0 \ln(\frac{T_i}{T_0})] \tag{3.19}$$

The discharging depth, *D*, is,

$$D = \frac{E_{PCM} + E_{Al}}{E_{PCM,store} + E_{Al,store}} \tag{3.20}$$

3.2.3 Charging experiments

(1) Experimental rig

Experimental rig included the compact TES device, a commercial air conditioner and a data acquisition system as shown in **Figure 3.10**. Cold air was acquired from a commercial air conditioner. To acquire inlet air with stable properties, a chamber with the size of 800 mm×800 mm×1000 mm was employed as an air reservoir. After the air was stabilized, it flowed through the TES device for charging.

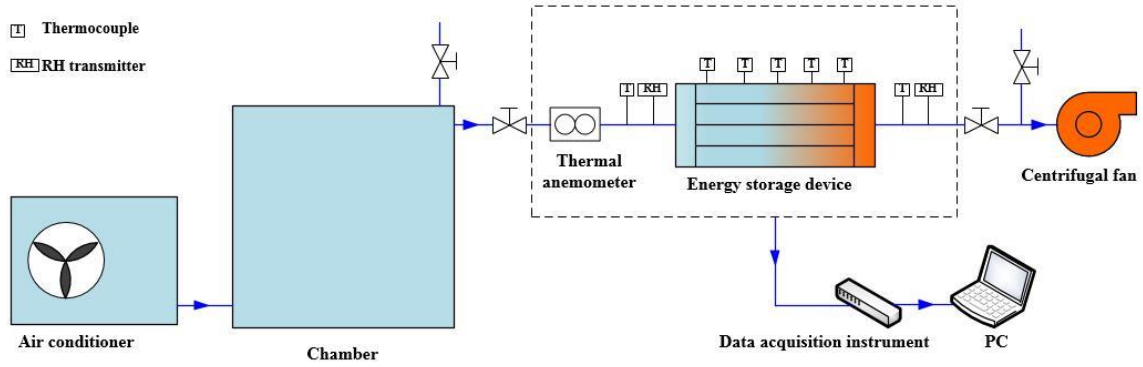

Figure 3.10: Schematics of the experimental rig for testing the TES device.

6 K-type thermocouples were fixed on the inlet and outlet of the device, with 3 at each side to acquire the inlet and outlet air temperatures. To study the internal temperature changes, another 20 K-type thermocouples were placed in 5 layers with 4 thermocouples in each layer along air flow direction. The thermocouples in each layer were located at different depths: 50 mm for T4-T8, 100 mm for T9-T13, 150 mm for T14-T18, and 200 mm T19-T23, shown in **Figure 3.11**.

An orchestrator data logger system with 64 channels including a 7320 measurement module and a 7020 Analog I/p module was used to record all the data. Two RH & T transmitters were used to measure the inlet and outlet air relative humidity and temperature. A thermal anemometer was used to measure the inlet air velocity. Air velocities at different points were measured to acquire the average value. The uncertainties of the measurement were 0.3% for thermocouples, 3.0% for RH &T transmitters and 1.0% for thermal anemometer, which indicated the good reliability of the experimental data.

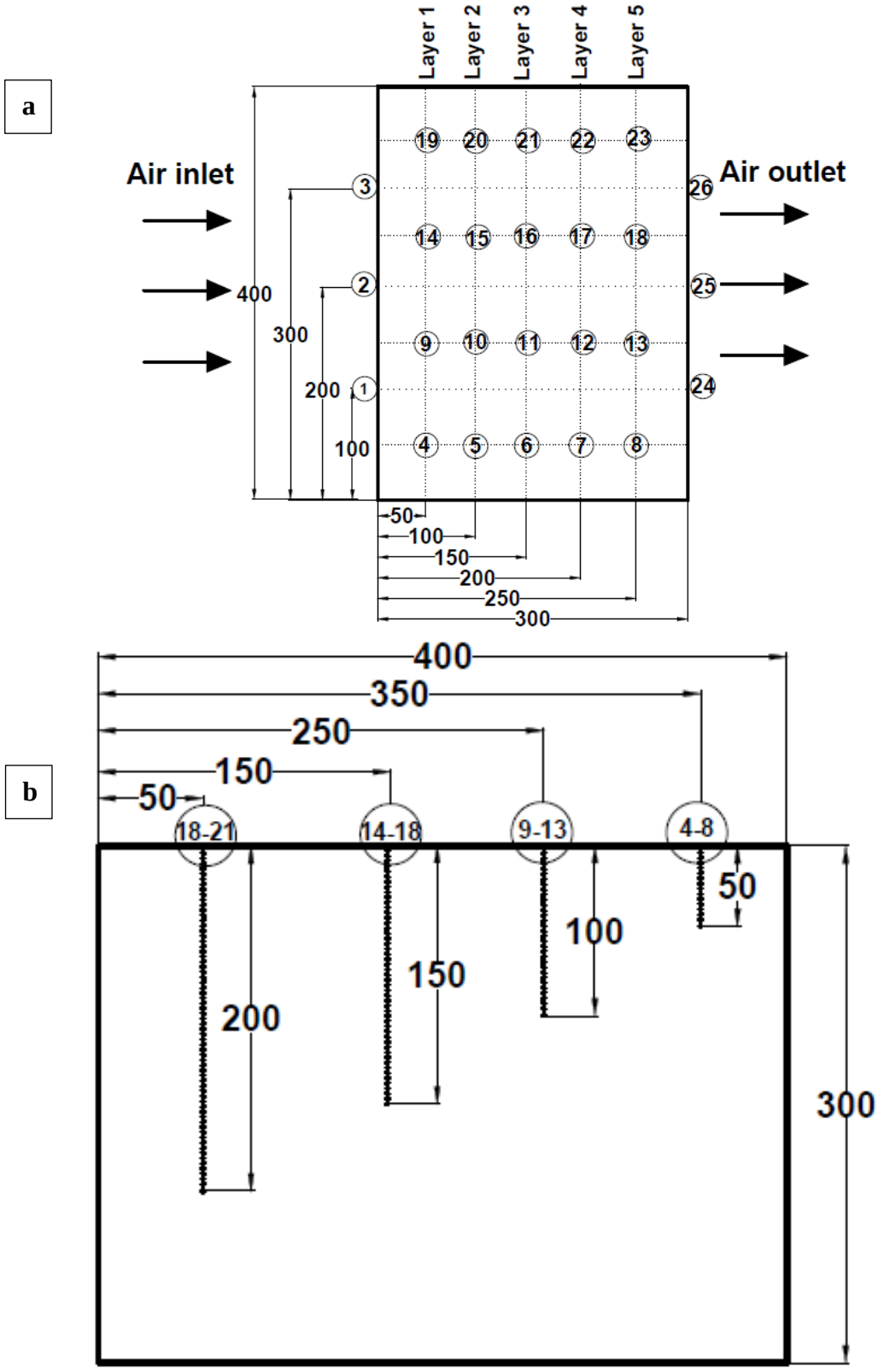

Figure 3.11: Top view (a) and cross section (b) of the TES device, the number i in the cycles corresponding to the Ti in the text (i=4-21), unit: mm.

(2) Performance indexes

(a).Transient charging rate

Charging rate, W_a, is the amount of cold energy released per second by air, and could be calculated as follows.

$$W_a = \dot{m}_a (H_{a,out}(t) - H_{a,in}(t)) \tag{3.21}$$

where, $\dot{m}_a$ is the average mass flow rate of air; t is the time; $H_{a,in}$ and $H_{a,out}$ are the inlet and outlet enthalpy of air, respectively.

(b).Charging thermal efficiency

The total cold energy released by air (Q_a) and total cold energy absorbed by the PCM (Q_{PCM}) are calculated using Eqs. (3.22) and (3.23), respectively.

$$Q_a = \int_0^t W_a dt \tag{3.22}$$

$$Q_{PCM} = m_{PCM}\left[c_{p,l}\left(T_i - T_{m,high}\right) + \Delta H_{PCM} + c_{p,s}\left(T_{m,low} - T_e\right)\right] \tag{3.23}$$

where, m_{PCM} and ΔH_{PCM} are the mass and latent heat capacity of PCM, respectively; $c_{p,l}$ and $c_{p,s}$ are the liquid and solid specific heat capacities; T_e and T_s are the end and initial temperatures of PCM. $T_{m,low}$ and $T_{m,high}$ are the low (17 ^{o}C) and high (19 ^{o}C) congealing temperatures, respectively.

The total cold energy absorbed by the aluminum frame of the TES device, Q_{Al}, can be calculated by Eq.(3.24).

$$Q_{Al} = m_{Al} c_{p,Al} (T_i - T_e) \tag{3.24}$$

where, m_{Al} and $c_{p,Al}$ are the mass and specific heat capacity of aluminum, respectively.

The charging thermal efficiency, η_{th}, is defined by Eq. (3.25).

$$\eta_{th} = \frac{Q_{PCM} + Q_{Al}}{Q_a} \tag{3.25}$$

(c).Charging exergy efficiency

The specific flow exergy of air, e_a, is given by Eq.(3.26).

$$e_a = (c_{p,a} + \omega c_{p,v})T_0(\frac{T_{a,in} - T_{a,out}}{T_0} - \ln\frac{T_{a,in}}{T_{a,out}}) \tag{3.26}$$

where, $c_{p,a}$ and $c_{p,v}$ are the specific heat capacity of dry air and vapor. T_0 is the ambient temperature. $T_{a,in}$ and $T_{a,out}$ are the air temperatures at the inlet and outlet of the TES device.

The total flow exergy of moist air, E_a, is given by Eq. (3.27).

$$E_a = \dot{m}_a \int_0^t e_a dt \tag{3.27}$$

The total exergy absorbed by PCM, E_{PCM}, is acquired by Eq. (3.28).

$$E_{PCM} = m_{PCM} c_{p,l}[(T_{m,high} - T_i) - T_0 \ln(\frac{T_{m,high}}{T_i})] + m_{PCM}\Delta H_{PCM}[(\frac{T_0}{T_{m,ave}}) - 1] + m_{PCM} c_{p,s}[(T_e - T_{m,low}) - T_0 \ln(\frac{T_e}{T_{m,low}})] \tag{3.28}$$

where, the first part is the supheating exergy, the second part the latent heat exergy, and the last part the subcooling exergy. $T_{m,ave}$ is the average congealing temperature 18^{o}C.

The total exergy lose from the aluminum (frame of the TES device), E_{Al}, is calculated in the following.

$$E_{Al} = m_{Al} c_{p,Al} T_0[(\frac{T_e - T_i}{T_0}) - \ln(\frac{T_e}{T_i})] \tag{3.29}$$

The charging exergy efficiency, η_{ex}, is defined by Eq. (3.30).

$$\eta_{ex} = \frac{E_{PCM} + E_{Al}}{E_a} \tag{3.30}$$

(d).Optimal charging depth

During the charging process, exergy efficiency will vary with time. When the dynamic exergy efficiency reaches the maximum value, further charging will not be energy-efficient. The optimal charging depth (D_{ch}) is

defined as the ratio of exergy stored in PCMs at the maximum exergy efficiency to that when the TES device is fully charged.

$$D_{ch} = \frac{E_{PCM}(t_{\max})}{E_{PCM}(t_e)} \tag{3.31}$$

where, t_{max} represents the time when the maximum exergy efficiency is obtained; t_e is the time when the TES device is fully charged.

3.2.4 Heat transfer experiments

(1) Experimental rig

The experimental rig is mainly consisted of an air conditioner the TES device, and a data acquisition instrument as shown in **Figure 3.12**. Hot air and cold air are provided by an air heater and an air conditioner respectively. In order to get the desirable inlet air temperature, an insulated chamber with the size of 800 mm (height)*800mm (width) *1000 mm (length) is used to uniformly mix the air from the air conditioner and air heater. Then, the stable air was blown through the TES device. A centrifugal fan with a frequency converter is used to obtain the required inlet air velocity.

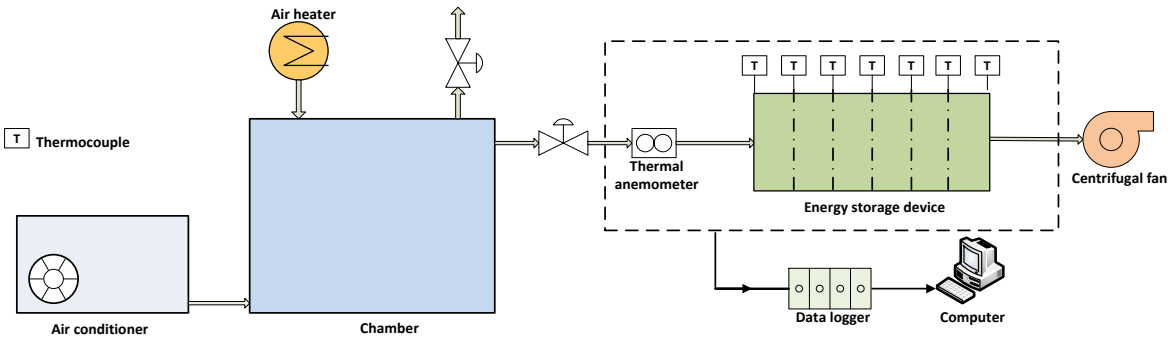

Figure 3.12: Schematics of the experimental rig for the heat transfer experiments.

An orchestrator data logger system was used to collect all the data. Forty-Two T-type thermocouples (of 0.3% accuracy) were employed to reflect the temperature distribution and the phase change period. A thermal anemometer was employed to measure the inlet air velocity (1% uncertainty). Different points of air velocity were measured to acquire the average value.

The device was divided into 6 layers along the air flow direction, with a length of 50mm for each layer. In order to obtain the temperature difference between the air flow and PCM, 42 T-type thermocouples were distributed over overall seven axial locations inside the device. These axial locations are 0mm, 50mm, 100mm, 150mm, 200mm, 250mm and 300mm from the front of the device. Each location contains six thermocouples. For thermocouples T1-T7, T15-T21 and T29-T35, they were inserted in the air flow channels to record the air temperature. The other 21 thermocouples marked as T8-T14, T22-T28 and T36-T42 were installed in the PCM channels to obtain the corresponding PCM temperature. The distribution of thermocouples is shown in **Figure 3.13 a**. The depth of thermocouples from the top surface of the device for T1-14, T15-28 and T29-42 is 250 mm, 150 mm and 50 mm respectively, as shown in **Figure 3.13 b**.

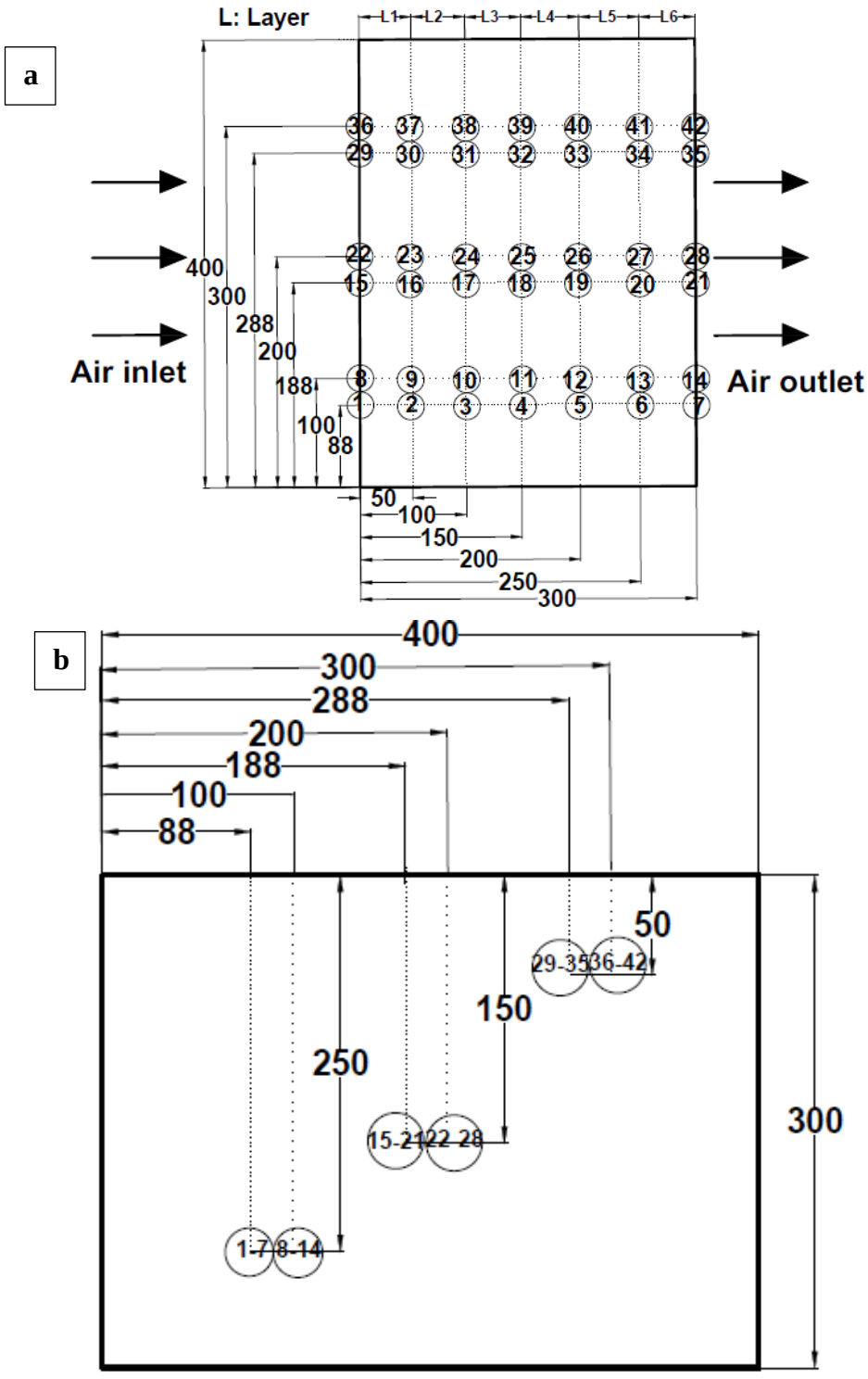

Figure 3.13: Top view (a) and cross section (b) of the TES device, unit: mm.

(2) Performance indexes

(a). Charging and discharging times

The charging time is defined as the period when the temperature of PCM drops from 19°C to 17°C, while the discharging time is given as the lasting time for PCM temperature increasing from 17°C to 19°C.

(b). Heat flux

The transient heat flux between the air flow and the PCM is evaluated through air side using the Eq.(3.32) as follows:

$$Q_{tj,layerl} = mc_{p,a}\left(T_{a,tj,layeri,e} - T_{a,tj,layerl,i}\right) \quad j = 1,2,\cdots,n, l = 1,2,\cdots,6. \tag{3.32}$$

where $Q_{,tj,layerl}$ is the transient heat flux of layer l calculated by air flow, $\dot{m}$ m is the mass flow rate of air flow, $c_{p,a}$ is the specific capacity of air, $T_{a,tj,\ layerl,e}$ and $T_{a,tj,layerl,i}$ are the transient air temperatures at the end and inlet of layer l and time tj.

(c). Transient heat transfer coefficient

The transient heat transfer coefficient between the air flow and PCM is calculated through Eq. (3.33)as expressed below.

$$K_{tj,layerl} = \frac{Q_{tj,layerl}}{A\Delta T_{LMTD,tj,layerl}}, \quad j = 1,2,\cdots,n, l = 1,2,\cdots,6. \tag{3.33}$$

where, $K_{tj,layerl}$ is the transient heat transfer coefficient at layer l and time tj; A is the surface area of the TES device on the air flow side of each layer; $\Delta T_{LMTD,tj,layerl}$ is the transient logarithmic mean temperature difference at layer l and time t_j calculated using Eq. (3.34),

$$\Delta T_{LMTD,tj,layerl} = \frac{\Delta T_{tj,layerl,e} - \Delta T_{tj,layerl,i}}{ln(\Delta T_{tj,layerl,e}/\Delta T_{tj,layerl,i})} \quad j = 1,2,\cdots,n, l = 1,2,\cdots,6. \tag{3.34}$$

where, the $\Delta T_{tj,layerl,e}$ and $\Delta T_{tj,layerl,i}$ are the temperature differences between the air flow and the corresponding PCM at the end and inlet of layer l and time tj respectively.

(d). Average heat transfer coefficient

The transient average heat transfer coefficient $K_{tj,ave}$ is defined as the average of transient heat transfer coefficient of the total six layers by using Eq.(3.35).

$$K_{tj,ave} = \frac{K_{tj,layer1} + K_{tj,layer2} + \cdots + K_{tj,layer6}}{6}, \quad j = 1, 2, \cdots, n \tag{3.35}$$

where $K_{tj,,layer1}$ *to* $K_{tj,,layer6}$ is the transient heat transfer coefficient corresponding to the layer 1 to layer 6 respectively.

(e). Overall heat transfer coefficient

The overall heat transfer coefficient K_{ov} between the air flow and PCM for the whole device is given by assessing the average of all the transient heat transfer coefficients, as shown in Eq.(3.36).

$$K_{ov} = \frac{K_{t1,ave} + K_{t2,ave} + \cdots + K_{tn,ave}}{n} \tag{3.36}$$

3.2.5 System experiments

(1) Experimental rig

An experimental rig was designed and constructed for studying the performance of the PCM based air-conditioning system (PCM-AC) and comparing its performance with that of a traditional air conditioning (AC) unit. **Figure 3.14**. shows schematically of the PCM-AC system, which consisted mainly of a conventional air conditioner, a PCM-based TES unit(see Section 3.2), a temperature-controlled room(testing space), a fan, various piping and valves, and a data-logging unit. The testing space had an internal dimension of 2.0 m(length)×2.0 m(width)×2.2 m(height) for simulating a transport vehicle carriage.The room was insulated all around with polyurethane foam panels with a thickness of 10mm. The heat load inside(testing space) was generated from an electrical heater. The fan was a centrifugal type equipped with a frequency converter for air velocity control. In a typical experiment, the electrical heater was switched on to warm up the testing space to 30^{o}C. The air conditioner and centrifugal fan were then started with the outlet temperature of the air conditioner set at 22^{o}C.The cold air from the air conditioner went through the TES unit before entering the room for providing cooling.The air from the testing space was then returned to the inlet of the air conditioner to close the loop.

The data-logging unit consisted of various sensors, for measuring temperature, humidity, velocity and electrical power, interfaced to a computer via Orchestrator data-loggers. The temperature measurements were done by 26

T-type (all 0.3% accuracy): three installed I the air duct between the air conditioner outlet and TES unit inlet to obtain the outlet ait temperature of the air conditioner; three in the air duct between the TES unit and the room to determine the testing space inlet air temperature, twenty in the interior of the PCM side of the unit(see Section 3.2) to investigate the transient temperature of the PCM; and ten on the walls and ceilings of the room(see **Figure 3.16** for the locations). Two relative humidity sensors(3.0% accuracy) were installed in the experimental rig with one inserted into air duct between the TES unit and the room to determine relative humidity of the air entering the testing space, and the other in the center of the testing space. A velocity meter(1.0% accuracy) was located at the inlet of the room to measure the air velocity into the testing space. The transient input electrical power of the air conditioner was recorded by an energy logger(1.0% accuracy). **Figure 3.15** shows a photograph of the whole experimental testing rig.

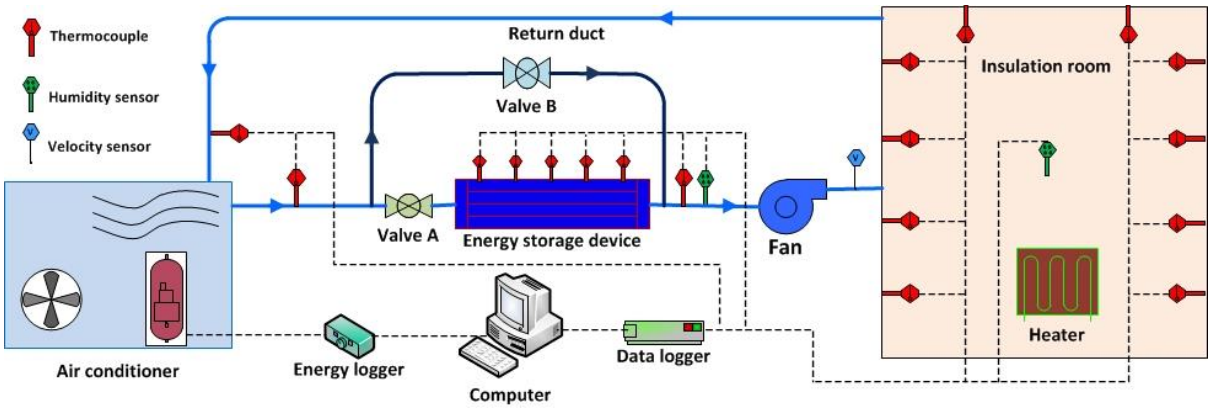

Figure 3.14: Schematics of the experimental rig for the PCM-AC.

1: Air conditioner; **2:** Energy storage device; **3:** Centrifugal fan;
4: Insulation room; **5:** Return duct; **6:** Data logger.

Figure 3.15: The photograph of the experimental testing rig.

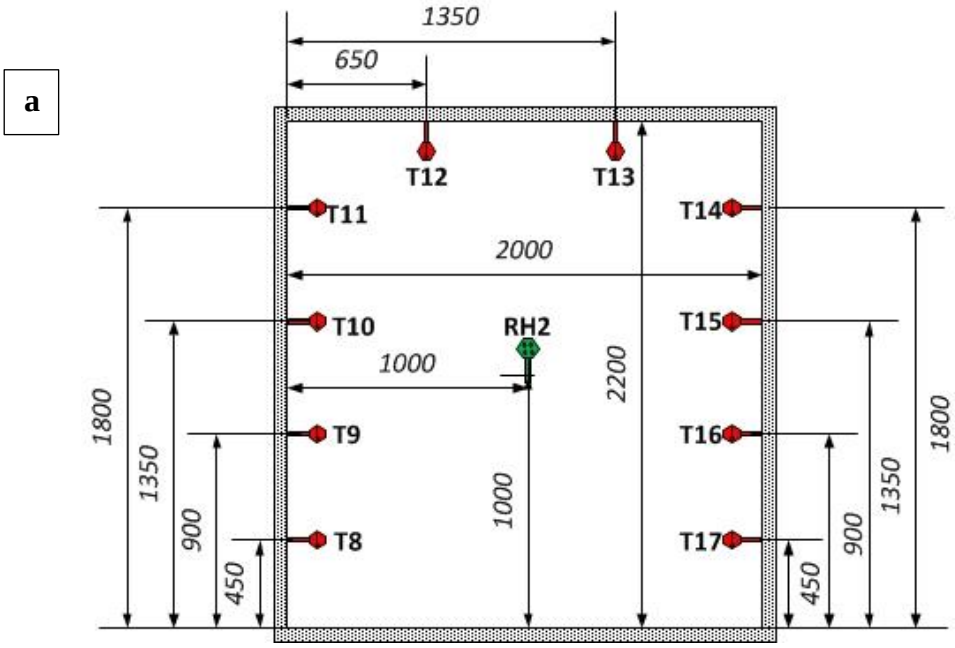

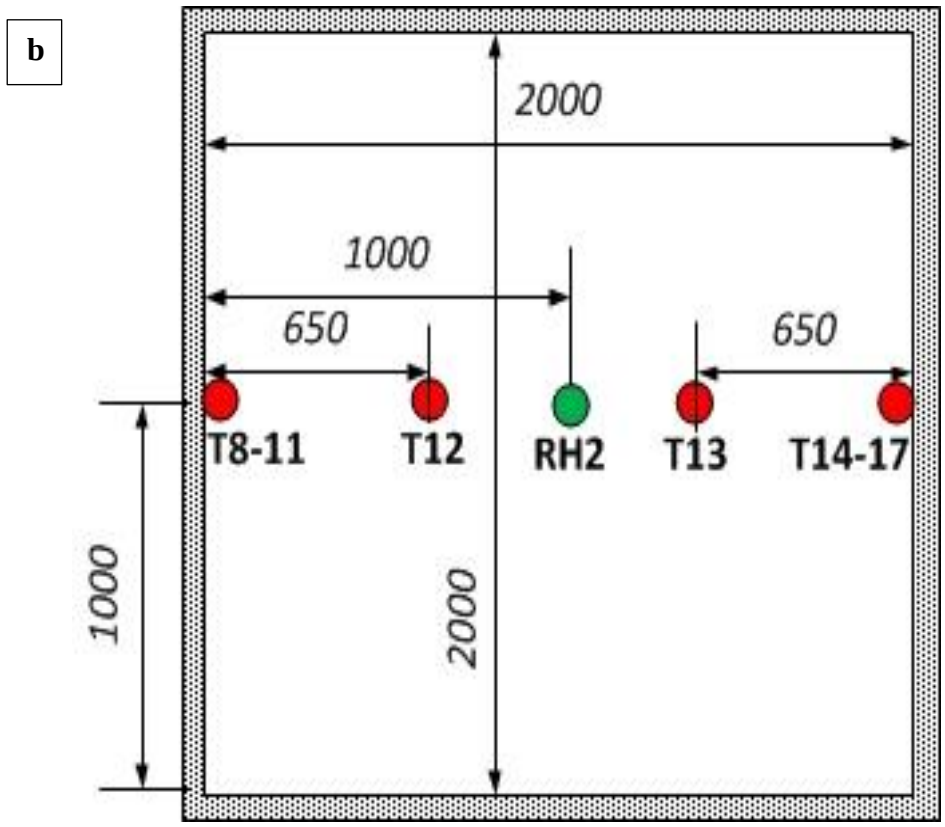

Figure 3.16: Locations of the sensors inside the insulation room (*a*: Cross section, *b*: Top view, unit: *mm*).

The polyurethane foam panels with a thickness of 100 mm are used for the insulation walls and ceiling. Ten T-type thermocouples (of 0.3% accuracy) are installed on the walls and ceiling of the insulation room. One relative humidity sensor (of 3.0% accuracy) is used to determine the relative humidity of the room. The locations of the sensors are shown in **Figure 3.16**. The PCM based TES unit is shown in Section 3.2. As mentioned , there are twenty thermocouples inserted in the interior of PCM based TES unit for measuring the transient responses of the temperature and their locations are shown in **Figure 3.17**.

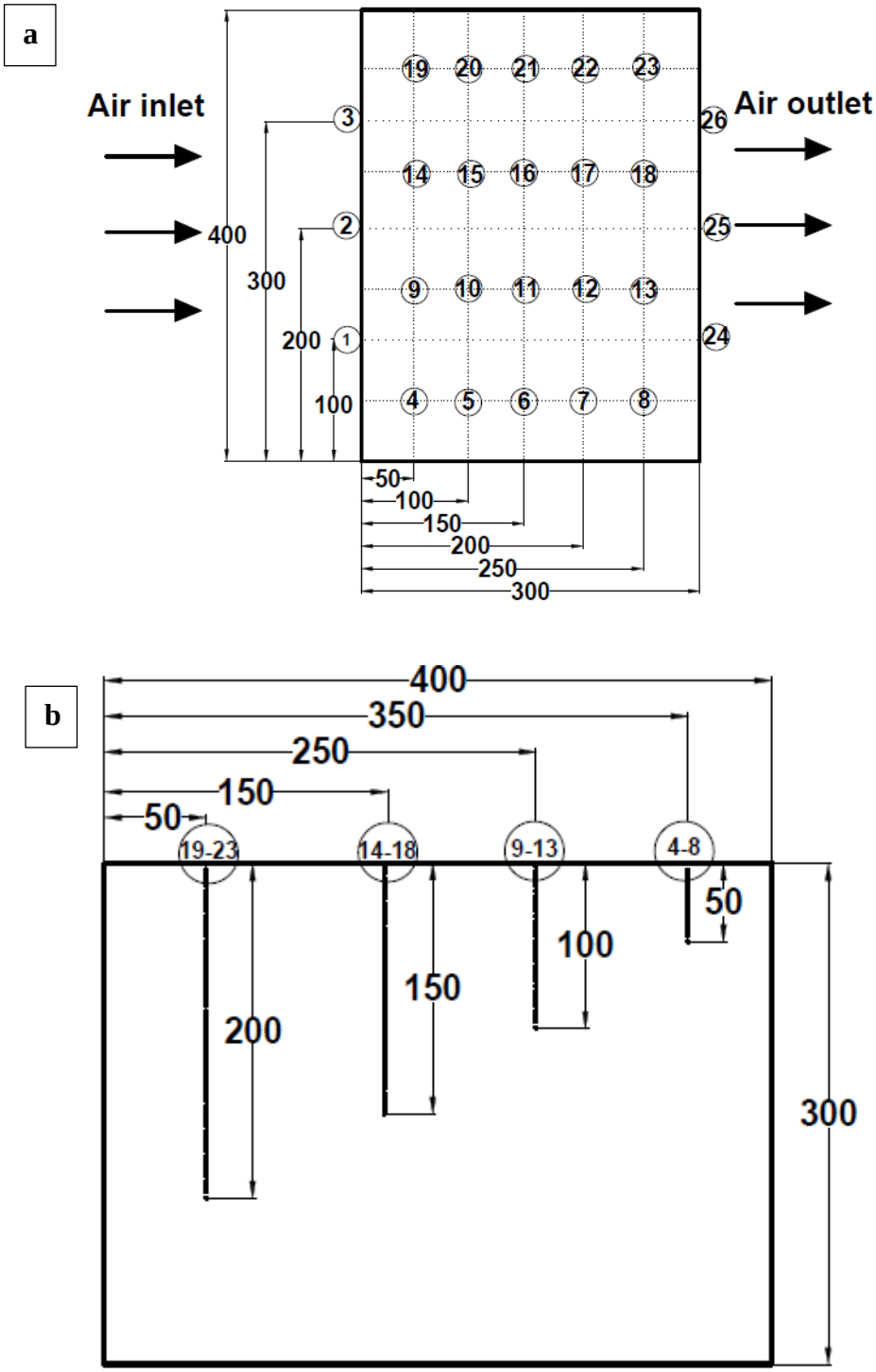

Figure 3.17: Locations of the thermocouple positions inside the TES unit(numbered between 4 and 23):Top view (a); and cross-sectional view (b).

(2) Performance indexes

(a). Electricity saving

The electricity saved by the use of PCM-AC, EC_s, is defined by the following:

$$Ec_s = Ec_{NOR} - Ec_{PCM} \tag{3.37}$$

Where EC_{NOR} is the consumed electricity by the AC; EC_{PCM} is the electricity consumed by the PCM-AC.

The percentage of electricity saving percent is therefore calculated by:

$$Ec_s\% = \frac{(Ec_{NOR} - Ec_{PCM})}{Ec_{NOR}} \times 100\% \tag{3.38}$$

(b). Coefficient of performance (COP)

The system *COP* is defined by:

$$COP = \left| \frac{Q_a}{W_{AC}} \right| \tag{3.39}$$

Where Q_a is the heat flux transferred by air flow; W_{AC} is the power consumption of the air conditioner. The heat transferred by air flow is given by:

$$Q_a = m_a \cdot c_{p,a} \cdot (T_{a,i} - T_{a,e}) \tag{3.40}$$

Where m_a is the air mass flow rate; $c_{p,a}$ is the specific heat capacity of the air; $T_{a,e}$ and $T_{a,i}$ are the air temperature at the exit and inlet of the TES unit, respectively.

(c). Emergency cooling time

In case of the breakdown of the air conditioner and/or electrical power supply fault, cooling cannot be provided by the air-conditioning unit and the room temperature will increase if there are no cold sources. Assuming that the cooling supply must be on when the room temperature is higher than 28^{o}C, the emergency cooling time is defined as the period from the point when the air conditioning stops working and the point when the room temperature rises at 28^{o}C.

(d). Economic analysis

We use the Net present value (NPV) to evaluate the economic feasibility of an investment project. The NPV examines costs and revenues while taking into consideration the time value of money. Considering a project of intel examines costs and revenues while taking into consideration the time value of money. Considering a project of integrating a PCM based TES into a conventional air conditioning system, its NPV can be written as Eq.(3.41) ,

$$NPV = \sum_{y=1}^{lifetime} \frac{C_{red}}{(1+r)^{y}} - C_{inv} \tag{3.41}$$

Where the superscript *lifetime* denotes the service life of the TES unit and r is the discount rate. In this study, the discount rate is chosen as 4%, which is a reasonable value to evaluate the economic performance of decoupled energy storage technologies in the UK[200]. C_{inv} in Eq.(3.41) denotes the total initial investment cost, which consists of two parts: the cost for the TES unit without PCM, C_{ESD}; and the cost for PCM, C_{PCM}. C_{red} in Eq.(3.41) represents the annual cost reduction by the application of PCM-AC system (the cost reduction per day is equal to the cost variation before and after the application of storage system), which, if we assume the system operates 200 days per year, can be given by:

$$C_{red} = D_{ope} * (EC_{Nor} - EC_{PCM}) \tag{3.42}$$

Where Ec_{Nor} represents the daily electricity cost of the normal system and Ec_{PCM} means the electricity cost of the system integrated with the PCM based TES. With the C_{inv} and C_{red}, one can estimate the static payback period as：

$$payback\ \ period = \frac{C_{inv}}{C_{red}} \tag{3.43}$$

Where the cost reduction is assumed to be the same every year.

3.2.6Uncertainly analysis

The overall uncertainty of the measurement results, δR , is due to uncertainties of measurements of various parameters denoted as δX_n [201], which can be calculated by Eq.(3.44).

$$\delta R = \sqrt{\sum_{n=1}^{N} \left(\frac{\partial R}{\partial X_n} \right)^2 \left(\delta X_n \right)^2} \tag{3.44}$$

Under the conditions of this study, the calculated overall uncertainty of the working period is 6.47%, the discharging depth is 9.25% and the discharging power is 8.28%. The overall uncertainty of discharging thermal efficiency and discharging exergy efficiency is 8.98% and 8.64% respectively.

The maximum uncertainty of the transient charging rate is 7.28%; the maximum uncertainty of charging thermal efficiency and exergy efficiency is 8.98% and 7.64% respectively; the maximum uncertainty of the optimal charging depth is 7.91%. The maximum uncertainty of the heat flux is 5.28%; the maximum uncertainty of transient heat transfer coefficient is 5.64%; the maximum uncertainty of the overall heat transfer coefficient is 5.91%. The maximum uncertainty of the COP is 7.6 %.All the maximum uncertainty is within 10%. Therefore, the experimental data is reliable and acceptable. These indicate the reliability of the experiment results.

Chapter 4 Results and Discussions (I): Modelling and experimental validation

4.1 Numerical simulation

Having established confidence in the numerical modelling, the TES device with four fin configurations were simulated. PCMs with different thermal conductivities were also studied for comparison with eh use of fins. Based on the modelling results, a TES device was designed and tested. The results are presented and discussed in the following subsections.

4.1.1 Comparison of TES performances between different fin configurations

During charge, the inlet air velocity and temperature were set at respectively 1.2m/s and 11^{o}C(284.15K). The measured PCM thermal conductivity was used. **Figure 4.1**. As can be seen, the axial air velocity distribution is parabolic in the no fins configuration(**Figure 4.1d**). This indicates a laminar flow regime-consistent with the low Re number (~325) condition. In both fins case, however, the air flow pattern changes significantly, showing regions with increased velocity and flow disturbance(**Figure 4.1c**). Correspondingly, the air temperature increases quickly in both fins case (**Figure 4.1a**) compared to that in the no fins situation (**Figure 4.1b**) due to heat transfer enhancement induced by the air flow turbulence.

Figure 4.2.shows the PCM temperature and liquid fraction contours. One can see that the PCM temperature decreases fast in the both fins case with(**Figure 4.2a)** than that without fins (**Figure 4.2b**). The solidification starts from regions close to the clapboard in no fins case (**Figure 4.2d**), whereas it starts in areas close to the clapboard and the fins in the both fins case (**Figure 4.2c**). The liquid fraction of the PCM reduces around 40% in 58s in both fins case, while it only reduces by ~10% in 295s in the no fins configuration. These results clearly demonstrate a significant heat transfer enhancement by using the both fins configuration due to the increased heat transfer area and air flow disturbance.

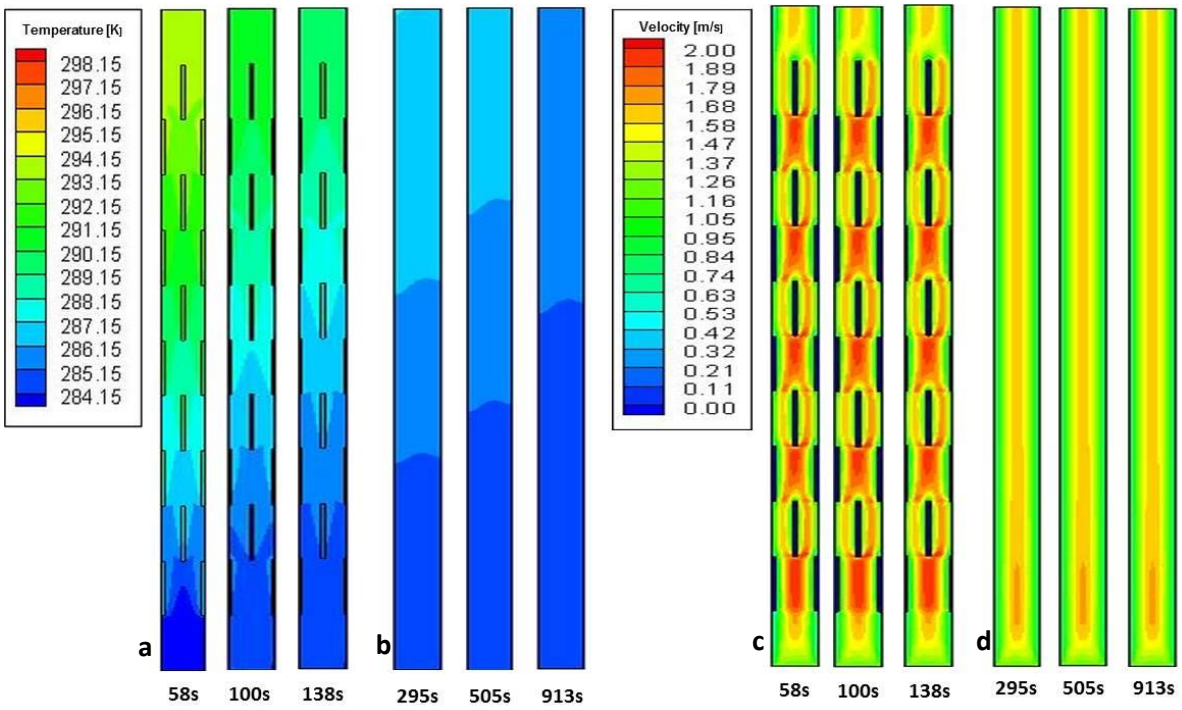

Figure 4.1: Air temperature and velocity contours of the charge process: (a). Air temperature for the both fins configuration, (b). Air temperature for the no fins configuration, (c). Air velocity for the both fins configuration, (d). Air velocity for the no fins configuration.

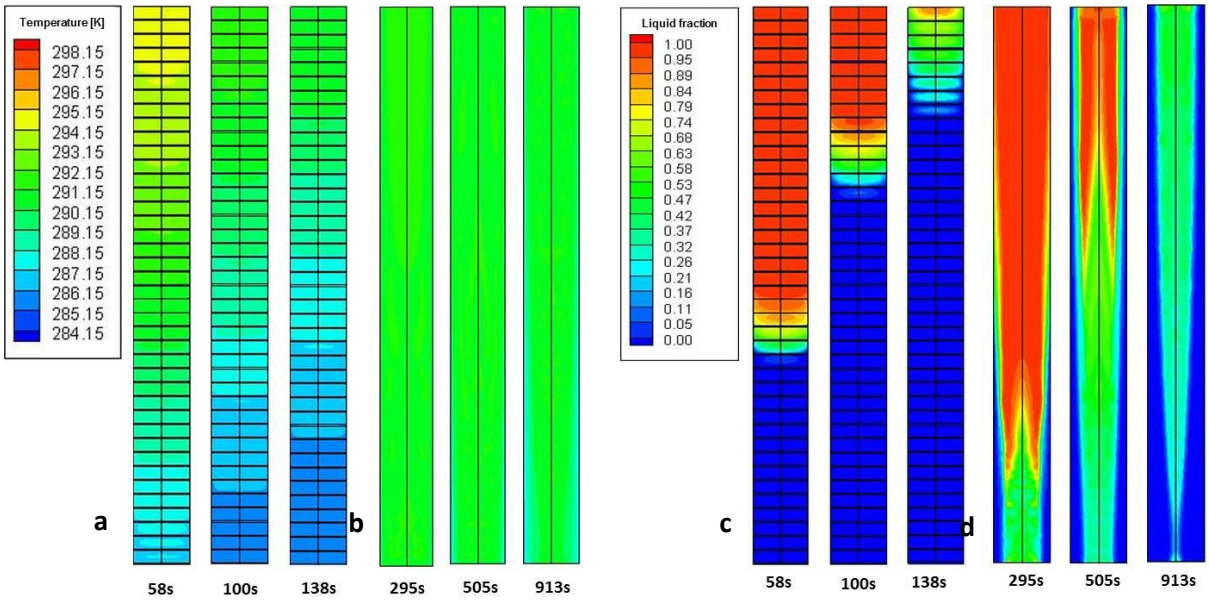

Figure 4.2: PCM temperature and liquid fraction contours during charge: (a). PCM temperature for the both fins case; (b). PCM temperature for the no fins case;(c). PCM liquid fraction for the both fins scenario; (d). PCM liquid fraction for the no fins case.

During discharge, the inlet air velocity and temperature were set at respectively 1.2m/s and 39 ^{o}C (T_{air}=312.15K). The simulated results are shown in **Figure 4.1** and **Figure 4.2**. Similar to the charging behaviour shown in **Figure 4.1** and **Figure 4.2**, more turbulent air flow (**Figure 4.3d**) and faster air temperature reduction (**Figure 4.3b**) can be clearly seen in both fins case than that in no fins situation (**Figure 4.3a** & **Figure 4.3 c**). The PCM starts to melt from areas surrounding fins and the clapboard in both fins case while the melting process starts only from locations close to the clapboard in on fins case. The liquid fraction of PCM increases at a much quicker rate in both fins case (**Figure 4.4c**) than that in the no fins configuration.

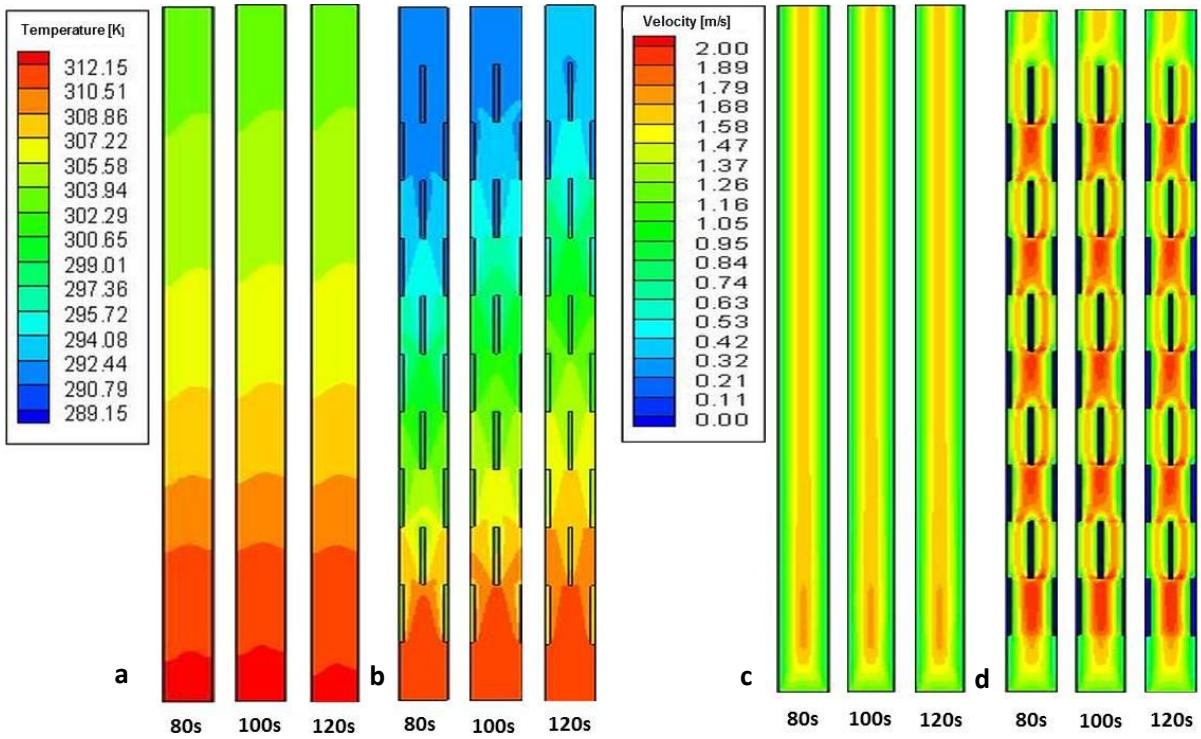

Figure 4.3: Air temperature and velocity contours of discharging process: (a).Air temperature for the no fins case; (b). Air temperature for the both fins case; (c). Air velocity for the no fins case; (d). Air velocity for the both fins case.

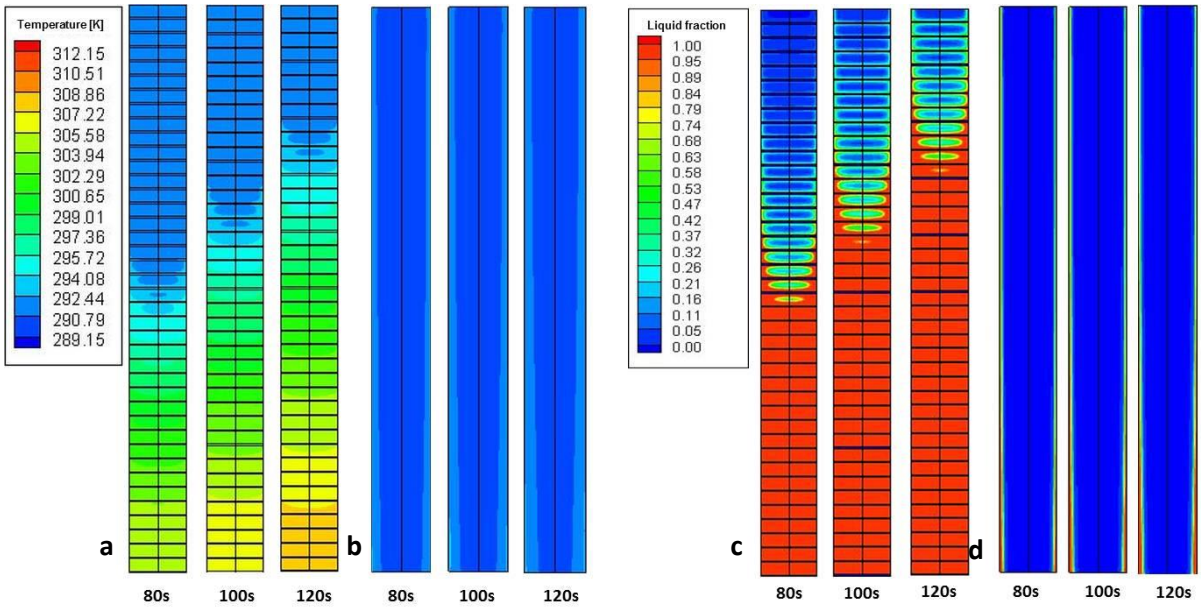

Figure 4.4: PCM temperature and liquid fraction contours of discharging process: (a). PCM temperature for the both fins case; (b). PCM temperature for the no fins case; (c). PCM liquid fraction for the both fins case; (d). PCM liquid fraction for the no fins case.

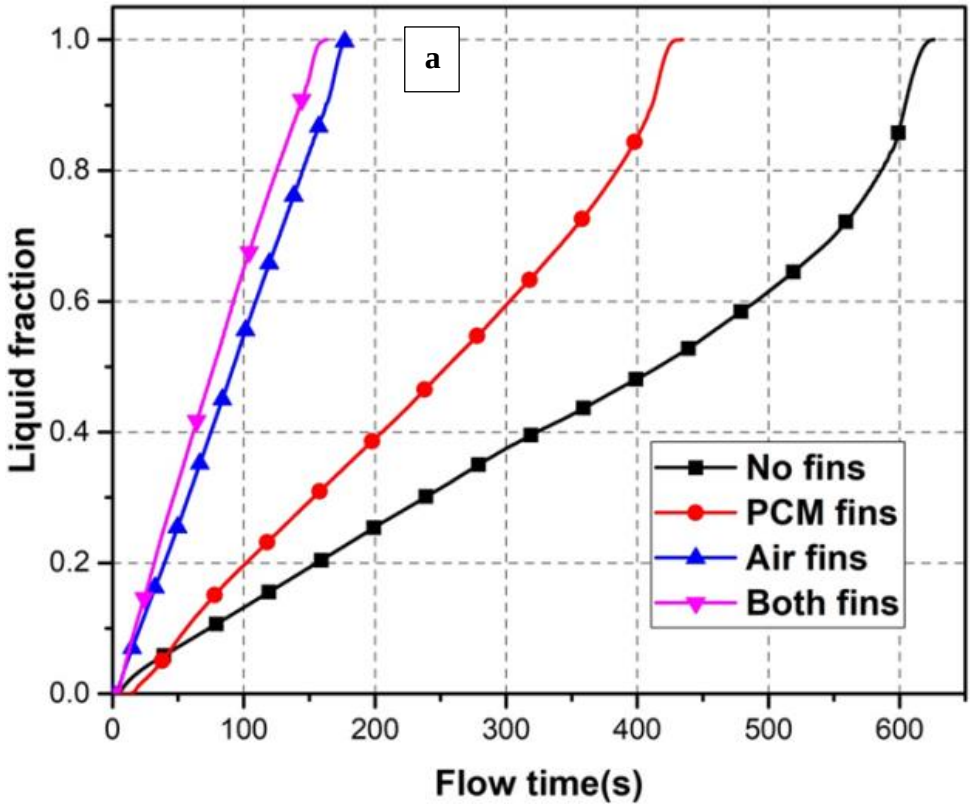

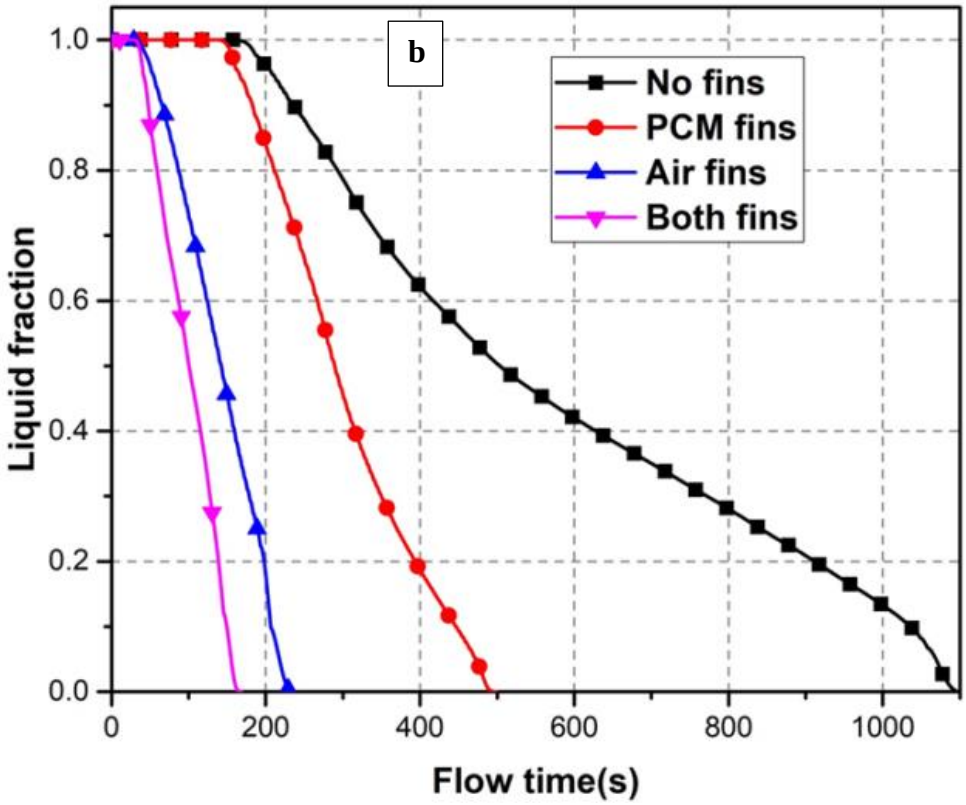

Figure 4.5: Evolution of the liquid fraction during the discharge (a) and charge (b) process with various configurations.

The liquid fraction data in the charge and discharge process shown graphically in **Figure 4.1** to **Figure 4.4** are respectively plotted in **Figure 4.5a** and **Figure 4.5b**. as a function of time. One can see that discharge (melting) process takes ~625s in the no fins case without fins (**Figure 4.5a**); this reduces to 164s for the both fins case. The discharge times for the air fins only and PCM only configurations are 180s and 430s, respectively. In other words, the discharge time reduces by approximately 74% with both fins, 715 with air fins and 31% with PCM fins, in comparison with the no fin case. These data also clearly demonstrate that the air fins are more effective that the use of PCM fins under the conditions of this study (typically used in air conditioning operations).

Figure 4.5b. shows the change of liquid fraction during the charge (solidification) process. The total charge time is found to be 1095s without fins, 168s with both fins, 234s with air fins only and 487s with PCM fins only. Correspondingly, the charge time reduces by approximately 85% with both fins, 79% with air fins and 56% with PCM fins. Clearly, the air fins are more effective than the PCM fins in the charging process. These results are similar to the discharge process discussed above.

4.1.2 Effects of PCM thermal conductivities

From the discussion above, both the air fins and PCM fins contribute to TES device performance enhancement to a significant extent and the air fins are more effective. A question is raised-can we enhance the PCM ide performance through modifying the thermal conductivity of the PCMs? To answer this question, PCMs with different thermal conductivities were examined through modelling and the results were compared with the use of fins. In the modelling, only air fins were used whereas the PCM fins were not used.

Figure 4.6. shows the results. One can see that the discharge time decreases with the increasing PCM thermal conductivity. When the PCM thermal conductivity increases from 0.2(the PCM used in this work) to 1.05 W/m·K, the discharge time reduces to be comparable to the use of the both fins configuration (**Figure 4.6a**). Similarly, for the charging process(**Figure 4.6b**), a PCM with a thermal conductivity of ~0.78 W/m·K would give the same heat transfer enhancement as the use of PCM fins. These comparisons indicate that a similar extent of heat transfer performance enhancement can be achieved by either extending heat transfer area through fins or by using PCMs with a high thermal conductivity(~5 times the PCM thermal conductivity used in this work).

The use of fins will result in a slightly higher manufacture cost and less space for PCM. However, PCMs with desirable phase change temperature and latent heat often do not meet the high thermal conductivity requirement and the modification PCMs by using highly thermally conductive additives also reduces the space or PCM, increases the costs and in some cases increases the complexity(e.g.phase separation). Therefore, the use of fins is still a highly effective option.

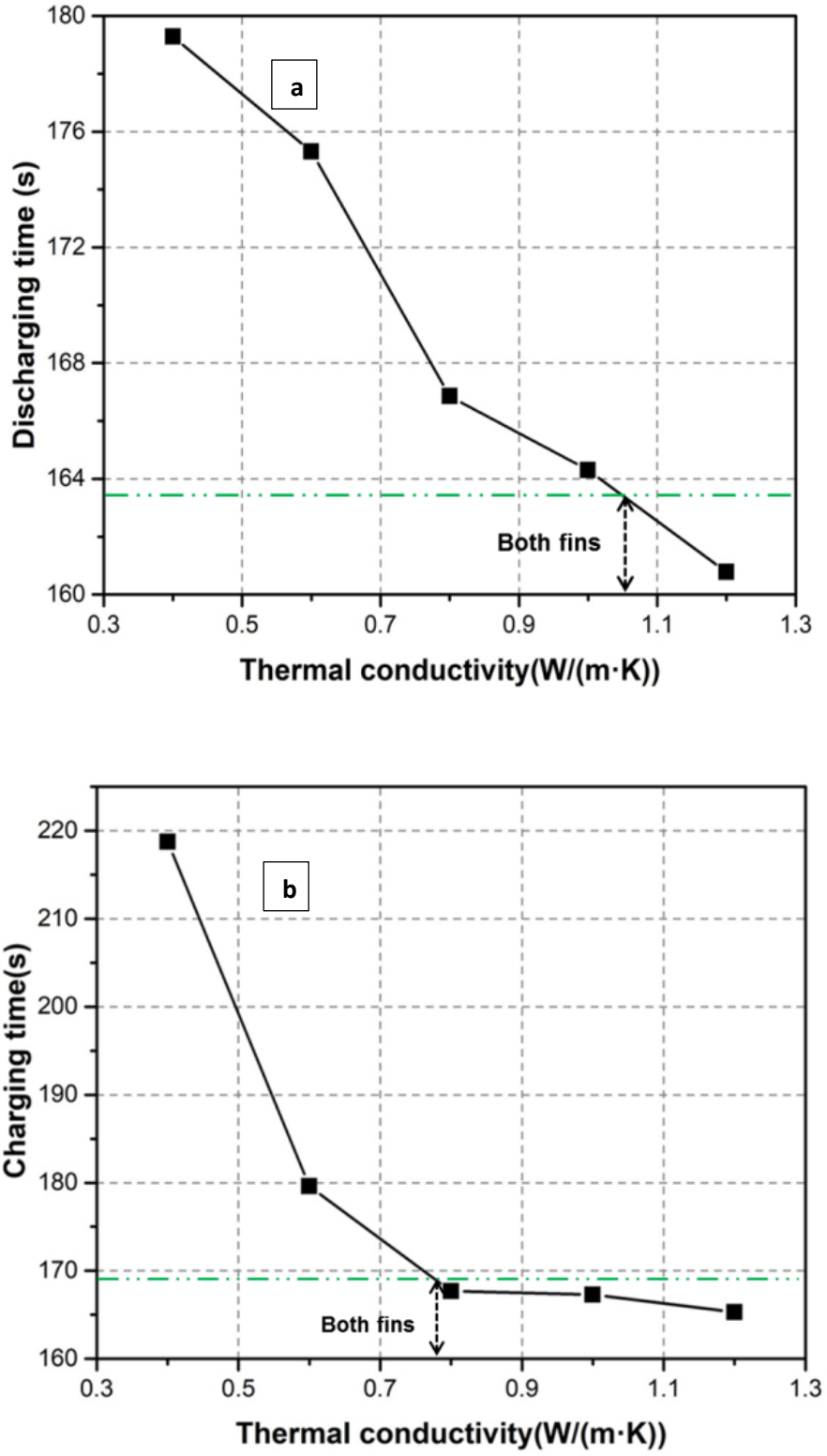

Figure 4.6: Discharge time (a) and charge(b) time with PCM at different thermal conductivity.

4.2 Performance of the TES device with both fins

Based on the results present above, a TES device with both fins was designed and manufactured and integrated with an air conditioning unit; see Section 3.1.3 for the experiment system. The charge and discharge behaviour of such system was investigated and the results are presented in the following.

4.2.1 Evolution of PCM temperature during charge and discharge processes

The charge and discharge behaviour was studied at different inlet air temperatures with a constant average air velocity at 1.25 m/s. **Figure 4.7** and **Figure 4.8**. show the results respectively during discharge and charge process. One can see that the temperature profiles at T1, T3, T5, T7 and T9 are almost the same as those respectively at T2, T4, T6, T8 and T10, indicating a rather uniform lateral temperature distribution in the designed TES device(refer to **Figure 3.4**).

Figure 4.7.also shows that the melting front of the PCM(denoted by the sudden temperature increase) moves with time and the front is diffusive due to reasons mentioned earlier. At the inlet air temperatures studied in this work(30°C and 39°C), the outlet air temperature is seen to be cooled down to around 18°C in seconds and such a temperature is kept constant for ~3600s and 2300s respectively for the air inlet temperatures of 30°C and 39°C.

During charge (**Figure 4.8**), a similar conclusion to the discharge process can be drawn in terms of the lateral temperature distribution uniformity. One can also notice that the motion of the solidification front of the PCM with time as well as the diffusive nature of the solidification front at different axial positions. A comparison between **Figure 4.8a** and **Figure 4.8b** also suggests that a significantly increased charge time would be needed for charges at a high charge temperature; see below for a quantitative comparison.

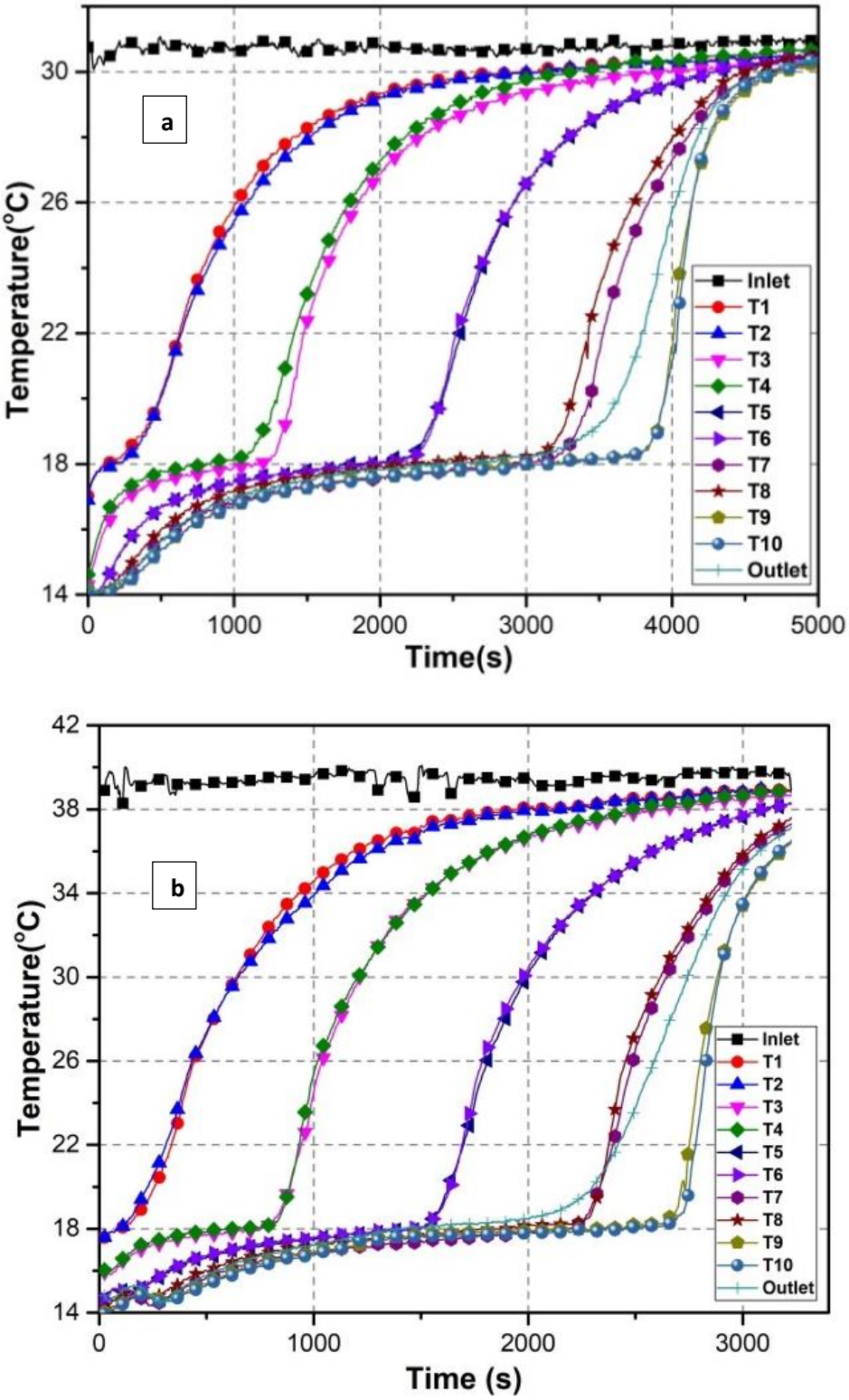

Figure 4.7: Evolution of axial temperature of air and PCM during discharge with air inlet temperature of 30°C(a) and 39°C(b).

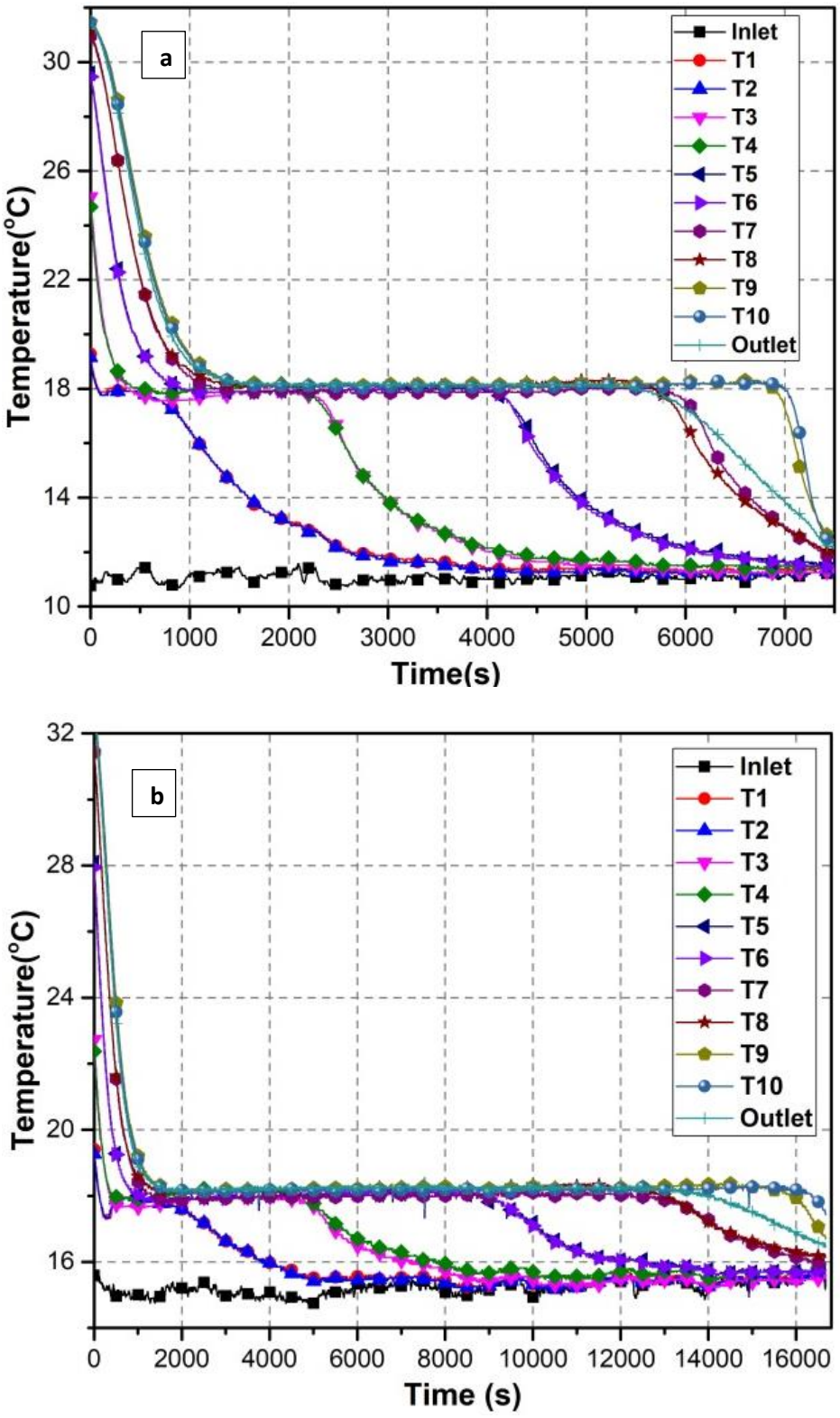

Figure 4.8: Evolution of axial temperature of air and PCM during charge with an inlet air temperature of 11°C(a) and 15°C(b).

4.2.2 TES device operating duration

For normal operation of an air-conditioning system, the outlet air temperature is expected to be between 16-20°C. As a result, we take the operating duration(also termed as the working period) as the period when the TES device has an outlet air temperature between 16-20°C. In addition, we expect an efficient PCM TES device should maintain the outlet air temperature stabilised around the phase change point and hence we regard the PCM based TES device as optimal if the deviation is within 1°C form the phase change point, namely, between 17°C and 19°C in this study, for a long period.

Figure 4.9. shows the operating duration of the designed TES device. One can see that, with a decrease in the inlet air temperature from 40°C to 30°C, the operating duration increases by 58.4%. With the inlet temperature decreases, both the operating duration and optimal operating duration increase, and the optimal operating duration accounts for 67.3%, 56.0% and 56.1% of the total operating period at inlet air temperature at 30°C, 35°C and 40°C respectively.

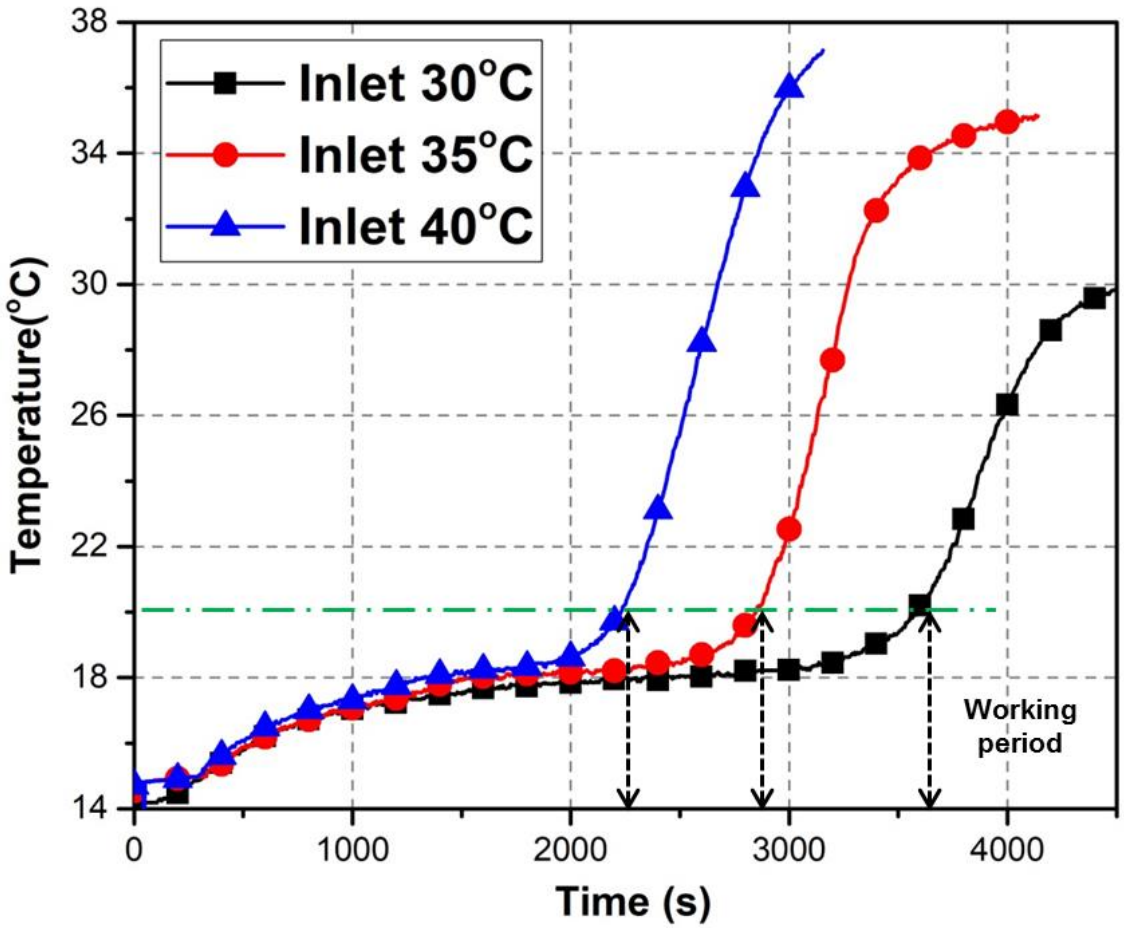

Figure 4.9: Operating duration for the designed TES at inlet air velocity at 1.25m/s.

4.2.3 Comparison of air outlet temperature of the system with and without the TES device

Figure 4.10 compares the air outlet temperature of air conditioning system with and without TES device. It can be seen that the system with the TES device provides a smooth outlet air temperature, whereas the air outlet temperature fluctuates significantly between ~0°C and 17°C every ~300s. Such a highly frequent and high amplitude fluctuation would imply a more frequent start-stop of the compressor, leading to a higher energy consumption and increased level of noise effect. This also clearly demonstrates that the TES based air-conditioning system gives a significantly improved thermal comfort, a much lower noise effect and potentially a lower energy consumption.

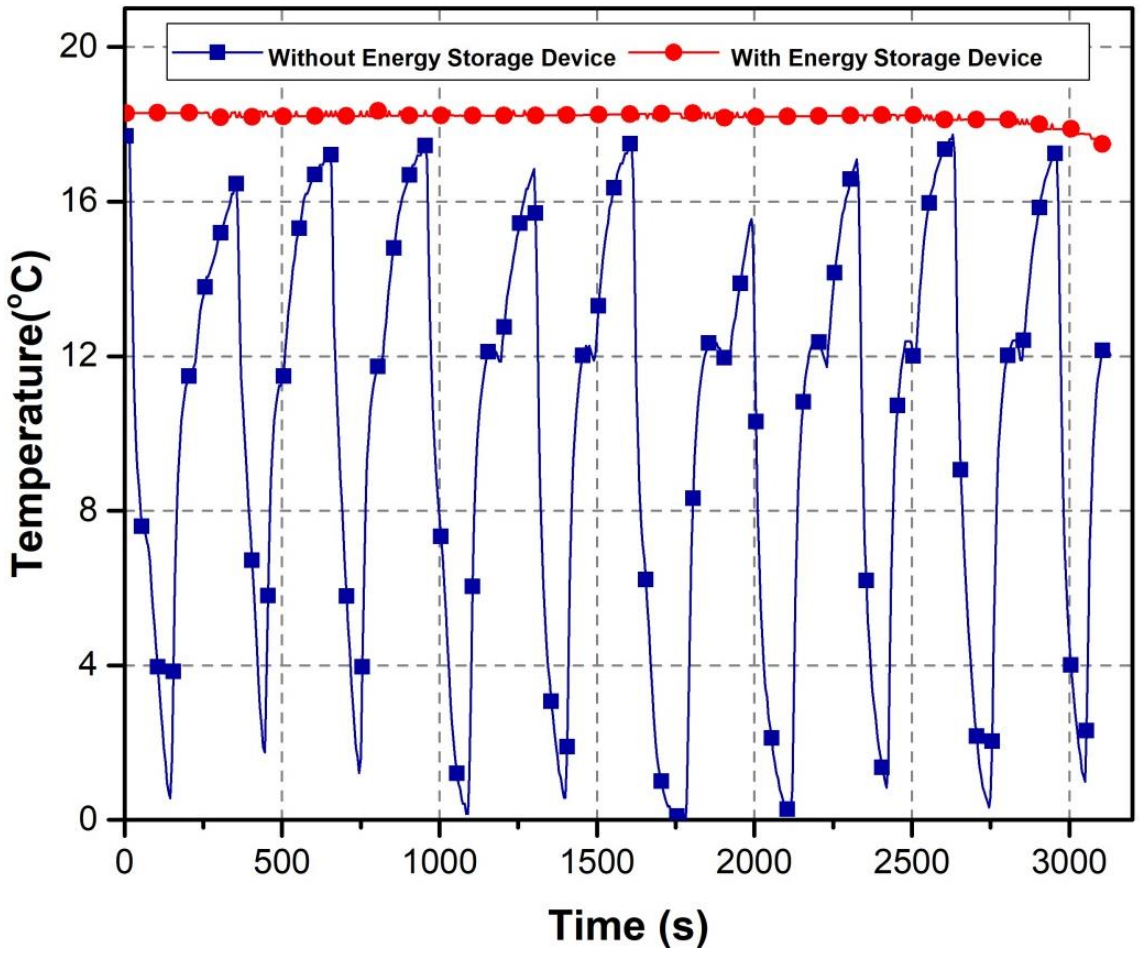

Figure 4.10: Comparison of the air outlet temperature of the system with and without TES device.

4.3 Summary

The effects of utilizing fins in both air and PCM sides were investigated numerically and experimentally. The effects of air fins, PCM fins and model PCMs with different thermal conductivities on the total heat transfer rate during the melting and solidification processes were compared. The charging and discharging behaviours of air conditioning system with the TES device installed were investigated experimentally.

Both the air fins and PCM fins could contribute to the increase of the heat transfer rate with the total reduction of charging and discharging times approximately 85% and 74%, respectively. Hot inlet air could be cooled down by the TES device to the desired temperature range of 16-20°C in seconds showing fast response. What's more, the outlet air has a stable temperature around 18°C for a long time, which is favourable to improve thermal comfort of the transport compartments. The quick thermal response at the beginning of the discharging (cooling) process and the long-period constant outlet air temperature around the PCM phase change point indicates the great advantages of employing the compact latent heat TES device. Hence, an optimum TES device was designed based on the results.

Chapter 5 Results and Discussions (II):

Discharging and Charging performance

A novel compact TES device containing PCM (RT 18 HC) was designed, the charging and discharging performance was experimentally studied in this chapter.

5.1 Discharging performance

In a typical experiment, the TES device was charged by flowing the cold air flow from the air conditioner, which has a temperature of approximately 11oC. The air flow from the TES outlet was vented to the environment. The air temperature from the outlet of the TES was monitored for controlling the charge process, which was stopped when there is no change to the air outlet temperature. The discharging process was then started with all the sensors and data-logging unit checked. The discharging process involved flowing an air through the TES device with the air temperature controlled by mixing the cold air from air-conditioner and hot air from the air heater in the chamber. The inlet air from the chamber was cooled down when flowing through the TES device. To study the performance of the TES device, three different inlet air temperatures (25, 28 and 30 °C) and velocities (0.70 m/s, 0.85 m/s and 1.2 m/s) were examined.

5.1.1 Evolution of PCM temperature over time

Figure 5.1 shows the time dependence of PCM temperatures at two depths of 50mm and 250mm from the TES device surface in the air flow direction for an air temperature of 25 ^{o}C and air flow velocity of 0.85m/s. As shown in **Figure 5.1 a**, with time evolution, the first layer (T6), second layer (T7), third layer (T8) and fourth layer (T9) start melting in turn. At time less than 25 s, only the first layer melts, while the other layers remain in subcooling; when time is longer than 150, 225, 315 s, the second layer, third layer and fourth layer start melting respectively. At time 685 s, the first layer becomes superheating, while the others stay in melting. At 1675, 2005 and 2465 s, the second layer, third layer, and fourth layer go into the superheating region, respectively. It can be clearly seen that the melting time extends along the air flow direction. It is around 660 s for the first layer, 1525s for the second layer, 1780s and 2150s for the third and fourth layers respectively. This is due to the fact that the inlet air temperature of the latter layer is lower than that of the former layer, which results in a small temperature difference of heat transfer between the air and PCM and consequently small heat transfer capacity when the heat transfer coefficient does not change much. Similar phenomena could be found in all layers and one more example at the depth of 50 mm is shown in **Figure 5.1b**.

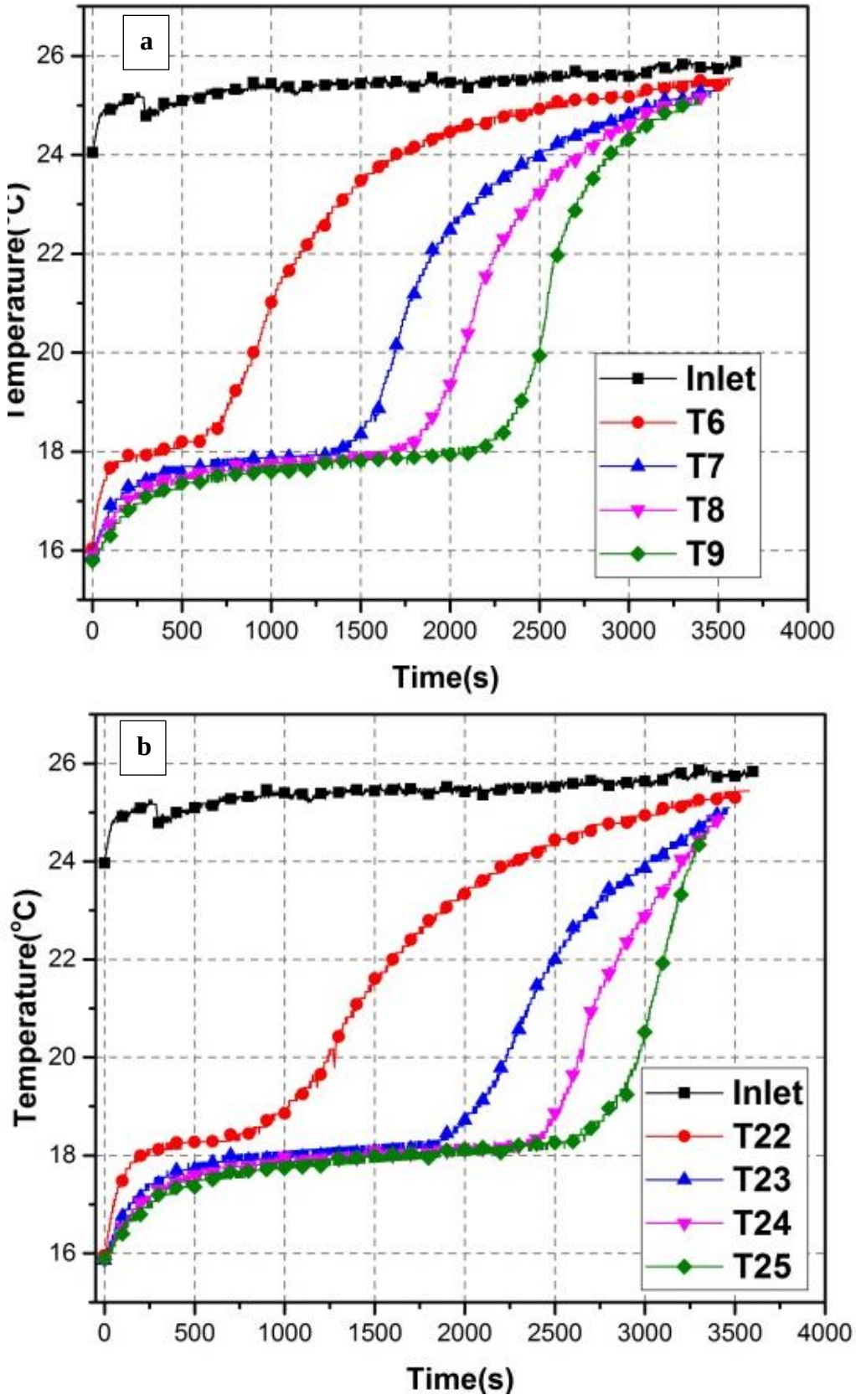

Figure 5.1: Evolution of axial temperature of PCM with processing time at inlet air temperature and velocity 25 °C and 0.85 m/s (a: Depth 250 mm, b: Depth 50 mm).

Figure 5.2 shows the radial temperature distribution of PCM in the TES device, where thermocouples for T6 (8), T10 (12), T14 (16), T18 (20) and T22 (24) are located at the depth of 250, 200, 150, 100 and 50 mm, respectively. As shown, PCM at the bottom (T22 and T24) have longer melting time, compared with that in the other positions, which is possibly due to the turbulence and convection flows in the air flow channel, where cold air prefers going down to the bottom and hot air going up to the top, and correspondingly PCM at the bottom melts slower.

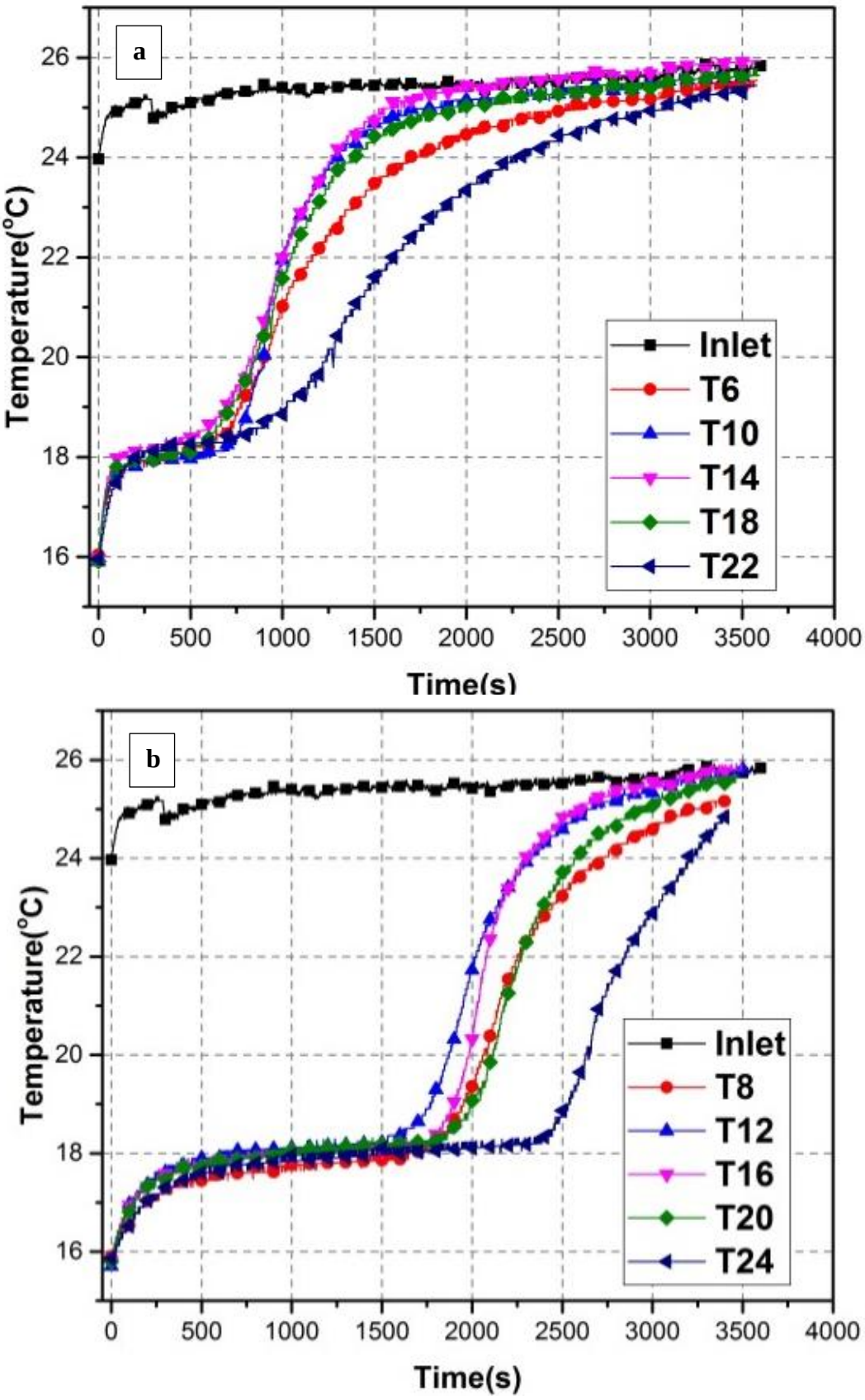

Figure 5.2: Evolution of radial temperature of PCM with processing time at inlet air temperature and velocity 25 °C and 0.85 m/s (a: Layer 1, b: Layer 3).

5.1.2 Outlet air temperature and working period

In the rail carriages, the desired supply air temperature is in the range of 16-20 ^{o}C. Hence, the outlet air temperature will be a key parameter to evaluate the performance of the TES device. As shown in **Figure 5.3**, the outlet air of the TES device could reach the desired temperature (16 ^{o}C) in seconds for all the studied inlet air temperature and velocity conditions, illustrating good heat transfer performance of the TES device. With time, the outlet air temperature is seen to increase first quickly from 16 to 17 ^{o}C, then very slowly from 17 to 19 ^{o}C, and, finally quickly again to reach the inlet air temperature. Both initial and final fast increases in the temperature is mainly due to the release of a small amount of sensible heat in the sub-cooling (solid) and sup-heating (liquid) regions (specific heat capacity ~2kJ/kg·K over a small temperature difference), respectively. The slow increase is due to the latent heat of the PCM in the phase change region (220 kJ/kg).

At a given air velocity, the outlet air temperature reaches 20^{o}C more quickly at a higher inlet air temperature. This is due to the greater temperature difference between the air and PCM, leading to a faster heat transfer. Given the inlet air temperature, a shorter duration is needed for the outlet air temperature to reach 20 ^{o}C at a higher air velocity. This is mainly due to an increased heat transfer coefficient due to the increased air velocity. The results indicate that the TES device could supply stable air temperature of ~18 ^{o}C for ~1 hour under suitable inlet air temperatures and/or air velocities, thus enabling an easy control to achieve thermal comfort of passengers in rail cabins.

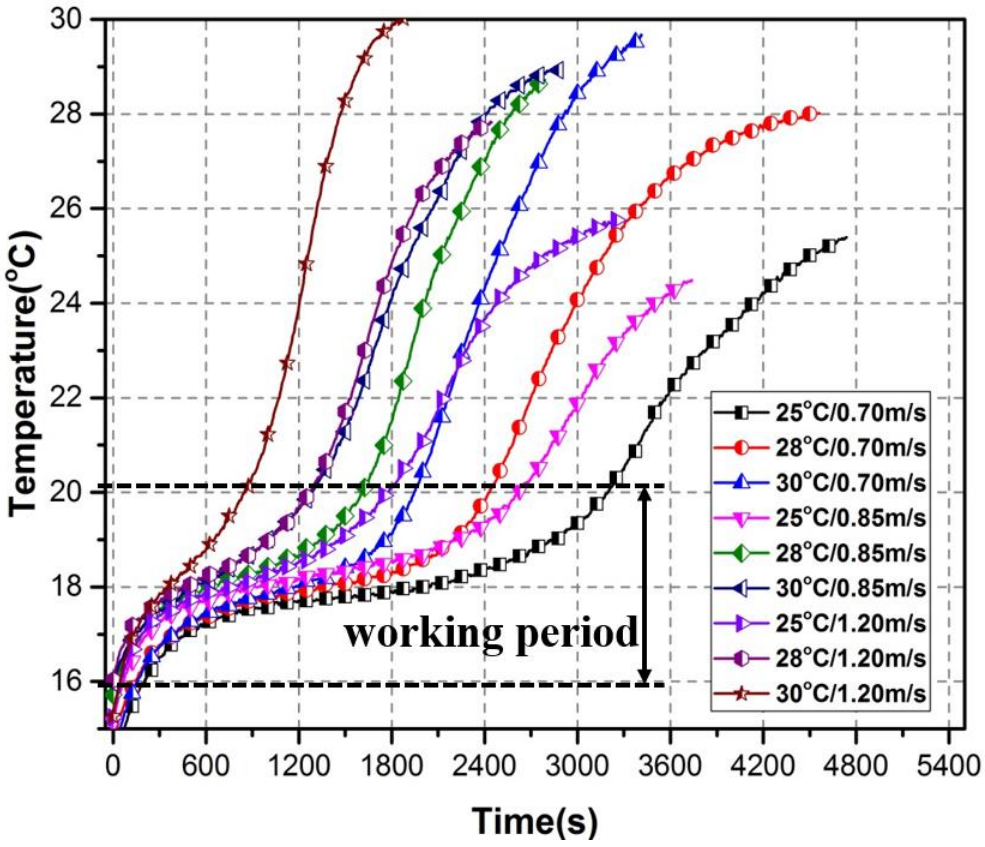

Figure 5.3: Evolution of outlet air temperature with processing time at different inlet air temperature and velocities.

Working period is a parameter showing how long the TES device could work. **Figure 5.4** shows the working period under different air inlet temperatures and velocities. One can see that the higher the inlet air temperature or the velocity, the lower the working period. For a given air velocity of 0.7 m/s, the working period decreases from 3080 to 1775 s when the inlet air temperature increases from 25 to 30 ^{o}C. This is because a higher inlet air temperature gives a greater temperature difference, leading to faster consumption of the cold energy stored in the TES device. At an inlet air temperature of 30 ^{o}C, the working period decreases from 1775 to 815 s when air velocity increases from 0.7 to 1.2 m/s, which results mainly from the increase in the heat transfer coefficient and air mass flow rate.

5.1.3 Discharging depth

For the TES device, it is valuable to evaluate the degree of the stored cold energy being released during the discharging process. **Figure 5.4** shows the discharging depth at different inlet air temperatures and velocities.

One can see that the discharging depth is above 97% under all investigated conditions, indicating a high heat transfer performance of the TES device. At a given inlet air velocity of 1.2 m/s, the discharging depth slightly decreases from 98.1% to 97.10% when the air temperature increases from 25 ^{o}C to 30 ^{o}C. Such a trend is also noticed when the inlet air velocity is increased at a given inlet air temperature. This is because an increase in either the inlet air temperature or the air velocity increases the air heat load. However, the change in the discharge depth is small under the conditions investigated in this study. These indicate the high heat transfer performance of the TES device that can work efficiently over a fairly wide range of operating conditions, providing relatively high tolerance for the design of the integrated PCM based TES device with the air-conditioning system.

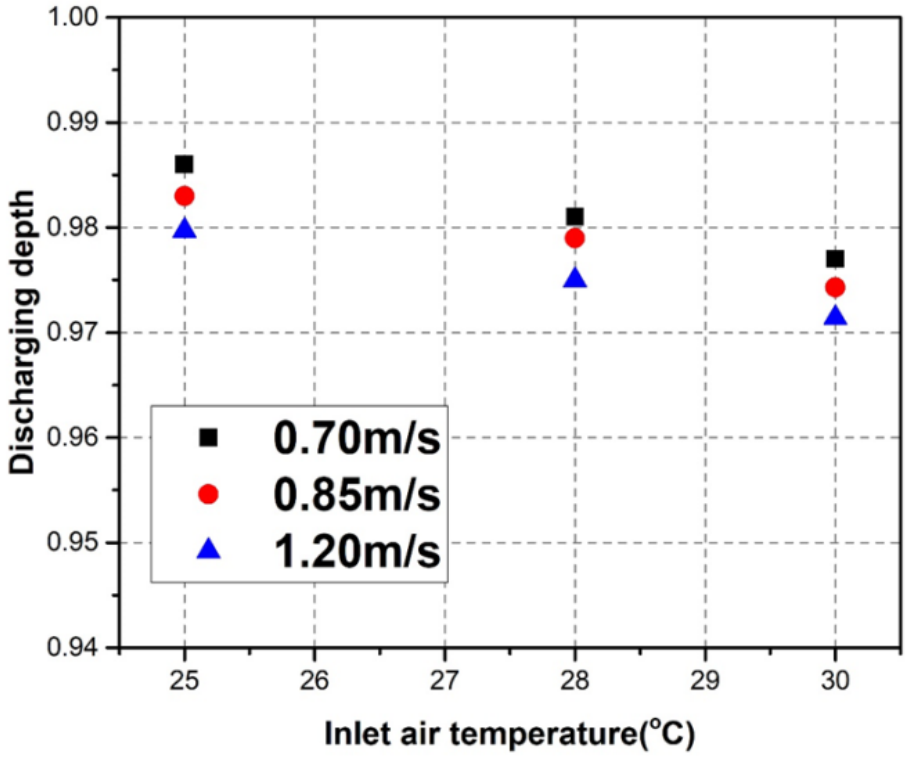

Figure 5.4: Discharging depth with different inlet air temperature and velocity.

5.1.4 Discharging power

Discharging power is of great importance to the TES device, which reflects its cooling capacity. **Figure 5.5** shows the transient discharging power during the working period at different inlet air temperatures. As shown in **Figure 5.5a**, at inlet air temperatures 28 and 30 ^{o}C, the average discharging power is 1.10 and 1.30 kW, respectively. Higher inlet air temperature is favourable to the discharging power. Air velocity also has a large

effect on the discharging power, as shown in **Figure 5.5b**. When the inlet air temperature is 28^{o}C, the average discharging powers are 1.10, 1.20, and 1.70 kW at air velocity 0.7, 0.85 and 1.2 m/s respectively. Larger air velocity is beneficial to exact more cooling capacity.

The results also indicate that the designed TES device has flexibility in regulating the output cooling power, with a maximum of 2.6 kW and a turndown ratio of ~2.4 under the conditions of this study. The results also indicate that the PCM based TES can also be a back-up on top of peak shaving for mechanical refrigeration systems.

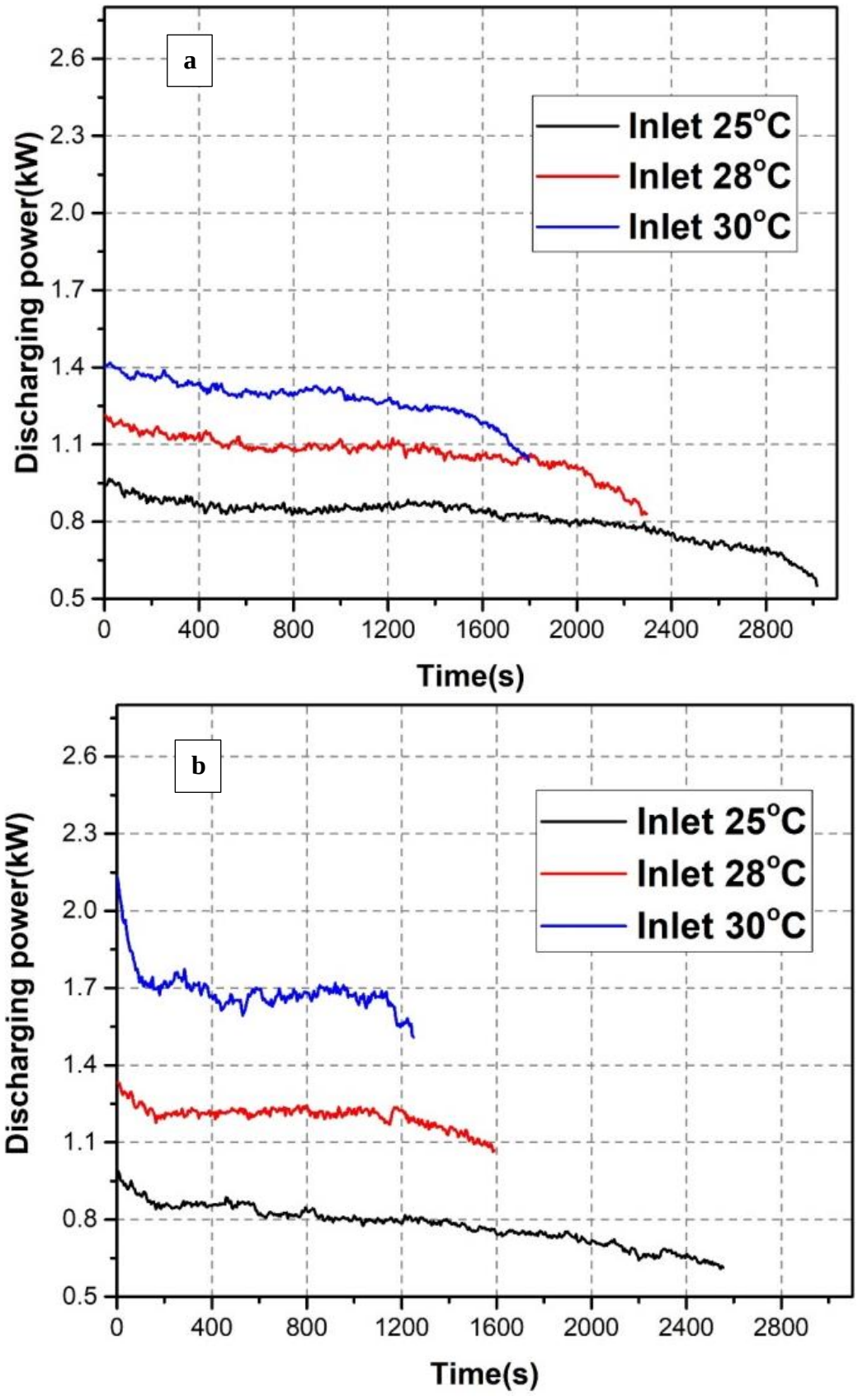
a
Inlet 25°C
Inlet 28°C
Inlet 30°C
Discharging power(kW)
Time(s)
b
Inlet 25°C
Inlet 28°C
Inlet 30°C
Discharging power(kW)
Time(s)

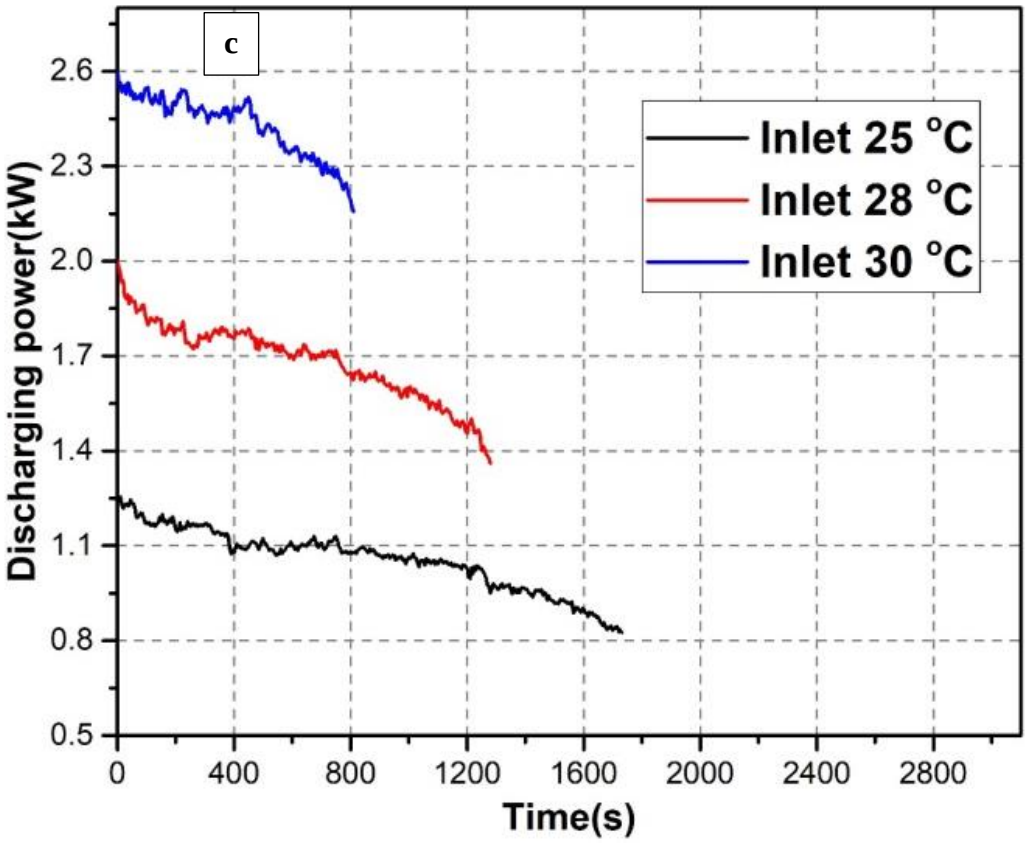

Figure 5.5: Discharging power during working period with different inlet air temperature and velocity (a: 0.70 m/s; b: 0.85 m/s; c:1.20 m/s).

5.1.5 Discharging thermal efficiency

Discharging thermal efficiency is a parameter that assesses thermal insulation performance of the TES device, which is shown in **Figure 5.6**. It could be seen that the discharging thermal efficiency is quite high. For the velocities of 0.7, 0.85 and 1.2 m/s, the thermal efficiencies for the investigated temperature range could reach 86.79% - 99.80%. This indicates good thermal insulation for the designed device and investigated processing conditions.

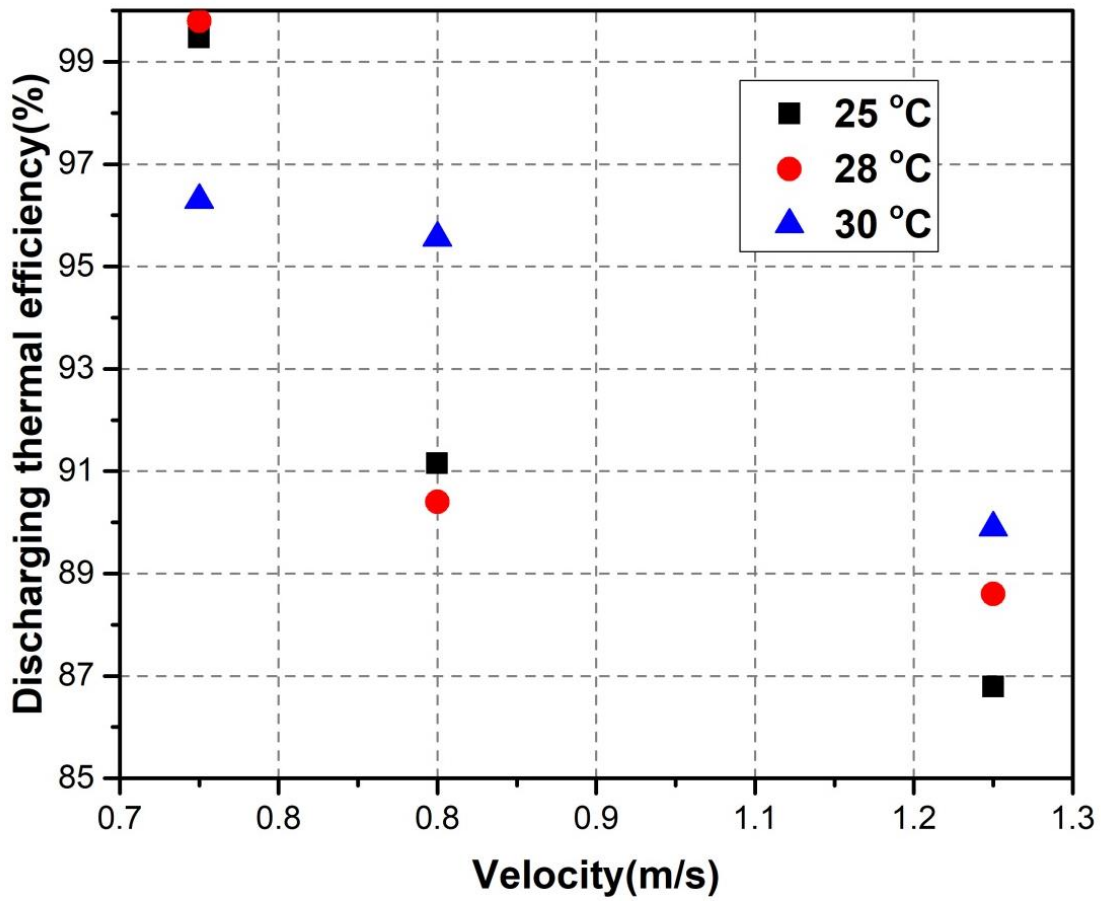

Figure 5.6: Discharging thermal efficiency with different inlet air temperature and velocity.

5.1.6 Discharging exergy efficiency

Discharging exergy efficiency presents the irreversible energy loss due to the temperature difference during heat transfer. **Figure 5.7** shows the influence of air velocity and temperature on exergy efficiency. For all the given velocities, with the increase of inlet air temperature, the discharging efficiency drops. It declines from 43.34% to 41.23% when the temperature increases from 25 to 30 ^{o}C at the velocity of 0.70 m/s. This is due to the larger temperature difference between heat transfer fluid and storage material.

The obtained results also show that the discharging exergy efficiencies decrease with the increase of the inlet air velocity. For the temperature at 25 ^{o}C, the discharging efficiency declines from 43.34% to 40.32% with the velocity increases from 0.70 to 1.20 m/s. For the certain amount of energy storage materials and heat transfer area, the higher air flow rate leads to more exergy loss.

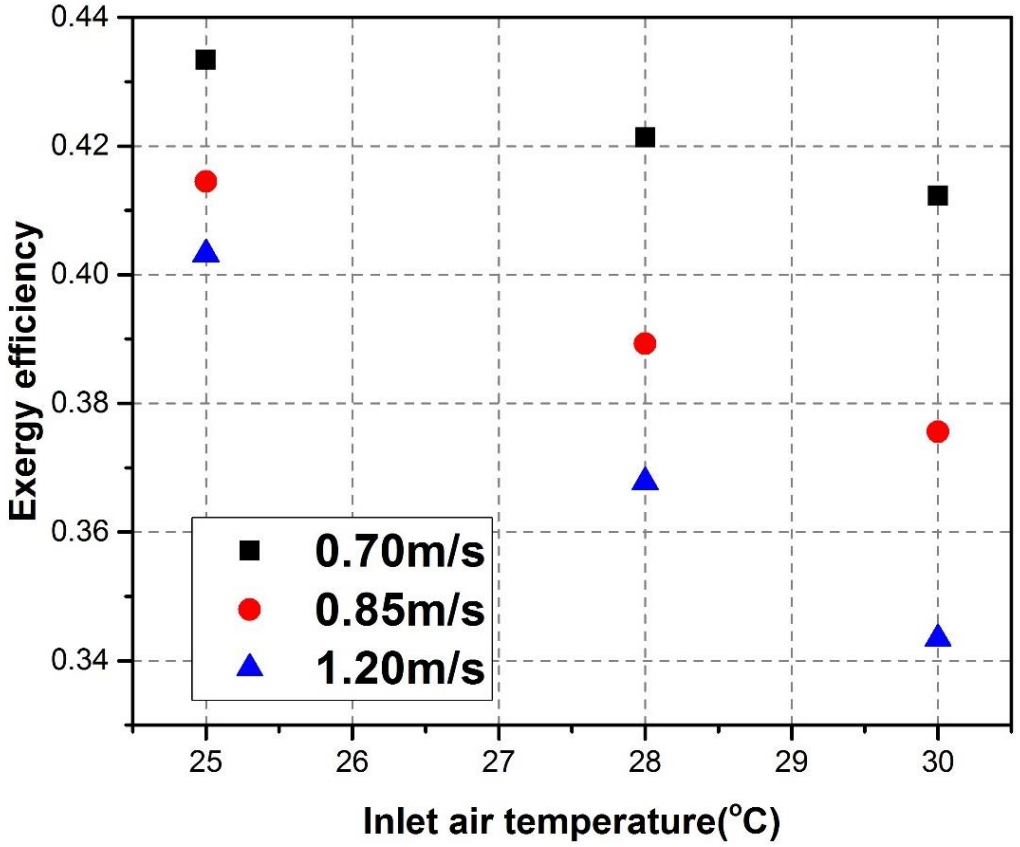

Figure 5.7: Discharging exergy efficiency with different inlet air temperature and velocity.

5.2 Charging performance

5.2.1 Evolution of PCM temperature with charging time

Figure 5.8shows the temperature distributions of PCM in the air flow direction at the inlet air temperature 11 °C, velocity 0.70 m/s and the initial PCM temperature 30 °C. As shown in **Figure 5.8 a**, with time evolution, the first layer (T4), second layer (T5), third layer (T6), fourth layer (T7) and the fifth layer (T8) begin to congeal in turn. When time is less than 125 s, only the first layer congeals, while the other layers remain in superheating; when time is beyond 550 s, the last layer starts to congeal. As time increases to 1275 s, the first layer becomes solid totally indicating the complete charging, while the other layers finish charging at 2100, 2900, 3420 and 3775 s respectively. It could be clearly seen that the congealing time extends gradually from the first layer to the last layer. This is due to the fact that the air temperature at the latter layer is higher than that of the former layer, which results in a lower temperature difference of heat transfer between the air and PCM in the latter layer and

consequently less heat transfer capacity when the heat transfer coefficient does not change much. Similar phenomena could be found at different depths of thermocouples and the results at depth 150 mm are shown in **Figure 5.8b**.

In addition, the congealing behaviours of PCM in the radial direction/depth are also revealed, through placing thermocouples at different depths in each layer. As shown in **Figure 5.9**, taking the first layer and last layer as examples, it can be found that the bottom part of PCM (T19 and T23) congeals slower than other positions and has longer congealing time. The reason is not clear right now and remains to be disclosed.

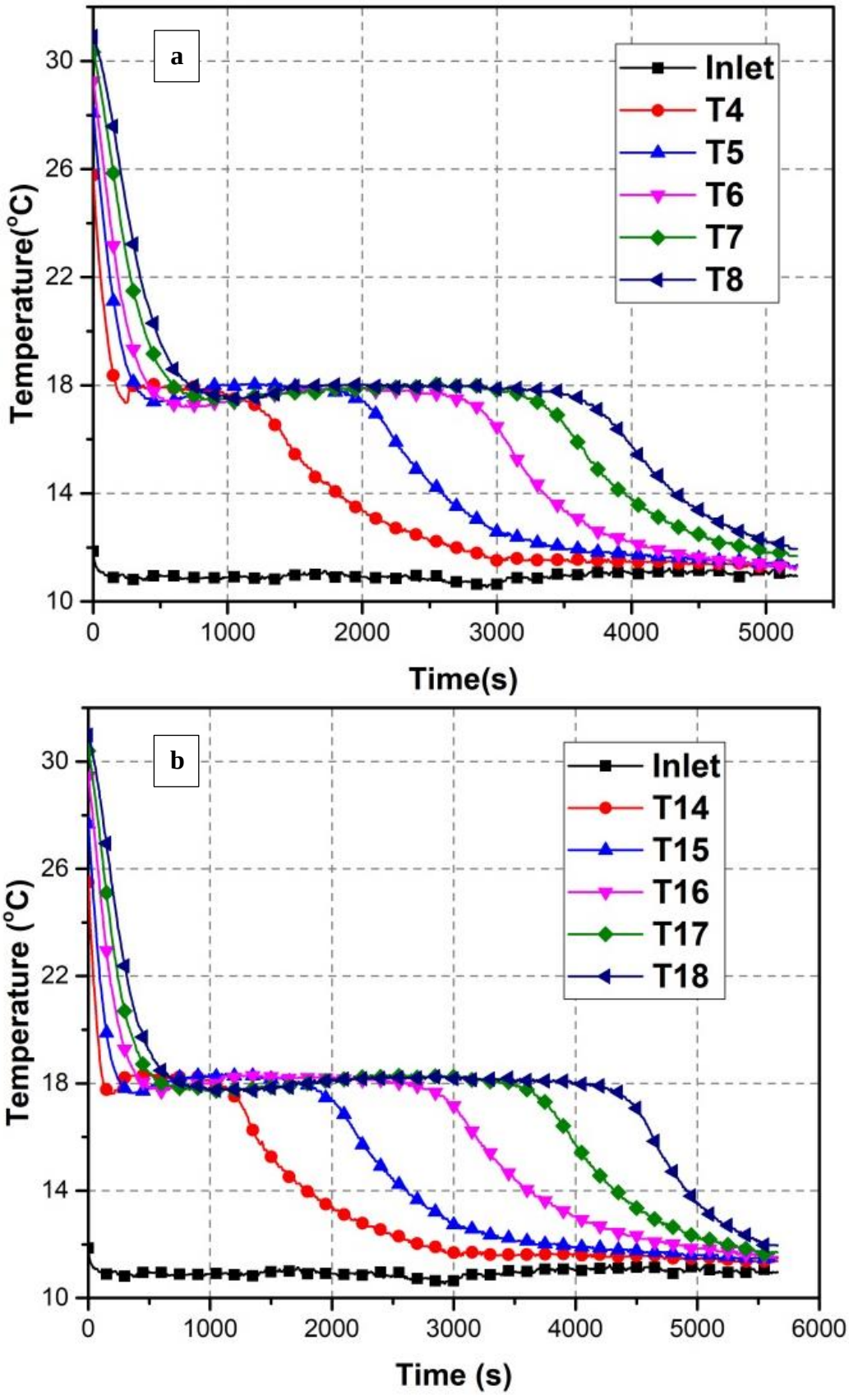

Figure 5.8: Evolution of axial temperature of PCM with the charging time at inlet air temperature 11°C, velocity 0.70 m/s, initial PCM temperature 30°C and depths: (a) 50 mm, , (b) 150 mm.

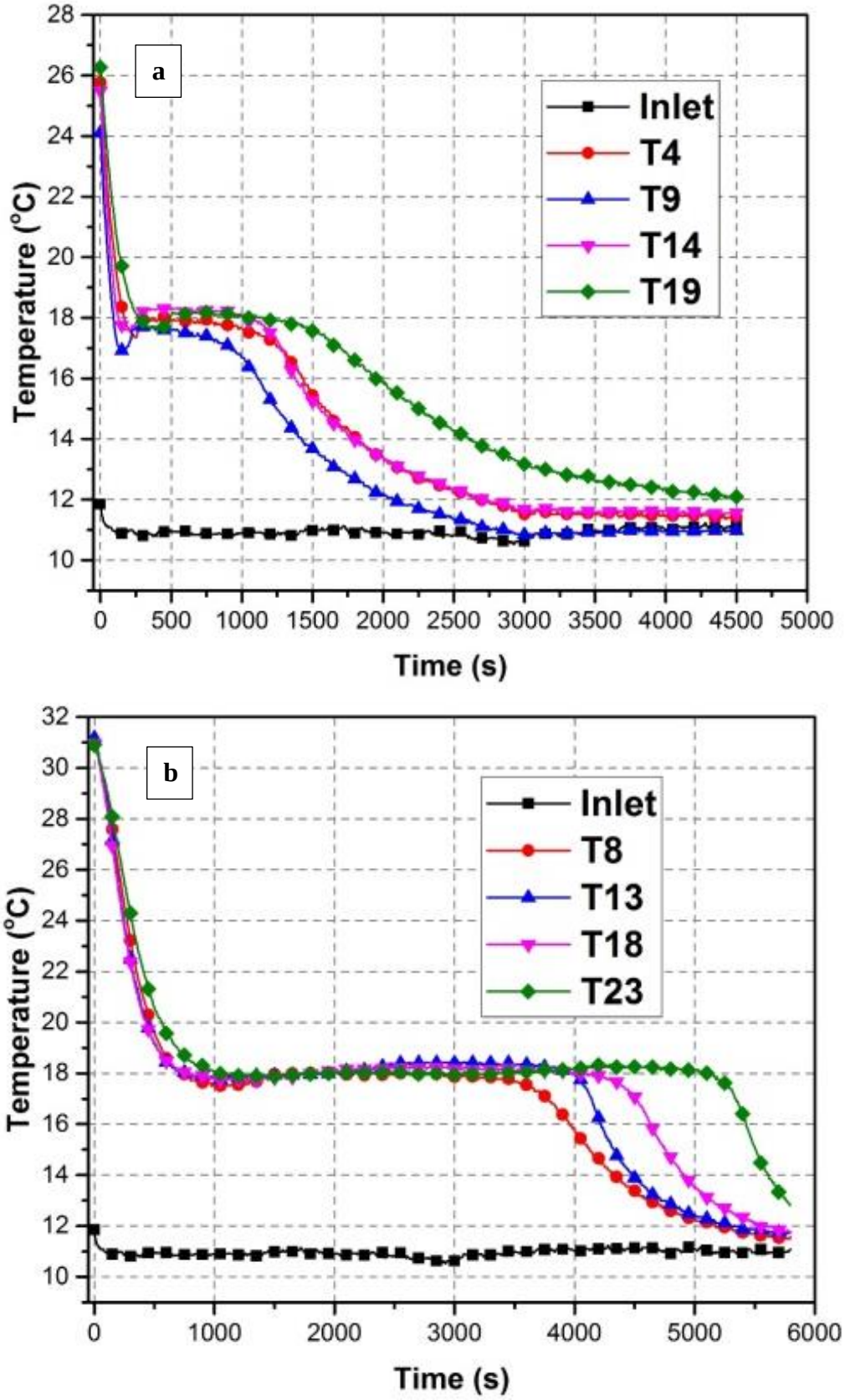

Figure 5.9. Evolution of radial temperature of PCM with the processing time at inlet air temperature 11 °C and velocity 0.70 m/s (a: Layer 1, b: Layer 5).

5.2.2 Charging time

Charging time shows how long the TES device can be fully charged. **Figure 5.10** illustrates the variations of charging time with different inlet air temperatures and velocities. As can be seen, the charging time increases with the inlet air temperature and decreases with the inlet air velocity. At the air velocity 0.7 m/s, as inlet air temperature decreases from 15 to 11 ^{o}C, the charging time decreases around 50% from 10450 s to 5340 s. This is due to the fact that the higher temperature difference leads to the larger heat transfer capacity, and correspondingly the cold energy of the air will be stored in the PCMs faster. At inlet air temperature 15 ^{o}C, when air velocity increases from 0.7 to 1.2 m/s, the charging time decreases around 27% from 10450 s to 7635 s, which results from the increased heat transfer coefficient and air mass flow rate.

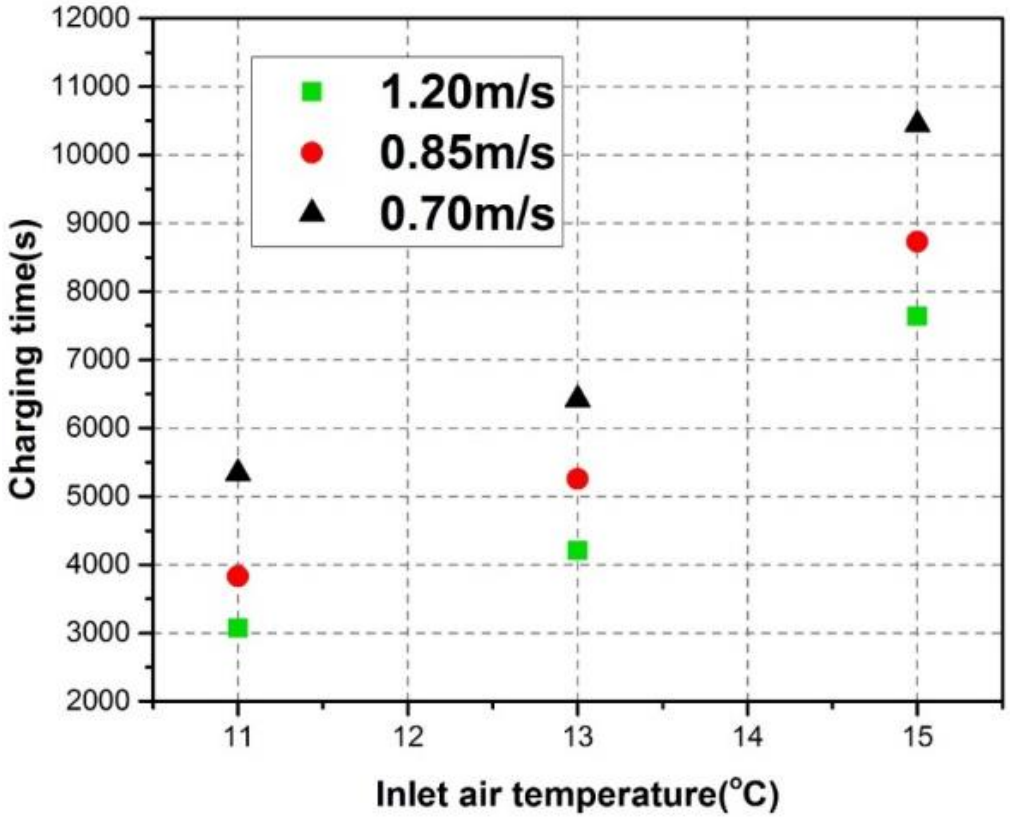

Figure 5.10: Charging time at different inlet air temperature and velocity.

5.2.3 Transient charging rate

Charging rate is of great importance to the TES device, which reflects its heat transfer characteristics. **Figure 5.11** illustrates the transient charging rate under different inlet air temperature and velocity. As shown, with time evolution, the charging rate decreases sharply at the beginning (superheating period of PCMs) and then keeps relative stable for a long time (phase change period of PCMs). Finally, it decreases gradually to 0 kJ/s (subcooling period of PCMs). What's more, when the charging temperature decreases, the steady charging rate will be higher correspondingly. For the given inlet air temperature 11^{o}C, the steady charging rate increases from 0.80 to 1.30 kJ/s as the air velocity increases from 0.70 to 1.20 m/s.

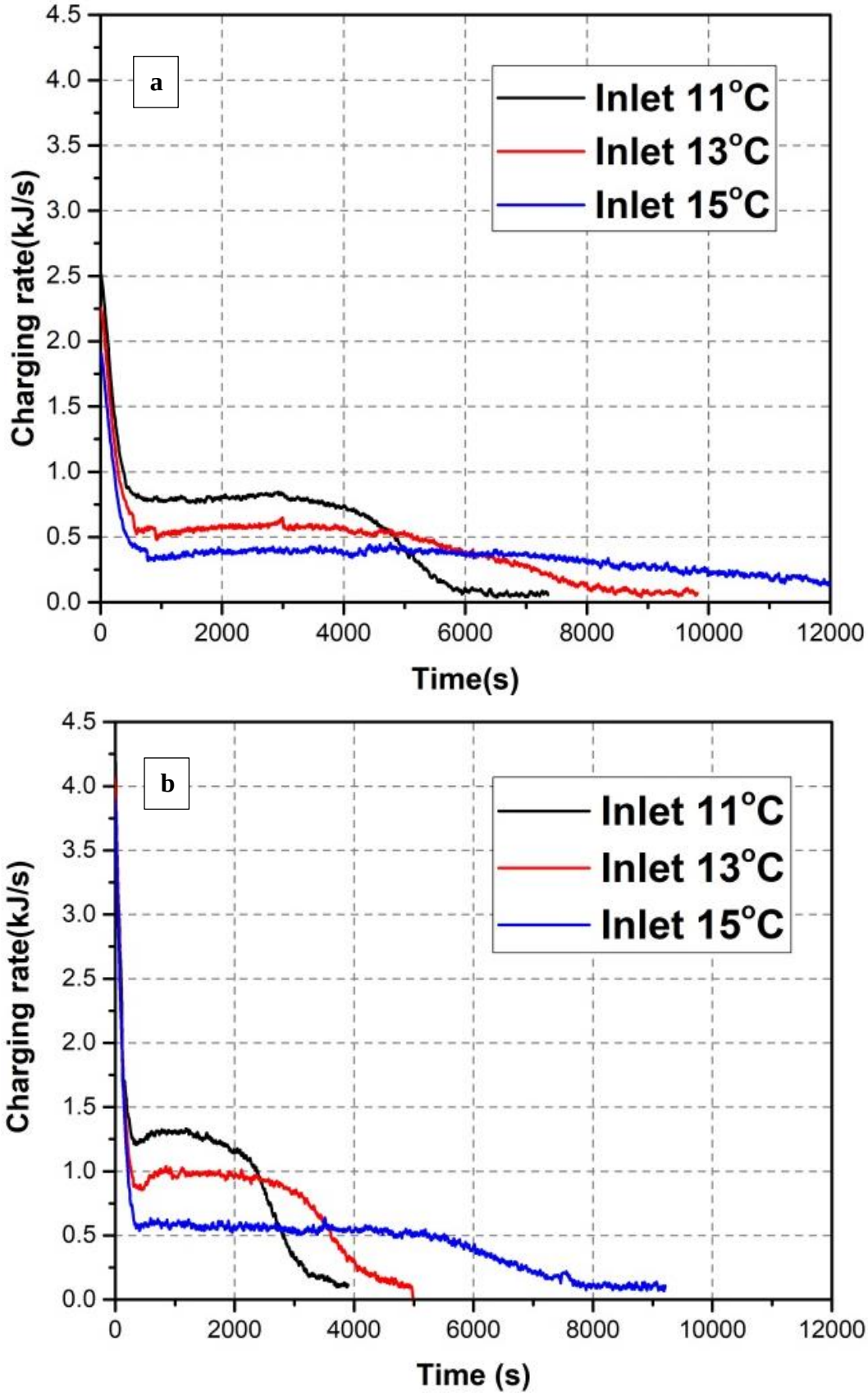

Figure 5.11: Transient charging rate at different inlet air temperature and velocity (a: 0.70 m/s, b:1.20 m/s).

5.2.4 Charging thermal efficiency

Table 5.1 shows the thermal efficiency of the charging process. It can be seen that the charging thermal efficiency is quite high, which indicates good heat transfer and thermal insulation. For the air velocity 0.7, 0.85 and 1.2 m/s and inlet temperature 11^0C, the thermal efficiency within the studied temperature range could reach 72.91%, 87.01% and 84.72%, respectively.

Table 5.1: Thermal efficiency of the whole charging process.

Inlet air temperature (°C)	Inlet air velocity (m/s)		
	0.70	0.85	1.20
11	72.91%	87.01%	84.72%
13	70.82%	82.22%	79.94%
15	66.74%	77.35%	71.98%

5.2.5 Charging exergy efficiency

Charging exergy efficiency represents the energy utilization effectiveness in the charging process and also indicates the irreversible energy loss due to the heat transfer. During the charging process, exergy efficiency varies significantly as shown in **Figure 5.12**. With time evolution, the exergy efficiency initially increases significantly and then decreases gradually. There exists the maximum exergy efficiency under studied conditions. As shown in **Figure 5.12 a**, at inlet air temperature 11 ^{o}C and velocity 0.70m/s , exergy efficiency rises dramatically from 6.0% to 80.0%, and drops generally from 80.0% to 48.5%. The maximum exergy efficiency, 80.0%, is obtained at charging time 20.5 minutes. In addition, with the increase of inlet air temperature, the maximum exergy efficiency increases due to the decrease of the temperature differences of heat transfer between the air and PCMs. **Figure 5.12 b** shows the similar phenomena with inlet air velocity 1.2 m/s.

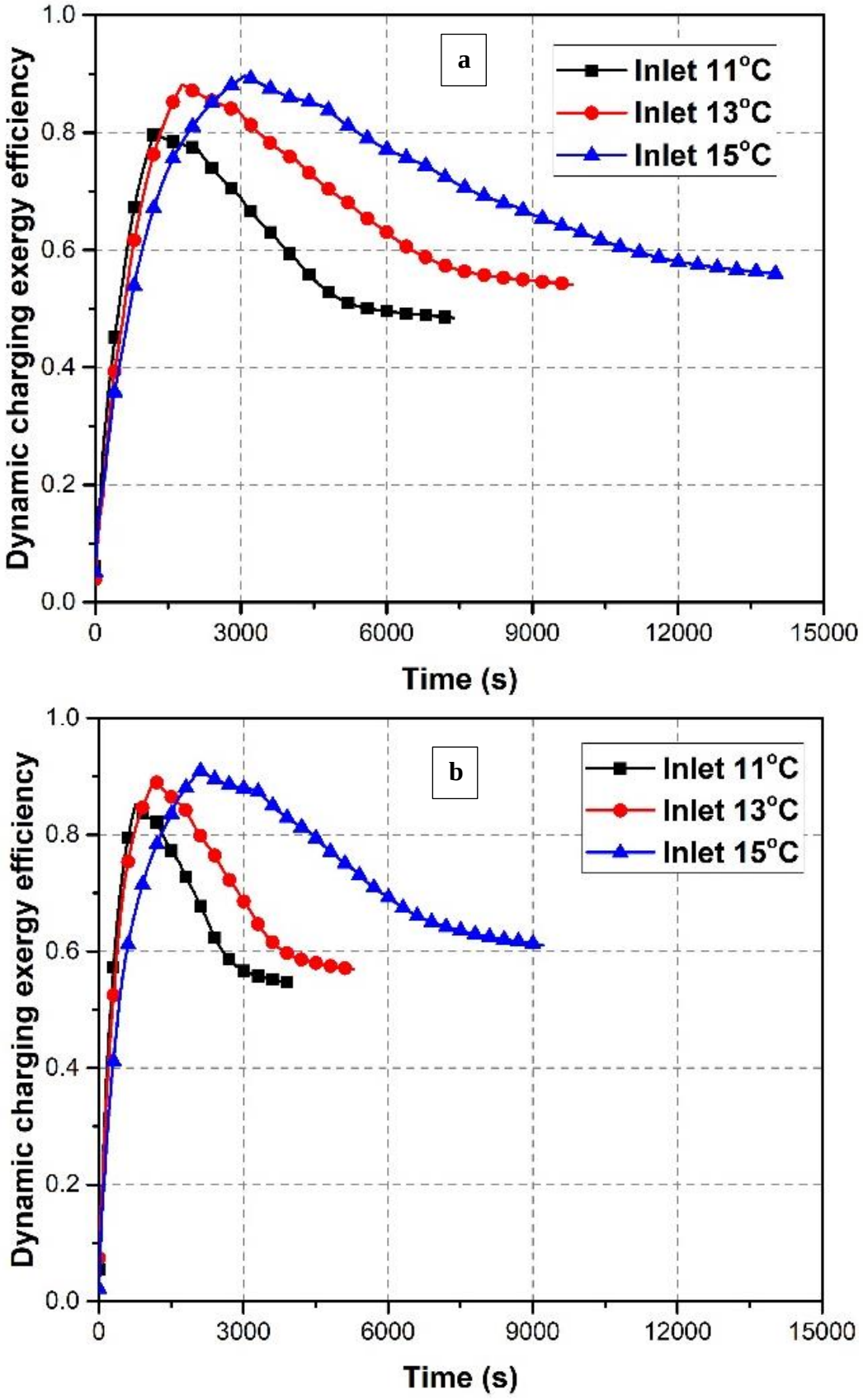

Figure 5.12: Dynamic exergy efficiency with different inlet air temperature and velocity (a: 0.70 m/s, b: 1.20 m/s).

Figure 5.13 shows the overall exergy efficiency when the charging process is finished, at different inlet air velocity and temperature. For all the given air velocities, higher exergy efficiency is obtained at the higher inlet air temperature.

For a given air temperature, with the increase of air velocity, the maximum overall exergy efficiency is obtained. For the air temperature at 11 ^{o}C, the overall exergy efficiency increases from 49.80% to 59.03%, and then decreases to 56.17% as the air velocity increases from 0.70 to 1.20 m/s, which is due to a combined result from the decreased charging time and increased air mass flow rate.

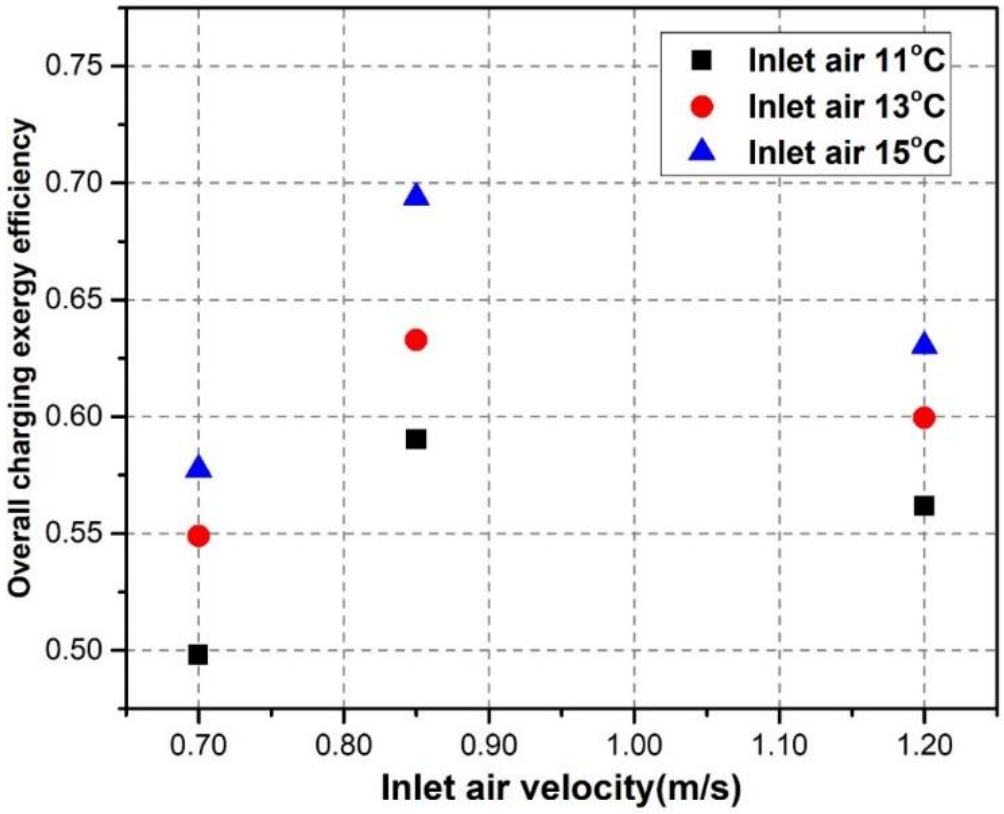

Figure 5.13: Overall exergy efficiency of the whole charging process.

5.2.6 Optimal charging depth and charging time

As shown in **Figure 5.13**, there exists the maximum charging exergy efficiency. Hence, it is valuable to evaluate the optimal charging depth, which is defined as the ratio of PCM stored exergy at the peak exergy efficiency to that when the charging process is finished.

Figure 5.14 shows the optimal charging depth with different inlet air velocity and temperature. The optimal charging depth rises with the increases of inlet air temperature and velocities. For the air velocity at 0.70 m/s, with air temperature increasing from 11 to 15 ^{o}C, the optimal charging depth goes up from 47.2% to 55.0% gradually. For the given inlet air temperature, the optimal charging depth increases gradually with the increase of inlet air velocity. For example at the air temperature 15 ^{o}C, the optimal charging depth increases from 54.9% to 57.1% as air velocity increases from 0.7 to 1.2 m/s. Under studied conditions, the optimal charging depth varies between 47% and 58%, which is a vital parameter for the design of charging process.

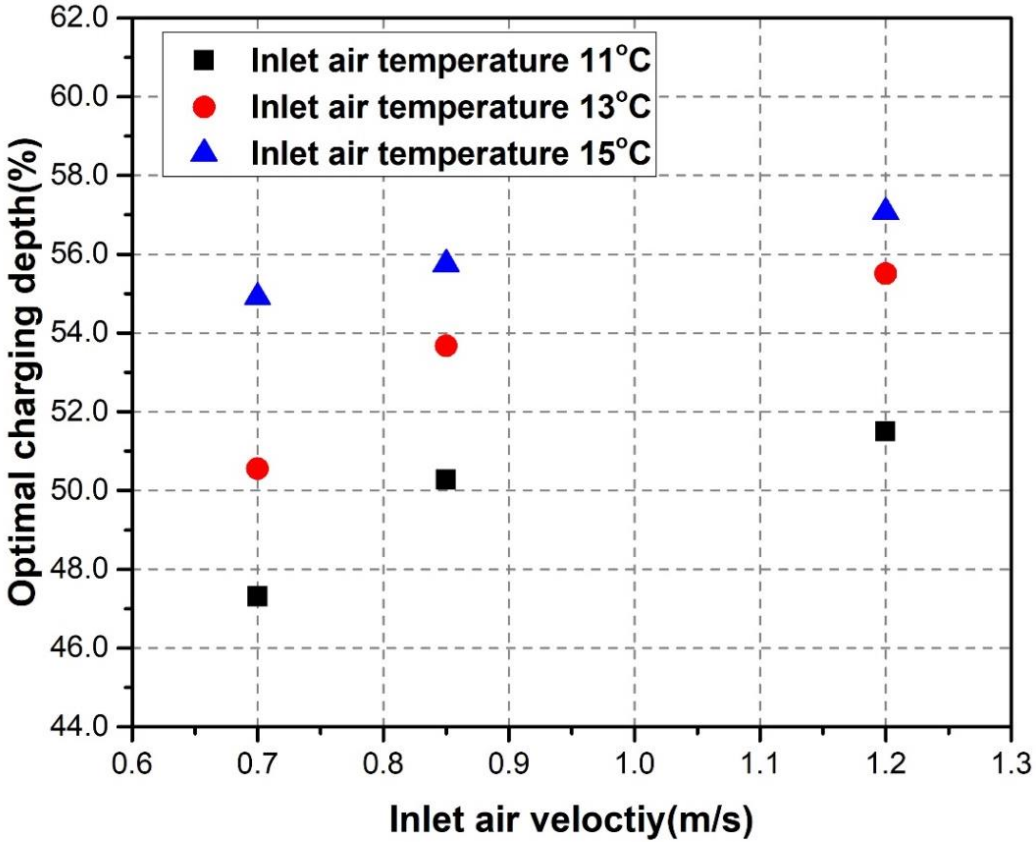

Figure 5.14: Optimal charging depth with different inlet air temperature and velocity.

In the charging process, the optimal charging time defined as the time when optimum charging depth is reached can be used for the guideline of operating management. **Figure 5.15** shows the optimal charging time as a function of inlet air velocity at different temperatures. The optimal charging time decreases with increasing inlet air velocity and decreasing inlet air temperature. For the air velocity at 0.70 m/s, the optimal charging time is 20.5, 30.0 and 51.7 mins at inlet air temperature 11,13 and 15 ^{o}C respectively.

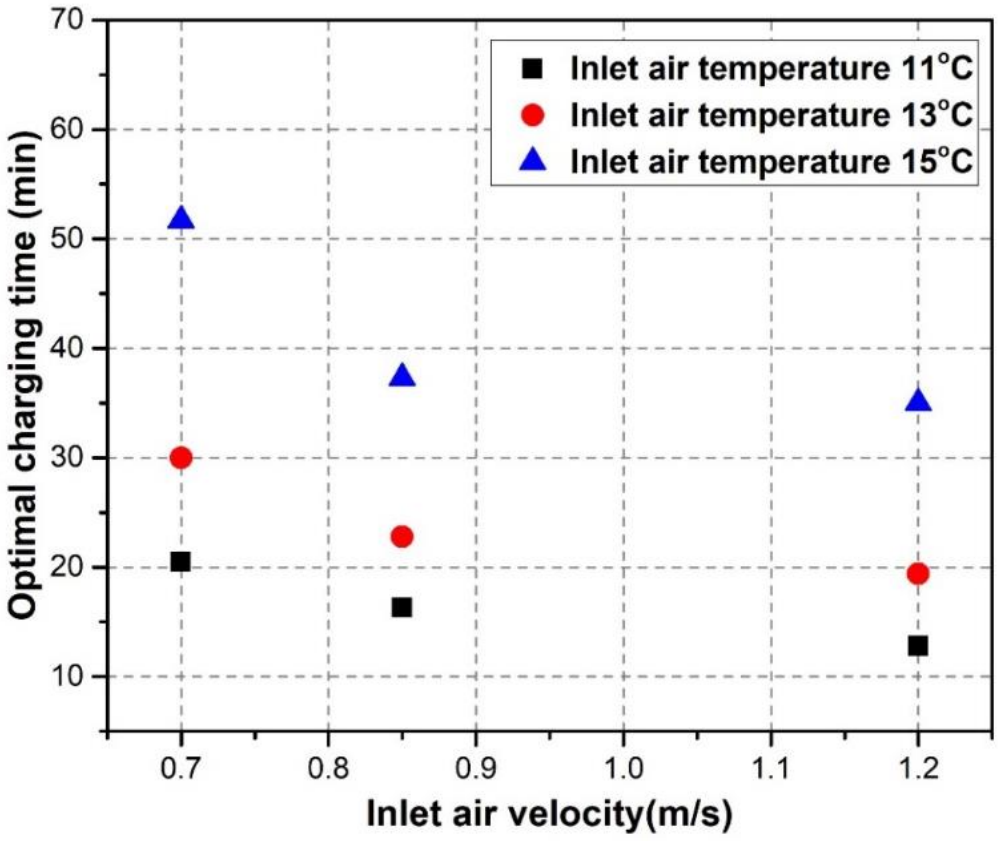

Figure 5.15: Optimal charging time with different inlet air temperature and velocity.

5.3 Summary

A novel compact TES device containing PCM (RT 18 HC) was designed, the charging and discharging performance was experimentally studied. Both the energy and exergy analysis reveals that the designed device has excellent thermal performance with discharging depth higher than 97%. Hot inlet air could be cooled down by the TES device to the desired temperature range of 16-20 ^{o}C in seconds showing fast response. The designed TES device has flexible charging rates with the maximum value of 1.3 kJ/s, high thermal efficiencies around 87% and overall exergy efficiencies up to 70%. In summary, the designed TES device is feasible to be used in air conditioning system to meet the fast-changing cooling load and improve the thermal comfort of compartments.

Chapter 6 Results and Discussions (III): Heat transfer coefficient

The heat transfer characteristics including the charging and discharging time, transient heat flux and especially the heat transfer coefficient of the device were revealed in this chapter.

6.1 The time-evolution of air and PCM temperatures

The time-evolution of air and PCM temperatures during the charging process with an inlet air temperature of 11°C and a velocity of 1.00m/s is illustrated in **Figure 6.1**. In this figure, the temperature of the PCM is initially kept at 30°C, which ensures all the PCM to be in full liquid state. As shown, after the air is introduced in the device the temperatures of the air at all layers almost immediately (within seconds) increase to the PCM temperature because of the hot device (30°C). As the time evolution and continuous air flow through the air temperatures quickly reduce in the sequence from layer 1 to layer 6 during 20 ~ 400 s (**Figure 6.1 a**). As a consequence, the PCM temperature also quickly reduces to phase change temperature (**Figure 6.1b**) because of the fast heat transfer from PCM to cool air and smaller sensible heat of PCM. This stage is related to the sensible heat transfer of PCM and defined as overheating period, After t >20-400s, PCM starts to solidify from the layer 1 to layer 6 in turn and the PCM temperature keeps at the phase change temperature around 18°C. Correspondingly, the air temperature also maintains 16-18°C for a relatively long time due to the large latent heat capacity during phase change period. This second stage corresponds to the phase transition period. After the phase change complete, the temperatures of both PCM and air gradually reduce to nearly inlet ait temperature (11°C) showing the third super cooling period. At this stage, the device achieves an approx. equilibrium where the air and PCM are of similar temperature 11^0C and there is almost no heat transfer between the air and PCM.

The charging time increases with a prolonged axial length. For example, the charging times for the axial length denoted at 50 and 200mm are 740s and 2095s respectively. **Figure 6.2** reveals the time-evolution of temperatures measured by thermocouples distributed inside the air and the corresponding PCM channels during the discharging process with an inlet air temperature and velocity at 25°C and 1.00m/s respectively. The initial temperature of the PCM is kept at 11°C during this set of experiments.

As shown in **Figure 6.2 a**, after the air is introduced in the device the temperatures of the air at all layers almost immediately (within seconds) decrease to the PCM temperature because of the cold device (11°C). As the time evolution and continuous air flow through the air temperatures quickly increase in the sequence from layer 1 to layer 6 during 20 ~ 400 s (**Figure 6.2a**). Correspondingly, the PCM temperature also quickly increases to phase

change temperature (**Figure 6.2b**) because of the fast heat transfer from air to PCM and smaller sensible heat of PCM. This stage is related to the sensible heat transfer of PCM and defined as super cooling period, After t >20-400s, PCM starts to liquefy (**Figure 6.2b**) from the layer 1 to layer 6 in turn and the PCM temperature keeps at the phase change temperature around 18°C. Correspondingly, the air temperature also maintains 17-19 °C for a relatively long period due to the large latent heat capacity during phase change period. This second stage corresponds to the phase transition period. After the phase change complete, the temperatures of both PCM and air gradually increase to nearly inlet ait temperature (25°C) showing the third overheating period. At this stage, the device achieves an approx. equilibrium where the air and PCM are of similar temperature 25°C and there is almost no heat transfer between the air and PCM. The discharging time demonstrates an upward trend with the increased axial length. For the locations at 50 and 200mm, the discharging time is 515s and 1700s respectively.

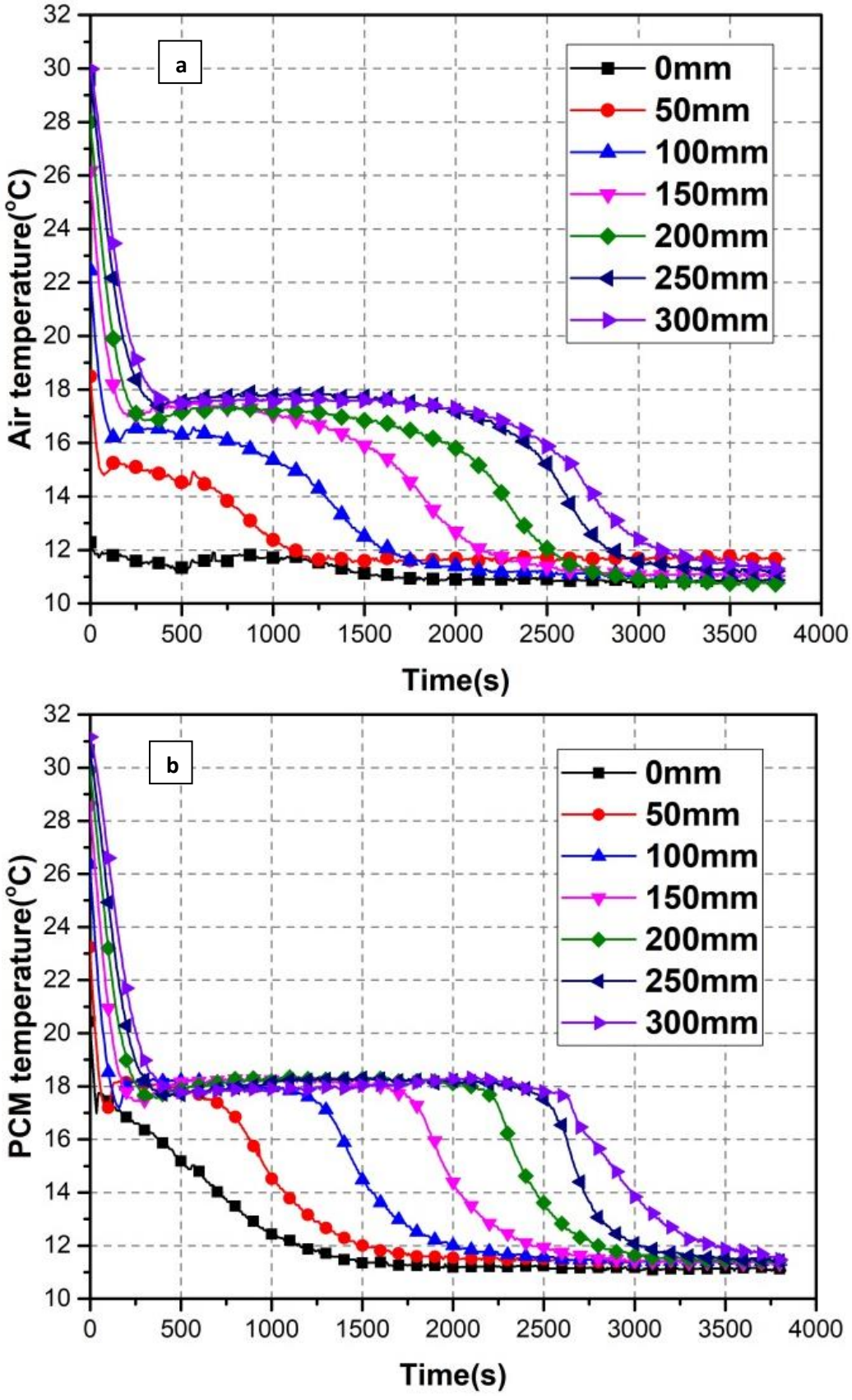

Figure 6.1: Evolution of axial temperature of air and PCM during charging process at inlet air temperature 11°C, velocity 1.00m/s and initial PCM 30°C, (a: air temperature, b: PCM temperature).

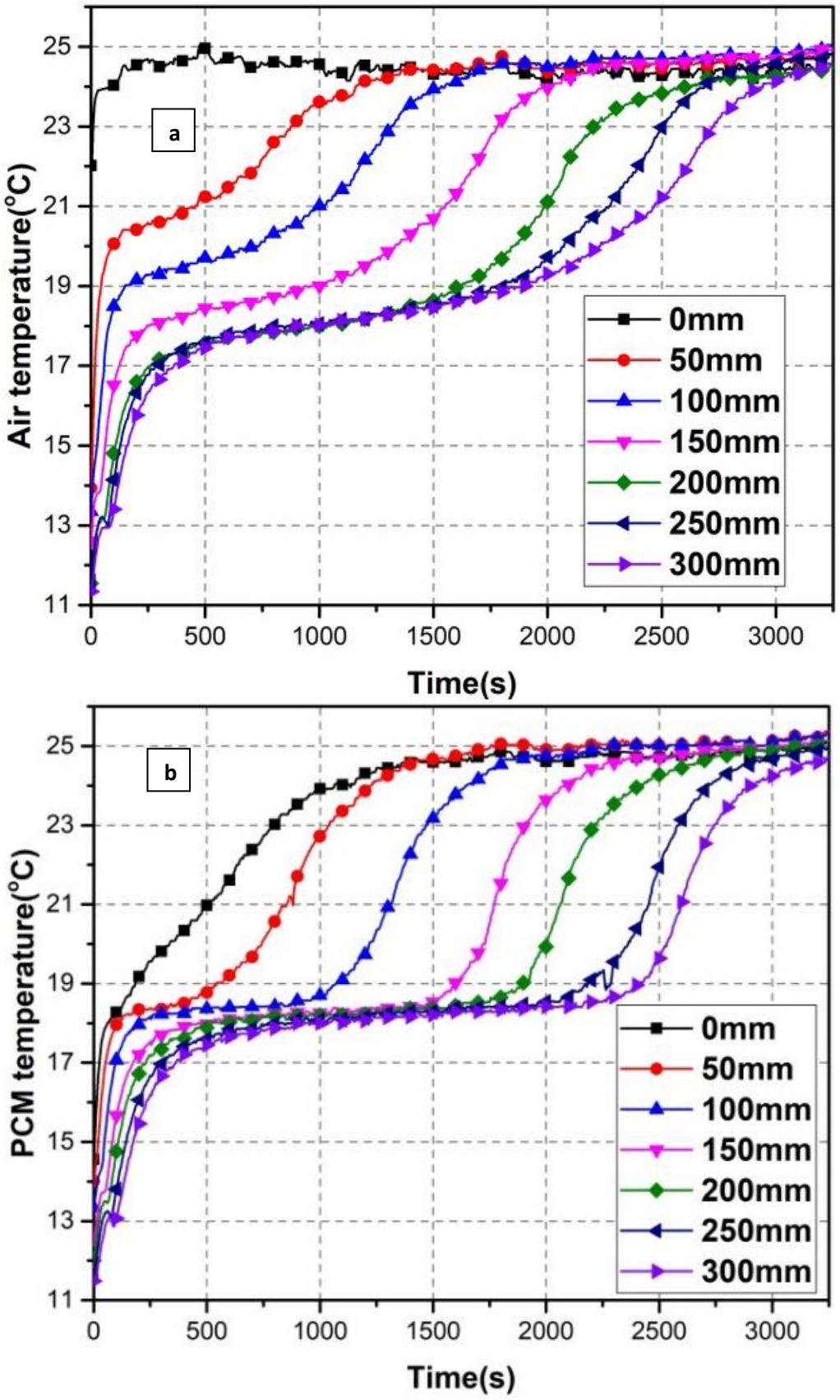

Figure 6.2. Evolution of axial temperature of air and PCM during discharging process at inlet air temperature 25 °C, velocity 1.00m/s and initial PCM 11°C (a: air temperature, b: PCM temperature).

6.2 Charging and discharging time

The total charging time is given as the time required for the temperature of the liquid PCM decreasing from the beginning to 17 ^{o}C. The entire discharging time is defined as the period when the PCM temperature increases from the beginning to 19 ^{o}C. **Figure 6.3** illustrates the charging and discharging time at different locations and inlet air velocities. For the given inlet air temperature and location, with the inlet air velocity increases, both the charging time and discharging time go down. For instance, at the axial position of 300mm the charging time declines from 2690s to 1965s (**Figure 6.3a**) and the discharging time decreases from 2415s to 1930s when velocity changes from 1.00m/s to 1.45m/s (**Figure 6.3b**).

More important, the variables to determine charging and discharging times are the temperature difference between the inlet air and PCM combined with the inlet air velocity. For the inlet air temperature at 11 and 25 °C, the temperature difference is the same for the charging and discharging processes. However, it can be easily noticed that the discharging time is obviously shorter than charging time with the given inlet air velocities. For instance, with the inlet air velocity at 1.45 m/s, the charging and discharging times with the axial length at 250mm are 1810s and 1645s respectively. The charging time is 10.03% longer than the discharging time. Hence, the heat transfer coefficient for the charging and discharging processes needs to be analysed to explain the time difference.

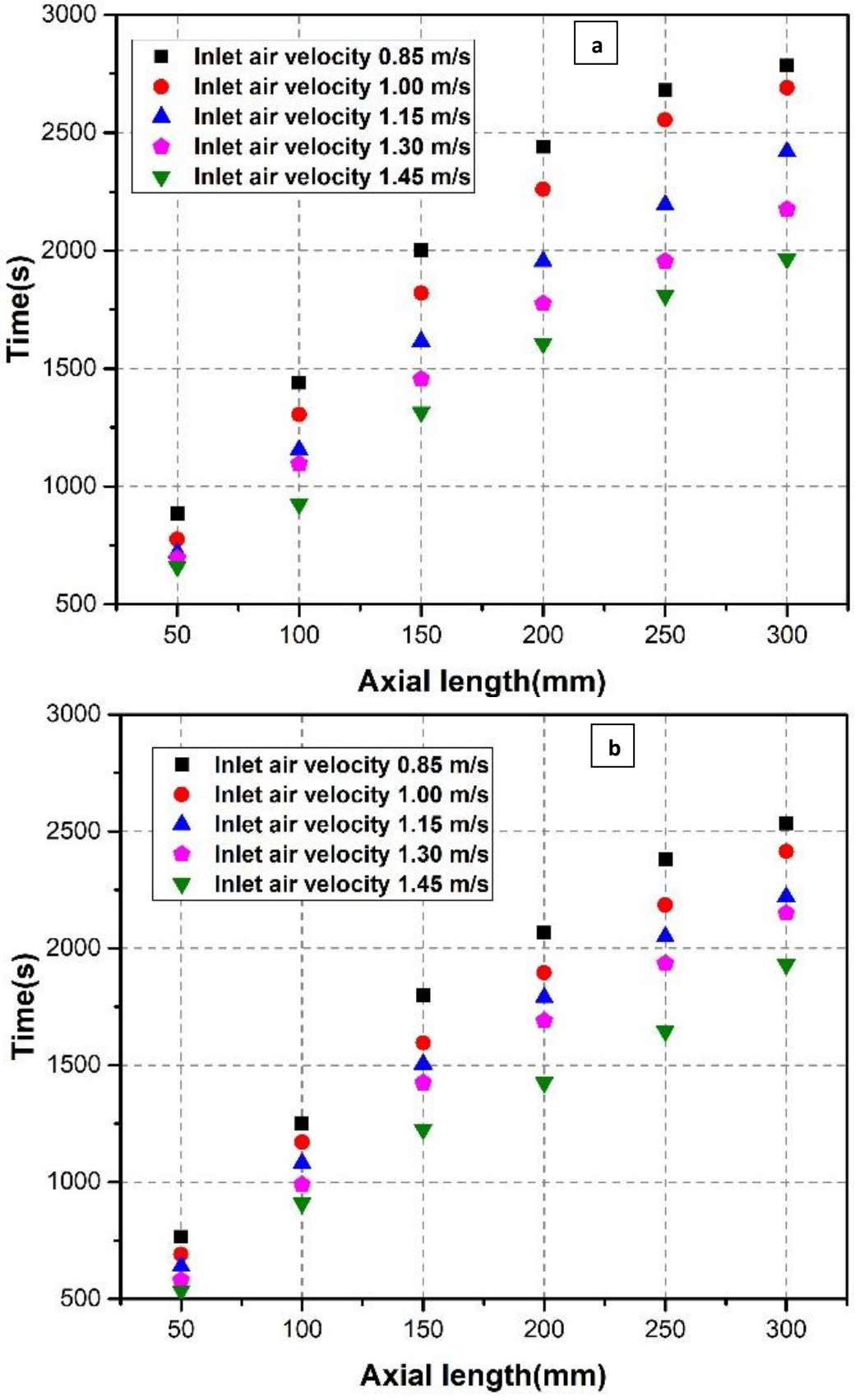

Figure 6.3: Charging (a: inlet air temperature 11°C) and discharging time (b: inlet air temperature 25°C) as a function of axial locations at diffident inlet air velocities.

6.3 Transient air temperature difference

The transient air temperature difference between the inlet and outlet of each layer is used to evaluate the transient heat flux. The results are summarised in **Figure 6.4**. For the charging process, shown in **Figure 6.4a**, after air is introduced the transient air temperature differences at all layers immediately increase within a few seconds because of the cold air and hot device. Then they quickly decrease (t<20-250s) because of the sensible heat transfer of PCM at overheating period. After t >20-250s, the air temperature difference of the first layer shows a relatively constant period and then decreases to near zero. It can be explained by that the air temperature always keeps relatively stable at the inlet and performs a nearly constant temperature in phase change period and then decreased temperature gradually down to the inlet temperature after the phase change complete at the outlet (with axial length at 50mm). Correspondingly, the air temperature difference maintains practically constant at phase change period and decreases at super cooling stage.

For the other layers, the transient air temperature differences start to increase from the layer 1 to layer 4 in turn (similar behaviours at layers 5 and 6, data not shown). These can be explained by that the solidification starts from layer 1 to layer 6 in the sequence. When the solidification complete at the inlet of the layer then the temperature starts to decrease while the solidification is not complete at the outlet of the layer, which leads to the increased air temperature difference. After the phase change complete for all the PCM in the layer the temperatures at both inlet and outlet decrease towards the initial air temperature at the inlet of the device and then the air temperature difference decrease gradually to zero. This is relating to the super cooling period.

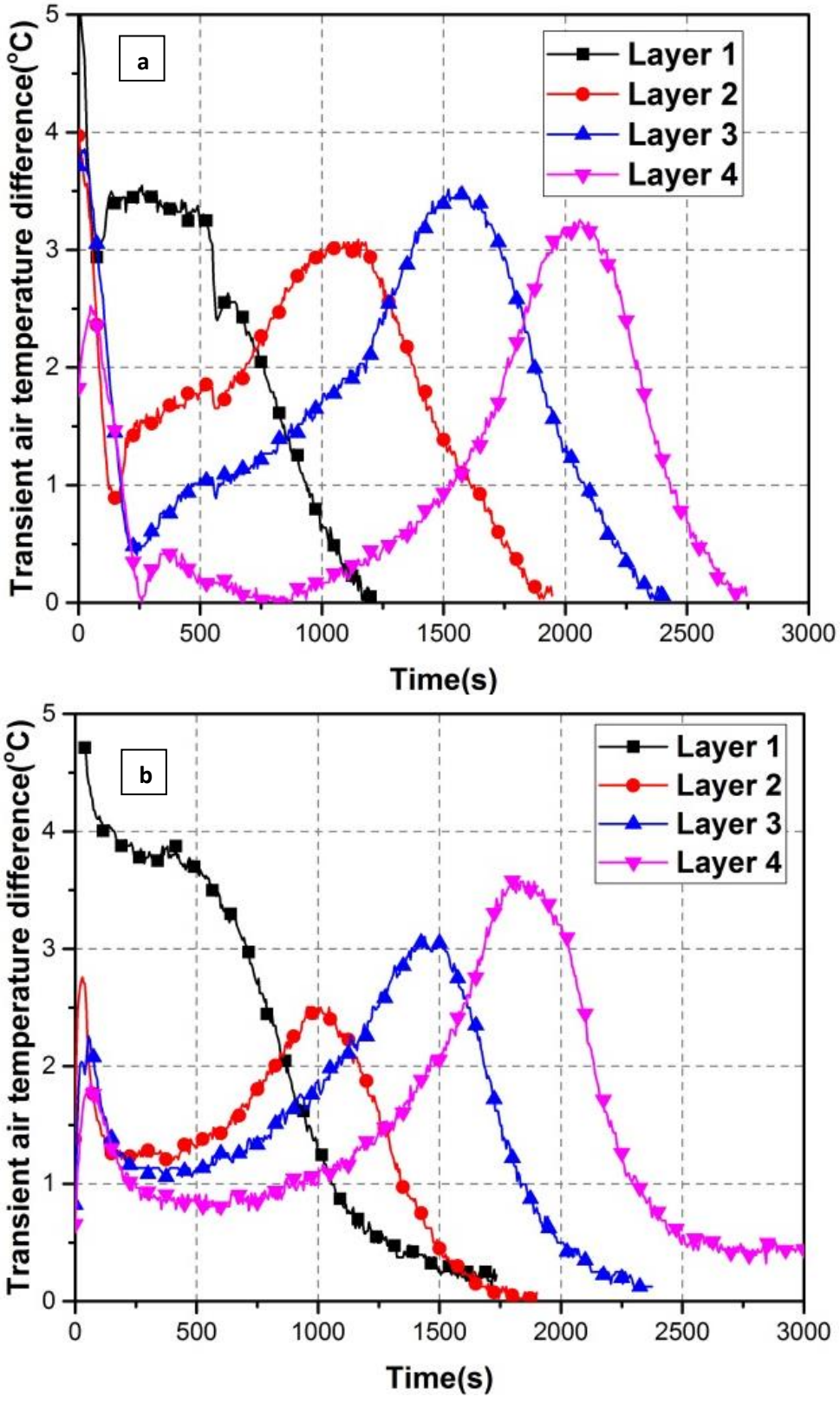

Figure 6.4: Transient air temperature difference (a) charging process at inlet air temperature 11 °C and velocity 1m/s, initial PCM temperature 31°C; (b)discharging process at inlet air temperature 25 °C and velocity 1m/s, initial PCM temperature 11°C.

The air temperature difference for the discharging process is given in **Figure 6.4b**. Similar to the charging process, after air is introduced, the transient air temperature differences at all layers immediately increase within a few seconds because of the cold air and hot device. Then they quickly decrease (t<20-250s) because of the sensible heat transfer of PCM at super cooling period. After t >20-250s, the air temperature difference of the first layer shows a relatively constant period and then decreases to near zero. It can be explained by that the air temperature always keeps relatively stable at the inlet and performs a nearly constant temperature in phase change period and then increased temperature towards its inlet value after the phase change complete at the outlet (with axial length at 50mm). Correspondingly, the air temperature difference maintains practically constant at phase change period and decreases at overheating stage.

For the other layers, the transient air temperature differences start to increase from the layer 1 to layer 4 in turn (similar behaviours at layers 5 and 6, data not shown). These can be explained by that the melting starts from layer 1 to layer 6 and from inlet to outlet at teach layer in the sequence. When the melting completes at the inlet but not at the outlet of the layer the inlet temperature starts to increase and the outlet temperature still maintains at phase change temperature. This will lead to the gradually increased temperature difference. After the phase change complete for all the PCM in the layer the temperatures at both inlet and outlet increase towards the initial air temperature at the inlet of the device and then the air temperature difference decrease towards zero, which relates to the overheating period.

6.4 Transient heat flux

The transient heat flux of the charging and discharging processes are shown in **Figure 6.5 a** and **Figure 6.5 b** respectively. It is not surprised that the evolution of transient heat flux with time follows the same pattern as the air temperature difference because it is calculated according to the air temperature difference between the inlet and outlet of each layer .

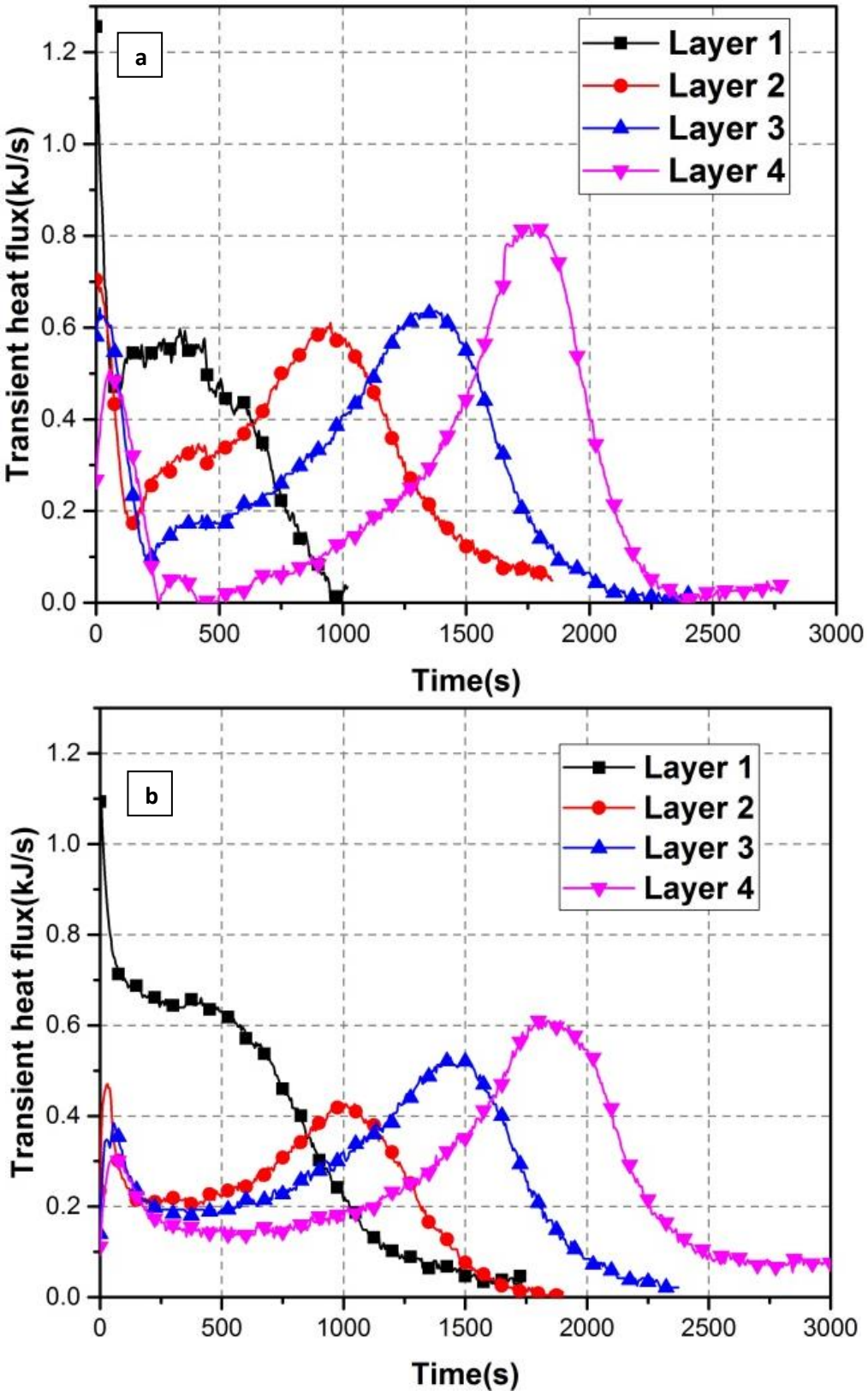

Figure 6.5: Transient heat flux at different inlet air temperature and velocity (a) charging process at inlet air temperature 11 °C and velocity 1m/s, initial PCM temperature 26 °C; (b) discharging process at inlet air temperature 25 °C and velocity 1m/s, initial PCM temperature 11 °C.

6.5 Transient temperature difference between air and PCM

The temperature difference between air flow and PCM is shown in **Figure 6.6**. For the charging process which is shown in **Figure 6.6a**, the temperature difference at the different axial locations except the inlet point performs the similar fluctuations. For the axial length at 0mm, the downward temperature difference is caused by the decreasing temperature of the inlet part of the device. For the other locations, the air temperature drops constantly, while for the PCM side, the temperature undergoes three stages. For the overheating stage, the PCM temperature drops with the downward of air. Meanwhile, the air temperature decreases faster due to the smaller specific heat capacity. This leads to PCM temperature approaches to that of air more quickly which causes the temperature difference to drop. After that, when the PCM phase change occurs, the temperature of PCM keeps relatively constant while the air temperature drops with the cold absorbed by the liquid PCM. The absorbing rate slows down with the percent of liquid PCM declines. Hence, a slight upward of temperature difference can be noticed after axial location longer than 100 mm. For the final stage, the PCM temperature drops due to the termination of phase transition. During this period, the decreased PCM temperature leads to the drop of temperature difference.

For the discharging process, indicated in **Figure 6.6b**, the temperature difference except the inlet also shows the fluctuated trend. At the inlet point, the temperature difference drops with the device was heated up. For the other axial lengths, the temperature difference lifts at first because of the faster air temperature increase rate. Then, with the beginning of the phase change of PCM, the temperature of PCM keeps relatively stable. While for the air side, the temperature goes up continuously. Due to the excellent heat transfer, the air temperature rises slightly and then faster with the consumption of solid PCM. Hence, an upward temperature difference was obtained. Finally, with the end of phase transition of PCM, both the air and PCM temperature rises, a drop of temperature difference decreases.

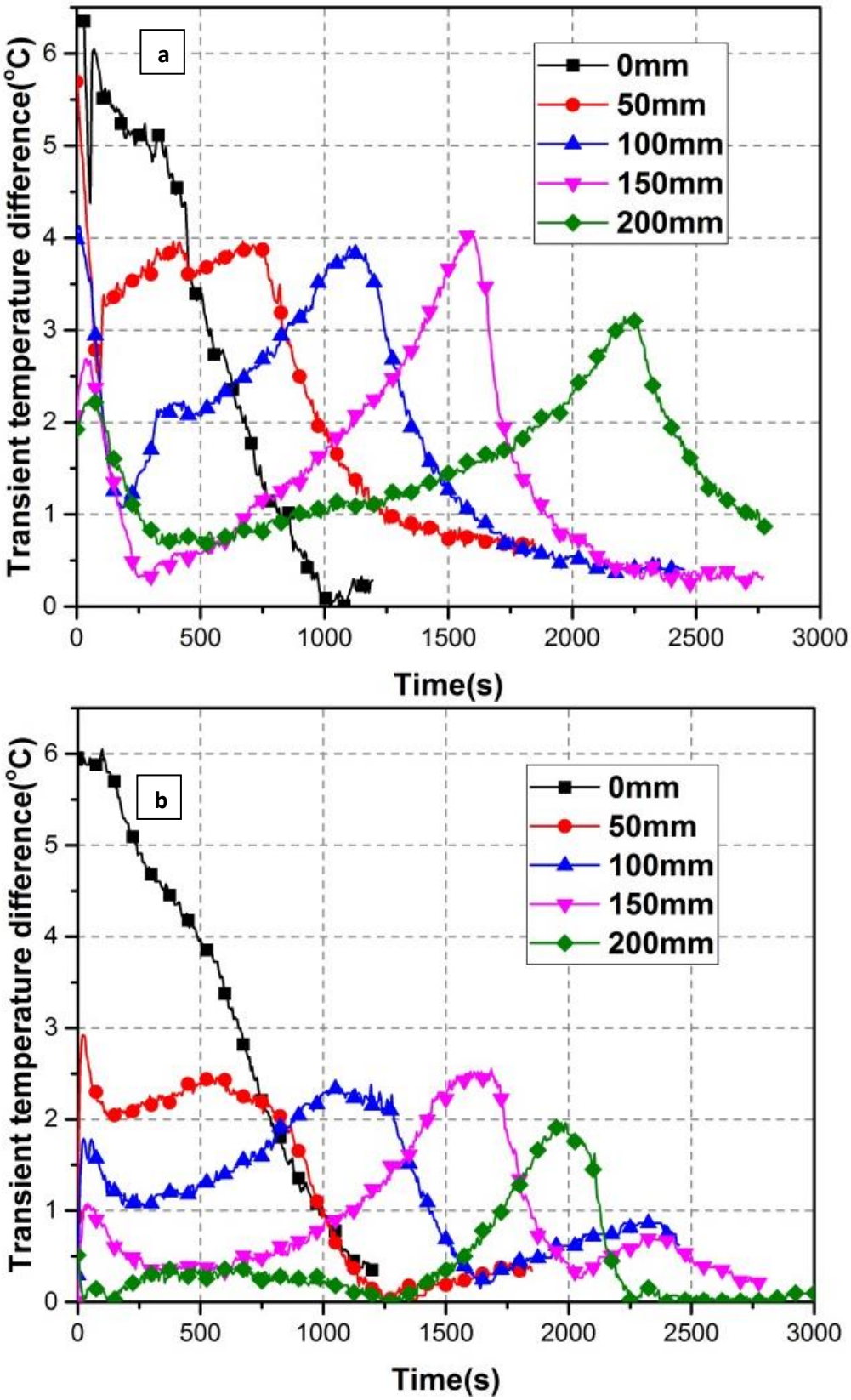

Figure 6.6: Temperature difference between PCM and air at different locations (a) charging process at inlet air temperature 11°C and velocity 1m/s, initial PCM temperature 26 °C; (b) discharging process at inlet air temperature 25 °C and velocity 1m/s, initial PCM temperature 11 °C.

6.6 Heat transfer coefficient

The transient heat transfer coefficient is shown in **Figure 6.7**. For the charging process (**Figure 6.7a**), the transient heat transfer coefficient lifts quickly at first. This is due to the large initial temperature gradient between the air and PCM. After that, the transient heat transfer coefficient drops fast which is because the PCM is in overheating period, the PCM temperature is approaching the air temperature fast which leads to the narrowing air temperature difference between air flow and PCM. Then, the PCM starts to phase change, due to the good heat transfer performance, the air temperature also keeps relatively stable. Hence, a relative stable transient heat transfer coefficient can be noticed. The final stage shows a downward tendency which indicates the end of the phase transition. With the start of the super cooling of PCM, the temperature for both the PCM and air goes down simultaneously. This causes a drop in the air and PCM temperature difference compared with that of the phase transition period.

Meanwhile, for the discharging process, given in **Figure 6.7b**, the transient heat transfer coefficient performs a quick up and down which is similar with that of charging process. This is also because of the quick heat exchange between the PCM and air in the sensible period. After that the transient heat transfer coefficient shows a slowly growing tendency which is also because of the phase transition. The PCM temperature keeps relatively stable, while the air drops slightly with desorbing heat to the PCM.

The overall heat transfer coefficients for the charging and discharging processes under the given conditions are revealed in **Figure 6.8**. For both the charging and discharging processes, the overall heat transfer coefficients go up with the rise of the inlet air velocity. Besides, the larger temperature difference between the inlet air and PCM phase change point contributes to a higher overall heat transfer coefficient. The more important thing is that when compared with the overall heat transfer coefficient with the same inlet temperature difference and air velocity for the charging and discharging processes, the heat transfer coefficient of the charging process is smaller than that of the discharging process. For instance, with the inlet air velocity at 1.45 m/s and the temperature difference between the inlet air and phase change point at 7 °C, the overall heat transfer coefficient of charging process (inlet air temperature at 11 °C) is 640W m^{-2} K^{-1}, while the overall heat transfer coefficient of discharging process (inlet air temperature at 25 °C) is 920W m^{-2} K^{-1}. The difference of overall heat transfer coefficient for the charging and discharging processes can help to understand why the charging time is longer than discharging time. With a higher overall heat transfer coefficient value under the same condition for the discharging process, the discharging rate is faster than the charging speed.

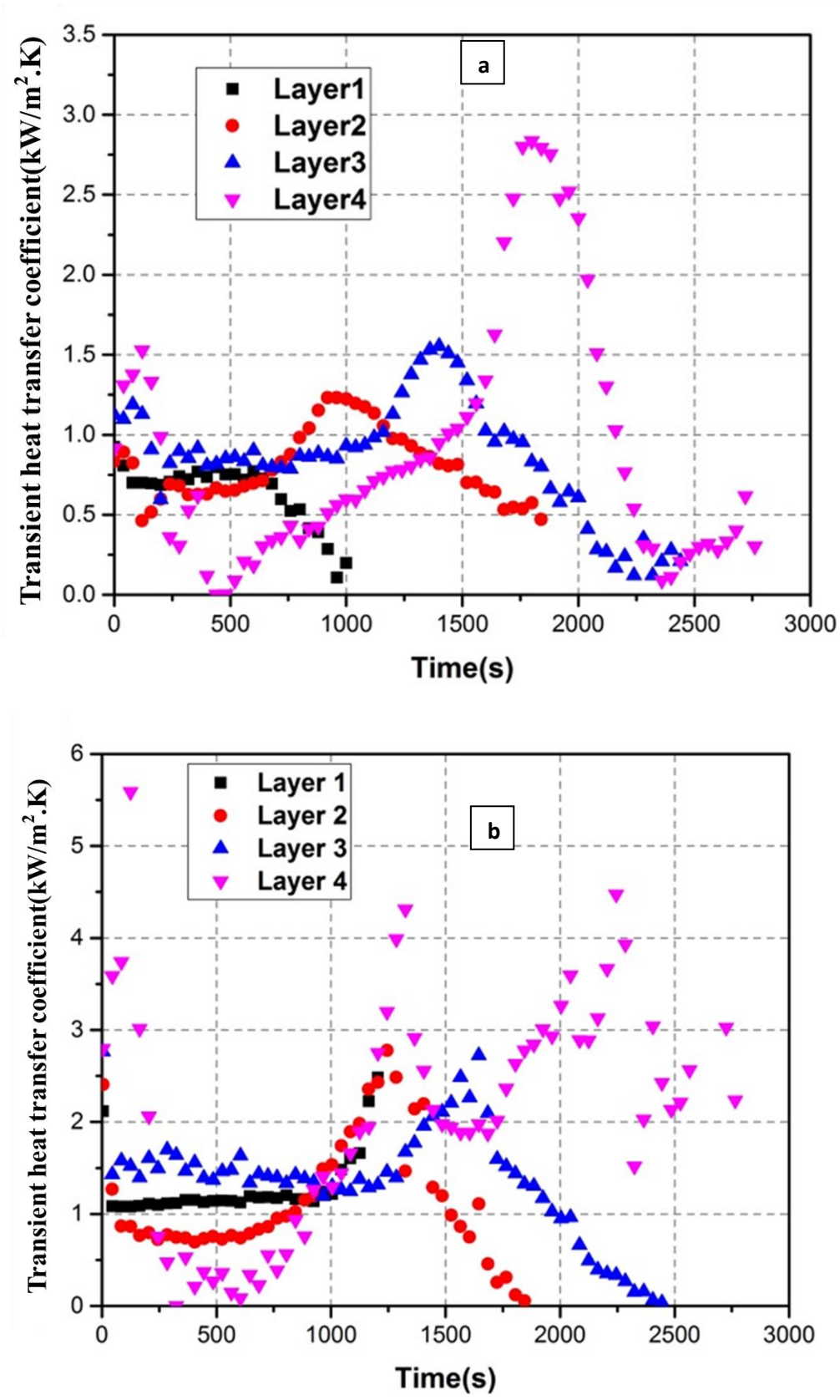

Figure 6.7: Transient heat transfer coefficient with different inlet air temperature and velocity (a) charging process at inlet air temperature 11 °C and velocity 1m/s, PCM temperature 26 °C; (b) discharging process at inlet air temperature 25 °C and velocity 1m/s, PCM temperature 11 °C.

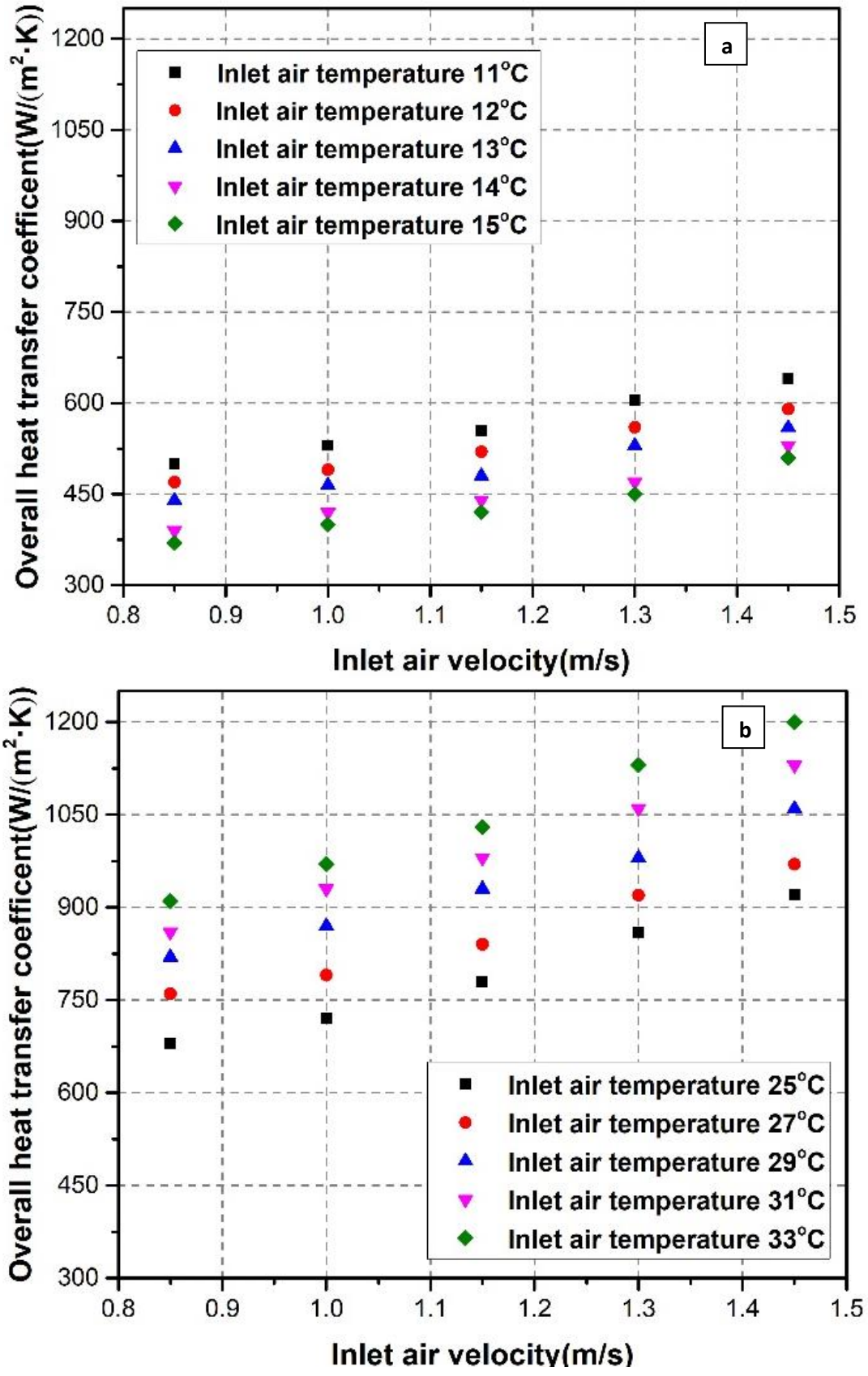

Figure 6.8: Overall heat transfer coefficient for (a) charging process, initial PCM temperature 26 °C and (b) discharging process initial PCM temperature 11 °C.

6.7 Empirical equations

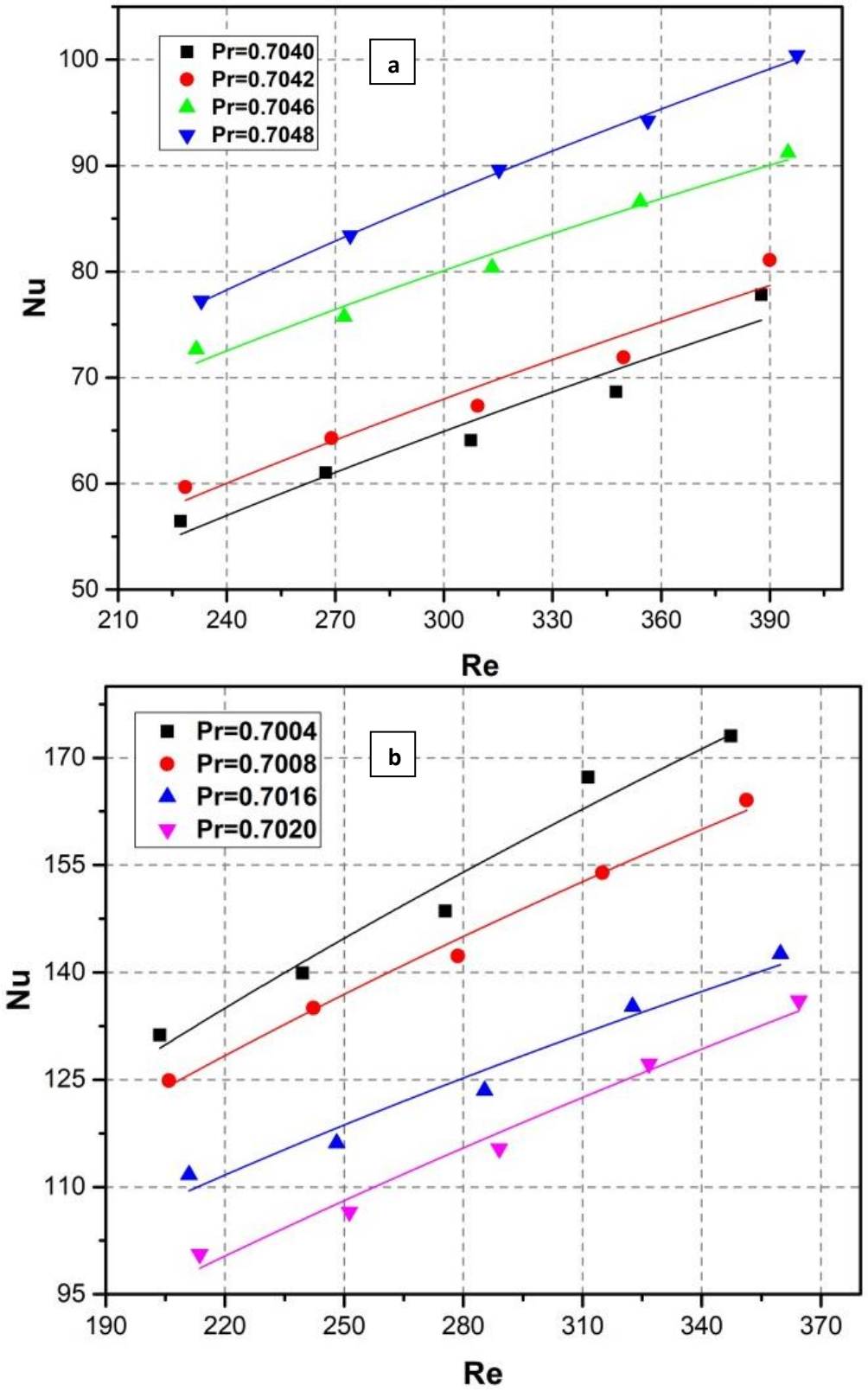

Figure 6.9: Variation of Nusselt number with Reynolds number for charging (a) and discharging (b) processes.

An effort has been made to process the experimental data in terms of non-dimensionless numbers for the overall heat transfer coefficient with an aim to obtain an empirical relationship for using in actual PCM based TES device design and optimization. **Figure 6.9** illustrates the Nusselt number as a function of Reynolds number at different Prandtl numbers for the discharging and charging processes. **Figure 6.9a** illustrates the variations of Nusselt number with Reynolds numbers for the charging process. Similarly, inlet air velocity contributes to the overall heat transfer performance dramatically. For the discharging process, shown in **Figure 6.9b**, the Nusselt number goes up with the increase of Reynolds number at the given Prandtl number. This means that higher velocity leads to better heat transfer performance.

Experiment results can be modelled by the correlations of the Nusselt number and Reynolds number (Jo et al. 2014). For the charging process, the empirical relationship of Nusselt number with Reynolds number and Prandtl number is given in Eq.(6.1) with a coefficient of determination equal to 0.9992.

$$Nu = 3.32012\,\mathrm{Re}^{0.56278}\,\mathrm{Pr}^{0.28612} \tag{6.1}$$

For discharging process the Nusselt number can be expressed by the Reynolds number and Prandtl number in Eq. (6.2) empirically with a coefficient of determination equal to 0.9994.

$$Nu = 13.59905\,\mathrm{Re}^{0.42252}\,\mathrm{Pr}^{0.26267} \tag{6.2}$$

6.8 Validation of the empirical equations

The empirical equations are validated by the experimental results with Prandtl number at 0.7012, shown in **Figure 6.10**. The average error for the charging and discharging processes between the empirical and experimental Nusselt is 2.33% and 1.65%, with the largest uncertainly is 5.08% and 4.32% respectively. These indicate that the empirical equations perform good reliability and can be used as the guide for the design of the proposed TES device under the given scale.

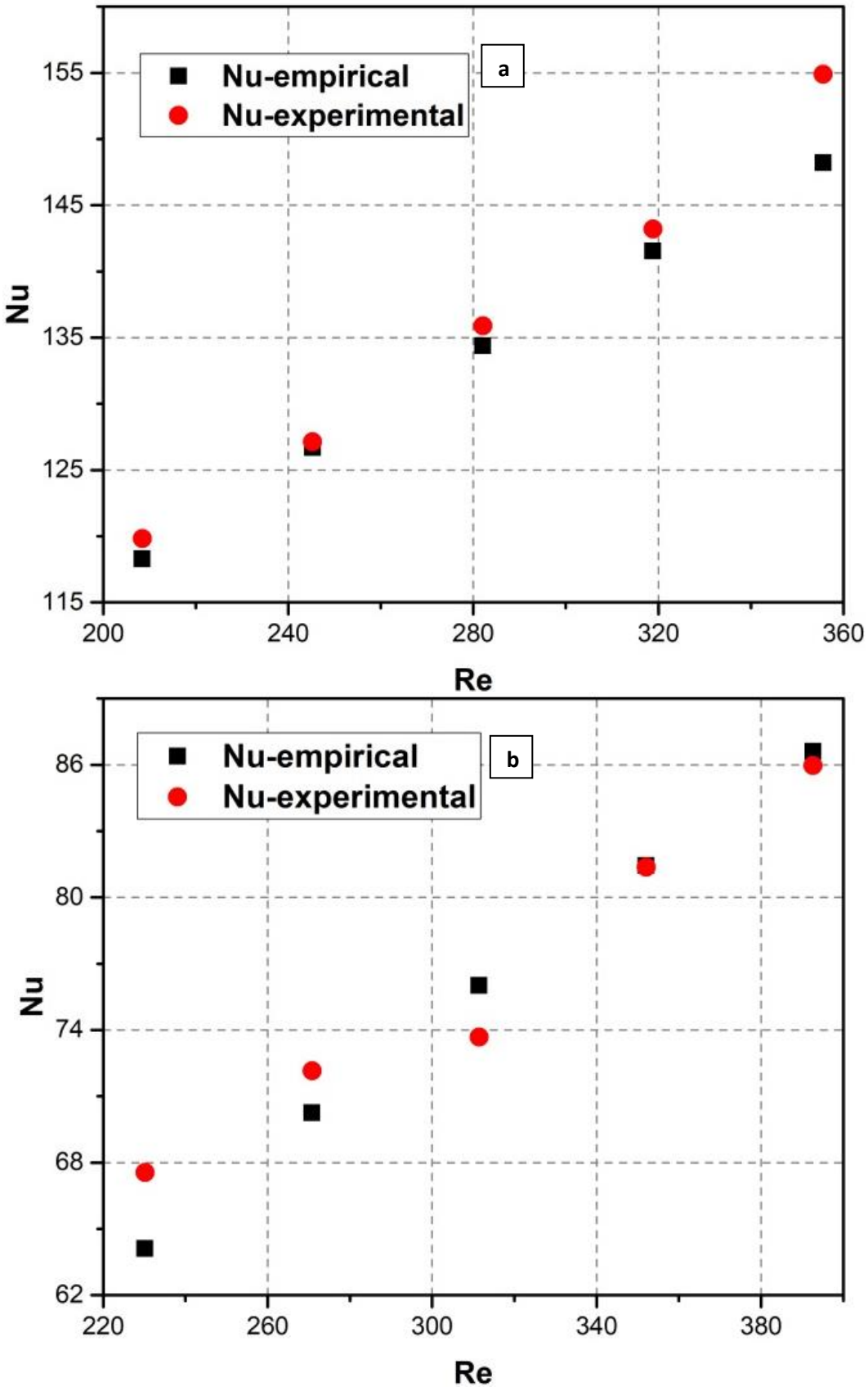

Figure 6.10: Comparison of the empirical and experimental Nusselt number during discharging (a) and charging (b) process.

6.8 Summary

The heat transfer coefficient of the device was revealed in this chapter. Empirical equations with high coefficients of determination above 0.99 for Nusselt number with Reynolds number and Prandtl number were developed. The validations between the empirical and experimental Nusselt number showed good reliability, with the average error for the charging and discharging process was 2.33% and 1.65% respectively. The concluded equations can be used as the guideline for the design of such novel TES devices for transport air conditioning applications under various scenarios.

Chapter 7 Results and Discussions (IV): System performance and Economic analysis

This chapter proposes to add a TES device filled with PCM in the AC (denoted as PCM-AC). Experimental study was conducted on the PCM-AC and comparisons are made between the AC and PCM-AC.

7.1 Average room temperature changes in the initial transient stage

Before an experiment is started, the TES device is in equilibrium with the surroundings and is unchanged. The air conditioner is started first to charge the TES device rather than to cool down the room(the testing room) initilally; see **Figure 7. 3**. One can see that it takes some ~75 mins for the room to achieve the set temperature(22°C), which is stabilised therefore with a very low temperature fluctuation frequency and amplitude. Without the use of the TES device, the room can reach the set temperature quickly, in 15 mins, but then fluctuates around the set temperature at a high frequency with a large amplitude; see later for more discussion.

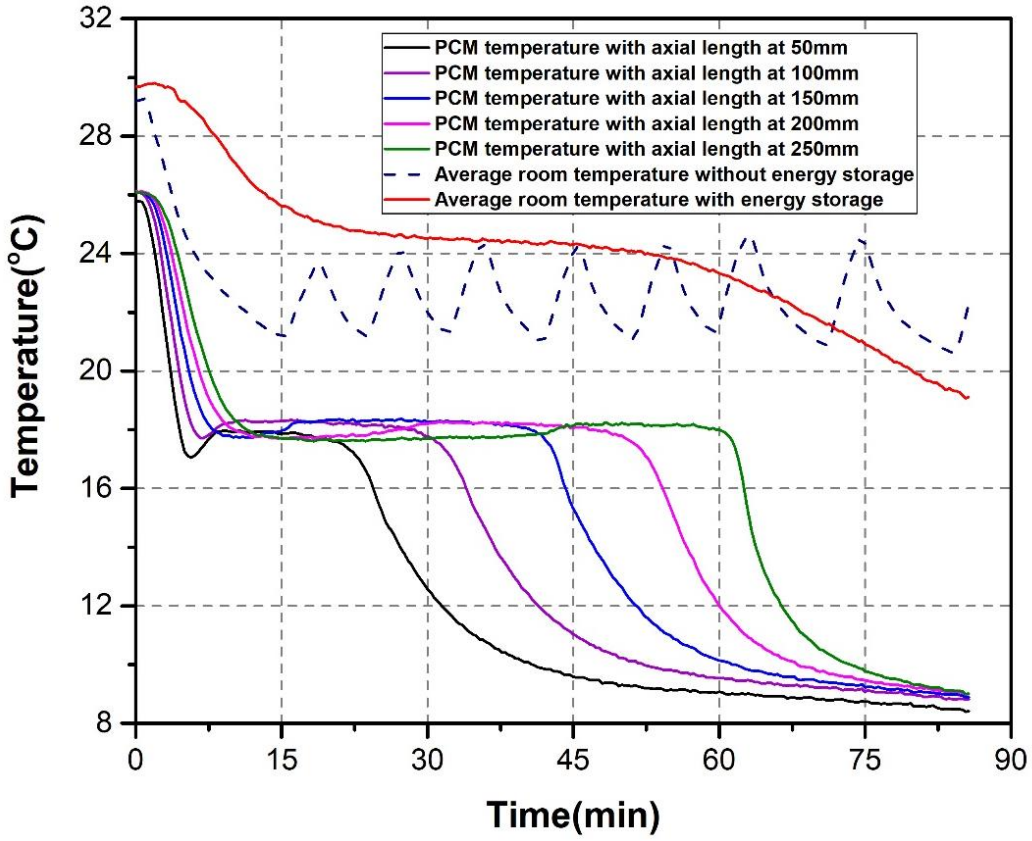

Figure 7. 3: Time evolution of average room temperature without (a) and with (b) TES device.

7.2 Average room temperature changes in the steady state stage

The time evolution of the average room(testing room) temperature for the AC and PCM-AC systems is illustrated in **Figure 7. 4**. where the PCM temperatures are also given. One can see clearly that the temperature fluctuations in the testing space are reduced significantly due to the integration of the PCM based TES unit: ~4.31°C for the AC case vs. ~2.56°C for the PCM-AC case. This represents 40.60% reduction in the temperature fluctuation and hence an improved thermal comfort.

7.3 Relative humidity in the room(testing space)

Relative humidity is another important indicator to the thermal comfort. Fig. shows the results with the TES device. One can see the relative humidity in the room fluctuates between a narrow range 27-40% (33.5%+/-20%). Without the use of the TES device, however, the room relative humidity varies significantly between 38 and 65%(51.5%+/-26.2%), due to mainly results from the large changes in the room temperature (see **Figure 7. 5**).Clearly, the use of TES device can narrow down the humidity fluctuations and provide the potential for improving the thermal comfort. The results also show that the use of the TES device has a dehumidification function on the air due to the stored cold energy in the storage device. Note that this work represents the first effort to demonstrate the PCM-AC in an industrial relevant scale and the humidity range has not been tailored to meet the optimal thermal comfort needs, which will be a subject for the future work.

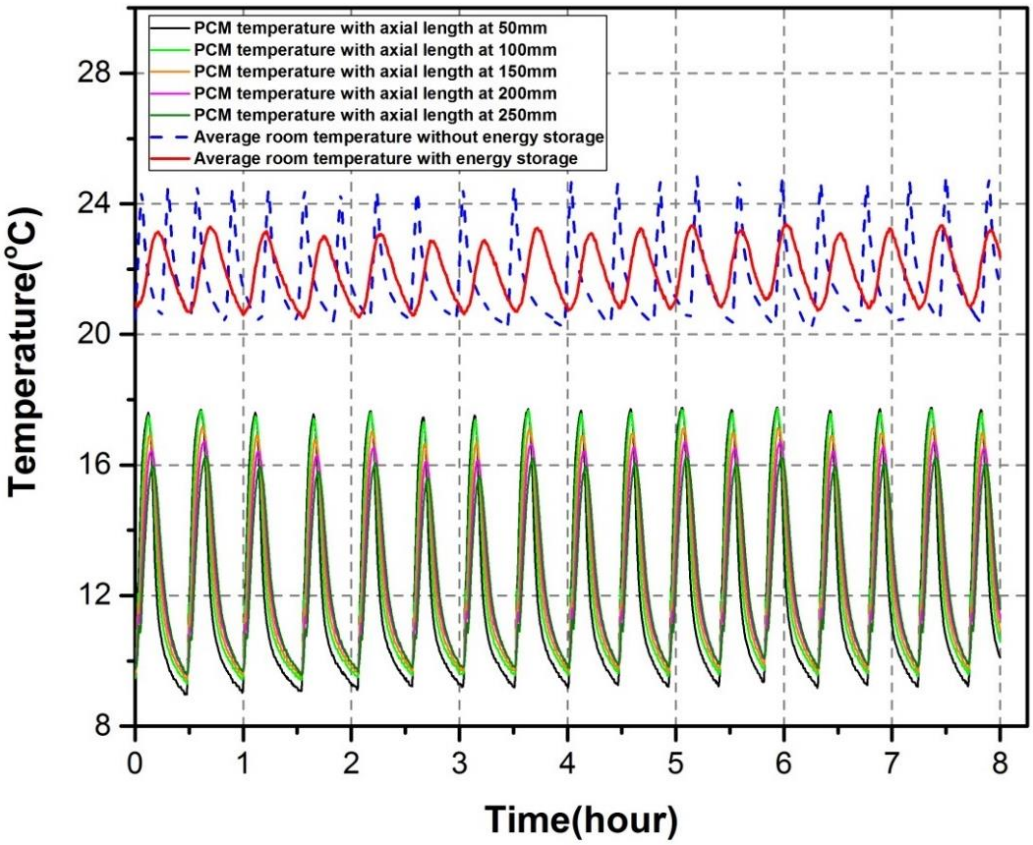

Figure 7. 4: Time evolution of the average room temperature with and without TES device.

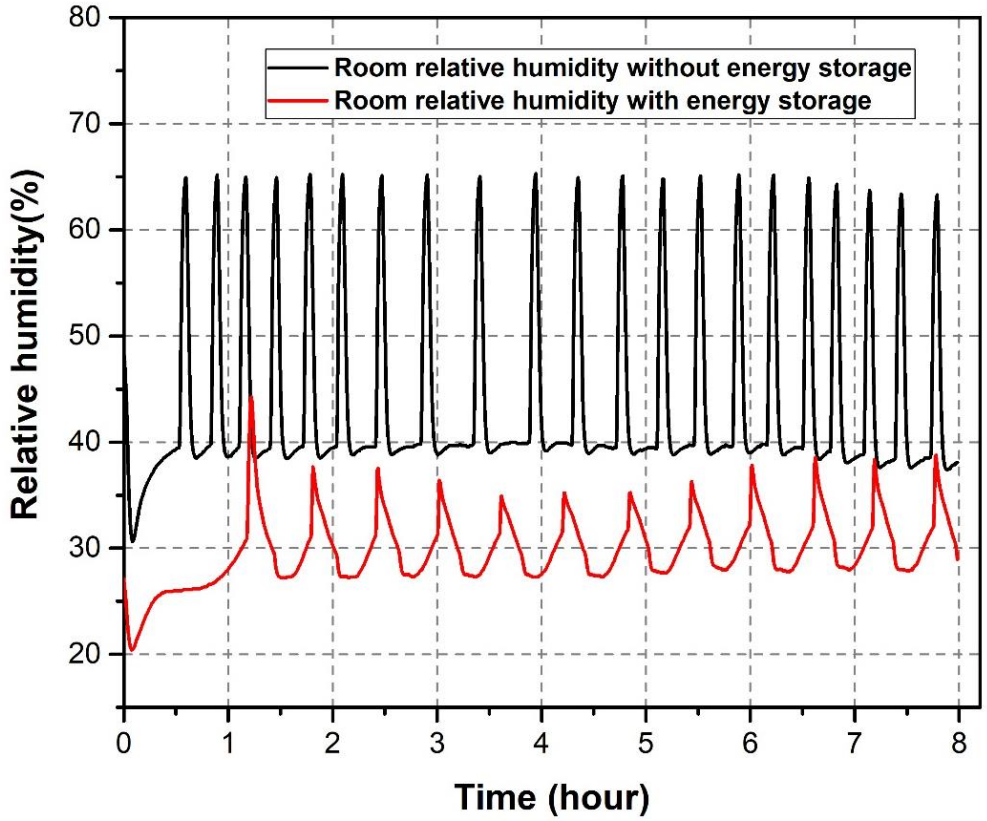

Figure 7. 5: Time evolution of the relative humidity in the testing space with and without the TES device.

7.2 ON-OFF times and power consumption of the compressor

Figure 7. 6. shows the number of ON-OFF cycles as a function of time for both the AC and PCM-AC scenarios. The ON-OFF times of the compressor with the AC scenario are 22 over an 8-hour duration, whereas that with the PCM-AC case over the same operation duration are 16. This represents a 275 reduction in the ON-OFF times. This is because that, during the OFF period, the return air from the testing space is cooled down by the TES device.

Figure 7. 6. also compares the power consumptions of the compressor with the AC and the PCM-AC scenarios. One can find by simple calculation that the daily electrical power consumption of the system with the PCM-AC is 1.29 kWh lower than that of the system with the AC over the 8 hours of testing operation, which represents a percent saving of 17.82%. As a result, the decreased ON-OFF times not only contribute to the saving of the electrical consumption, but are expected to enhance the life-span of the compressor due to the reduced the start-stop frequency.

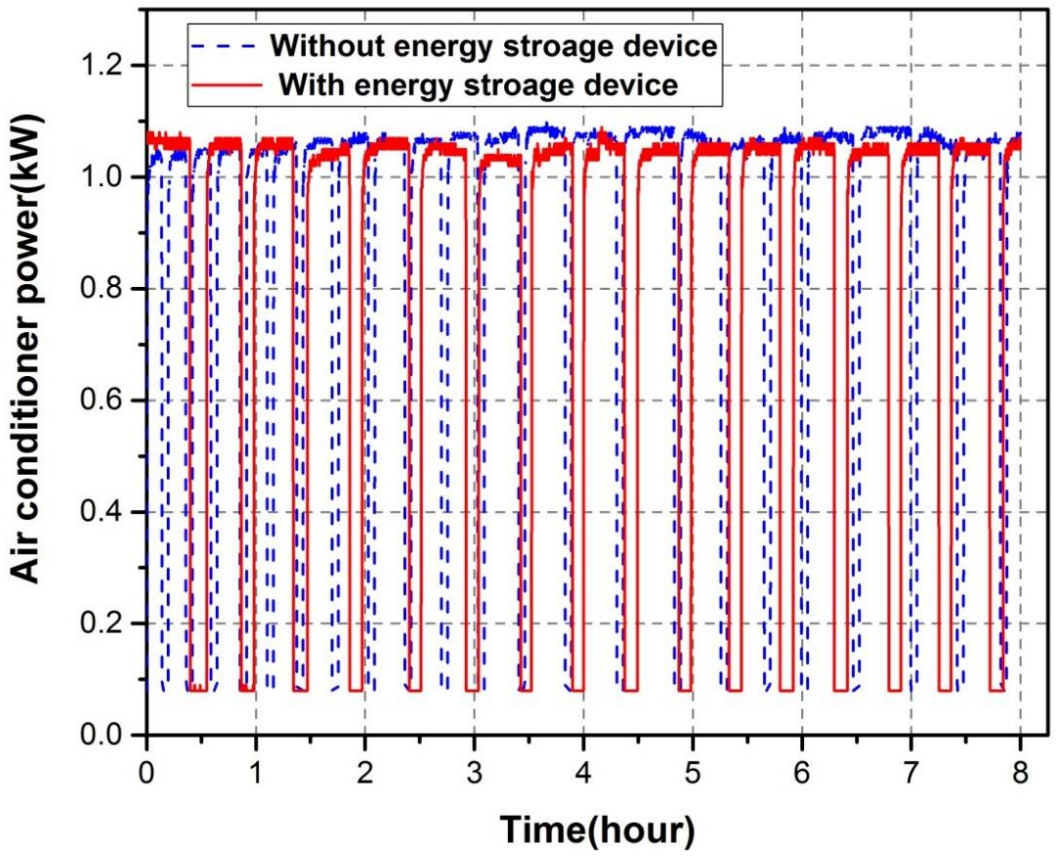

Figure 7. 6: Time evolution of power consumption of the compressor with and without TES device.

7.3 Transient and average COP

Figure 7. 7. compares the transient COP of the system with the AC and the CPM-AC scenarios. Over the operating duration of the 8 hours, the average COP for the AC and the PCM-AC cases is respectively 1.47 and 1.75. This indicates that a 19.05% increase in the average COP with the use of the PCM based TES unit, consistent with the analyses in Section 7.2.

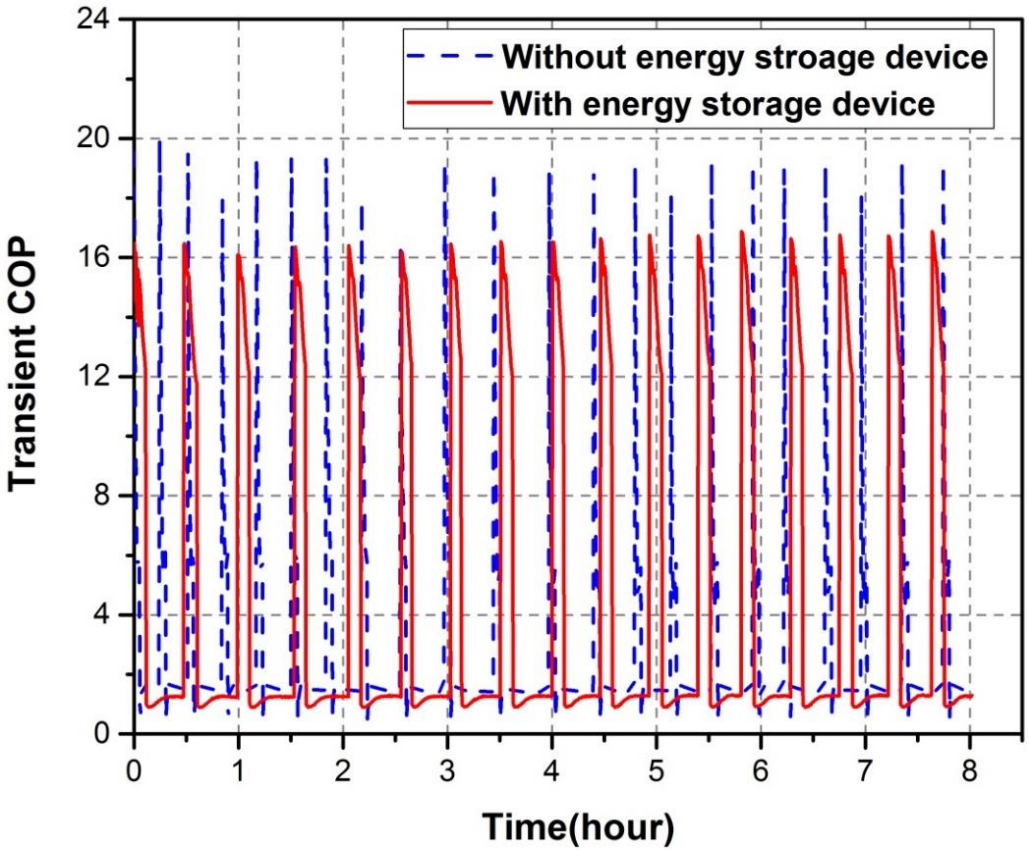

Figure 7. 7: Time evolution of average COP with and without TES device.

7.4 Emergency cooling time

The emergency cooling times with and without the TES device are compared in **Figure 7. 8**. For the AC scenario, the room(testing space) temperature rises sharply after the stop of the air conditioner, giving an emergency cooling duration of only 10.42 minutes(**Figure 7. 8a**). With the use of the PCM based TES(the PCM-AC case), the emergency cooling time is seen to prolonged to 95 minutes(**Figure 7. 8b**), which is almost 9 times of the AC case. The PCM-AC therefore provides a great potential for emergency cooling applications.

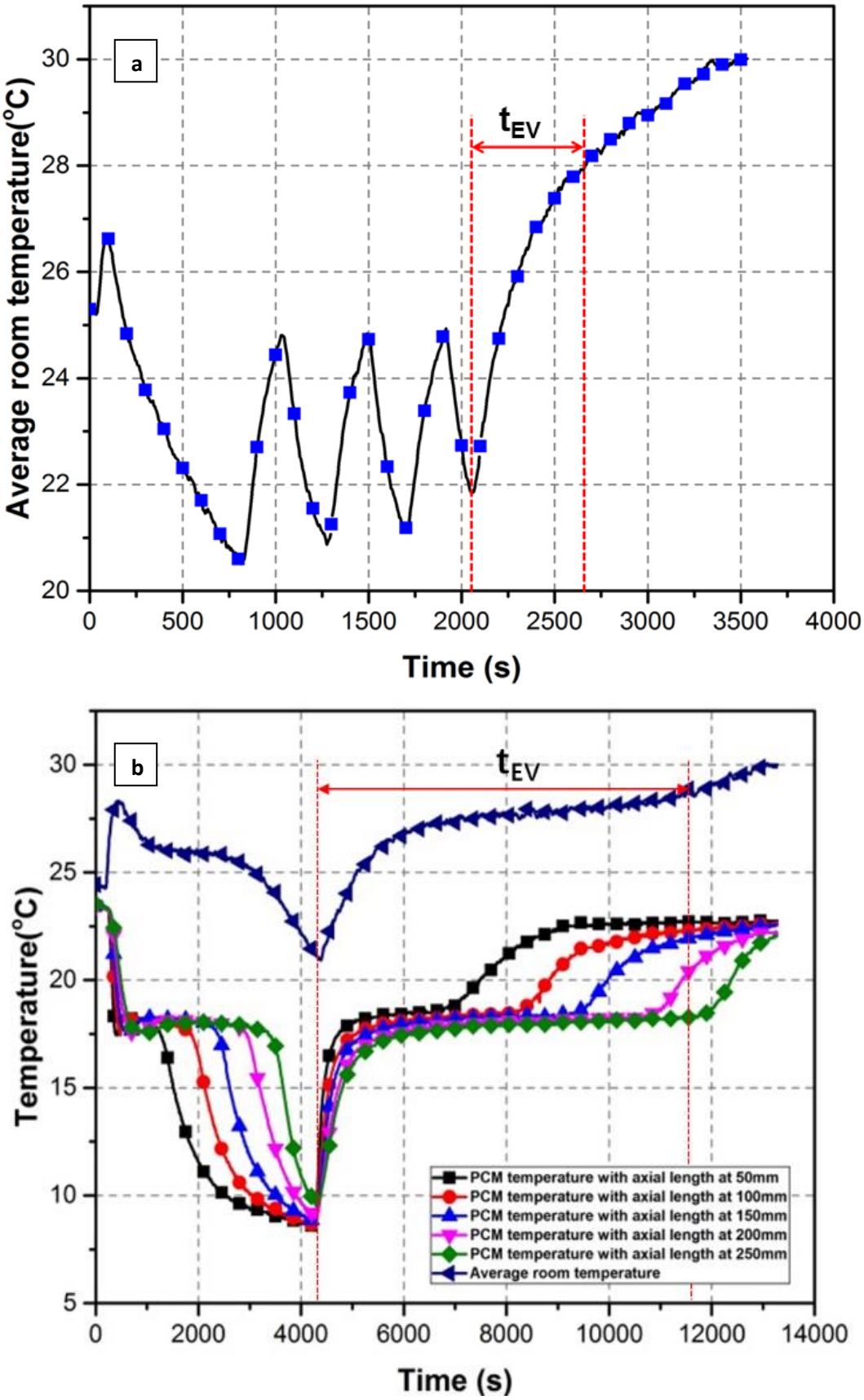

Figure 7. 8: Time evolution of average room temperature without (a) and with (b) TES device.

7.5 Economic evaluation

Table 7.1 shows the data for the economic analyses of the AC and PCM-AC scenarios. The electrical power consumptions for the AC and the PCM-AC cases are from experimental measurements; see Section 4. For details.

As the PCM-AC system uses 10kgs of PCM, the initial investment is £123.7, and the NPV is £289.37, demonstrating a high profitability for the investment project. Meanwhile, the payback period of the PCM-AC system is ~ 3.3 years. Clearly, both the electricity price and the operating strategy affect the economic performance of the PCM-AC system. More profits could be obtained if the system is applied in a location with a high electricity price or is operated in a peak-load shifing mode. It should be noted that the PCM used here is technical grade, which is very expensive. For large scale applications, an industrial grade PCM should be used, which has a price currently at £2.83/kg and the payback period could be reduced to ~1.83 years.

Table 7.1: Key parameters for the economic analysis.

Properties	The normal system	The PCM based system
Operating day	200 d/y	
Operating time	8 h/d	
Lifetime	15 year	
Discount rate	4%	
Electricity cost	14.4 pence/kWh[1]	
Electrical power consumption	7.24 kWh/d	5.95 kWh/d
TES device cost	£0	£40
Technical grade PCM price	£0	£8.37/kg
PCM amount	0 kg	10 kg

7.6 Summary

This chapter experimentally investigated the air conditioning system integration with a TES device filled with PCM. Compared with the AC, space temperature fluctuation of the PCM-AC was decreased to 2.56°C; the ON-OFF cycles of the compressor in the PCM-AC were reduced by 27%; the overall COP was increased by 19.05%; the emergency ventilation and cooling time was prolonged by up to 9 times. What's more, the economic evaluation showed that the electrical cost of the PCM-AC could be saved by up to 17.82%; the payback period was around 3.3 years and could be reduced to 1.83 years when using industrial grade PCM. Economic analyses show that the PCM-AC is profitable and has a payback period of 5.89~3.3 years; hence the proposed PCM-AC is feasible for real application.

Chapter 8 Conclusions and Recommendations

The effects of utilizing fins in both air and PCM sides were investigated numerically and experimentally. The effects of air fins, PCM fins and model PCMs with different thermal conductivities on the total heat transfer rate during the melting and solidification processes were compared. An optimum TES device was designed based on the results. The charging and discharging behaviours of air conditioning system with the TES device installed were investigated experimentally. The following results are obtained:

Both the air fins and PCM fins could contribute to the increase of the heat transfer rate with the total reduction of charging and discharging times approximately 85% and 74% respectively. The addition of air fins increases the charging/discharging rate more significantly than PCM fins. During the charging and discharging processes, the outlet air temperature could reach the required value in seconds and keep constant at the phase change range of the PCM with the addition of both fins. Alternatively to using PCM fins, the same heat transfer enhancement can be achieved by increasing the thermal conductivity of the PCMs to 1.05 and 0.78 W m^{-1} K^{-1} for discharging and charging processes respectively, which is 5 to 4 times than that of paraffin (0.2W m^{-1} K^{-1}). This provides the guidelines for the selection of PCMs and the design of PCM based TES device.

Evolutions of PCM temperature with discharging time both in the axial and radial directions are investigated. The discharging performances including the discharging time, discharging depth, discharging power, thermal efficiency and exergy efficiency are disclosed with different inlet air temperatures and velocities. The designed TES device is flexible to adjust its output cooling capacity, with the maximum value of 2.6 kW, which indicates its great potential to match the frequent fluctuations of cooling load in the transport compartments. What's more, it has high heat transfer performance, with the discharging depth higher than 97%. Higher inlet air temperature or velocity will decrease the discharging time, and decreasing the inlet air temperature or velocity is beneficial to the discharging exergy efficiency, which varies from 34% to 44%. Hot inlet air could be cooled down by the TES device to the desired temperature range of 16-20^{o}C in seconds showing fast response. What's more, the outlet air has a stable temperature around 18^{o}C for a long time.

The charging performances, including the charging time, transient charging rate, charging thermal efficiency, dynamic and overall exergy efficiency, the optimal charging depth and charging time, are disclosed at different inlet air temperatures and velocities. PCM at different layers is charged successively in the axial direction (air flow direction), and the outlet air has almost the same temperature trends as the last layer PCM, which indicates the designed TES device has excellent heat transfer performance. In addition, the time evolution of PCM temperature in the radial direction shows that the bottom PCM congeals slower than that at the other positions. The designed TES device has flexible charging rates with the maximum value of 1.3 kJ/s, high

thermal efficiencies around 87% and overall exergy efficiencies up to 70%. Lower inlet air temperature or higher air velocity could shorten the whole charging time, which varies from 50 to 174.2 mins.

The analysis of dynamic charging exergy efficiency shows that with time evolution, the charging exergy efficiency increases significantly at beginning, and then decreases gradually. The maximum charging exergy efficiency is around 90% under studied conditions. What's more, for the given inlet air velocity, the maximum exergy efficiency increases with the increase of inlet air temperature.The optimal charging depth and charging time are obtained which can be used as guidelines for real operation optimization. The optimal charging depth increases with the increase of inlet air temperature or velocity, and varies between 46% and 58% under studied conditions; the corresponding optimal charging time increases with increasing inlet air temperature and decreasing air velocity, and varies from 10 to 52 mins.

The heat transfer characteristics including the charging and discharging time, transient heat flux and especially the heat transfer coefficient of the device were revealed. A difference between the charging and discharging times under the same inlet conditions was noticed and explained by revealing the overall heat transfer coefficient for the charging and discharging processes. Nusselt number can be well related to Reynolds number and Prandtl number using well developed equations. The validations between the experiments and predicted Nusselt number show good reliability, with the average error for the charging and discharging process is 2.33% and 1.65% respectively. The concluded equations can be the guideline for the design of such novel TES devices for transport air conditioning applications.

Finally, Experimental study is conducted on the PCM-AC and comparisons are made between the AC and PCM-AC. Main conclusions are as follows. The PCM-AC improves the room thermal comfort; the room temperature fluctuation is reduced from 4.31°C to 2.56°C. The ON-OFF times of the compressor in the PCM-AC are decreased by 27% with the electrical power consumption of the PCM-AC is saved by ~17.82%, which contributes to the increase of COP by 19.05%. The PCM-AC has the function for emergency cooling when there is power off or the air conditioner beaks down; the emergency cooling time of the PCM-AC is 95 minutes, which is almost 9 times of that for the AC. Economic analyses show that the PCM-AC is profitable and has a payback period of 3.3 years , with potential drop to 1.83 years; hence the proposed PCM-AC is feasible for real application.

The quick thermal response at the beginning of the discharging (cooling) process and the long-period constant outlet air temperature around the PCM phase change point indicates the great advantages of employing the compact latent heat TES device to the air conditioning system. The constant outlet air temperature could

stabilize the output power of the compressor which could reduce the energy waste and the noise. The long working periods due to the large energy storage capacity could meet the operational requirements. These innovative conclusions show the advantages of using latent heat energy storage system in the air conditioning system.

Hence, in the future, the prototypes of PCM-AC should be designed based on the concluded results. They should be tested on the demonstration train to obtain the performance under real operating conditions. Firstly, the cooling performace should be compared with that of the traditional system under the real ambient. Secondly, The operating strategy should be optimised, especially the charging mode. Thirdly, the charging factility should be designed according to the operating strategy of the trains. If peak electricity policy applies, the cold energy used for charging the on-board TES devices should be generated during off-peak period. Finally, the energy saving, thermal comfort, noise reduction should be evaluated.

List of Publications

Journal Paper

Nie B, She X, Du Z, Xie C, Li Y, Z He, Ding Y. System performance and economic assessment of a thermal energy storage based air-conditioning system for transport applications. *Applied Energy 251(2019)113254.*

Nie B, She X, Zou B, Li Y, Ding Y. A PCM-air thermal energy storage device - improved discharging properties for transport cooling application. (Under review, *Energy* jounral);

Nie B, She X, Yu Q, Li Y, Ding Y. Experimental study of charging a compact PCM energy storage device for transport application with dynamic exergy analysis. (Revised manuscript submited, *Energy Conversion and Management* jounral);

Nie B, Li Y, Ding Y. Performance enhancement of a phase-change-material based thermal energy storage device for air-conditioning applications: Numerical analyses and experimental validation. (Under review, *Applied Energy* jounral);

Nie B, She X, Zhang T, Zhao Y, Li Y, Ding Y. Development of heat transfer coefficient based design method of cold energy storage device for transport cooling applications (Under review, *Applied Energy* jounral);

Nie B, She X, Zou B, Zhang T, Li Y, Ding Y. Review on phase change materials based cold thermal energy storage applications. (Preparing to submit to *Renewable & Sustainable Energy Reviews* jounral);

Conference Paper

Nie B, She X, Navarro H, Smith DP, Sciacovelli A, Ding Y. Charging properties of a compact energy storage device for transport air conditioning applications. Energy Procedia 2017;142:3531–6. Cardiff, UK.

Patents

Electric vehicle air conditioner technology and system using thermal energy storage, CN107696823A, 2018-02-16.

Vehicle Charging, PCT/GB2019/050483, 2019-02-21.

Bibliography

[1] González-Gil A, Palacin R, Batty P, Powell JP. A systems approach to reduce urban rail energy consumption. Energy Convers Manag 2014;80:509–24. doi:10.1016/j.enconman.2014.01.060.

[2] Bolton G. Auxiliary power systems for rolling stock, Professional Development Course on Electric Traction Systems. IET 13th n.d.

[3] Jankowski NR, McCluskey FP. A review of phase change materials for vehicle component thermal buffering. Appl Energy 2014;113:1525–61. doi:10.1016/j.apenergy.2013.08.026.

[4] Agyenim F, Hewitt N, Eames P, Smyth M. A review of materials, heat transfer and phase change problem formulation for latent heat thermal energy storage systems (LHTESS). Renew Sustain Energy Rev 2010;14:615–28. doi:10.1016/j.rser.2009.10.015.

[5] Sharma A, Tyagi V V., Chen CR, Buddhi D. Review on thermal energy storage with phase change materials and applications. Renew Sustain Energy Rev 2009;13:318–45. doi:10.1016/j.rser.2007.10.005.

[6] Oró E, de Gracia A, Castell A, Farid MM, Cabeza LF. Review on phase change materials (PCMs) for cold thermal energy storage applications. Appl Energy 2012;99:513–33. doi:10.1016/j.apenergy.2012.03.058.

[7] Reyes A, Henríquez-Vargas L, Aravena R, Sepúlveda F. Experimental analysis, modeling and simulation of a solar energy accumulator with paraffin wax as PCM. Energy Convers Manag 2015;105:189–96. doi:10.1016/j.enconman.2015.07.068.

[8] Abokersh MH, El-Morsi M, Sharaf O, Abdelrahman W. An experimental evaluation of direct flow evacuated tube solar collector integrated with phase change material. Energy 2017;139:1111–25. doi:10.1016/j.energy.2017.08.034.

[9] Diaconu BM, Cruceru M. Novel concept of composite phase change material wall system for year-round thermal energy savings. Energy Build 2010;42:1759–72. doi:10.1016/j.enbuild.2010.05.012.

[10] Parameshwaran R, Kalaiselvam S. Energy efficient hybrid nanocomposite-based cool thermal storage air conditioning system for sustainable buildings. Energy 2013;59:194–214. doi:10.1016/j.energy.2013.06.064.

[11] Xia M, Yuan Y, Zhao X, Cao X, Tang Z. Cold storage condensation heat recovery system with a novel composite phase change material. Appl Energy 2016;175:259–68. doi:10.1016/j.apenergy.2016.05.001.

[12] Conklin JC, Szybist JP. A highly efficient six-stroke internal combustion engine cycle with water injection for in-cylinder exhaust heat recovery. Energy 2010;35:1658–64. doi:10.1016/j.energy.2009.12.012.

[13] Chiu JNW, Gravoille P, Martin V. Active free cooling optimization with thermal energy storage in Stockholm. Appl Energy 2013;109:523–9. doi:10.1016/j.apenergy.2013.01.076.

[14] Barzin R, Chen JJJ, Young BR, Farid MM. Application of PCM energy storage in combination with night ventilation for space cooling. Appl Energy 2015;158:412–21. doi:10.1016/j.apenergy.2015.08.088.

[15] Medved S, Arkar C. Correlation between the local climate and the free-cooling potential of latent heat storage. Energy Build 2008;40:429–37. doi:10.1016/j.enbuild.2007.03.011.

[16] Takeda S, Nagano K, Mochida T, Shimakura K. Development of a ventilation system utilizing thermal energy storage for granules containing phase change material. Sol Energy 2004;77:329–38. doi:10.1016/j.solener.2004.04.014.

[17] Arkar C, Medved S. Free cooling of a building using PCM heat storage integrated into the ventilation system. Sol Energy 2007;81:1078–87. doi:10.1016/j.solener.2007.01.010.

[18] Zalba B, Marín JM, Cabeza LF, Mehling H. Free-cooling of buildings with phase change materials. Int J Refrig 2004;27:839–49. doi:10.1016/j.ijrefrig.2004.03.015.

[19] Walsh BP, Murray SN, O'Sullivan DTJ. Free-cooling thermal energy storage using phase change materials in an evaporative cooling system. Appl Therm Eng 2013;59:618–26. doi:10.1016/j.applthermaleng.2013.06.008.

[20] Osterman E, Butala V, Stritih U. PCM thermal storage system for "free" heating and cooling of buildings. Energy Build 2015;106:125–33. doi:10.1016/j.enbuild.2015.04.012.

[21] Sun X, Zhang Q, Medina MA, Liao S. Performance of a free-air cooling system for telecommunications base stations using phase change materials (PCMs): In-situ tests. Appl Energy 2015;147:325–34. doi:10.1016/j.apenergy.2015.01.046.

[22] De Gracia A, Navarro L, Castell A, Ruiz-Pardo Á, Álvarez S, Cabeza LF. Thermal analysis of a ventilated facade with PCM for cooling applications. Energy Build 2013;65:508–15. doi:10.1016/j.enbuild.2013.06.032.

[23] Mosaffa AH, Infante Ferreira CA, Talati F, Rosen MA. Thermal performance of a multiple PCM thermal storage unit for free cooling. Energy Convers Manag 2013;67:1–7. doi:10.1016/j.enconman.2012.10.018.

[24] Liu Z, Zhao D, Wang Q, Chi Y, Zhang L. Étude Sur La Performance D'Un Réfrigérateur Domestique Refroidi Par Air Utilisant Des Matériaux À Changement De Phase Pour L'Entreposage Frigorifique. Int J Refrig 2017;79:130–42. doi:10.1016/j.ijrefrig.2017.04.009.

[25] Beck M, Müller K, Arlt W. Storing surplus solar energy in low temperature thermal storage for refrigeration applications. Energy Build 2016;122:192–8. doi:10.1016/j.enbuild.2016.04.041.

[26] Liu M, Saman W, Bruno F. Development of a novel refrigeration system for refrigerated trucks incorporating phase change material. Appl Energy 2012;92:336–42. doi:10.1016/j.apenergy.2011.10.015.

[27] Liu M, Saman W, Bruno F. Computer simulation with TRNSYS for a mobile refrigeration system incorporating a phase change thermal storage unit. Appl Energy 2014;132:226–35. doi:10.1016/j.apenergy.2014.06.066.

[28] Glouannec P, Michel B, Delamarre G, Grohens Y. Experimental and numerical study of heat transfer across insulation wall of a refrigerated integral panel van. Appl Therm Eng 2014;73:194–202.

doi:10.1016/j.applthermaleng.2014.07.044.

[29] Yusufoglu Y, Apaydin T, Yilmaz S, Paksoy HO. Improving performance of household refrigerators by incorporating phase change materials. Int J Refrig 2015;57:173–85. doi:10.1016/j.ijrefrig.2015.04.020.

[30] Shukla AK. Development and Optimization of PCM Based Technology for Cooling Applications for Improvement of Fuel Efficiency in Commercial Vehicle 2018. doi:10.4271/2017-01-0150.Copyright.

[31] Azzouz K, Leducq D, Gobin D. Performance enhancement of a household refrigerator by addition of latent heat storage. Int J Refrig 2008;31:892–901. doi:10.1016/j.ijrefrig.2007.09.007.

[32] Ahmed M, Meade O, Medina MA. Reducing heat transfer across the insulated walls of refrigerated truck trailers by the application of phase change materials. Energy Convers Manag 2010;51:383–92. doi:10.1016/j.enconman.2009.09.003.

[33] Zarajabad OG, Ahmadi R, Ghaffari S. Numerical Investigation of Cold Thermal Energy Storage Using Phase Change Material in Freezer 2017;2:1–6.

[34] Wang F, Maidment G, Missenden J, Tozer R. The novel use of phase change materials in refrigeration plant. Part 3: PCM for control and energy savings. Appl Therm Eng 2007;27:2911–8. doi:10.1016/j.applthermaleng.2005.06.010.

[35] Gin B, Farid MM. The use of PCM panels to improve storage condition of frozen food. J Food Eng 2010;100:372–6. doi:10.1016/j.jfoodeng.2010.04.016.

[36] Cheng W long, Ding M, Yuan X dong, Han BC. Analysis of energy saving performance for household refrigerator with thermal storage of condenser and evaporator. Energy Convers Manag 2017;132:180–8. doi:10.1016/j.enconman.2016.11.029.

[37] Fioretti R, Principi P, Copertaro B. A refrigerated container envelope with a PCM (Phase Change Material) layer: Experimental and theoretical investigation in a representative town in Central Italy. Energy Convers Manag 2016;122:131–41. doi:10.1016/j.enconman.2016.05.071.

[38] Sepe R, Armentani E, Pozzi A. Development and stress behaviour of an innovative refrigerated container with PCM for fresh and frozen goods. Multidiscip Model Mater Struct 2015;11:202–15. doi:10.1108/MMMS-05-2014-0030.

[39] Khan IH, Afroz HMM, Karim MA. Effect of PCM on temperature fluctuation during the door opening of a household refrigerator. Int J Green Energy 2017;14:379–84. doi:10.1080/15435075.2016.1261705.

[40] Kilic GA, Yalcin E, Aydın AA. Experimental analysis of a cold store integrated with phase change material : a case study 2016;48:195–8.

[41] Elarem R, Mellouli S, Abhilash E, Jemni A. Performance analysis of a household refrigerator integrating a PCM heat exchanger. Appl Therm Eng 2017;125:1320–33. doi:10.1016/j.applthermaleng.2017.07.113.

[42] Raja M, Yadav GMP. Experimental Investigation on Cascade Refrigeration System with And without Phase Change Material 2015;4.

[43] Bruno F, Hudson J, Henshall P, Belusko M. Evaluation of PCM Thermal Storage Demonstration System for Cold Storage n.d.

[44] Bista S, Hosseini SE, Owens E, Phillips G. Performance improvement and energy consumption reduction in refrigeration systems using phase change material (PCM). Appl Therm Eng 2018;142:723–35. doi:10.1016/J.APPLTHERMALENG.2018.07.068.

[45] Krishnan S, Garimella S V, Kang SS. Materials for Transient Thermal Management of Electronics. IEEE Trans Components Packag Technol 2005;28:281–9.

[46] Hasan A, Hejase H, Abdelbaqi S, Assi A, Hamdan M. Comparative Effectiveness of Different Phase Change Materials to Improve Cooling Performance of Heat Sinks for Electronic Devices. Appl Sci 2016;6:226. doi:10.3390/app6090226.

[47] Behi H, Ghanbarpour M, Behi M. Investigation of PCM-assisted heat pipe for electronic cooling. Appl Therm Eng 2017;127:1132–42. doi:10.1016/j.applthermaleng.2017.08.109.

[48] Krishna J, Kishore PS, Solomon AB. Heat pipe with nano enhanced-PCM for electronic cooling application. Exp Therm Fluid Sci 2017;81:84–92. doi:10.1016/j.expthermflusci.2016.10.014.

[49] Yang L, Peng H, Ling X, Dong H. Numerical analysis on performance of naphthalene phase change thermal storage system in aluminum plate-fin unit. Heat Mass Transf Und Stoffuebertragung 2014;51:195–207. doi:10.1007/s00231-014-1400-7.

[50] Sharma S, Tahir A, Reddy KS, Mallick TK. Performance enhancement of a Building-Integrated Concentrating Photovoltaic system using phase change material. Sol Energy Mater Sol Cells 2016;149:29–39. doi:10.1016/j.solmat.2015.12.035.

[51] Karthick A, Murugavel KK, Ramanan P. Performance enhancement of a building-integrated photovoltaic module using phase change material. Energy 2018;142:803–12. doi:10.1016/j.energy.2017.10.090.

[52] Duan X, Naterer GF. Heat transfer in phase change materials for thermal management of electric vehicle battery modules. Int J Heat Mass Transf 2010;53:5176–82. doi:10.1016/j.ijheatmasstransfer.2010.07.044.

[53] Fathabadi H. High thermal performance lithium-ion battery pack including hybrid active-passive thermal management system for using in hybrid/electric vehicles. Energy 2014;70:529–38. doi:10.1016/j.energy.2014.04.046.

[54] Lu Y, Wei F, Lai D, Shi W, Wang F, Gao C, et al. A novel personal cooling system (PCS) incorporated with phase change materials (PCMs) and ventilation fans: An investigation on its cooling efficiency. J Therm Biol 2015;52:137–46. doi:10.1016/j.jtherbio.2015.07.002.

[55] Mokhtari Yazdi M, Sheikhzadeh M, Dabirzadeh A, Chavoshi E. Modeling the efficiency and heat gain of a phase change material cooling vest: The effect of ambient temperature and outer isolation. J Ind Text 2016;46:436–54. doi:10.1177/1528083715589746.

[56] Mokhtari Yazdi M, Sheikhzadeh M, Borhani S. Modeling the heat transfer in a PCM cooling vest. J

Text Inst 2015;106:1003–12. doi:10.1080/00405000.2014.959800.

[57] Yazdi MM, Sheikhzadeh M, Chavoshi SE. Modeling the performance of a PCM cooling vest considering its side effects. Int J Cloth Sci Technol 2015;27:573–86. doi:10.1108/IJCST-01-2014-0018.

[58] Itani M, Ghaddar N, Ouahrani D, Ghali K, Khater B. An optimal two-bout strategy with phase change material cooling vests to improve comfort in hot environment. J Therm Biol 2018;72:10–25. doi:10.1016/j.jtherbio.2017.12.005.

[59] Park J, Kim T, Leigh SB. Application of a phase-change material to improve the electrical performance of vertical-building-added photovoltaics considering the annual weather conditions. Sol Energy 2014;105:561–74. doi:10.1016/j.solener.2014.04.020.

[60] Atkin P, Farid MM. Improving the efficiency of photovoltaic cells using PCM infused graphite and aluminium fins. Sol Energy 2015;114:217–28. doi:10.1016/j.solener.2015.01.037.

[61] Luo Z, Huang Z, Xie N, Gao X, Xu T, Fang Y, et al. Numerical and experimental study on temperature control of solar panels with form-stable paraffin/expanded graphite composite PCM. Energy Convers Manag 2017;149:416–23. doi:10.1016/j.enconman.2017.07.046.

[62] Nada SA, El-Nagar DH, Hussein HMS. Improving the thermal regulation and efficiency enhancement of PCM-Integrated PV modules using nano particles. Energy Convers Manag 2018;166:735–43. doi:10.1016/j.enconman.2018.04.035.

[63] Hasan A, McCormack SJ, Huang MJ, Sarwar J, Norton B. Increased photovoltaic performance through temperature regulation by phase change materials: Materials comparison in different climates. Sol Energy 2015;115:264–76. doi:10.1016/j.solener.2015.02.003.

[64] Stropnik R, Stritih U. Increasing the efficiency of PV panel with the use of PCM. Renew Energy 2016;97:671–9. doi:10.1016/j.renene.2016.06.011.

[65] Aelenei L, Pereira R, Gonçalves H, Athienitis A. Thermal performance of a hybrid BIPV-PCM: Modeling, design and experimental investigation. Energy Procedia 2014;48:474–83. doi:10.1016/j.egypro.2014.02.056.

[66] Hasan A, McCormack SJ, Huang MJ, Norton B. Evaluation of phase change materials for thermal regulation enhancement of building integrated photovoltaics. Sol Energy 2010;84:1601–12. doi:10.1016/j.solener.2010.06.010.

[67] Qiu Z, Ma X, Zhao X, Li P, Ali S. Experimental investigation of the energy performance of a novel Micro-encapsulated Phase Change Material (MPCM) slurry based PV/T system. Appl Energy 2016;165:260–71. doi:10.1016/j.apenergy.2015.11.053.

[68] Gao X, Yuan Y, Wu H, Cao X, Zhao X. Coupled cooling method and application of latent heat thermal energy storage combined with pre-cooling of envelope: Optimization of pre-cooling with intermittent mode. Sustain Cities Soc 2018;38:370–81. doi:10.1016/j.scs.2018.01.014.

[69] Veerakumar C, Sreekumar A. Phase change material based cold thermal energy storage: Materials, techniques and applications - A review. Int J Refrig 2016;67:271–89. doi:10.1016/j.ijrefrig.2015.12.005.

[70] Ferrer G, Solé A, Barreneche C, Martorell I, Cabeza LF. Corrosion of metal containers for use in PCM energy storage. Renew Energy 2015;76:465–9. doi:10.1016/j.renene.2014.11.036.

[71] Vasu A, Hagos FY, Noor MM, Mamat R, Azmi WH, Abdullah AA, et al. Corrosion effect of phase change materials in solar thermal energy storage application. Renew Sustain Energy Rev 2017;76:19–33. doi:10.1016/j.rser.2017.03.018.

[72] Mohamed SA, Al-Sulaiman FA, Ibrahim NI, Zahir MH, Al-Ahmed A, Saidur R, et al. A review on current status and challenges of inorganic phase change materials for thermal energy storage systems. Renew Sustain Energy Rev 2017;70:1072–89. doi:10.1016/j.rser.2016.12.012.

[73] Browne MC, Boyd E, McCormack SJ. Investigation of the corrosive properties of phase change materials in contact with metals and plastic. Renew Energy 2017;108:555–68. doi:10.1016/j.renene.2017.02.082.

[74] Zhang S, Wu W, Wang S. Experimental investigations of Alum/expanded graphite composite phase change material for thermal energy storage and its compatibility with metals. Energy 2018. doi:10.1016/j.energy.2018.07.075.

[75] Deng Y, Li J, Qian T, Guan W, Wang X. Preparation and Characterization of KNO3/Diatomite Shape-Stabilized Composite Phase Change Material for High Temperature Thermal Energy Storage. J Mater Sci Technol 2017;33:198–203. doi:10.1016/j.jmst.2016.02.011.

[76] Chandel SS, Agarwal T. Review of current state of research on energy storage, toxicity, health hazards and commercialization of phase changing materials. Renew Sustain Energy Rev 2017;67:581–96. doi:10.1016/j.rser.2016.09.070.

[77] Shukla A, Buddhi D, Sawhney RL. Thermal cycling test of few selected inorganic and organic phase change materials. Renew Energy 2008;33:2606–14. doi:10.1016/j.renene.2008.02.026.

[78] Regin AF, Solanki SC, Saini JS. Heat transfer characteristics of thermal energy storage system using PCM capsules: A review. Renew Sustain Energy Rev 2008;12:2438–51. doi:10.1016/j.rser.2007.06.009.

[79] Baetens R, Jelle BP, Gustavsen A. Phase change materials for building applications: A state-of-the-art review. Energy Build 2010;42:1361–8. doi:10.1016/j.enbuild.2010.03.026.

[80] Ushak S, Gutierrez A, Galleguillos H, Fernandez AG, Cabeza LF, Grágeda M. Thermophysical characterization of a by-product from the non-metallic industry as inorganic PCM. Sol Energy Mater Sol Cells 2015;132:385–91. doi:10.1016/j.solmat.2014.08.042.

[81] Huang Q, Lu G, Wang J, Yu J. Thermal decomposition mechanisms of MgCl2·6H2O and MgCl2·H2O. J Anal Appl Pyrolysis 2011;91:159–64. doi:10.1016/j.jaap.2011.02.005.

[82] Farid MM, Khudhair AM, Razack SAK, Al-Hallaj S. A review on phase change energy storage: Materials and applications. Energy Convers Manag 2004;45:1597–615. doi:10.1016/j.enconman.2003.09.015.

[83] Li G, Hwang Y, Radermacher R, Chun HH. Review of cold storage materials for subzero applications. Energy 2013;51:1–17. doi:10.1016/j.energy.2012.12.002.

[84] Jeong SG, Kim S, Cha J, Kim S, Seo J, Lee JH. Preparation of thermal-enhanced epoxy resin adhesive with organic PCM for applying wood flooring. J Therm Anal Calorim 2014;117:1027–34. doi:10.1007/s10973-014-3862-8.

[85] Akeiber H, Nejat P, Majid MZA, Wahid MA, Jomehzadeh F, Zeynali Famileh I, et al. A review on phase change material (PCM) for sustainable passive cooling in building envelopes. Renew Sustain Energy Rev 2016;60:1470–97. doi:10.1016/j.rser.2016.03.036.

[86] Tang Y, Lin Y, Jia Y, Fang G. Improved thermal properties of stearyl alcohol/high density polyethylene/expanded graphite composite phase change materials for building thermal energy storage. Energy Build 2017;153:41–9. doi:10.1016/j.enbuild.2017.08.005.

[87] Tang Y, Jia Y, Alva G, Huang X, Fang G. Synthesis, characterization and properties of palmitic acid/high density polyethylene/graphene nanoplatelets composites as form-stable phase change materials. Sol Energy Mater Sol Cells 2016;155:421–9. doi:10.1016/j.solmat.2016.06.049.

[88] Tang Y, Su D, Huang X, Alva G, Liu L, Fang G. Synthesis and thermal properties of the MA/HDPE composites with nano-additives as form-stable PCM with improved thermal conductivity. Appl Energy 2016;180:116–29. doi:10.1016/j.apenergy.2016.07.106.

[89] Motahar S, Alemrajabi AA, Khodabandeh R. Enhanced thermal conductivity of n-octadecane containing carbon-based nanomaterials. Heat Mass Transf Und Stoffuebertragung 2016;52:1621–31. doi:10.1007/s00231-015-1678-0.

[90] Raam Dheep G, Sreekumar A. Influence of nanomaterials on properties of latent heat solar thermal energy storage materials - A review. Energy Convers Manag 2014;83:133–48. doi:10.1016/j.enconman.2014.03.058.

[91] Németh B, Németh ÁS, Tóth J, Fodor-Kardos A, Gyenis J, Feczkó T. Consolidated microcapsules with double alginate shell containing paraffin for latent heat storage. Sol Energy Mater Sol Cells 2015;143:397–405. doi:10.1016/j.solmat.2015.07.029.

[92] Lv P, Liu C, Rao Z. Experiment study on the thermal properties of paraffin/kaolin thermal energy storage form-stable phase change materials. Appl Energy 2016;182:475–87. doi:10.1016/j.apenergy.2016.08.147.

[93] Xu B, Li Z. Paraffin/diatomite/multi-wall carbon nanotubes composite phase change material tailor-made for thermal energy storage cement-based composites. Energy 2014;72:371–80. doi:10.1016/j.energy.2014.05.049.

[94] Fan L, Khodadadi JM. Thermal conductivity enhancement of phase change materials for thermal energy storage: A review. Renew Sustain Energy Rev 2011;15:24–46. doi:10.1016/j.rser.2010.08.007.

[95] Liu L, Su D, Tang Y, Fang G. Thermal conductivity enhancement of phase change materials for thermal energy storage: A review. Renew Sustain Energy Rev 2016;62:305–17. doi:10.1016/j.rser.2016.04.057.

[96] Li J, He L, Liu T, Cao X, Zhu H. Preparation and characterization of PEG/SiO2 composites as shape-stabilized phase change materials for thermal energy storage. Sol Energy Mater Sol Cells

2013;118:48–53. doi:10.1016/j.solmat.2013.07.017.

[97] Karaipekli A, Biçer A, Sarı A, Tyagi VV. Thermal characteristics of expanded perlite/paraffin composite phase change material with enhanced thermal conductivity using carbon nanotubes. Energy Convers Manag 2017;134:373–81. doi:10.1016/j.enconman.2016.12.053.

[98] Atinafu DG, Dong W, Huang X, Gao H, Wang G. Introduction of organic-organic eutectic PCM in mesoporous N-doped carbons for enhanced thermal conductivity and energy storage capacity. Appl Energy 2018;211:1203–15. doi:10.1016/j.apenergy.2017.12.025.

[99] Zou D, Ma X, Liu X, Zheng P, Hu Y. Thermal performance enhancement of composite phase change materials (PCM) using graphene and carbon nanotubes as additives for the potential application in lithium-ion power battery. Int J Heat Mass Transf 2018;120:33–41. doi:10.1016/j.ijheatmasstransfer.2017.12.024.

[100] Ji H, Sellan DP, Pettes MT, Kong X, Ji J, Shi L, et al. Enhanced thermal conductivity of phase change materials with ultrathin-graphite foams for thermal energy storage. Energy Environ Sci 2014;7:1185–92. doi:10.1039/C3EE42573H.

[101] Deng Y, Li J, Qian T, Guan W, Li Y, Yin X. Thermal conductivity enhancement of polyethylene glycol/expanded vermiculite shape-stabilized composite phase change materials with silver nanowire for thermal energy storage. Chem Eng J 2016;295:427–35. doi:10.1016/j.cej.2016.03.068.

[102] Şahan N, Fois M, Paksoy H. Improving thermal conductivity phase change materials - A study of paraffin nanomagnetite composites. Sol Energy Mater Sol Cells 2015;137:61–7. doi:10.1016/j.solmat.2015.01.027.

[103] Yang Z, Zhou L, Luo W, Wan J, Dai J, Han X, et al. Thermally conductive, dielectric PCM–boron nitride nanosheet composites for efficient electronic system thermal management. Nanoscale 2016;8:19326–33. doi:10.1039/C6NR07357C.

[104] Kalaiselvam S, Parameshwaran R, Harikrishnan S. Analytical and experimental investigations of nanoparticles embedded phase change materials for cooling application in modern buildings. Renew Energy 2012;39:375–87. doi:10.1016/j.renene.2011.08.034.

[105] Chandrasekaran P, Cheralathan M, Kumaresan V, Velraj R. Enhanced heat transfer characteristics of water based copper oxide nanofluid PCM (phase change material) in a spherical capsule during solidification for energy efficient cool thermal storage system. Energy 2014;72:636–42. doi:10.1016/j.energy.2014.05.089.

[106] Wang F, Zhang C, Liu J, Fang X, Zhang Z. Highly stable graphite nanoparticle-dispersed phase change emulsions with little supercooling and high thermal conductivity for cold energy storage. Appl Energy 2017;188:97–106. doi:10.1016/j.apenergy.2016.11.122.

[107] Parameshwaran R, Deepak K, Saravanan R, Kalaiselvam S. Preparation, thermal and rheological properties of hybrid nanocomposite phase change material for thermal energy storage. Appl Energy 2014;115:320–30. doi:10.1016/j.apenergy.2013.11.029.

[108] Kumaresan V, Chandrasekaran P, Nanda M, Maini AK, Velraj R. Role of PCM based nanofluids for energy efficient cool thermal storage system. Int J Refrig 2013;36:1641–7. doi:10.1016/j.ijrefrig.2013.04.010.

[109] Fu W, Liang X, Xie H, Wang S, Gao X, Zhang Z, et al. Thermophysical properties of n-tetradecane@polystyrene-silica composite nanoencapsulated phase change material slurry for cold energy storage. Energy Build 2017;136:26–32. doi:10.1016/j.enbuild.2016.12.001.

[110] Zhu ZQ, Huang YK, Hu N, Zeng Y, Fan LW. Transient performance of a PCM-based heat sink with a partially filled metal foam: Effects of the filling height ratio. Appl Therm Eng 2018;128:966–72. doi:10.1016/j.applthermaleng.2017.09.047.

[111] Isa MHM, Zhao X, Yoshino H. Preliminary study of passive cooling strategy using a combination of PCM and copper foam to increase thermal heat storage in building facade. Sustainability 2010;2:2365–81. doi:10.3390/su2082365.

[112] Tian Y, Zhao CY. A numerical investigation of heat transfer in phase change materials (PCMs) embedded in porous metals. Energy 2011;36:5539–46. doi:10.1016/j.energy.2011.07.019.

[113] Yang J, Yang L, Xu C, Du X. Experimental study on enhancement of thermal energy storage with phase-change material. Appl Energy 2016;169:164–76. doi:10.1016/j.apenergy.2016.02.028.

[114] Lafdi K, Mesalhy O, Shaikh S. Experimental study on the influence of foam porosity and pore size on the melting of phase change materials. J Appl Phys 2007;102. doi:10.1063/1.2802183.

[115] Xiao X, Zhang P, Li M. Preparation and thermal characterization of paraffin/metal foam composite phase change material. Appl Energy 2013;112:1357–66. doi:10.1016/j.apenergy.2013.04.050.

[116] Wang Z, Zhang Z, Jia L, Yang L. Paraffin and paraffin/aluminum foam composite phase change material heat storage experimental study based on thermal management of Li-ion battery. Appl Therm Eng 2015;78:428–36. doi:10.1016/j.applthermaleng.2015.01.009.

[117] Zhao CY, Lu W, Tian Y. Heat transfer enhancement for thermal energy storage using metal foams embedded within phase change materials (PCMs). Sol Energy 2010;84:1402–12. doi:10.1016/j.solener.2010.04.022.

[118] Li WQ, Qu ZG, He YL, Tao WQ. Experimental and numerical studies on melting phase change heat transfer in open-cell metallic foams filled with paraffin. Appl Therm Eng 2012;37:1–9. doi:10.1016/j.applthermaleng.2011.11.001.

[119] Zhou D, Zhao CY. Experimental investigations on heat transfer in phase change materials (PCMs) embedded in porous materials. Appl Therm Eng 2011;31:970–7. doi:10.1016/j.applthermaleng.2010.11.022.

[120] Li WQ, Qu ZG, He YL, Tao YB. Experimental study of a passive thermal management system for high-powered lithium ion batteries using porous metal foam saturated with phase change materials. J Power Sources 2014;255:9–15. doi:10.1016/j.jpowsour.2014.01.006.

[121] Hussain A, Tso CY, Chao CYH. Experimental investigation of a passive thermal management system

for high-powered lithium ion batteries using nickel foam-paraffin composite. Energy 2016;115:209–18. doi:10.1016/j.energy.2016.09.008.

[122] Wang C, Lin T, Li N, Zheng H. Heat transfer enhancement of phase change composite material: Copper foam/paraffin. Renew Energy 2016;96:960–5. doi:10.1016/j.renene.2016.04.039.

[123] El Qarnia H, Draoui A, Lakhal EK. Computation of melting with natural convection inside a rectangular enclosure heated by discrete protruding heat sources. Appl Math Model 2013;37:3968–81. doi:10.1016/j.apm.2012.08.021.

[124] Jmal I, Baccar M. Numerical study of PCM solidification in a finned tube thermal storage including natural convection. Appl Therm Eng 2015;84:320–30. doi:10.1016/j.applthermaleng.2015.03.065.

[125] Mat S, Al-Abidi AA, Sopian K, Sulaiman MY, Mohammad AT. Enhance heat transfer for PCM melting in triplex tube with internal-external fins. Energy Convers Manag 2013;74:223–36. doi:10.1016/j.enconman.2013.05.003.

[126] Ogoh W, Groulx D. Effects of the heat transfer fluid velocity on the storage characteristics of a cylindrical latent heat energy storage system: a numerical study. Heat Mass Transf 2012;48:439–49. doi:10.1007/s00231-011-0888-3.

[127] Liu Z, Sun X, Ma C. Experimental study of the characteristics of solidification of stearic acid in an annulus and its thermal conductivity enhancement. Energy Convers Manag 2005;46:971–84. doi:10.1016/j.enconman.2004.05.011.

[128] Rabienataj Darzi AA, Jourabian M, Farhadi M. Melting and solidification of PCM enhanced by radial conductive fins and nanoparticles in cylindrical annulus. Energy Convers Manag 2016;118:253–63. doi:10.1016/j.enconman.2016.04.016.

[129] Joybari MM, Haghighat F, Seddegh S, Al-Abidi AA. Heat transfer enhancement of phase change materials by fins under simultaneous charging and discharging. Energy Convers Manag 2017;152:136–56. doi:10.1016/j.enconman.2017.09.018.

[130] Raud R, Cholette ME, Riahi S, Bruno F, Saman W. Design optimization method for tube and fin latent heat thermal energy storage systems. Energy 2017;134:585–94. doi:10.1016/j.energy.2017.06.013.

[131] Bourne S, Novoselac A. Compact PCM-based thermal stores for shifting peak cooling loads. Build Simul 2015;8:673–88. doi:10.1007/s12273-015-0243-6.

[132] Tay NHS, Belusko M, Bruno F. Designing a PCM storage system using the effectiveness-number of transfer units method in low energy cooling of buildings. Energy Build 2012;50:234–42. doi:10.1016/j.enbuild.2012.03.041.

[133] Wu S, Fang G, Chen Z. Discharging characteristics modeling of cool thermal energy storage system with coil pipes using n-tetradecane as phase change material. Appl Therm Eng 2012;37:336–43. doi:10.1016/j.applthermaleng.2011.11.046.

[134] Zhai XQ, Cheng XW, Wang C, Wang RZ. Experimental investigation and performance analysis of a fin tube phase change cold storage unit for high temperature cooling application. Energy Build 2015;89:9–

17. doi:10.1016/j.enbuild.2014.12.021.

[135] Antony Aroul Raj V, Velraj R. Heat transfer and pressure drop studies on a PCM-heat exchanger module for free cooling applications. Int J Therm Sci 2011;50:1573–82. doi:10.1016/j.ijthermalsci.2011.01.025.

[136] Hed G, Bellander R. Mathematical modelling of PCM air heat exchanger. Energy Build 2006;38:82–9. doi:10.1016/j.enbuild.2005.04.002.

[137] Zhao D, Tan G. Numerical analysis of a shell-and-tube latent heat storage unit with fins for air-conditioning application. Appl Energy 2015;138:381–92. doi:10.1016/j.apenergy.2014.10.051.

[138] Teggar M, Mezaache EH. Numerical investigation of a PCM heat exchanger for latent cool storage. Energy Procedia 2013;36:1310–9. doi:10.1016/j.egypro.2013.07.149.

[139] Mosaffa AH, Talati F, Basirat Tabrizi H, Rosen MA. Analytical modeling of PCM solidification in a shell and tube finned thermal storage for air conditioning systems. Energy Build 2012;49:356–61. doi:10.1016/j.enbuild.2012.02.053.

[140] Hu Y, Heiselberg PK. A new ventilated window with PCM heat exchanger—Performance analysis and design optimization. Energy Build 2018;169:185–94. doi:10.1016/j.enbuild.2018.03.060.

[141] Dolado P, Lazaro A, Delgado M, Peñalosa C, Mazo J, Marin J, et al. An Approach to the Integrated Design of PCM-Air Heat Exchangers Based on Numerical Simulation: A Solar Cooling Case Study. Resources 2015;4:796–818. doi:10.3390/resources4040796.

[142] Allouche Y, Varga S, Bouden C, Oliveira AC. Experimental determination of the heat transfer and cold storage characteristics of a microencapsulated phase change material in a horizontal tank. Energy Convers Manag 2015;94:275–85. doi:10.1016/j.enconman.2015.01.064.

[143] Marín JM, Zalba B, Cabeza LF, Mehling H. Improvement of a thermal energy storage using plates with paraffin-graphite composite. Int J Heat Mass Transf 2005;48:2561–70. doi:10.1016/j.ijheatmasstransfer.2004.11.027.

[144] Castell A, Belusko M, Bruno F, Cabeza LF. Maximisation of heat transfer in a coil in tank PCM cold storage system. Appl Energy 2011;88:4120–7. doi:10.1016/j.apenergy.2011.03.046.

[145] Diaconu BM, Varga S, Oliveira AC. Experimental assessment of heat storage properties and heat transfer characteristics of a phase change material slurry for air conditioning applications. Appl Energy 2010;87:620–8. doi:10.1016/j.apenergy.2009.05.002.

[146] Weng YC, Cho HP, Chang CC, Chen SL. Heat pipe with PCM for electronic cooling. Appl Energy 2011;88:1825–33. doi:10.1016/j.apenergy.2010.12.004.

[147] Usman H, Ali HM, Arshad A, Ashraf MJ, Khushnood S, Janjua MM, et al. An experimental study of PCM based finned and un-finned heat sinks for passive cooling of electronics. Heat Mass Transf Und Stoffuebertragung 2018:1–12. doi:10.1007/s00231-018-2389-0.

[148] Garg H, Pandey B, Saha SK, Singh S, Banerjee R. Design and analysis of PCM based radiant heat

exchanger for thermal management of buildings. Energy Build 2018;169:84–96. doi:10.1016/j.enbuild.2018.03.058.

[149] Al-Abidi AA, Mat S, Sopian K, Sulaiman MY, Mohammad AT. Internal and external fin heat transfer enhancement technique for latent heat thermal energy storage in triplex tube heat exchangers. Appl Therm Eng 2013;53:147–56. doi:10.1016/j.applthermaleng.2013.01.011.

[150] Peng H, Ling X. Numerical modeling and experimental verification of flow and heat transfer over serrated fins at low Reynolds number. Exp Therm Fluid Sci 2008;32:1039–48. doi:10.1016/j.expthermflusci.2007.11.021.

[151] Tao YB, He YL. Numerical study on performance enhancement of shell-and-tube latent heat storage unit. Int Commun Heat Mass Transf 2015;67:147–52. doi:10.1016/j.icheatmasstransfer.2015.07.013.

[152] Sciacovelli A, Gagliardi F, Verda V. Maximization of performance of a PCM latent heat storage system with innovative fins. Appl Energy 2015;137:707–15. doi:10.1016/j.apenergy.2014.07.015.

[153] Ye WB, Zhu DS, Wang N. Numerical simulation on phase-change thermal storage/release in a plate-fin unit. Appl Therm Eng 2011;31:3871–84. doi:10.1016/j.applthermaleng.2011.07.035.

[154] Stritih U. An experimental study of enhanced heat transfer in rectangular PCM thermal storage. Int J Heat Mass Transf 2004;47:2841–7. doi:10.1016/j.ijheatmasstransfer.2004.02.001.

[155] Farrington R, Rugh J. Impact of Vehicle Air-Conditioning on Fuel Economy, Tailpipe Emissions, and Electric Vehicle Range. Earth Technol Forum 2000:http://www.nrel.gov/docs/fy00osti/28960.pdf. doi:NREL/CP-540-28960.

[156] Kambly KR, Bradley TH. Estimating the HVAC energy consumption of plug-in electric vehicles. J Power Sources 2014;259:117–24. doi:10.1016/j.jpowsour.2014.02.033.

[157] Lambert MA, Jones BJ. Automotive adsorption air conditioner powered by exhaust heat. Part 1: Conceptual and embodiment design. Proc Inst Mech Eng Part D J Automob Eng 2006;220:959–72. doi:10.1243/09544070JAUTO221.

[158] Anderson RJ, Findlay NS, Graham DJ. Maximising the potential for metros to reduce energy consumption and deliver low-carbon transportation in cities. Transp Res Board 91st Annu Meet 2012:1–13.

[159] Zhou D, Zhao CY, Tian Y. Review on thermal energy storage with phase change materials (PCMs) in building applications. Appl Energy 2012;92:593–605. doi:10.1016/j.apenergy.2011.08.025.

[160] Xu B, Li Z. Paraffin/diatomite composite phase change material incorporated cement-based composite for thermal energy storage. Appl Energy 2013;105:229–37. doi:10.1016/j.apenergy.2013.01.005.

[161] Kang Y, Jeong SG, Wi S, Kim S. Energy efficient Bio-based PCM with silica fume composites to apply in concrete for energy saving in buildings. Sol Energy Mater Sol Cells 2015;143:430–4. doi:10.1016/j.solmat.2015.07.026.

[162] Devaux P, Farid MM. Benefits of PCM underfloor heating with PCM wallboards for space heating in

winter. Appl Energy 2017;191:593–602. doi:10.1016/j.apenergy.2017.01.060.

[163] Li Y, Huang G, Xu T, Liu X, Wu H. Optimal design of PCM thermal storage tank and its application for winter available open-air swimming pool. Appl Energy 2018;209:224–35. doi:10.1016/j.apenergy.2017.10.095.

[164] Xiang B, Cao X, Yuan Y, Sun L, Wu H, Haghighat F. A novel hybrid energy system combined with solar-road and soil-regenerator: Dynamic model and operational performance. Energy Convers Manag 2018;156:376–87. doi:10.1016/j.enconman.2017.11.066.

[165] Pasupathy A, Velraj R, Seeniraj R V. Phase change material-based building architecture for thermal management in residential and commercial establishments. Renew Sustain Energy Rev 2008;12:39–64. doi:10.1016/j.rser.2006.05.010.

[166] Tyagi V V., Kaushik SC, Tyagi SK, Akiyama T. Development of phase change materials based microencapsulated technology for buildings: A review. Renew Sustain Energy Rev 2011;15:1373–91. doi:10.1016/j.rser.2010.10.006.

[167] Allouche Y, Varga S, Bouden C, Oliveira AC. Dynamic simulation of an integrated solar-driven ejector based air conditioning system with PCM cold storage. Appl Energy 2017;190:600–11. doi:10.1016/j.apenergy.2017.01.001.

[168] Hoseini Rahdar M, Emamzadeh A, Ataei A. A comparative study on PCM and ice thermal energy storage tank for air-conditioning systems in office buildings. Appl Therm Eng 2016;96:391–9. doi:10.1016/j.applthermaleng.2015.11.107.

[169] Ascione F, Bianco N, De Masi RF, de' Rossi F, Vanoli GP. Energy refurbishment of existing buildings through the use of phase change materials: Energy savings and indoor comfort in the cooling season. Appl Energy 2014;113:990–1007. doi:10.1016/j.apenergy.2013.08.045.

[170] Qi L, Pan H, Zhu X, Zhang X, Salman W, Zhang Z, et al. A portable solar-powered air-cooling system based on phase-change materials for a vehicle cabin. Energy Convers Manag 2017;150:148–58. doi:10.1016/j.enconman.2017.07.067.

[171] Ramakrishnan S, Wang X, Sanjayan J, Wilson J. Thermal performance of buildings integrated with phase change materials to reduce heat stress risks during extreme heatwave events. Appl Energy 2017;194:410–21. doi:10.1016/j.apenergy.2016.04.084.

[172] Sage-Lauck JS, Sailor DJ. Evaluation of phase change materials for improving thermal comfort in a super-insulated residential building. Energy Build 2014;79:32–40. doi:10.1016/j.enbuild.2014.04.028.

[173] Hasnain SM. Review on sustainable thermal energy storage technologies, Part II: cool thermal storage. Energy Convers Manag 1998;39:1139–53. doi:10.1016/S0196-8904(98)00024-7.

[174] Yau YH, Rismanchi B. A review on cool thermal storage technologies and operating strategies. Renew Sustain Energy Rev 2012;16:787–97. doi:10.1016/j.rser.2011.09.004.

[175] Moreno P, Solé C, Castell A, Cabeza LF. The use of phase change materials in domestic heat pump and air-conditioning systems for short term storage: A review. Renew Sustain Energy Rev 2014;39:1–13.

doi:10.1016/j.rser.2014.07.062.

[176] Chen SL, Chen CL, Tin CC, Lee TS, Ke MC. An experimental investigation of cold storage in an encapsulated thermal storage tank. Exp Therm Fluid Sci 2000;23:133–44. doi:Doi 10.1016/S0894-1777(00)00045-5.

[177] Tan H, Li Y, Tuo H, Zhou M, Tian B. Experimental study on liquid/solid phase change for cold energy storage of Liquefied Natural Gas (LNG) refrigerated vehicle. Energy 2010;35:1927–35. doi:10.1016/j.energy.2010.01.006.

[178] Fang G, Liu X, Wu S. Experimental investigation on performance of ice storage air-conditioning system with separate heat pipe. Exp Therm Fluid Sci 2009;33:1149–55. doi:10.1016/j.expthermflusci.2009.07.004.

[179] Al-Aifan B, Parameshwaran R, Mehta K, Karunakaran R. Évaluation De La Performance D'Un Volume De Frigorigène Variable Combiné À Un Système De Stockage D'Énergie Thermique Froide Pour Des Applications De Conditionnement D'Air. Int J Refrig 2017;76:271–95. doi:10.1016/j.ijrefrig.2017.02.008.

[180] Sun X, Zhang Q, Medina MA, Liu Y, Liao S. A study on the use of phase change materials (PCMs) in combination with a natural cold source for space cooling in telecommunications base stations (TBSs) in China. Appl Energy 2014;117:95–103. doi:10.1016/j.apenergy.2013.12.010.

[181] Jia J, Lee WL. Experimental investigations on using phase change material for performance improvement of storage-enhanced heat recovery room air-conditioner. Energy 2015;93:1394–403. doi:10.1016/j.energy.2015.10.053.

[182] Zhao D, Tan G. Experimental evaluation of a prototype thermoelectric system integrated with PCM (phase change material) for space cooling. Energy 2014;68:658–66. doi:10.1016/j.energy.2014.01.090.

[183] Parameshwaran R, Kalaiselvam S. Energy conservative air conditioning system using silver nano-based PCM thermal storage for modern buildings. Energy Build 2014;69:202–12. doi:10.1016/j.enbuild.2013.09.052.

[184] Castell A, Martorell I, Medrano M, Pérez G, Cabeza LF. Experimental study of using PCM in brick constructive solutions for passive cooling. Energy Build 2010;42:534–40. doi:10.1016/j.enbuild.2009.10.022.

[185] Chaiyat N. Energy and economic analysis of a building air-conditioner with a phase change material (PCM). Energy Convers Manag 2015;94:150–8. doi:10.1016/j.enconman.2015.01.068.

[186] Allouche Y, Varga S, Bouden C, Oliveira A. A Trnsys simulation of a solar-driven ejector air conditioning system with an integrated PCM cold storage. AIP Conf Proc 2017;1814. doi:10.1063/1.4976240.

[187] Said MA, Hassan H. An experimental work on the effect of using new technique of thermal energy storage of phase change material on the performance of air conditioning unit. Energy Build 2018;173:353–64. doi:10.1016/j.enbuild.2018.05.041.

[188] Aljehani A, Razack SAK, Nitsche L, Al-Hallaj S. Design and optimization of a hybrid air conditioning system with thermal energy storage using phase change composite. Energy Convers Manag 2018;169:404–18. doi:10.1016/j.enconman.2018.05.040.

[189] Chen X, Zhang Q, Zhai ZJ, Wu D, Liao S. Experimental study on operation characteristics of a novel refrigeration system using phase change material. Energy Build 2017;150:516–26. doi:10.1016/j.enbuild.2017.05.069.

[190] Jarzyna W, Zielinski D, Aftyka M, Fatyga K. Cold Storage-Supported Air Conditioning System in Urban Transport Vehicles. J Ecol Eng 2016;17:120–7. doi:10.12911/22998993/65460.

[191] Kabeel AE, Abdelgaied M, Al Ali M. Energy saving potential of a solar assisted desiccant air conditioning system for different types of storage. Environ Prog Sustain Energy 2017;0:1–7. doi:10.1002/ep.12795.

[192] Mosaffa AH, Garousi Farshi L. Exergoeconomic and environmental analyses of an air conditioning system using thermal energy storage. Appl Energy 2016;162:515–26. doi:10.1016/j.apenergy.2015.10.122.

[193] Navidbakhsh M, Shirazi A, Sanaye S. Four e analysis and multi-objective optimization of an ice storage system incorporating PCM as the partial cold storage for air-conditioning applications. Appl Therm Eng 2013;58:30–41. doi:10.1016/j.applthermaleng.2013.04.002.

[194] Diaconu BM, Varga S, Oliveira AC. Numerical simulation of a solar-assisted ejector air conditioning system with cold storage. Energy 2011;36:1280–91. doi:10.1016/j.energy.2010.11.015.

[195] Akeiber HJ, Hosseini SE, Hussen HM, Wahid MA, Mohammad AT. Thermal performance and economic evaluation of a newly developed phase change material for effective building encapsulation. Energy Convers Manag 2017;150:48–61. doi:10.1016/j.enconman.2017.07.043.

[196] Peng H, Ling X. Analysis of heat transfer and flow characteristics over serrated fins with different flow directions. Energy Convers Manag 2011;52:826–35. doi:10.1016/j.enconman.2010.08.008.

[197] Peng H, Ling X, Li J. Performance investigation of an innovative offset strip fin arrays in compact heat exchangers. Energy Convers Manag 2014;80:287–97. doi:10.1016/j.enconman.2014.01.050.

[198] Bertrand O, Binet B, Combeau H, Couturier S, Delannoy Y, Gobin D, et al. Melting driven by natural convection A comparison exercise: first results. Int J Therm Sci 1999;38:5–26. doi:10.1016/S0035-3159(99)80013-0.

[199] Zukowski M. Mathematical modeling and numerical simulation of a short term thermal energy storage system using phase change material for heating applications. Energy Convers Manag 2007;48:155–65. doi:10.1016/j.enconman.2006.04.017.

[200] Xie C, Hong Y, Ding Y, Li Y, Radcliffe J. An economic feasibility assessment of decoupled energy storage in the UK: With liquid air energy storage as a case study. Appl Energy 2018;225:244–57. doi:10.1016/j.apenergy.2018.04.074.

[201] Moffat RJ. Describing the uncertainties in experimental results. Exp Therm Fluid Sci 1988;1:3–17.

doi:10.1016/0894-1777(88)90043-X.